5-29-2023 10:00 AM

Hydrothermal Liquefaction (HTL) of Lignocellulosic Biomass for Biocrude Production: Reaction Kinetics and Corrosion-Resistance Performance of Candidate Alloys for Reactors

Haoyu Wang,

Supervisor: Dr. Chunbao Charles Xu, *The University of Western Ontario*
Co-Supervisor: Dr. Yimin Zeng, *NRCan, CanmetMATERIALS*
A thesis submitted in partial fulfillment of the requirements for the Doctor of Philosophy degree in Chemical and Biochemical Engineering

Recommended Citation

Wang, Haoyu, "Hydrothermal Liquefaction (HTL) of Lignocellulosic Biomass for Biocrude Production: Reaction Kinetics and Corrosion-Resistance Performance of Candidate Alloys for Reactors" (2023). *Electronic Thesis and Dissertation Repository*. 9333.
https://ir.lib.uwo.ca/etd/9333

Abstract

In recent years, the rapid increase in the demand for clean energy and green chemicals as well as concerns over the supply and environmental impacts associated with fossil. resources have stimulated intensive research on conversion of bioresources, such as lignocellulosic biomass and biowaste, into energy, fuels, chemicals, and materials.

Hydrothermal liquefaction (HTL) is a unique thermochemical conversion process, particularly applicable for the conversion of wet biomass and biowaste feedstocks. Most of the biomass HTL studies are conducted in batch reactor and focus on the effects of catalysts, reaction temperature and time on production efficiency and chemical properties of the products. Besides, HTL process is operating usually in a reaction medium in the presence of hot-compressed water (under elevated temperature and high pressure) and usually an alkali catalyst. It is thus necessary to assess corrosion-resistance performance of various candidate alloys for reactors.

In this thesis work, a kinetic model based on chemical compositions (cellulose, hemicellulose, and lignin) was developed for predicting HTL product yields. Validation with our experimental results and the publicly available HTL data in literature obtained with lignocellulosic biomass feedstocks was performed to assess the quality/reliability of the model predictions. In addition, the influence of reaction atmosphere (N_2, H_2, and O_2) on HTL process was investigated in this thesis work. Bio-oils obtained under N_2 or H_2 exhibited higher energy recovery and better quality. Moreover, the comparison between the performance of batch and continuous-flow reactors in HTL of several lignocellulosic biomass and lignin-rich biomass (lignin and black liquor) was investigated. The continuous-flow operations resulted in slightly poorer qualities compared with those obtained from batch operations due to the relatively short reaction time. Furthermore, this thesis examined the corrosion modes and extents of SS316L for reactor construction under static and batch-mode catalytic HTL conversion of two typical biomass feedstocks, Bamboo and Black liquor. These results would be helpful for designing the HTL systems for continuous production and the development and deployment of HTL technology in Canada and the global bioenergy industry.

Keywords

Batch reactor, Black liquor, Continuous reactor, Corrosion, Kinetic model, Hydrothermal liquefaction, Lignin, Lignocellulosic biomass, Model compounds, Reaction atmosphere, Reaction network, SS316L

Co-Authorship Statement

Chapter 2 Literature Review

Authors: Haoyu Wang, Haoyang Li, Xue Han, Yimin Zeng, Chunbao Charles Xu

This chapter was accepted by Elsevier for publication as a book chapter (Biomass Conversion by Liquefaction Technology) in Encyclopedia of Renewable Energy, Sustainability and the Environment.

Chapter 3 Hydrothermal Liquefaction of Pinewood Sawdust: Influence of Reaction Atmosphere

Authors: Haoyu Wang, Yipei Jiang, Even Park, Xue Han, Yimin Zeng, Chunbao Charles Xu

This chapter was published in Sustainability. Wang H, Jiang Y, Park E, Han X, Zeng Y, Xu C. Hydrothermal Liquefaction of Pinewood Sawdust: Influence of Reaction Atmosphere. *Sustainability*. 2023; 15(8):6698. https://doi.org/10.3390/su15086698

The experimental work was conducted by Haoyu Wang, Yipei Jiang and Evan Park under the supervision of Prof. Chunbao (Charles) Xu and Prof. Yimin Zeng. Writing, sample characterizations and data analysis were conducted by Haoyu Wang and Yipei Jiang. The work was reviewed and revised by Prof. Chunbao (Charles) Xu, Prof. Yimin Zeng, and Dr. Xue Han.

Chapter 4 Development of a Kinetic Model based on Chemical Compositions of Lignocellulosic Biomass for Predicting Yields from Hydrothermal Liquefaction under N_2 Atmosphere

Authors: Haoyu Wang, Xue Han, Yimin Zeng, Chunbao Charles Xu

This chapter was submitted to Renewable Energy. The experimental work was conducted by Haoyu Wang under the supervision of Prof. Chunbao (Charles) Xu and Prof. Yimin

Zeng. Writing, data analysis and software programming were performed by Haoyu Wang. The work was reviewed and revised by Prof. Chunbao (Charles) Xu, Prof. Yimin Zeng, and Dr. Xue Han.

Chapter 5 Production of Bio-oils or De-polymerized Lignin from Technical Lignin through Hydrothermal Liquefaction: Comparison of Batch and Continuous-flow Operations

Authors: Haoyu Wang, Mingyuan Zhang, Xue Han, Yimin Zeng, Chunbao Charles Xu

The experimental work was conducted by Haoyu Wang under the supervision of Prof. Chunbao (Charles) Xu and Prof. Yimin Zeng and the assistance of Mingyuan Zhang. Design, commissioning, and modification of the reactor setup were conducted by Haoyu Wang. Writing, sample characterization, and data analysis were performed by Haoyu Wang. The work was reviewed and revised by Prof. Chunbao (Charles) Xu, Prof. Yimin Zeng, and Dr. Xue Han. This chapter will be submitted to a journal for publication.

Chapter 6 Production of Bio-oils from Various Bio-feedstocks through Hydrothermal Liquefaction: Comparison of Batch and Continuous-flow Operations

Authors: Haoyu Wang, Mingyuan Zhang, Xue Han, Yimin Zeng, Chunbao Charles Xu

This chapter was published in Biomass and Bioenergy. Wang H, Zhang M, Han X, Zeng Y, Xu C. Production of bio-oils from various bio-feedstocks through hydrothermal liquefaction: Comparison of batch and continuous-flow operations. *Biomass and Bioenergy*. 2023; 173:106810. https://doi.org/10.1016/j.biombioe.2023.106810.

The experimental work was conducted by Haoyu Wang under the supervision of Prof. Chunbao (Charles) Xu and Prof. Yimin Zeng and the assistance of Mingyuan Zhang. Design, commissioning, and modification of the reactor setup were conducted by Haoyu Wang. Writing, sample characterization, and data analysis were performed by Haoyu

Wang. The work was reviewed and revised by Prof. Chunbao (Charles) Xu, Prof. Yimin Zeng, and Dr. Xue Han.

Chapter 7 Roles of Biomass Feedstocks and Corresponding Organic Products in Corrosion of SS316L under Hydrothermal Liquefaction (HTL) Conversion

Authors: Haoyu Wang, Minkang Liu, Vahid Dehnavi, Xue Han, Yimin Zeng, Chunbao (Charles) Xu

The experimental work was conducted by Haoyu Wang and Minkang Liu under the supervision of Prof. Chunbao (Charles) Xu and Prof. Yimin Zeng and the assistance of Haoyang Li. Fresh samples were prepared by Dr. Minkang Liu. Corrosion samples characterizations were performed by Haoyu Wang, Dr. Minkang Liu, and Dr. Vahid Dehnavi. Writing and data analysis were performed by Haoyu Wang and Dr. Minkang Liu. The work was reviewed and revised by Prof. Chunbao (Charles) Xu, Prof. Yimin Zeng, Dr. Xue Han. This chapter will be submitted to a journal for publication.

Acknowledgments

Though only my name appears on the cover of this dissertation, it would not have been possible to finish this work without the help of so many people who have contributed to its production.

I would like to express my sincere gratitude to my supervisors: Dr. Chunbao (Charles) Xu and Dr. Yimin Zeng for their continuous support of my PhD study and research, for their patience, motivation, enthusiasm, immense knowledge, and valuable guidance.

I would like to thank Dr. Zhongshun (Sean) Yuan for his recommendations and comments on my research and Dr. Xue Han for her assistance at all levels of the research project.

I thank Fang (Flora) Cao, Dr. Minkang Liu and Dr. Kaiyang Li for their contributions and assistance on the analysis and characterization of my samples.

I also thank my fellow colleagues at the Institute for Chemicals and Fuels from Alternative Resources (ICFAR) for their assistance and friendship.

I would like to acknowledge the financial support from the department of Natural Resources Canada (NRCan) OERD Clean Energy and Forest Innovation programs, as well as from the Natural Science and Engineering Research Council of Canada (NSERC).

Last but not the least, I`m truly thankful to my families for their unconditional love and continued support throughout my entire life.

Table of Contents

List of Tables

List of Figures

List of Appendices

List of Abbreviations and Symbols

Abbreviation	Meaning
AP	Aqueous-phase products
BPR	Back pressure regulator
FIB	Focus Ion Beam microscope
FT-IR	Fourier-transform infrared spectroscopy
GC-MS	Gas chromatography–mass spectrometry
GPC	Gel permeation chromatography
HHV	Higher heating value
HTL	Hydrothermal liquefaction
MAPE	Mean absolute percentage error
RMSD	Root mean square deviation
SEM	Scanning electron microscope
SR	Solid residue
SS	Stainless steel
TAN	Total acid number
TEM	Transmission electron microscopy
TGA	Thermogravimetric analysis
XRD	X-ray diffraction
A	Arrehenius constant
d	Alloy density
E	Activation energy
f	Minimum sum of squred error
k	Reaction rate constant
M_n	Nmuber average molecular weight
M_w	Weight avergae molecular weight
R	Molar gas constant
S	Surface area of alloy sample
T	Reaction Temperature
Δm	Mass loss of alloy sample

X_{feed}	Mass fraction of feedstock
X_{oil}	Mass fraction of biocrude
X_{SR}	Mass fraction of solide residue
X_{AP}	Mass fraction of aqueous-phase product
X_{gas}	Mass fraction of gas
x_i	Mass fraction of compositional component
Y_{cal}	Simulation results
Y_{exp}	Experimetal data
$\widehat{Y_\imath}$	Predicted yield of each product
Y_i	Experimental result from HTL of real biomass
$\widehat{y_\imath}$	Calculated yield of each product from the kinetic model

Chapter 1

1 General Introduction

The main objectives of this PhD project were to develop a generalized kinetic model based on chemical compositions (cellulose, hemicellulose, and lignin) for predicting HTL product yields (gas, liquid, and solid residue) from various types of lignocellulosic biomass with different chemical compositions, and investigate the product yields and corrosion-resistance performance of various candidate alloys in HTL of various types of lignocellulosic biomass under varying conditions, particularly atmosphere and type of reactors (batch and continuous-flow).

1.1 Background and Knowledge Gaps

The depletion of fossil resources and increasing environmental concerns have attracted intensive R&D works on the utilization of clean and renewable alternatives to replace fossil fuels for production of energy, fuels, chemicals and materials [1, 2]. Among all the identified alternatives, biomass resources, such as lignocellulosic biomass (e.g., forestry residues, agricultural residues), food waste and algal biomass, are abundant and promising candidates for both energy and chemical production owing to their renewability and “net-zero carbon emission” characteristics [3-8]. The biomass resources are estimated to be 146 billion tons per annum [9], among which lignocellulosic biomasses (forestry and agricultural residues) has received a particular interest over the past decades as the residues are seen as bio-wastes and presented in abundant amounts in forestry and agricultural sectors.

Direct utilization of biomass is challenging, not only because it is usually bulky and hence difficult to transport, handle, and store, but also because it has a much lower energy density based on either volume or mass compared to fossil fuels [10]. Therefore, it is necessary to convert raw biomass materials effectively and efficiently into gaseous or liquid biofuels for final applications. The developed conversion technologies are categorized into biochemical and thermochemical methods. Biochemical conversion is aided by enzymes and bacteria, primarily involving the fermentation of wet carbohydrate materials into bioethanol and anaerobic digestion to generate biogas under ambient operating conditions [11-13]. The biochemical processes are very sensitive to operating conditions (pH, temperature, etc.) and quite slow (usually requiring days and weeks to complete), hence less efficient [4]. In contrast, thermochemical processes, including direct combustion, gasification, pyrolysis or liquefaction, are more efficient than the biochemical conversion in terms of processing time and the ability to process various types of the biomass feedstocks [8].

Hydrothermal liquefaction (HTL) is a unique thermochemical conversion process, particularly applicable for the conversion of wet biomass feedstocks, such as "black liquor" from pulp mills, wastewater sludge, food wastes and newly harvested algal biomass, etc. [10, 14, 15]. The biocrude (or bio-oil) obtained from the HTL have higher chemical stability , lower oxygen and water content, and higher heating value (25–35 MJ/kg) compared to pyrolysis oils [16, 17]. HTL processes are operated in hot pressurized water, water-alcohol mixed solvent, or other organic solvents in the temperature range of 200–400 °C and the pressure range of 5–25 MPa with/without homogenous or heterogenous catalyst to directly decompose the macromolecules of biomass into biocrude products - fragments of light molecules [18].

To date, most of the biomass HTL studies focus on the effects of catalysts, reaction temperature and time on production efficiency and chemical properties of the products. However, the process itself still suffers from lack of predictability for different types of lignocellulosic biomass (with varying chemical compositions of cellulose, hemicellulose, and lignin). Thus, a kinetic model based on textural compositions (cellulose, hemicellulose, and lignin) would be particularly useful for predicting HTL product yields (gas, liquid, and solid residue) from various types of lignocellulosic biomass with different chemical compositions, and for elucidating the reaction pathways and mechanisms in HTL of lignocellulosic biomass. Such kinetic models are also helpful for scaling up the HTL reactors for industrial application of HTL process.

Intensive efforts made in biomass HTL were conducted in batch reactors. However, precise control of residence time and pressure in a batch reactor are quite challenging due to the variability in reactor heating/cooling rates, and the autogenic pressure (temperature, solvent and reactor volume dependent) during the HTL processes [19]. Thus, the findings from batch processing cannot be directly and effectively applied to the continuous-flow processes, which are more desirable for future industrial scale applications of the HTL technology [20]. Recently, there is a growing focus on the upscaling of HTL processes, transitioning from lab-scale experiments to pilot-scale plants that operate using continuous flow processes [21-24]. However, limited information is available on the comparisons between the batch- and continuous modes of biomass HTL operations (especially lignocellulosic and lignin-rich biomass) in terms of product distribution and properties. Also, the performance of continuous HTL processes for biomass types has not been sufficiently investigated.

Another important issue for industrial application of HTL process is related to the unwanted corrosion issue for the reactor and downstream processing equipment, which has not received sufficient attention but must be addressed. A range of oxygenated/corrosive compounds, such as organic acids, aggressive sulfur and/or chlorinated compounds, can be produced during the biomass conversion processes, consequently creating highly corrosive environments to the reactor construction alloys [25]. Besides, HTL process is operating usually in a reaction medium in the presence of hot-compressed water (under elevated temperature and high pressure) and usually an alkali catalyst [26-28]. In the sub-/supercritical region, the ionization constant of water increases while the dielectric constant of water drops, which allows water to dissolve organic compounds and provides an acidic medium for the hydrolysis reactions [29], possibly leading to a remarkable change in the chemical dissolution of surface oxide layers formed on HTL reactor alloys [30, 31]. In addition, several pioneer studies suggested that the presence of an alkaline catalyst could cause a remarkable increase in corrosion rate as the formed surface scale was composed of porous hydroxides with high solubility in high temperature aqueous environments instead of stable and compact oxides [32, 33]. It is thus necessary to assess corrosion-resistance performance of various candidate alloys for reactors to establish guidelines for selecting proper (cost-effective) materials for HTL reactor construction and to develop corrosion-preventing strategies to achieve long-term operation of HTL processes. To the best of our knowledge, several types of commercial steels and alloys have the potential for the construction of HTL reactors due to their wide utilization in high temperature aqueous environments [34]. However, very few efforts have been employed to investigate eth performance of steels and alloys in HTL of real biomass environment.

1.2 Objectives

To address the above knowledge gaps, the main objectives of this PhD proejct are to:

(1) Develop a kinetic model based on chemical compositions (cellulose, hemicellulose, and lignin) for predicting HTL product yields (gas, liquid, and solid residue) from various types of lignocellulosic biomass with different chemical compositions.

(2) Compare the performance of HTL conversion of various biomass feedstocks in continuous-flow HTL reactors and batch reactors.

(3) Investigate the corrosion-resistance performance of various candidate alloys in HTL of various types of lignocellulosic biomass under varying conditions, in order to establish guidelines for selecting proper materials for HTL reactor construction and to develop corrosion-preventing strategies to achieve long-term operation of HTL reactors.

(4) Accelerate the development and deployment of HTL technology in Canada and the global bioenergy industry in a cost-competitive manner.

This research would provide valuable assistance in choosing an effective process for biomass liquefaction. By utilizing the developed kinetic model, the influence of the biochemical composition of feedstocks, as well as reaction conditions such as temperature and reaction time, can be assessed more accurately on product yields. Furthermore, this kinetic model would be more useful in the design of large-scale reactors and enable thorough techno-economic analysis of the process by integration with heat and mass balance models. In addition, the outcomes from the comparison of batch- and continuous HTL process would be helpful in designing the HTL systems for commercialized production of biocrude and drop-in fuels at a larger scale, using lignocellulosic biomass or biowaste. This work is also expected to determine the influence of biomass type and the role of converted products on corrosion in HTL biorefining environments and partially support the development of applicable materials technology solutions for the construction of industrial HTL plants.

1.3 Research Approaches and Methodologies

As discussed above, this research can be divided into three main phases. The first phase involved the development of a kinetic model to predict product yields from hydrothermal liquefaction (HTL) of lignocellulosic biomass based on its chemical compositions (contents of cellulose, hemicellulose, and lignin) and validation with our experimental results from batch-mode HTL of real biomass under N_2 atmosphere and the publicly available HTL data in literature obtained with lignocellulosic biomass feedstocks. The second phase focused on comparing the performance of HTL of various types of bio-feedstocks in a continuous-flow reactor and a batch reactor in terms of product yields and chemistry of the bio-oils and energy recovery potential. The third phase was investigating the corrosion-resistance performance of various candidate alloys in HTL of various types of lignocellulosic biomass.

The experiments were conducted in batch and continuous flow reactors. **Figure 1.1-1.3** show the images of the reactors used. The batch reactors are 100 mL and 500 mL stainless steel stirred reactors (Parr 4590 and 4575A Bench top reactor), equipped with a mixer, heater, thermocouple, controller, and pressure gage. The continuous-flow HTL experiments were conducted on a plug flow HTL reactor (with a maximum slurry feeding capacity of 6 kg/h) designed and custom-built at our lab. **Figure 1.4** is the schematic diagram of the continuous-flow reactor for biomass HTL.

Typical analyses of HTL products were performed using gas chromatograph-mass spectrometer (GC-MS), gas chromatograph equipped with a thermal conductivity detector (GC-TCD), Fourier transform infrared spectrometer (FT-IR), thermal gravimetric analysis (TGA), elemental analysis (CHNS). The corrosion products were characterized using scanning electron microscope equipped with energy dispersive X-ray spectroscopy (SEM-EDX), X-ray diffraction (XRD), Focus Ion Beam microscope (FIB), and transmission electron microscope (TEM).

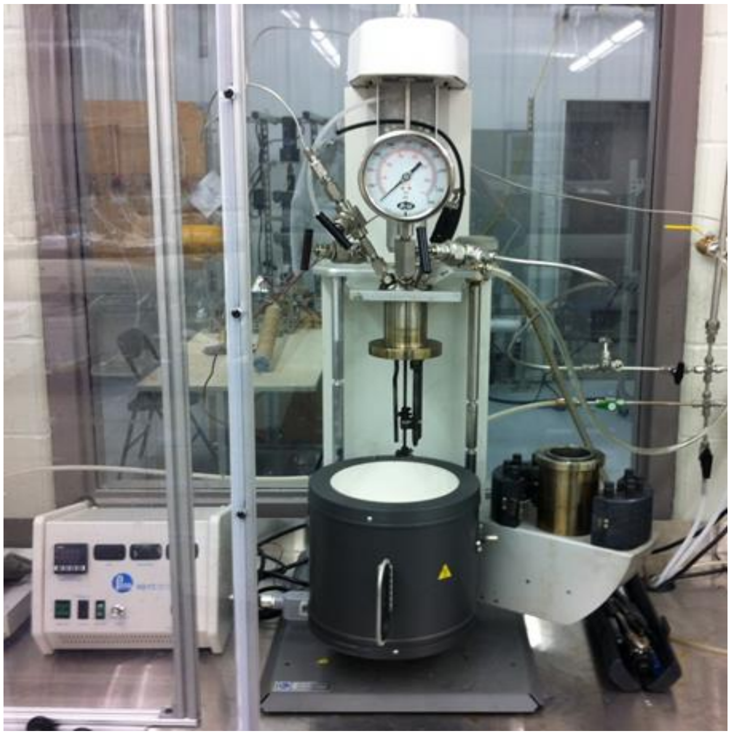

Figure 1.1: Photo of the 500 ml batch reactor used in this work.

Figure 1.2: Photo of the 100 ml batch reactor used in this work.

Figure 1.3: Photo of the continuous-flow reactor used in this work.

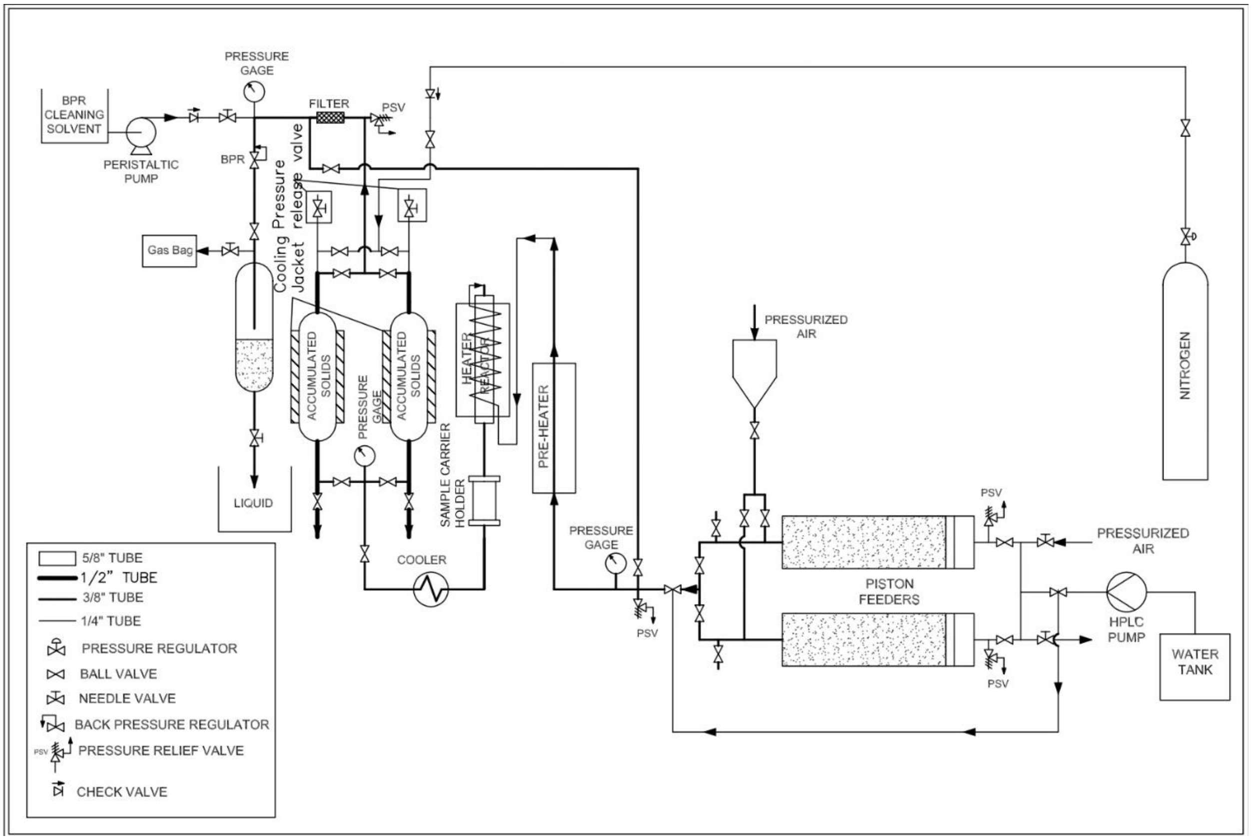

Figure 1.4: Schematic diagram of the continuous-flow reactor.

1.4 Thesis Overview

Chapter 1 provides a general introduction of the importance of replacing fossil fuels with biomass-derived fuels, introduction of hydrothermal liquefaction and its challenges. The research objectives, approaches and methodology, and thesis structure are also outlined.

Chapter 2 introduces the effects of major process parameters, such as reaction temperature, residence time, catalysts, biomass type, and biomass to solvent ratio on biomass HTL. The HTL process modelling and limitations, the corrosion issues in HTL reactor, and challenges of HTL scaling up are reviewed as well.

Chapter 3 presents investigation on the effects of reactor atmosphere on HTL of pinewood.

Chapter 4 proposes a universal reaction network and a kinetic model based on the experimental results obtained from HTL of biomass model compounds. Validation with our experimental results and the publicly available HTL data in literature obtained with lignocellulosic biomass feedstocks was performed to assess the quality/reliability of the model predictions.

Chapter 5 compares the performance of HTL of various types of technical lignin (alkali lignin and kraft lignin) in a continuous-flow reactor and a batch reactor in terms of product yields and chemistry of the bio-oils or depolymerized lignin and energy recovery potential.

Chapter 6 compares the performance of HTL of various bio-feedstocks (cornstalk, pinewood, and black liquor) in a continuous-flow reactor and a batch reactor in terms of product yields and chemistry of the bio-oils and energy recovery potential.

Chapter 7 presents the examination of the corrosion modes and extents of Cr-bearing SS316L constructional candidate under static and batch-mode catalytic HTL conversion of two typical biomass feedstocks (bamboo and black liquor). The possible roles of organic compounds on the sample surface were also introduced.

Chapter 8 presents the main conclusions obtained from the present research and recommendations for future work.

1.5 References

[1] H.C. Ong, W.-H. Chen, A. Farooq, Y.Y. Gan, K.T. Lee, V. Ashokkumar, Catalytic thermochemical conversion of biomass for biofuel production: A comprehensive review, Renewable and Sustainable Energy Reviews 113 (2019) 109266.

[2] S. Pang, Advances in thermochemical conversion of woody biomass to energy, fuels and chemicals, Biotechnology advances 37(4) (2019) 589-597.

[3] I.A. Basar, H. Liu, H. Carrere, E. Trably, C. Eskicioglu, A review on key design and operational parameters to optimize and develop hydrothermal liquefaction of biomass for biorefinery applications, Green Chemistry 23(4) (2021) 1404-1446.

[4] A. Gollakota, N. Kishore, S. Gu, A review on hydrothermal liquefaction of biomass, Renewable and Sustainable Energy Reviews 81 (2018) 1378-1392.

[5] P. McKendry, Energy production from biomass (part 1): overview of biomass, Bioresource technology 83(1) (2002) 37-46.

[6] I. Mead, International energy outlook 2017, US Energy InformationAdministration (2017).

[7] M. Kumar, Y. Sun, R. Rathour, A. Pandey, I.S. Thakur, D.C. Tsang, Algae as potential feedstock for the production of biofuels and value-added products: Opportunities and challenges, Science of the Total Environment 716 (2020) 137116.

[8] T.H. Seehar, S.S. Toor, K. Sharma, A.H. Nielsen, T.H. Pedersen, L.A. Rosendahl, Influence of process conditions on hydrothermal liquefaction of eucalyptus biomass for biocrude production and investigation of the inorganics distribution, Sustainable Energy & Fuels 5(5) (2021) 1477-1487.

[9] B.-H. Cheng, B.-C. Huang, R. Zhang, Y.-L. Chen, S.-F. Jiang, Y. Lu, X.-S. Zhang, H. Jiang, H.-Q. Yu, Bio-coal: A renewable and massively producible fuel from lignocellulosic biomass, Science advances 6(1) (2020) eaay0748.

[10] C. Xu, J. Lancaster, Conversion of secondary pulp/paper sludge powder to liquid oil products for energy recovery by direct liquefaction in hot-compressed water, Water research 42(6-7) (2008) 1571-1582.

[11] R. Ahorsu, F. Medina, M. Constantí, Significance and challenges of biomass as a suitable feedstock for bioenergy and biochemical production: A review, Energies 11(12) (2018) 3366.

[12] C. Sawatdeenarunat, K. Surendra, D. Takara, H. Oechsner, S.K. Khanal, Anaerobic digestion of lignocellulosic biomass: challenges and opportunities, Bioresource technology 178 (2015) 178-186.

[13] A. Ward, D. Lewis, F. Green, Anaerobic digestion of algae biomass: a review, Algal research 5 (2014) 204-214.

[14] F. Conti, S.S. Toor, T.H. Pedersen, T.H. Seehar, A.H. Nielsen, L.A. Rosendahl, Valorization of animal and human wastes through hydrothermal liquefaction for biocrude production and simultaneous recovery of nutrients, Energy conversion and management 216 (2020) 112925.

[15] C. Tian, B. Li, Z. Liu, Y. Zhang, H. Lu, Hydrothermal liquefaction for algal biorefinery: A critical review, Renewable and Sustainable Energy Reviews 38 (2014) 933-950.

[16] R. Shu, J. Long, Y. Xu, L. Ma, Q. Zhang, T. Wang, C. Wang, Z. Yuan, Q. Wu, Investigation on the structural effect of lignin during the hydrogenolysis process, Bioresource technology 200 (2016) 14-22.

[17] S. Bensaid, R. Conti, D. Fino, Direct liquefaction of ligno-cellulosic residues for liquid fuel production, Fuel 94 (2012) 324-332.

[18] A. Dimitriadis, S. Bezergianni, Hydrothermal liquefaction of various biomass and waste feedstocks for biocrude production: A state of the art review, Renewable and Sustainable Energy Reviews 68 (2017) 113-125.

[19] B. Patel, K. Hellgardt, Hydrothermal upgrading of algae paste in a continuous flow reactor, Bioresource technology 191 (2015) 460-468.

[20] D. Castello, T.H. Pedersen, L.A. Rosendahl, Continuous hydrothermal liquefaction of biomass: A critical review, Energies 11(11) (2018) 3165.

[21] Y. Fan, C. Prestigiacomo, M. Gong, T. Tietz, U. Hornung, N. Dahmen, Comparative investigation on the value-added products obtained from continuous and batch hydrothermal liquefaction of sewage sludge, Frontiers in Environmental Science 10 (2022) 996353.

[22] P.A. Marrone, D.C. Elliott, J.M. Billing, R.T. Hallen, T.R. Hart, P. Kadota, J.C. Moeller, M.A. Randel, A.J. Schmidt, Bench-Scale Evaluation of Hydrothermal Processing Technology for Conversion of Wastewater Solids to Fuels, Water Environment Research 90(4) (2018) 329-342.

[23] K. Anastasakis, P. Biller, R.B. Madsen, M. Glasius, I. Johannsen, Continuous hydrothermal liquefaction of biomass in a novel pilot plant with heat recovery and hydraulic oscillation, Energies 11(10) (2018) 2695.

[24] I. Johannsen, B. Kilsgaard, V. Milkevych, D. Moore, Design, modelling, and experimental validation of a scalable continuous-flow hydrothermal liquefaction pilot plant, Processes 9(2) (2021) 234.

[25] M.P. Brady, J.R. Keiser, D.N. Leonard, L. Whitmer, J.K. Thomson, Corrosion considerations for thermochemical biomass liquefaction process systems in biofuel production, JOM 66(12) (2014) 2583-2592.

[26] R.F. Beims, Y. Hu, H. Shui, C.C. Xu, Hydrothermal liquefaction of biomass to fuels and value-added chemicals: Products applications and challenges to develop large-scale operations, Biomass and Bioenergy 135 (2020) 105510.

[27] S. Sahu, N. Sahoo, S. Naik, D. Mahapatra, Advancements in hydrothermal liquefaction reactors: Overview and prospects, Bioreactors (2020) 195-213.

[28] R.K. Mishra, P. Kumar, K. Mohanty, Hydrothermal liquefaction of biomass for bio-crude production: A review on feedstocks, chemical compositions, operating parameters, reaction kinetics, techno-economic study, and life cycle assessment, Fuel 316 (2022) 123377.

[29] S. Machmudah, Q. Shiddiqi, A. Kharisma, W. Widiyastuti, H. Kanda, S. Winardi, M. Goto, Subcritical water extraction of xanthone from mangosteen (Garcinia Mangostana Linn) pericarp, J Adv Chem Eng 5(117) (2015) 2.

[30] M. Liu, Y. Zeng, J.-L. Luo, Influence of Major Operating Parameters (Temperature, Pressure, and Flow Rate) on the Corrosion of Candidate Alloys for the Construction of Hydrothermal Liquefaction Biorefining Reactors, Energy & Fuels 36(6) (2022) 3134-3153.

[31] D. Gómez-Briceño, F. Blázquez, A. Sáez-Maderuelo, Oxidation of austenitic and ferritic/martensitic alloys in supercritical water, The Journal of Supercritical Fluids 78 (2013) 103-113.

[32] C.A. de Wolf, H.A. Nasr-El-Din, A. Bouwman, E.R. Bang, E. Naylor, Corrosion rates of Cr-and Ni-based alloys with organic acids and chelating agents used in stimulation of deep wells, SPE Production & Operations 32(02) (2017) 208-217.

[33] J. Shao, C. Du, X. Zhang, L. Cui, Effects of lead on the initial corrosion behavior of 316LN stainless steel in high-temperature alkaline solution, Acta Metallurgica Sinica

32(1) (2019) 89-97.

[34] M. Liu, Y. Zeng, J.-L. Luo, Roles of Major Alloying Elements in Steels and Alloys on Corrosion under Biomass Hydrothermal Liquefaction (HTL) Conversion, Corrosion Science (2023) 111148.

Chapter 2

2 Literature Review

Hydrothermal liquefaction (HTL) is a promising thermochemical technology that converts wet biomass and biowaste feedstocks into bio-oils and valuable biochemicals. HTL processes are usually operated in hot pressurized water, water-alcohol mixture, with /without other organic solvents at 200–400 °C and pressures up to 25 MPa with/without catalysts. Compared with biochemical and other thermochemical conversion methods, HTL provides a cost-effective solution to the bioenergy industry on the use of wet biomass streams, especially industrial and municipal biowastes. This chapter introduces the fundamental concepts and major process parameters of HTL and reviews the most recent research and development (R&D) progress in this field.

2.1 Chemical Compositions of Biomass

During hydrothermal liquefaction, biomass is subjected to a series of reactions. The basic reaction pathway involves three major steps: depolymerization followed by decomposition and recombination. In essence, the biomass is broken down either by thermal decomposition or hydrolytic depolymerization in hot-compressed water or heated solvents, resulting in the formation of monomers and unit structures. The produced macromolecules or fractured units undergo further degradation or decomposition, leading to the production of intermediates. These reactive fragments and intermediates are then reassembled through re-polymerization, condensation, and cyclization reactions, generating high molecular weight oil (bio-oil) while producing aqueous, gas, and char side products [1, 2]. Various types of biomasses are available for HTL conversion. Lignocellulosic biomass and algal biomass are the most investigated in HTL [3].

Lignocellulosic biomass consists of different components, including three major chemical components (cellulose, hemicellulose and lignin) and other minor components (proteins and lipids) [4, 5]. Algae, on the other hand, has three major components: carbohydrates, lipids, and proteins [6]. Each component undergoes distinct chemical conversion routes in HTL, as summarized below.

Cellulose is a linear polysaccharide with a high molecular weight and composed of anhydro glucose monomer units and crystalline structure, making it insoluble in water. However, it can dissolve in supercritical - or subcritical water with high ionic property. At temperature, > 240 °C, decomposition of cellulose increases with an increase in temperature [7].

Hemicellulose is a branched polymer with non-crystalline and random structure and thus easily hydrolysable [2]. In comparison with cellulose, hemicellulose possesses a weaker structure and is more susceptible to intramolecular hydrogen bonding, making it easier for its molecules to break apart. During hydrothermal processing, hemicellulose can be hydrolyzed easily at temperatures above 180 °C. The hydrolysis produces a mixture of polysaccharides composed mainly of five-carbon (xylose and arabinose) and six-carbon sugars (glucose, galactose and mannose), as well as formic/acetic acid, pyran derivatives and aldehydes [8].

Lignin is an aromatic heteropolymer with a high molecular. As schematically shown below, lignin consists of three major phenylpropanoid building units: coniferyl, sinapyl, and *p*-coumaryl alcohols, making it the most valuable natural source of phenolic compounds [9]. The inter-monomeric linkage in lignin is connected most frequently (over 60%) by β-O-4 aryl ether bond as well as β-O-4 ether bonds and C-C bonds. Lignin is commonly associated with hemicellulose both physically and chemically through covalent bonds [10]. In contrast to cellulose and hemicellulose, lignin is relatively resistant to chemical or enzymatic degradation. The major compounds formed during hydrothermal processing of lignin or lignocellulosic biomass are phenolic compounds [2, 11].

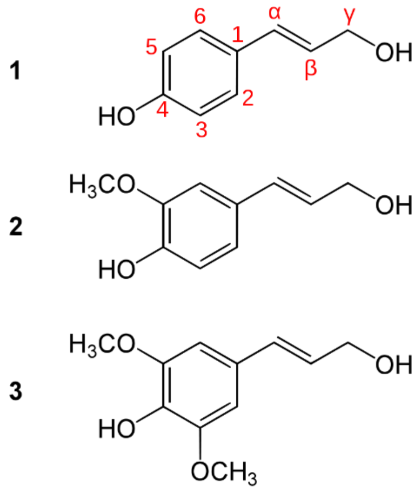

Figure 2.1: Three common monolignols: paracoumaryl alcohol (1), coniferyl alcohol (2) and sinapyl alcohol (3).

Lipids are hydrophobic organic compounds, the majority of which are made up of triglycerides (TAGs), a combination of tri-esters of fatty acids and glycerol [1]. Fats are easily dissolved with solvents due to the dielectric constant of water at sub-critical conditions [12-14]. This phenomenon directly impacts the stability of TAGs, leading to the formation of glycerol, the major by-product of biodiesel industry which consists of fatty acids, methanol, and salts. The degradation of glycerol produces acetaldehydes, formaldehyde, acrolein, allyl alcohol, propionaldehyde, ethanol, CO_2, CO, and H_2.

Proteins, formed from amino acids, are the major components of microbial or algal [15, 16]. During hydrothermal liquefaction, the peptide chain of proteins undergoes deamination and decarboxylation reactions, producing hydrocarbons, aldehydes, amines, and acids. Further degradation leads to the formation of carboxylic acids, acetic acid, propionic acid, n-butyric acid, and iso-butyric acids [17-19].

2.2 Effects of Process Condition

2.2.1 Effects of Temperature

Temperature is an important process parameter that could greatly influence the yield of HTL products. Generally, increasing temperature enhances the fracture of chemical bonds and the depolymerization of biomass. Consequently, the concentration of free radicals and the probability of repolymerization of fragmented molecular are increased, leading to an increase in the total yield of bio-oil [3]. After the oil yield reaches the maximum value, further increasing temperature could inhibit oil production because other reactions, including the secondary decomposition and Boudouard gas reactions to produce gas products and the recombination/condensation reactions of intermediates (free radicals) to generate char, become dominant at higher temperatures [20-22].

Zhu et al. [23] investigated the HTL of barley straw at various temperatures ranging from 280 to 400 °C. The yield of bio-oil reached a maximum of 34.9 wt.% at 300 °C. Further increasing temperature to 400 °C resulted in a decrease in bio-oil yield to 19.9 wt.%. Later, Jindal and Jha [24] examined the effects of temperature on HTL of waste furniture sawdust. The sawdust conversion and bio-oil yield significantly increased from 37.5 and 4.6 wt.% to 61.6 and 12.7 wt.% respectively with increasing temperature from 180 °C to 280 °C. However, further increase in temperature caused a reduction in both sawdust conversion bio-oil yield. HTL of eucalyptus was conducted at 260 - 320 °C in subcritical water [25]. At 300 °C for 30 min, a high yield of bio-oil (30.1 wt.%) was generated, which thereafter declined marginally as the temperature climbed further.

A similar trend was reported in the HTL of algal biomass. Reddy et al. investigated the temperature effect on HTL of Nannochloropsis gaditana and Chlorella sp. at 180 - 330 °C [26]. Maximum bio-oil yields of 47.5 wt.% and 32.5 wt.% for Nannochloropsis sp. and Chlorella sp. respectively were obtained at 300 °C. Further increase in temperature reduced bio-oil yield. He et al. [27] researched the impact of temperature on Nannochloropsis sp. as well. The maximum bio-oil yield of 54.11 wt.% was obtained at 320 °C and then showed a slight decline with a further increase in temperature to 340 °C. Biswas et al. performed HTL of sargassum tenerrimum and the total bio-oil yield obtained was 11.5%, 16.3% and 14.7% at 260 °C, 280 °C, and 300 °C, respectively [28].

Temperature affects chemical properties of produced bio-oil as well. Villaver et al. performed the HTL of spirulina platensis at 280, 320, and 350 °C, and discovered that the maximum HHV of bio-oil (36.99 MJ/kg) and lowest nitrogen content were achieved at 350 °C, while the highest energy recovery from the microalgae (76.8%) was obtained at

280 °C [29]. According to Zhu et al. [30], increasing temperature could make the produced bio-oil to have a higher calorific value owing to the decreased oxygen content and increased carbon content in the produced bio-oil. Higher temperatures are anticipated to be more favorable for deoxygenation, hence producing more unsaturated molecules. However, the oil yield would decrease due to condensation and cracking reactions, even though the quality of the bio-oil generated at a higher temperature improves. Thus, there shall be an optimum temperature for maximizing both output and quality of bio-oil derived from a specific biomass feedstock.

2.2.2 Effects of Residence Time

The residence time of biomass in an HTL process would strongly influence the yields, components, and properties of bio-oil products, and hence the optimization of residence times is necessary [3, 31]. In a HTL process a shorter residence time is found to be generally preferred for bio-oil production, especially at a low biomass-to-water ratio [31-33]. On the other hand, a longer reaction time would induce repolymerization of the intermediate products, which lowered the yield of bio-oil [3, 34].

By extending the reaction time from 5 min to 30 min, Yang et al. investigated the HTL of waste coffee residues [35]. The bio-oil yield increased to 31.6% when the retention time was increased to 10 min. However, the bio-oil yield declined to 22.7% when the retention period was increased to 30 min, due to the repolymerization of bio-oils, accompanied by the marginally increased yield of solid residues. In addition, previous studies have also shown a correlation between reaction time and temperature. Kaur et al. performed HTL of castor residue at 260–300 °C for 15–90 min [36]. The greatest bio-oil production (15.8 wt.%) was achieved at 300 °C for 60 min. At 280 °C, the maximum yield of biochar was reached at 30 min but decreased slightly in the 60- and 90-min runs, while at 300 °C, the biochar yield continued to increase until 90 min. He et al. reported similar trends when performing HTL tests using an algal biomass Spirulina platensis at 250–350 °C for 0–60 min. [37]. The residence times to reach maximum bio-oil yields at 340 °C and 300 °C were 30 min and 60 min, respectively.

2.2.3 Effects of Biomass Feedstocks

Various types of biomass feedstocks have been studied, including algae, lignocellulosic biomass, food waste, manure, etc. [38-45]. Feedstock types and compositions could significantly affect the overall bio-oil yield and compositions. This is because major textural components of biomass, i.e., lignin, hemicelluloses, cellulose, protein, and lipid behave differently during HTL conversion. Generally, the conversion efficiency of different biomass constituents decreases in the order of lipids > proteins > hemicellulose > cellulose > lignin. Therefore, the more lignin that the biomass contains, the higher operating temperature was required [39, 46]. Tian et al. examined four types of crop straws (including corn straw, peanut straw, soybean straw, and rice straw) at 320 °C for 60 min [40]. Soybean straw generated the highest bio-oil production, followed by rice straw, peanut straw, and corn straw. The significant difference in bio-oil yield was attributed to the different cellulose contents. Feng et al. investigated the effects of white pine bark, white spruce bark, and white birch bark on bio-oil yield in HTL at 300 °C for 15 min [45]. Results demonstrated that a higher lignin content in the biomass would generally lead to a higher bio-oil yield. However, an opposite trend was observed by Chan et al. when conducting the liquefaction of three types of oil palm biomass, namely, empty fruit bunch (EFB), palm mesocarp fiber (PMF), and palm kernel shell (PKS) at 330 °C and 25 MPa [47].

2.2.4 Effects of Mass Ratio of Water to Biomass

In a HTL process, mass ratio of water to biomass is considered as another key parameter which has remarkably impacts on bio-oil yield and compositions. In general, a high amount of water is desirable for more liquid products. Studies have revealed that a high solid-to-liquid ratio is unfavorable for the dissolving of biomass in water and retards the hydrolysis and liquefaction processes of the feedstock, consequently leading to decreased biomass conversion and bio-oil output [48]. The presence of high amount of water content can support the dissolving of biomass, provide sufficient hydrogen to stabilize the liquefaction intermediates, reduce the formation of solid residues and gases, and finally enhance the bio-oil output [24].

Ye et al. liquefied bamboo shoot shell in polyethylene glycol 400 and ethylene glycol at different liquid to solid ratio (3:1-6:1) [49]. They reported that a low liquefaction percentage was obtained at a lower liquid to solid ratio. The liquefaction percentage increased greatly when the liquid to solid ratio increased from 3:1 to 5:1. Malins et al. examined the influence of sewage sludge to water ratio (1:0-1:15) on HTL process of sewage sludge [48]. The results indicated that decreasing the sludge-to-water weight ratio boosted bio-oil production, energy recovery, and overall conversion. Yin et al. reported that when mass ratio of water to cattle manure decreased from 2.0 to 0.5, the corresponding bio-oil yield decreased sharply from 48.7 to 1.5 wt.% [41]. The decrease in oil yield was believed to be due to the conversion of bio-oil/intermediates into solid residue through self-condensation reactions.

2.2.5 Effects of Catalysts

Catalyst is another particularly important factor in HTL conversion. Catalysts effectively promote the decomposition of biomass macromolecules, lower the solid residue production while increasing the yield and calorific value of bio-oil and inhabiting side reactions like condensation and repolymerization of intermediates. Different kinds of homogenous and heterogenous catalysts have been introduced to HTL processes to improve liquefaction efficiency as well as bio-oil quality. **Table 2.1** lists some of the common catalysts applied to HTL process recently.

Table 2.1: Recent applications of catalysts in HTL of different biomass.

Biomass	Type	Catalyst	Main results	Ref.
Peanut shell	Wood	MgO, ZSM-5 and MgO + ZSM-5	Mixture of MgO + ZSM-5 achieved the highest bio-oil yield of 40.6 wt.%.	[50]
Larch Mongolian oak	Wood	K_2CO_3	The maximum bio-oil yields (27.7 wt.% for Mongolian oak and 25.7 wt.% for larch), and the highest carbon conversion ratio were obtained with 0.5 wt.% of catalyst.	[51]
Oak wood	Wood	Fe, Fe_3O_4 and Fe_2O_3	Highest bio-oil yield of 40.0% was obtained using Fe at 320 °C.	[52]

Corn straw	Wood	CuO + NaOH, NaOH and CuO	Mixture of CuO +NaOH achieved the highest bio-oil yield (26.6 wt.%) and conversion rate (85.6 wt.%).	[53]
Corn straw	Wood	Nano ferrite and NaOH	The maximum bio-oil yield of 31.3 wt.% was achieved using ZnFe2O4 + NaOH. The bio-oil yields obtained by single heterogeneous catalyst were lower than that of homogeneous catalyst.	[54]
Eucalyptus	Wood	NaOH, KOH, and Pd/C	The bio-oil yields obtained at 260 °C using NaOH, KOH, and Pd/C were 61.2 wt.%, 57.7 wt.% and 36.8 wt.%.	[55]
Ulva prolifera	Algae	KOH, NaOH and Na_2CO_3	Maximum bio-oil yield (26.7 wt.%) was observed with KOH (0.1 g) catalyst.	[56]
Ulva prolifera	Algae	ZSM-5, Y-Zeolite and Mordenite	ZSM-5 (15.0 wt.%) catalyst promotes the bio-oil yield to 29.3 wt.% and deoxygenation process.	[57]
Chlorella	Algae	Pt/C, Ru/C, and Pt/C + Ru/C	The addition of catalyst (Pt/C, Ru/C, or Pt/C + Ru/C) decrease the water-soluble bio-oil fraction in total bio-oil.	[58]
Spirulina platensis	Algae	CeO_2	Conversion rate and bio-oil production were enhanced using 0.2g of CeO_2 at 250 °C for 30 min.	[59]
Nannochloropsis	Algae	M (Fe, Co, Ni, Mo and Mn)/TiO_2	Ni/TiO_2 was the most effective catalyst to improve the yield and quality of bio-oil and the liquefaction conversion.	[60]
Spirulina	Algae	Pd/HZSM-5@MS and Pd/HZSM-5 (MS: meso-SiO_2)	Pd/HZSM-5@MS-catalyzed HTL achieved a high bio-oil output of 37.3% and a low coke yield of 8.6 %.	[61]

Spirulina platensis	Algae	Co/BC, Ni/BC, CoO_x/BC, NiO/BC (BC: biochar)	BC catalyst improved the bio-oil yield, and the highest bio-oil yield was 36.6 wt.% using Ni/BC.	[62]

As summarized in the above Table, the most commonly used catalysts are homogeneous alkaline catalysts [63]. Previous studies showed the application of homogeneous alkaline catalysts would significantly enhance the liquefaction of lignocellulosic biomass into bio-oil products [23, 64]. During the HTL treatment of pinewood sawdust, the effectiveness of alkaline catalysts on the feedstock conversion was reported to decline in the order of $K_2CO_3 > KOH > Na_2CO_3 > NaOH$ [65]. In contrast, the addition of mineral acid catalysts, such as sulfuric acid, promoted the condensation and re-polymerization processes of intermediate products, resulting in an increased char yield and a decreased oil yield [23, 66]. Furthermore, mineral acid catalysts would corrode core biorefinery equipment as well [67]. Although organic acids such as acetic acid and formic acid showed catalytic effect by improving the bio-oil yield, these acids were found to be consumed during the conversion likely due to the esterification reactions between carboxylic acids and the liquefaction productions, suggesting that they could act as both a catalyst and a reactant [68].

Recently, extensive studies have focused on employing heterogeneous catalysts in the biomass HTL process due to their great efficiency and easy separation from the liquid phase [69]. Gasification catalysts such as metals (Pt, Pd, Mo, Ni, and Ru) supported on active carbon (AC), SiO_2, Al_2O_3, and zeolite were extensively studied for biomass HTL [70, 71]. Pt/C, Pd/C, and Ru/C work well in terms of improving bio-oil quality by increasing the H/C ratio. Alternatively, Pt/C, Ni/SiO_2-Al_2O_3, and sulfide CoMo/γ-Al_2O_3 could effectively lower down the bio-oil O/C ratio [71]. Zeolite catalysts also exhibit superior catalytic performance in HTL as well. Ma et al. conducted HTL of Ulva prolifera using three zeolites-based catalysts (ZSM-5, Y-Zeolite and Mordenite) [57]. They reported that the bio-oil output was up to 29.3 wt.% with the ZSM-5 catalyst at a loading of 15.0 wt.% at 280 °C. Meanwhile, using a zeolite catalyst increased the HHV of bio-oil from 21.2 MJ/kg to 34.8 MJ/kg. The ZSM-5 catalytic liquefaction process resulted in more de-oxygenation than that of the Y-zeolite or mordenite catalyst.

Among all the homogeneous and heterogeneous catalysts, alkaline catalysts are still the most promising catalysts for HTL of biomass, as they could effectively enhance bio-oil yield by 50–135%, neutralize the pH of the reaction media, avoid the repolymerization of biocrude-forming intermediates, and thus significantly inhibit the formation of solid residue [66].

2.3 Modelling of Hydrothermal Liquefaction

For the design and commercialization of HTL process, it is important to comprehend the formation mechanisms and reaction kinetics for various chemical products. Recently, several studies on the kinetics of HTL of various biomass feedstocks in lab-scale batch reactors were reported. Zhang et al. developed a kinetic model for the HTL of softwood kraft lignin based on the mechanism of two separated reaction phases (the fast and the slow reaction) in the temperature range of 300–380 °C. [72]. Hardi et al. used a face centered central composite design to correlate the yields and properties of sawdust HTL products with HTL temperature, time, and feedstock concentration [73]. However, these models are only applicable to the specific feedstocks used in the corresponding studies. Thus, innovations have been made to develop product yield-prediction models for biomass based on biomass composition [46, 74, 75], whereas these models are only able to predict HTL product yields under specific processing conditions. Valdez et al. [76], Hietala et al. [77], and Vo et al. [78] further developed kinetic models of HTL reaction networks for the HTL of algal biomass based on the feedstock composition to estimate the product yields at varying reaction temperature/time. An example can be found in **Figure 2.2**. However, no existing models are suitable for the HTL of lignocellulosic biomass. The kinetic models established to date have restrictions in predicting the yields and quality of the products. More attention needs to be paid to developing a general kinetic model that incorporates the impacts of operational variables and feedstock compositions on product yields and properties. A few kinetic models have been integrated in Aspen- and CFD-based process simulations [79-81]. With no doubt, the reactor hydrodynamics and thorough simulation of the reaction kinetics with the application of simulators are highly valuable.

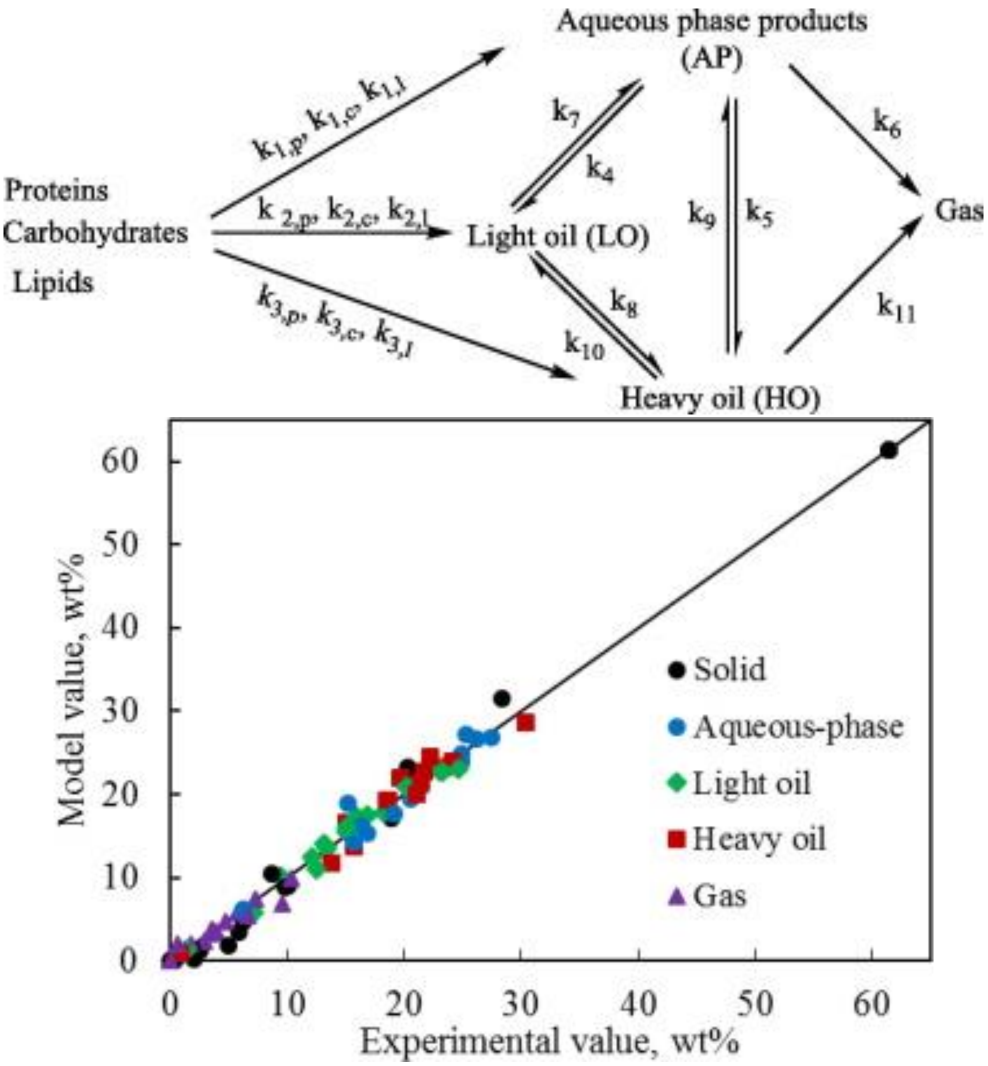

Figure 2.2: Hydrothermal liquefaction reaction network and comparison the experimental and calculated product yields from the hydrothermal liquefaction of Tetraselmis sp. under various HTL conditions [78].

2.4 HTL Reactor Configurations and Challenges

Intensive studies have been focused on biomass HTL studies in batch reactors and provided abundant information about the effects of different operating parameters and a variety of feedstocks on the yields and properties of bio-oils. Furthermore, the HTL reaction mechanisms have been well investigated for batch-mode operations. However, a batch HTL process is hard to scale up to an industrial level. It is more meaningful to develop continuous-flow HTL reactors. Despite the significant interest from industry, there are lack of advances in continuous-flow HTL processes due to their challenging performance problems and issues [66]. In the following section, recent progresses on continuous-flow biomass HTL, and the major issues towards continuous-flow operation will be provided and discussed.

2.4.1 Continuous Flow HTL Operations

One study by Fan et al. compared the bio-oil yield from sewage sludge HTL in a continuous-flow reactor with that in a batch reactor under the same conditions (350 °C and 8 min). A slightly higher bio-oil yield (33.1 wt.% vs. 30.8 wt.%) was observed in the batch reactor, while there was no significant difference in the bio-oil yield when using an instant heating rate to reach the desired temperature. With regard to the oil quantity, the continuous-flow HTL operation produced a bio-oil with lower nitrogen content than the batch-mode operation [82].

Researchers from the Pacific Northwest National Laboratory (PNNL) have accumulated considerable experience in continuous-flow biomass HTL. A recent continuous-flow HTL study by PNNL on various wet-waste feedstocks (fermentation waste, sludge, manure, food waste, and mixed waste) clearly demonstrated that an increase in the flow rate and the solid content of the feedstock improved the bio-oil yield. On the other hand, they used an alternative reactor system configuration by combining a continuous stirred tank reactor (CSTR) with a plug flow reactor (PFR). Prior to the PFR, the CSTR was heated to the desired temperature to reduce the impact of reactor blockage as a result of solid residue accumulation. When the CSTR was utilized, the average bio-oil yield for each feedstock type was noticeably improved. With regard to the bio-oil quality (heteroatom content, HHV, density, and total acid number), no obvious differences were observed with or without the insert of CSTR [83].

Efforts have been made to improve the continuous-flow HTL reactors. Anastasakis et al. first developed a hydraulic oscillation device with the intention of boosting the turbulence inside the tubular reactor in a pilot-scale biomass HTL system (with a capacity for feeding up to 100 L/h). The oscillators improved the overall mixing and heat transfer inside the reactor system by increasing the turbulence throughout the entire reactor. Moreover, they customized the heat exchanger, which recovered up to 80% of heat loss [84].

Aierzhati et al. proposed an innovative mobile pilot-scale HTL reactor (0.57 L/min) for food waste conversion, which can be easily delivered by truck. To demonstrate the economic viability of this mobile reactor system, a techno-economic analysis of food waste HTL was performed. When there is a widespread availability of biomass resources (more than 106 miles distance), the mobile HTL unit can be more cost-effective [85].

Although promising results about lab/pilot-scale continuous-flow HTL reactor design have been reported constantly around the world, none of the institutes or companies is able to expand beyond pilot plant scale due to capital investment and technical challenges described below.

2.4.2 HTL Reactor Corrosion Issues

Up to now, most of previous research on biomass HTL concentrated on optimizing the reaction conditions, reactor design, catalysts screening, and feedstock selection. However, Corrosion is one of the major concerns in the complex HTL environments. To ensure the cost-effective construction and long-term safe operations, it is crucial to understand the factors causing corrosion and develop practical corrosion control strategy.

2.4.2.1 Organic Acids

During HTL conversion, organic corrodents, such as butyric, acetic, and formic acids, are formed from the feedstocks. It is possible that the presence of these organic acids in the hot-compressed water within the HTL process will speed up the chemical loss of oxide scales that have accumulated on stainless steels at elevated temperatures [86, 87]. It was discovered that adding acetic acid to water would increase the number of protons in the pores of powder metallurgy stainless steels, which in turn accelerated the localized dissolving of metal oxide scales [88]. A recent study in simulated HTL conversion environments showed that the addition of 5% acetic acid into HTL conversion environments could not only accelerate the loss of the metal oxide scales formed on SS 310 and P91, but also cause the localized damage of these reactor constructional materials [89]. Thus, it is necessary to investigate the corrosive effects of organic acids on various reactor alloys during the HTL conversion.

2.4.2.2 Inorganic Contents

Typical industrial bio-wastes have been found to contain up to 15,000 and 13,200 ppm of Cl^- and S^{2-}, respectively [89]. The aggressive inorganic agents will be discharged during the HTL conversion of these bio-wastes. Cl^- and S^{2-} are known to trigger pitting corrosion and even stress corrosion cracking of Fe-based and Ni-based alloys in high-temperature aqueous media [90, 91]. However, it was found that the presence of low concentration (3500 ppm Cl^- and 2500 ppm S^{2-}) could not likely cause severe general corrosion damage on Fe-based steels containing 9-22% Cr, nor cause pitting initiation and propagation under simulated HTL conversion conditions [89]. However, it is unclear whether the accumulation of Cl^- and S^{2-} would cause corrosion of the HTL systems after relatively long-term operation. Once the contents of the ions exceed the critical level to initiate pitting, localized corrosion would become a serious concern due to the synergetic effects of pitting and stress loading from the high-pressure reaction media. More research is still required to assess the corrosion behaviors of pilot- and industrial-scale HTL processes.

2.4.2.3 Temperature

A generally accepted temperature range for biomass hydrothermal liquefaction is 200–400 °C. Different from the positive effects of elevated temperature on the bio-oil yield, increasing the reactor temperature would weaken the protectivity of the oxide layer towards the substrate [92]. However, Kritzer reported that the corrosion rate under subcritical water at 300 °C was higher than that in supercritical water at 500 °C, which could be explained by the different chemical properties between subcritical water (being more ionic) and supercritical water [93]. The impact of temperature on corrosion in subcritical water has been thoroughly investigated, but a general consensus about the temperature effect has not yet been established. A recent study indicated that there could be a transition temperature point (~ 310 °C) above which the corrosion rates of Cr-bearing steels will decrease with temperature [94]. At temperatures near or above the critical point (374 °C) where water is less ionic, chemical reactions instead of electrochemical reactions would dominate, limiting the formation of metal oxides on the surface of steels and alloys but reducing the oxides loss due to chemical dissolution [95]. Compared with batch-mode operation of HTL, the effect of temperature on reactor corrosion could be more complicated in a continuous-flow HTL process where a noticeable temperature gradient exists on the reactor materials. More research is needed to elucidate the role of temperature on reactor corrosion in order to ensure the safe and reliable operation of commercial HTL plants.

2.4.3 Char Formation and Clogging

Due to the fibrous structure of typical feedstock (lignocellulosic biomass) for HTL, solid residue (or char) can readily form, consequently clogging/damaging the continuous reactor system. Because of the smaller tube diameter, continuous reactor systems operated in laboratories using syringe or injector type pumps are prone to clogging [96]. The following sections discuss how to reduce solid formation and minimize the clogging problems for HTL operations.

2.4.3.1 Feedstock Pretreatment

In order to feed the feedstock into the system smoothly, the feedstock slurry should be evenly distributed, homogeneous, and stable. To this end, carboxymethyl cellulose (CMC) has been commonly applied as a sedimentation inhibitor and NaOH as a stabilizer in the preparation of stable feedstock slurry for feeding [97]. The blending process under mild temperatures (100 °C) was found to be an essential step to achieve stable dispersions, because it could break the fibrous structure of the feedstock that would cause problems of sedimentation and low dispersibility [97]. Different from that, Deraban et al. developed a mechanical way to pretreat a pumpable woody biomass feedstock slurry with more than 20 wt.% solid content, where wood powder was first mixed with water to allow the sorption of water into the wood pores, followed by the addition of recycled bio-oil to allow the water phase fill in the pores. Whereas the bio-oil would occupy the interparticle spaces and then act as a media fluid for the moist biomass particles [98].

2.4.3.2 System Configuration

To avoid system clogging caused by the solid feedstocks/char and less soluble oil products, it is important to choose the right conditions and use efficient separation methods, such as the application of organic solvents in the feed or common physical techniques (filtration and centrifugation) to treat the reactor effluent. Furthermore, the optimization of system configuration can be helpful for reducing clogging issues. The velocity profiles and fluid flow patterns of the slurry can be changed in the tubular reactors in different shapes or dimensions under continuous operation. Under some conditions, sedimentation could occur, leading to gradual accumulation of solids at some specific points and finally clogging of the system. For instance, clogging could be more common in steeper-angled bends. The following positions of the bend are subjected to more tendency of clogging: the tee of a horizontal tube with a vertical branch, and a U-shape bend [99]. Therefore, the bends of a continuous system should be kept as smooth as possible, and avoid 90 ° elbows [100].

2.4.3.3 Char Formation Control

Char or hydrochar is produced during HTL processes. The deposition of char would introduce plugging and scaling problems in continuous-flow systems, finally resulting in safety concerns and unwanted system failure. Meanwhile, the accumulation of char on the surfaces of heterogeneous catalysts could deactivate the catalyst by obstructing access to its active sites [101]. Thus, it is necessary to restrict the char formation. Among the proposed methods, the addition of suitable co-solvent (such as alcohol) and catalysts can effectively reduce char formation. For example, Ni/ZrO_2 and Ni/CeO_2 proved to have the potential for restricting char formation and enhancing the energy recovery from HTL of food waste [102]. Homogeneous catalysts, mainly alkaline and acid catalysts, show a great promise in biomass HTL as discussed previously. Even though an acid catalyst can improve the bio-oil yield, alkali catalysts would be more suitable since acidic conditions can promote polymerization/condensation of the reaction intermediates, resulting in more char formation [103]. Furthermore, the acid would corrode the HTL reactors. Alternatively, employing reducing gases such as H_2 or CO could stabilize the intermediate products of HTL, which prevents the condensation, cyclization, or repolymerization of the reaction intermediates, hence decreasing the char formation, and improving the bio-oil yield and quality [3].

2.5 Conclusions and Future Perspectives

HTL is a promising technology for producing clean and renewable energy and chemicals from widely distributed and abundant biomass resources, in particular high water containing bio-wastes such as wastewater sludge, food processing waste, algal biomass, “black liquor,” and lignin. Over the past decade, the effects of operating parameters (temperature, reaction time, feedstock type, liquid-to-solid ratio, and catalysts) on the yield and quality of bio-oil, have been extensively investigated, although mainly in bench-scale batch reactors. Several conversion kinetic models for predicting bio-oil yields with various biomass feedstocks have been proposed as well, and the development of more general models for bio-oil yield prediction is in progress. To advance the deployment of HTL technology in the bioenergy sector, efforts have been made on the development of continuous-flow HTL systems as they are more economical and scalable for industrial applications. Despite the above significant achievements, future works are urgently needed to address the following issues: (1) operation conditions to achieve the optimum yield and chemical composition of bio-oils; (2) knowledge gaps on affordable construction materials for long-term operation of HTL reactors with minimized corrosion; (3) better designs and efficient and effective ways to continuously feed the biomass slurry, with controlled char formation, to avoid clogging of the continuous-flow HTL systems.

2.6 References

[1] A. Gollakota, N. Kishore, S. Gu, A review on hydrothermal liquefaction of biomass, Renewable and Sustainable Energy Reviews 81 (2018) 1378-1392.

[2] S.S. Toor, L. Rosendahl, A. Rudolf, Hydrothermal liquefaction of biomass: a review of subcritical water technologies, Energy 36(5) (2011) 2328-2342.

[3] Y. Xue, H. Chen, W. Zhao, C. Yang, P. Ma, S. Han, A review on the operating conditions of producing bio-oil from hydrothermal liquefaction of biomass, International Journal of Energy Research 40(7) (2016) 865-877.

[4] J. Cai, Y. He, X. Yu, S.W. Banks, Y. Yang, X. Zhang, Y. Yu, R. Liu, A.V. Bridgwater, Review of physicochemical properties and analytical characterization of lignocellulosic biomass, Renewable and Sustainable Energy Reviews 76 (2017) 309-322.

[5] R. Ahorsu, F. Medina, M. Constantí, Significance and challenges of biomass as a suitable feedstock for bioenergy and biochemical production: A review, Energies 11(12) (2018) 3366.

[6] P. Das, V. Chandramohan, T. Mathimani, A. Pugazhendhi, A comprehensive review on the factors affecting thermochemical conversion efficiency of algal biomass to energy, Science of the Total Environment 766 (2021) 144213.

[7] O. Bobleter, Hydrothermal degradation of polymers derived from plants, Progress in polymer science 19(5) (1994) 797-841.

[8] C. Xu, J. Lancaster, Conversion of secondary pulp/paper sludge powder to liquid oil products for energy recovery by direct liquefaction in hot-compressed water, Water research 42(6-7) (2008) 1571-1582.

[9] T. Kanetake, M. Sasaki, M. Goto, Decomposition of a lignin model compound under hydrothermal conditions, Chemical Engineering & Technology: Industrial Chemistry-Plant Equipment-Process Engineering-Biotechnology 30(8) (2007) 1113-1122.

[10] H.A. Ruiz, R.M. Rodríguez-Jasso, B.D. Fernandes, A.A. Vicente, J.A. Teixeira, Hydrothermal processing, as an alternative for upgrading agriculture residues and marine biomass according to the biorefinery concept: a review, Renewable and Sustainable Energy Reviews 21 (2013) 35-51.

[11] M. Saisu, T. Sato, M. Watanabe, T. Adschiri, K. Arai, Conversion of lignin with supercritical water− phenol mixtures, Energy & Fuels 17(4) (2003) 922-928.

[12] M. Ravber, Ž. Knez, M. Škerget, Hydrothermal degradation of fats, carbohydrates and proteins in sunflower seeds after treatment with subcritical water, Chemical and Biochemical Engineering Quarterly 29(3) (2015) 351-355.

[13] T. Kocsisova, J. Juhasz, J. Cvengroš, Hydrolysis of fatty acid esters in subcritical water, European Journal of Lipid Science and Technology 108(8) (2006) 652-658.

[14] A.A. Peterson, F. Vogel, R.P. Lachance, M. Fröling, M.J. Antal Jr, J.W. Tester, Thermochemical biofuel production in hydrothermal media: a review of sub-and supercritical water technologies, Energy & environmental science 1(1) (2008) 32-65.

[15] C. Tian, B. Li, Z. Liu, Y. Zhang, H. Lu, Hydrothermal liquefaction for algal biorefinery: A critical review, Renewable and Sustainable Energy Reviews 38 (2014) 933-950.

[16] H. Li, Z. Liu, Y. Zhang, B. Li, H. Lu, N. Duan, M. Liu, Z. Zhu, B. Si, Conversion efficiency and oil quality of low-lipid high-protein and high-lipid low-protein microalgae via hydrothermal liquefaction, Bioresource technology 154 (2014) 322-329.

[17] L. Luo, J.D. Sheehan, L. Dai, P.E. Savage, Products and kinetics for isothermal hydrothermal liquefaction of soy protein concentrate, ACS Sustainable Chemistry & Engineering 4(5) (2016) 2725-2733.

[18] R. Obeid, D.M. Lewis, N. Smith, T. Hall, P. van Eyk, Reaction kinetics and characterisation of species in renewable crude from hydrothermal liquefaction of monomers to represent organic fractions of biomass feedstocks, Chemical Engineering Journal 389 (2020) 124397.

[19] J. Chen, J. Zhang, W. Pan, G. An, Y. Deng, Y. Li, Y. Hu, Y. Xiao, T. Liu, S. Leng, A novel strategy to simultaneously enhance bio-oil yield and nutrient recovery in sequential hydrothermal liquefaction of high protein microalgae, Energy conversion and management 255 (2022) 115330.

[20] Z. Abu El-Rub, E.A. Bramer, G. Brem, Review of catalysts for tar elimination in biomass gasification processes, Industrial & Engineering Chemistry Research 43(22) (2004) 6911-6919.

[21] Z. Zhu, S.S. Toor, L. Rosendahl, G. Chen, Analysis of product distribution and characteristics in hydrothermal liquefaction of barley straw in subcritical and supercritical water, Environmental Progress & Sustainable Energy 33(3) (2014) 737-743.

[22] N. Sharma, K.K. Jaiswal, V. Kumar, M.S. Vlaskin, M. Nanda, I. Rautela, M.S. Tomar, W. Ahmad, Effect of catalyst and temperature on the quality and productivity of HTL bio-oil from microalgae: A review, Renewable energy 174 (2021) 810-822.

[23] Z. Zhu, S.S. Toor, L. Rosendahl, D. Yu, G. Chen, Influence of alkali catalyst on product yield and properties via hydrothermal liquefaction of barley straw, Energy 80 (2015) 284-292.

[24] M.K. Jindal, M.K. Jha, Effect of process parameters on hydrothermal liquefaction of waste furniture sawdust for bio-oil production, RSC advances 6(48) (2016) 41772-41780.

[25] X. Wu, J. Zhang, Y. Huang, M. Li, J. Bian, F. Peng, Comparative investigation on bio-oil production from eucalyptus via liquefaction in subcritical water and supercritical ethanol, Industrial crops and products 140 (2019) 111695.

[26] H.K. Reddy, T. Muppaneni, S. Ponnusamy, N. Sudasinghe, A. Pegallapati, T. Selvaratnam, M. Seger, B. Dungan, N. Nirmalakhandan, T. Schaub, Temperature effect on hydrothermal liquefaction of Nannochloropsis gaditana and Chlorella sp, Applied Energy 165 (2016) 943-951.

[27] S. He, M. Zhao, J. Wang, Z. Cheng, B. Yan, G. Chen, Hydrothermal liquefaction of low-lipid algae Nannochloropsis sp. and Sargassum sp.: Effect of feedstock composition and temperature, Science of the Total Environment 712 (2020) 135677.

[28] B. Biswas, A.A. Kumar, Y. Bisht, R. Singh, J. Kumar, T. Bhaskar, Effects of temperature and solvent on hydrothermal liquefaction of Sargassum tenerrimum algae, Bioresource technology 242 (2017) 344-350.

[29] W.S. Villaver, R.B. Carpio, K.J. Yap, R. De Leon, Effects of temperature and reaction time on yield and properties of biocrude oil produced by hydrothermal liquefaction of Spirulina platensis, Int. J. Smart Grid Clean Energy 7 (2018).

[30] Z. Zhu, L. Rosendahl, S.S. Toor, D. Yu, G. Chen, Hydrothermal liquefaction of barley straw to bio-crude oil: Effects of reaction temperature and aqueous phase recirculation, Applied Energy 137 (2015) 183-192.

[31] R.K. Mishra, P. Kumar, K. Mohanty, Hydrothermal liquefaction of biomass for bio-crude production: A review on feedstocks, chemical compositions, operating parameters, reaction kinetics, techno-economic study, and life cycle assessment, Fuel 316 (2022) 123377.

[32] B. Zhang, M. von Keitz, K. Valentas, Thermochemical liquefaction of high-diversity grassland perennials, Journal of Analytical and Applied Pyrolysis 84(1) (2009) 18-24.

[33] Y. Xu, M. Li, Hydrothermal liquefaction of lignocellulose for value-added products: Mechanism, parameter and production application, Bioresource technology 342 (2021) 126035.

[34] F. Wang, Z. Chang, P. Duan, W. Yan, Y. Xu, L. Zhang, J. Miao, Y. Fan, Hydrothermal liquefaction of Litsea cubeba seed to produce bio-oils, Bioresource technology 149 (2013) 509-515.

[35] L. Yang, L. Nazari, Z. Yuan, K. Corscadden, C.C. Xu, Hydrothermal liquefaction of spent coffee grounds in water medium for bio-oil production, Biomass and Bioenergy 86 (2016) 191-198.

[36] R. Kaur, P. Gera, M.K. Jha, T. Bhaskar, Reaction parameters effect on hydrothermal liquefaction of castor (Ricinus Communis) residue for energy and valuable hydrocarbons recovery, Renewable energy 141 (2019) 1026-1041.

[37] Z. He, B. Wang, B. Zhang, H. Feng, S. Kandasamy, H. Chen, Synergistic effect of hydrothermal Co-liquefaction of Spirulina platensis and Lignin: Optimization of operating parameters by response surface methodology, Energy 201 (2020) 117550.

[38] E. Panisko, T. Wietsma, T. Lemmon, K. Albrecht, D. Howe, Characterization of the aqueous fractions from hydrotreatment and hydrothermal liquefaction of lignocellulosic feedstocks, Biomass and Bioenergy 74 (2015) 162-171.

[39] D.R. Vardon, B. Sharma, J. Scott, G. Yu, Z. Wang, L. Schideman, Y. Zhang, T.J. Strathmann, Chemical properties of biocrude oil from the hydrothermal liquefaction of Spirulina algae, swine manure, and digested anaerobic sludge, Bioresource technology 102(17) (2011) 8295-8303.

[40] Y. Tian, F. Wang, J.O. Djandja, S.L. Zhang, Y.P. Xu, P.G. Duan, Hydrothermal liquefaction of crop straws: Effect of feedstock composition, Fuel 265 (2020) 116946.

[41] S. Yin, R. Dolan, M. Harris, Z. Tan, Subcritical hydrothermal liquefaction of cattle manure to bio-oil: Effects of conversion parameters on bio-oil yield and characterization of bio-oil, Bioresource technology 101(10) (2010) 3657-3664.

[42] H. Bayat, F. Cheng, M. Dehghanizadeh, N. Soliz, C.E. Brewer, U. Jena, Hydrothermal liquefaction of food waste: Bio-crude oil Characterization, Mass and Energy Balance, 2019 ASABE Annual International Meeting, American Society of Agricultural and Biological Engineers, 2019, p. 1.

[43] T. Belkheiri, S.I. Andersson, C. Mattsson, L. Olausson, H. Theliander, L. Vamling, Hydrothermal liquefaction of kraft lignin in sub-critical water: the influence of the sodium and potassium fraction, Biomass Conversion and Biorefinery 8(3) (2018) 585-595.

[44] P. Biller, D. Lawson, R.B. Madsen, J. Becker, B.B. Iversen, M. Glasius, Assessment of agricultural crops and natural vegetation in Scotland for energy production by anaerobic digestion and hydrothermal liquefaction, Biomass Conversion and Biorefinery 7(4) (2017) 467-477.

[45] S. Feng, Z. Yuan, M. Leitch, C.C. Xu, Hydrothermal liquefaction of barks into bio-crude–Effects of species and ash content/composition, Fuel 116 (2014) 214-220.

[46] J. Lu, Z. Liu, Y. Zhang, P.E. Savage, Synergistic and antagonistic interactions during hydrothermal liquefaction of soybean oil, soy protein, cellulose, xylose, and lignin, ACS Sustainable Chemistry & Engineering 6(11) (2018) 14501-14509.

[47] Y.H. Chan, S. Yusup, A.T. Quitain, Y. Uemura, M. Sasaki, Bio-oil production from oil palm biomass via subcritical and supercritical hydrothermal liquefaction, The Journal of Supercritical Fluids 95 (2014) 407-412.

[48] K. Malins, V. Kampars, J. Brinks, I. Neibolte, R. Murnieks, R. Kampare, Bio-oil from thermo-chemical hydro-liquefaction of wet sewage sludge, Bioresource technology 187 (2015) 23-29.

[49] L. Ye, J. Zhang, J. Zhao, S. Tu, Liquefaction of bamboo shoot shell for the production of polyols, Bioresource technology 153 (2014) 147-153.

[50] M. Cao, C. Long, S. Sun, Y. Zhao, J. Luo, D. Wu, Catalytic hydrothermal liquefaction of peanut shell for the production aromatic rich monomer compounds, Journal of the Energy Institute 96 (2021) 90-96.

[51] H. Hwang, J.H. Lee, I.-G. Choi, J.W. Choi, Comprehensive characterization of hydrothermal liquefaction products obtained from woody biomass under various alkali catalyst concentrations, Environmental technology 40(13) (2019) 1657-1667.

[52] B. de Caprariis, I. Bavasso, M.P. Bracciale, M. Damizia, P. De Filippis, M. Scarsella, Enhanced bio-crude yield and quality by reductive hydrothermal liquefaction of oak wood biomass: Effect of iron addition, Journal of Analytical and Applied Pyrolysis 139 (2019) 123-130.

[53] Y. Chen, L. Dong, J. Miao, J. Wang, C. Zhu, Y. Xu, G. Chen, J. Liu, Hydrothermal liquefaction of corn straw with mixed catalysts for the production of bio-oil and aromatic compounds, Bioresource technology 294 (2019) 122148.

[54] Y. Chen, P. Duan, L. Dong, C. Zhu, L. Jin, F. Tian, The study of hydrothermal liquefaction of corn straw with Nano ferrite+ inorganic base catalyst system at low temperature, Bioresource technology 333 (2021) 125185.

[55] X. Wu, J. Zhang, M. Li, J. Bian, F. Peng, Catalytic hydrothermal liquefaction of eucalyptus to prepare bio-oils and product properties, Energy conversion and management 199 (2019) 111955.

[56] L. Yan, Y. Wang, J. Li, Y. Zhang, L. Ma, F. Fu, B. Chen, H. Liu, Hydrothermal liquefaction of Ulva prolifera macroalgae and the influence of base catalysts on products, Bioresource technology 292 (2019) 121286.

[57] C. Ma, J. Geng, D. Zhang, X. Ning, Hydrothermal liquefaction of macroalgae: Influence of zeolites based catalyst on products, Journal of the Energy Institute 93(2) (2020) 581-590.

[58] D. Xu, S. Guo, L. Liu, G. Lin, Z. Wu, Y. Guo, S. Wang, Heterogeneous catalytic effects on the characteristics of water-soluble and water-insoluble biocrudes in chlorella hydrothermal liquefaction, Applied Energy 243 (2019) 165-174.

[59] S. Kandasamy, B. Zhang, Z. He, H. Chen, H. Feng, Q. Wang, B. Wang, V. Ashokkumar, S. Siva, N. Bhuvanendran, Effect of low-temperature catalytic hydrothermal liquefaction of Spirulina platensis, Energy 190 (2020) 116236.

[60] W. Wang, Y. Xu, X. Wang, B. Zhang, W. Tian, J. Zhang, Hydrothermal liquefaction of microalgae over transition metal supported TiO2 catalyst, Bioresource technology 250 (2018) 474-480.

[61] C. Liu, L. Kong, Y. Wang, L. Dai, Catalytic hydrothermal liquefaction of spirulina to bio-oil in the presence of formic acid over palladium-based catalysts, Algal research 33 (2018) 156-164.

[62] B. Wang, Z. He, B. Zhang, Y. Duan, Study on hydrothermal liquefaction of spirulina platensis using biochar based catalysts to produce bio-oil, Energy 230 (2021) 120733.

[63] H. Mazaheri, K.T. Lee, S. Bhatia, A.R. Mohamed, Subcritical water liquefaction of oil palm fruit press fiber for the production of bio-oil: effect of catalysts, Bioresource technology 101(2) (2010) 745-751.

[64] Z. Bi, J. Zhang, E. Peterson, Z. Zhu, C. Xia, Y. Liang, T. Wiltowski, Biocrude from pretreated sorghum bagasse through catalytic hydrothermal liquefaction, Fuel 188 (2017) 112-120.

[65] S. Karagöz, T. Bhaskar, A. Muto, Y. Sakata, T. Oshiki, T. Kishimoto, Low-temperature catalytic hydrothermal treatment of wood biomass: analysis of liquid products, Chemical Engineering Journal 108(1-2) (2005) 127-137.

[66] I.A. Basar, H. Liu, H. Carrere, E. Trably, C. Eskicioglu, A review on key design and operational parameters to optimize and develop hydrothermal liquefaction of biomass for biorefinery applications, Green Chemistry 23(4) (2021) 1404-1446.

[67] L. Cao, C. Zhang, H. Chen, D.C. Tsang, G. Luo, S. Zhang, J. Chen, Hydrothermal liquefaction of agricultural and forestry wastes: state-of-the-art review and future prospects, Bioresource technology 245 (2017) 1184-1193.

[68] R. Shakya, J. Whelen, S. Adhikari, R. Mahadevan, S. Neupane, Effect of temperature and Na2CO3 catalyst on hydrothermal liquefaction of algae, Algal research 12 (2015) 80-90.

[69] Y. Wu, H. Wang, H. Li, X. Han, M. Zhang, Y. Sun, X. Fan, R. Tu, Y. Zeng, C.C. Xu, Applications of catalysts in thermochemical conversion of biomass (pyrolysis, hydrothermal liquefaction and gasification): A critical review, Renewable energy (2022).

[70] P. Biller, R. Riley, A. Ross, Catalytic hydrothermal processing of microalgae: decomposition and upgrading of lipids, Bioresource technology 102(7) (2011) 4841-4848.

[71] P. Duan, P.E. Savage, Hydrothermal liquefaction of a microalga with heterogeneous catalysts, Industrial & Engineering Chemistry Research 50(1) (2011) 52-61.

[72] B. Zhang, H.J. Huang, S. Ramaswamy, Reaction kinetics of the hydrothermal treatment of lignin, Biotechnology for fuels and chemicals, Springer2007, pp. 487-499.

[73] F. Hardi, M. Mäkelä, K. Yoshikawa, Non-catalytic hydrothermal liquefaction of pine sawdust using experimental design: material balances and products analysis, Applied Energy 204 (2017) 1026-1034.

[74] Y.H. Chan, A.T. Quitain, S. Yusup, Y. Uemura, M. Sasaki, T. Kida, Liquefaction of palm kernel shell to bio-oil using sub-and supercritical water: an overall kinetic study, Journal of the Energy Institute 92(3) (2019) 535-541.

[75] M. Déniel, G. Haarlemmer, A. Roubaud, E. Weiss-Hortala, J. Fages, Modelling and predictive study of hydrothermal liquefaction: application to food processing residues, Waste and Biomass Valorization 8(6) (2017) 2087-2107.

[76] P.J. Valdez, V.J. Tocco, P.E. Savage, A general kinetic model for the hydrothermal liquefaction of microalgae, Bioresource technology 163 (2014) 123-127.

[77] D.C. Hietala, J.L. Faeth, P.E. Savage, A quantitative kinetic model for the fast and isothermal hydrothermal liquefaction of Nannochloropsis sp, Bioresource technology 214 (2016) 102-111.

[78] T.K. Vo, S.S. Kim, H.V. Ly, E.Y. Lee, C.G. Lee, J. Kim, A general reaction network and kinetic model of the hydrothermal liquefaction of microalgae Tetraselmis sp, Bioresource technology 241 (2017) 610-619.

[79] R. Kumar, A review on the modelling of hydrothermal liquefaction of biomass and waste feedstocks, Energy Nexus (2022) 100042.

[80] J. Ni, L. Qian, Y. Wang, B. Zhang, H. Gu, Y. Hu, Q. Wang, A review on fast hydrothermal liquefaction of biomass, Fuel 327 (2022) 125135.

[81] C.L. Yiin, E. bin Odita, S.S.M. Lock, K.W. Cheah, Y.H. Chan, M.K. Wong, B.L.F. Chin, A.T. Quitain, S.K. Loh, S. Yusup, A review on potential of green solvents in hydrothermal liquefaction (HTL) of lignin, Bioresource technology (2022) 128075.

[82] Y. Fan, C. Prestigiacomo, M. Gong, T. Tietz, U. Hornung, N. Dahmen, Comparative investigation on the value-added products obtained from continuous and batch hydrothermal liquefaction of sewage sludge, Frontiers in Environmental Science 10 (2022) 996353.

[83] D. Cronin, A.J. Schmidt, J. Billing, T.R. Hart, S.P. Fox, X. Fonoll, J. Norton, M.R. Thorson, Comparative Study on the Continuous Flow Hydrothermal Liquefaction of Various Wet-Waste Feedstock Types, ACS Sustainable Chemistry & Engineering 10(3) (2021) 1256-1266.

[84] K. Anastasakis, P. Biller, R.B. Madsen, M. Glasius, I. Johannsen, Continuous hydrothermal liquefaction of biomass in a novel pilot plant with heat recovery and hydraulic oscillation, Energies 11(10) (2018) 2695.

[85] A. Aierzhati, J. Watson, B. Si, M. Stablein, T. Wang, Y. Zhang, Development of a mobile, pilot scale hydrothermal liquefaction reactor: Food waste conversion product analysis and techno-economic assessment, Energy Conversion and Management: X 10 (2021) 100076.

[86] I. Sekine, A. Masuko, K. Senoo, Corrosion behavior of AISI 316 stainless steel in formic and acetic acid solutions, Corrosion 43(9) (1987) 553-560.

[87] A. Invernizzi, E. Sivieri, S. Trasatti, Corrosion behaviour of duplex stainless steels in organic acid aqueous solutions, Materials Science and Engineering: A 485(1-2) (2008) 234-242.

[88] E. Otero, A. Pardo, M. Utrilla, F. Pérez, C. Merino, The corrosion behaviour of AISI 304L and 316L stainless steels prepared by powder metallurgy in the presence of organic acids, Corrosion science 39(3) (1997) 453-463.

[89] M. Liu, Y. Zeng, J.-L. Luo, Impacts of Catalyst, Inorganic and Organic Corrodants on Corrosion under Batch-mode Catalytic Biomass Hydrothermal Liquefaction Conversion, Corrosion Science (2022) 110409.

[90] D.-H. Xia, Y. Behnamian, J.-L. Luo, Factors influencing sulfur induced corrosion on the secondary side in pressurized water reactors (PWRs), Journal of the Electrochemical Society 166(2) (2019) C49.

[91] O.D. Azamata, T.Y. Jibatswen, O.C. Michael, Effect of chlorine and sulphur on stainless steel (AISI 310) due to high temperature corrosion, Am. J. Eng. Res 5 (2016) 266-270.

[92] K. Wang, J. Wang, W. Hu, Evaluation of temperature effect on the corrosion process of 304 stainless steel in high temperature water with electrochemical noise, Materials & Design 82 (2015) 155-163.

[93] P. Kritzer, Corrosion in high-temperature and supercritical water and aqueous solutions: a review, The Journal of Supercritical Fluids 29(1-2) (2004) 1-29.

[94] M. Liu, Y. Zeng, J.-L. Luo, Influence of Major Operating Parameters (Temperature, Pressure, and Flow Rate) on the Corrosion of Candidate Alloys for the Construction of Hydrothermal Liquefaction Biorefining Reactors, Energy & Fuels 36(6) (2022) 3134-3153.

[95] D. Guzonas, W. Cook, Cycle chemistry and its effect on materials in a supercritical water-cooled reactor: A synthesis of current understanding, Corrosion Science 65 (2012) 48-66.

[96] A.J. Mørup, J. Becker, P.S. Christensen, K. Houlberg, E. Lappa, M. Klemmer, R.B. Madsen, M. Glasius, B.B. Iversen, Construction and commissioning of a continuous reactor for hydrothermal liquefaction, Industrial & engineering chemistry research 54(22) (2015) 5935-5947.

[97] E. Lappa, P.S. Christensen, M. Klemmer, J. Becker, B.B. Iversen, Hydrothermal liquefaction of Miscanthus× Giganteus: Preparation of the ideal feedstock, Biomass and Bioenergy 87 (2016) 17-25.

[98] I.M. Dãrãban, L.A. Rosendahl, T.H. Pedersen, S.B. Iversen, Pretreatment methods to obtain pumpable high solid loading wood–water slurries for continuous hydrothermal liquefaction systems, Biomass and bioenergy 81 (2015) 437-443.

[99] G. Brown, Erosion prediction in slurry pipeline tee-junctions, Applied mathematical modelling 26(2) (2002) 155-170.

[100] F. Cheng, T. Le Doux, B. Treftz, S. Woolf, J. Yu, J. Miller, U. Jena, C.E. Brewer, Modification of a pilot-scale continuous flow reactor for hydrothermal liquefaction of wet biomass, MethodsX 6 (2019) 2793-2806.

[101] E. Furimsky, F.E. Massoth, Deactivation of hydroprocessing catalysts, Catalysis Today 52(4) (1999) 381-495.

[102] F. Cheng, G.A. Tompsett, D.V.F. Alvarez, C.I. Romo, A.M. McKenna, S.F. Niles, R.K. Nelson, C.M. Reddy, S. Granados-Fócil, A.D. Paulsen, Metal oxide supported Ni-impregnated bifunctional catalysts for controlling char formation and maximizing energy recovery during catalytic hydrothermal liquefaction of food waste, Sustainable Energy & Fuels 5(4) (2021) 941-955.

[103] M. Déniel, G. Haarlemmer, A. Roubaud, E. Weiss-Hortala, J. Fages, Energy valorisation of food processing residues and model compounds by hydrothermal liquefaction, Renewable and Sustainable Energy Reviews 54 (2016) 1632-1652.

Chapter 3

3 Hydrothermal Liquefaction of Pinewood Sawdust: Influence of Reaction Atmosphere

Abstract

Hydrothermal liquefaction (HTL) is a thermochemical process for production of bio-oils, commonly from wet biomass under inert atmosphere (N_2). Influence of reaction atmosphere on HTL of pinewood sawdust was investigated in this work, at 300 °C for 60 min with the presence of KOH or H_2SO_4 catalyst under N_2, H_2, and O_2 atmosphere, respectively. Very interestingly, the reaction atmosphere showed significant influence on both products' distribution and properties of the bio-oil. Generally, H_2 atmosphere enhanced biomass degradation in the presence of either KOH or H_2SO_4 catalyst, producing the highest bio-oil yield, lowest solid residue yield, and the best oil quality in terms of total acid number (TAN), viscosity and average molecular weights (M_n, M_w). Whereas the HTL in O_2 atmosphere showed the poorest performance in terms of yields and properties of bio-oils. The highest quality of bio-oil was produced using KOH catalyst in H_2 atmosphere produced the maximum bio-oil yield (approx. 34 wt.%) and the highest energy recovery (ER) in bio-oil (ER = 73.14%). The measured properties of the oil are as follows: TAN = 40.2 mg KOH/g, viscosity = 51.2 cp, Mn = 470 g/mol, Mw = 767 g/mol. In addition, the bio-oils produced in H_2 atmosphere contain more light oil (naphtha) fraction (23.9 wt.% with KOH and 16.5 wt.% with H_2SO_4) with lower boiling points, while those generated in O_2 atmosphere have more carboxylic acid compounds.

Keywords: Bio-oil properties, Hydrogen, H_2SO_4, KOH, Nitrogen, Oxygen, Pinewood sawdust, Products distribution, Reaction atmosphere

3.1 Introduction

The growing energy demand has led to extensive use and overexploitation of fossil resources, resulting in an energy crisis and severe environmental issues such as climate changes [1-3]. To mitigate the pressure from the global energy shortage and global warming due to fast increased CO_2 emission, as well as to satisfy the clean energy demand, sustainable development and carbon neutrality, biomass has gained immense interest for the production of energy, fuels, chemicals and materials [4, 5]. Biomass is a renewable and abundantly available resource from dedicated energy crops or various organic wastes, such as wood and forestry residues, agricultural crops and crop residues, marine products, wastewater sludge, microalgae, etc. [6-8].

Biomass can be converted into energy, fuels, and chemicals via biochemical and thermochemical conventional technologies. Biochemical treatments mainly refer to anaerobic digestion, fermentation, and photobiological hydrogen production. The objective of these treatments was to utilize various microorganisms or enzymes to convert the biomass into a variety of products and intermediates. This process offers an opportunity to produce an assortment of fuels and chemicals, including biogas, hydrogen, ethanol, butanol, acetone, and various organic acids [9]. However, biochemical processes are very sensitive to operating conditions (such as pH, temperature, and residence time) and quite slow (usually requiring days or weeks to complete) [10-12]. Thermochemical processes include gasification, hydrothermal liquefaction (HTL), pyrolysis, and combustion [13, 14]. Pyrolysis and HTL are two main thermochemical pathways developed for the transformation of raw biomass materials into liquid products that can be further processed to produce biofuels or bio-based chemicals. Compared with pyrolysis, HTL has gained increasing attention because it can produce high quality bio-oils (5%-20% oxygen) as the primary products with little gas generated [15], and more advantageously HTL can handle wet feedstocks (with >70% water content) without the requirement for drying [13, 16], and it typically operates at milder temperatures (250 °C - 400 °C), though under high pressure (50 bar - 250 bar) in an inert atmosphere (N_2) [6, 17, 18].

Many studies focus on the effects of HTL process parameters, e.g., reaction temperature, pressure, residence time, and types of solvent. Generally, operations at a moderate temperature between 250-350 °C obtain a higher bio-oil yield, however a too high temperature would reduce bio-crude yield and increase the amount of solid residue due to the reactions of bio-oil cracking and repolymerization/condensation of the reaction intermediates [16, 19-21]. Shortening residence time can prevent those reactions happening to a certain extent, resulting in an increased bio-oil yield. However, a too-short duration would cause incomplete biomass degradation, while a too long residence time would lead to polymerization/condensation of the reaction intermediates, reducing bio-oil yield [22]. Besides, a lower solid-to-liquid ratio increased the yield of bio-oil and inhibited formation of solid residues and gases owing to better dissolution of reaction intermediates/products in the liquid (water or a mixed solvent of water-organic solvent) and the enhanced hydrolysis reactions of the biomass [23]. Catalyst is another critical factor that affects HTL bio-oil yield and properties. Homogeneous catalysts, including soluble acids, base, and alkali salts, are commonly used in biomass HTL. Strong acids (sulfuric acid and hydrochloric acid) exhibited great performance in biomass conversion. However, strong acid could corrode the experimental equipment, and the biomass conversion might decrease when increasing the acid content over a certain level [24, 25], because acidic condition facilitates the condensation and re-polymerization reactions of the reaction intermediates, thereby reducing the yield of bio-oil. Alkaline catalysts such as NaOH, K_2CO_3, KOH, and Na_2CO_3 have been widely used in HTL processes [14]. Alkaline catalysts can neutralize the acid compounds in the hydrothermal products, which prevents the repolymerization/condensation of the reaction intermediates, thus reducing the formation of solid residue/char [26]. Recently, researchers have employed mathematical models to optimize the parameters of HTL of biomass. The goal of this optimization is to obtain bio-oil with high yield, high carbon and hydrogen content, and low heteroatom content, along with the corresponding reaction conditions and material composition. The primary methods include empirical summaries based on experimental laws, response surface method (RSM), kinetics modeling, and machine learning (ML). For example, Zhu et al. [27] utilized RSM to optimize reaction temperature, reaction time, catalyst dosage and biomass/water ratio for highest bio-oil yield. Obeid et al. [28] employed kinetics modeling to predict the distribution of bio-oil yield. Cheng et al. [29] used multiple linear regression (MLR), regression tree (RT) and random forest (RF) to predict the quantity and quality of biomass HTL products.

However, limited studies reported effects of the reaction atmosphere on biomass HTL with respect to the products distribution and properties of the bio-oil. HTL of biomass is typically operated in an inert atmosphere with pressurized nitrogen to avoid boiling of the reaction mixtures. Zhang et al. found using a reducing gas (CO, H_2) as the HTL reaction pressurizing gas could inhibit condensation, cyclisation, and re-polymerization of free radicals of the reaction intermediates, and hence stabilize the depolymerized lignocellulose fragments and reduce char formation [30]. Yin et.al reported that using CO and H_2 (respectively) as the reaction atmosphere in HTL of cattle manure led to increased bio-oil production by 5-15 wt.% [31]. Interestingly, Yin et al. also tested oxygen as an oxidative atmosphere for cattle manure HTL, resulting in much lower bio-oil yield compared with those obtained under N_2 and CO atmosphere, due to the oxidation of feedstocks/products in the presence of an excess of oxygen in the reactor [31]. In another research by Rahimi et al. in HTL conversion of lignin, oxygen atmosphere was found to promote cleavage of alkyl aryl ether units in lignin to promote yield of low molecular weight compounds such as vanillin and benzylic/aliphatic alcohols [32, 33] .

Lignocellulosic biomass is one of the most commonly used feedstocks for HTL process. However, no research has indicated which atmosphere (inert, oxidative, or reductive) works best for the HTL conversion of lignocellulosic biomass. In this study, we for the first time compared the oil product yield and properties from HTL of a typical lignocellulosic biomass - pinewood sawdust – under different reaction atmospheres (N_2, H_2, and O_2) on HTL of a typical lignocellulosic biomass - pinewood sawdust. The tests were conducted with a biomass-to-water ratio of 1:15 (w/w) at 300°C for 60 min under N_2, H_2, and O_2 atmosphere in the presence of a homogeneous catalyst: KOH or H_2SO_4. The bio-oil products were comprehensively characterized for their physicochemical properties, i.e., viscosity, total acid number (TAN), functional groups by Fourier-transform infrared spectroscopy (FT-IR), volatile compositions by gas chromatography-mass spectrometry (GC-MS), volatility by thermogravimetry analysis (TGA), and average molecular weights and distributions by gel permeation chromatography (GPC).

3.2 Materials and Methods

3.2.1 Materials

Pinewood sawdust was collected from a local sawmill (London, Canada). Prior to the HTL test, it was crushed and sieved to reduce particle size below 40 mesh, followed by pre-drying at 105 °C in an oven for 24 h. It contains 40.9 wt.% cellulose, 28.5 wt.% hemicellulose and 28.4 wt.% lignin. Its proximate analysis and ultimate analysis, were obtained from our previous work [34], as shown in **Table 3.1**. Potassium hydroxide (KOH, 99 wt.%) and sulfuric acid (H_2SO_4, 98 wt.%) were purchased from Sigma-Aldrich (Oakville, Canada), and VWR International (Mississauga, Canada), respectively. Reagent-grade acetone (99.8 wt.%) was received from Fisher Scientific (Ottawa, Canada). De-ionized water was used as the solvent in HTL experiments.

Table 3.1: Proximate analysis and ultimate analysis of the pinewood sawdust feedstock.

Proximate analysis(wt.%) [a]	
Volatile matter (VM)	85.35±0.99
Fixed carbon (FC)	14.02±0.92
Ash	0.63±0.07
Elemental analysis(wt.%) [a]	
C	48.24±0.82
H	4.72±0.12
O[b]	46.33±0.76
N	0.08±0.01
S	n.d. [c]
HHV(MJ/kg)[d]	14.78

[a]On dry basis; [b]Calculated by difference: %O = 100% - C% - H% - N% - S% - Ash%; [c] Not detected; [d] Higher heating value, calculated by Dulong equation [HHV (MJ/kg) = 0.338C + 1.428(H-O/8) + 0.095S].

3.2.2 Apparatus and Methods

3.2.2.1 HTL Experiments

The HTL experiments were conducted in a 100 ml Parr 4590 autoclave batch reactor (made of SS316L) equipped with a stirrer and temperature controller. In a typical HTL run, 2 g of pinewood sawdust together with 30 g de-ionized water (solid-to-liquid ratio is fixed as 1:15 w/w) were loaded into the reactor. The catalyst (KOH/H_2SO_4) dosage was set to be 5 wt.% with respect to the mass of dry biomass feedstock. The reactor was sealed, and the air inside was displaced by vacuuming and purging for three times with N_2, H_2, or O_2, followed by pressurizing the reactor to 20 bar using different N_2, H_2, or O_2. Then the reactor was heated under 100 rpm stirring to 300 °C and maintained at the temperature for 60 min for reaction (reported as the optimum condition for HTL of pinewood in previous studies [35-37]), followed by quenching in a water bath.

3.2.2.2 Products Separation

The products from the HTL experiments include gaseous products, bio-oil, aqueous-phase (AP) products, and solid residues (SR). After the reactor was quenched to room temperature, the gas products from HTL were vented into a gas bag and analyzed by Micro-GC-TCD (Agilent 3000). The gas products composition (mainly CO_2) was used for calculation of mass of gas products, M_{gas}. Then the reactor was opened and the solid/liquid products inside the reactor were first washed out with distilled water. The resulting suspension was filtered under vacuum through a pre-weighted VWR No. 413 filter paper. The filtrate was collected as the aqueous phase (AP) products. As the collected AP contains extra water from the above washing process, the accurate yield of AP products was calculated based on the mass balance of conversion processes as shown in Eqn. (3.4). The reactor was then further washed with reagent-grade acetone to collect the water-insoluble oil components. The mixture was filtered under vacuum through the same filter paper (VWR No. 413) retaining the solid residue on it. The solid residue or char was rinsed with additional acetone until the filtrate became colorless, followed by oven dried at 105 °C until attaining a constant weight to determine the mass of solid residue (M_{SR}). The filtrate was evaporated under reduced pressure at 50 °C until bio-oil was precipitated on the flask inner wall. The remaining aqueous solution was decanted and collected as the aqueous product (AP). The oily product sticking on the flask, designated as bio-oil or simply bio-oil, was weighed to determine the mass of bio-oil, $M_{bio\text{-}oil}$. The yields of the HTL products were calculated based on dry and ash-free mass of biomass feedstock, $M_{Biomass,daf}$, as follows:

$$Biocrude\ yield\ (wt.\%) = \frac{M_{biocrude}}{M_{Biomass,daf}} \times 100 \tag{3.1}$$

$$SR\ yield\ (wt.\%) = \frac{M_{SR}}{M_{Biomass,daf}} \times 100 \tag{3.2}$$

$$Gas\ yield\ (wt.\%) = \frac{M_{gas}}{M_{Biomass,daf}} \times 100 \tag{3.3}$$

$$AP\ yield\ (wt.\%) = 100 - Biocrude\ yeild - SR\ yield - Gas\ yield \tag{3.4}$$

$$Energy\ recovery\ (\%) = \frac{HHV_{biocrude}}{HHV_{Biomass}} \times Biocrude\ yield \tag{3.5}$$

3.2.2.3 Products Analysis

The composition of the collected gaseous products in the gas bag was analyzed with a Micro-GC-TCD (Agilent Micro-GC 3000) by injecting 50 ml of air as the internal standard. A PerkinElmer Fourier transform infrared spectrometer (FT-IR, Massachusetts, USA) was used to determine the functional groups of the bio-oil products. The bio-oil viscosity at 80 °C was measured using a Brookfield CAP 2000 + Viscometer. The weight/number average molecular weights (M_w, M_n), polydispersity index (PDI, =Mw/Mn), of the obtained bio-oil products were determined by Gel Permeation Chromatography (GPC-UV, Waters Breeze). Volatile compositions of the bio-oil products were analyzed by Gas Chromatograph-Mass Spectrometer (GC–MS, Agilent Technologies, 5977A MSD) equipped with an HP-5MS column (30 m × 250 μm × 0.25 μm). The GC temperature program was set as: held at 40 °C for 5 min, then increased at 10 °C/min to 150 °C and held for 2 min, increased at 10 °C/min to 290 °C and held for 5 min. The elemental compositions (C, H, N, and S) of the biomass feedstock and bio-oil products were analyzed on an elemental analyzer (Vario EL Cube). The O content was calculated by difference on a dry basis (%O = 100% - %Ash - %C - %H - %N -%S) where the ash content of biomass feedstock was determined by ashing at 700°C for 4 hours in a muffle furnace. The higher heating values (HHV) of the biomass feedstock, bio-oils, and solid residue were calculated by Dulong equation [HHV (MJ/kg) = 0.338C + 1.428(H-O/8) + 0.095S]. The proximate analysis (volatile matters and fixed carbon contents) of biomass feedstock and bio-oil products was determined on a thermogravimetric analyzer (Pris 1 TGA, Waltham, USA), where the sample was heated in 30 ml/min N_2 flow from 25 °C to 800 °C at 10 °C /min, followed by soaking at this temperature for 15 min in 30 mL/min air flow for ashing. The total acid number (TAN) of bio-oil was determined by titration on a pH meter (Titroline 7000) using 0.01 N KOH and phenolphthalein as the titration solution and indicator, respectively. TAN was calculated in milligrams of KOH/gram of the bio-oil sample as follows:

$$TAN = [(A - B)N \times 56.1]/W \tag{3.6}$$

where:

A = KOH solution required for titration of the sample, ml,

B = KOH solution required for titration of the blank, ml,

N = Normality of the KOH solution,

W = Mass of the bio-oil sample, g.

3.3 Results and Discussion

3.3.1 HTL Products Distribution

Figure 3.1 shows the products distribution in HTL of pinewood sawdust under N_2, H_2, and O_2, respectively, with KO or H_2SO_4 catalyst. As clearly shown in **Figure 3.1**, reaction atmosphere and catalyst both have significant influence on the products distribution in HTL of the woody biomass. In terms of bio-oil yield and biomass conversion (or SR yield), the alkali catalyst (KOH) outperformed the acid catalyst (H_2SO_4), and H_2 atmosphere was superior to both N_2 and O_2. The highest bio-oil yield (approx. 34 wt.%.) and maximum biomass conversion (approx. 91%, or SR ~ 9 wt.%) was achieved under the H_2 atmosphere with KOH catalyst. In contrast, the presence of O_2 atmosphere with KOH catalyst produced the lowest bio-oil yield (approx. 2 wt.%) and minimum biomass conversion (approx. 63%, or SR ~ 37 wt.%). Similar results were reported by Singh et al. [38] for HTL of rice straw under different reaction environments (N_2, O_2 and CO_2). Minimum bio-oil yield (3 wt.%) and conversion (73 wt.%) was achieved in the case of liquefaction using O_2. In addition, Peng et al. [39] reported that higher conversion and liquid product yield were observed in the HTL of cornstalk under reducing atmosphere (CO, H_2).

Pinewood sawdust is a typical woody biomass contains 60-70 wt.% holocellulose (cellulose and hemicellulose), 20-30 wt.% lignin, and 5-10 wt.% others (extractives and ash) [40]. Holocellulose includes polysaccharides with $\beta(1\rightarrow4)$ linkage [41], and lignin is well known a polymer of phenylpropane linked mainly by β-O-4 ether linkage. During HTL, $\beta(1\rightarrow4)$ linkage in holocellulose, and β-O-4 ether linkage in lignin can be broken via hydrolytic depolymerization, forming carbohydrate/phenolic monomers and oligomers as

HTL reaction intermediates, which would further undergo recombination reactions to form bio-oil including mixture of organic acids and phenolics [42]. The hydrolytic depolymerization process could be catalyzed by acid catalyst or self-catalyzed by the organic acids formed in the biomass HTL process. However the acid catalyst could catalyze the condensation/repolymerization reactions of the HTL reaction intermediates to form SR product, whereas an alkaline catalyst, e.g., KOH can neutralize the organic acids produced and inhibit condensation/repolymerization reactions [15], hence restricting SR yield and improving bio-oil yield, as evidenced by the results of this study (**Figure 3.1**). In addition to catalyzing the condensation/repolymerization reactions of the HTL reaction intermediates, an acid catalyst (e.g. H_2SO_4) could also catalyze decarboxylation and dehydration of the intermediates, leading to increased formation of SR [43, 44]. Thus, the above explains why the alkali catalyst (KOH) outperformed the acid catalyst (H_2SO_4) HTL of the woody biomass, leading to higher yields of bio-oil and lower yields of SR (**Figure 3.1**).

On the other hand, the significant effects of the atmosphere on the HTL products distribution should be discussed. First of all, the H_2 atmosphere could play positive roles in breaking of the β(1→4) linkage in holocellulose and β-O-4 ether linkage in lignin via reductive depolymerization and stabilizing the reaction intermediates [45], which would hence suppress the condensation/repolymerization reactions, restrict SR formation and improve bio-oil yield, as evidenced by the results of this study (**Figure 3.1**). In contrast, under O_2 atmosphere, the reaction intermediates are converted into more carboxylic compounds that promote the formation of SR product, accompanied by significantly reduced yields of bio-oil (**Figure 3.1**). More gaseous products were generated under O_2 atmosphere. Further analysis of the gas products indicates that the amount of produced CO_2 in O_2 atmosphere is much higher than those in N_2 or H_2 (**Table 3.2**), as a result of the enhanced decarboxylation and deep oxidation of the intermediates by O_2. In addition, the reductive environment (H_2) somewhat limits the production of CO_2. In a summary, among all three types of gas atmosphere examined, biomass HTL under H_2 atmosphere produced the highest bio-oil yields and the lowest SR yields. It is worth noting that although an inert atmosphere (N_2) exhibited an average performance in terms of bio-oil yield and biomass conversion, N_2 atmosphere is more economical and safer than H_2 and O_2, hence has been employed most often for biomass HTL.

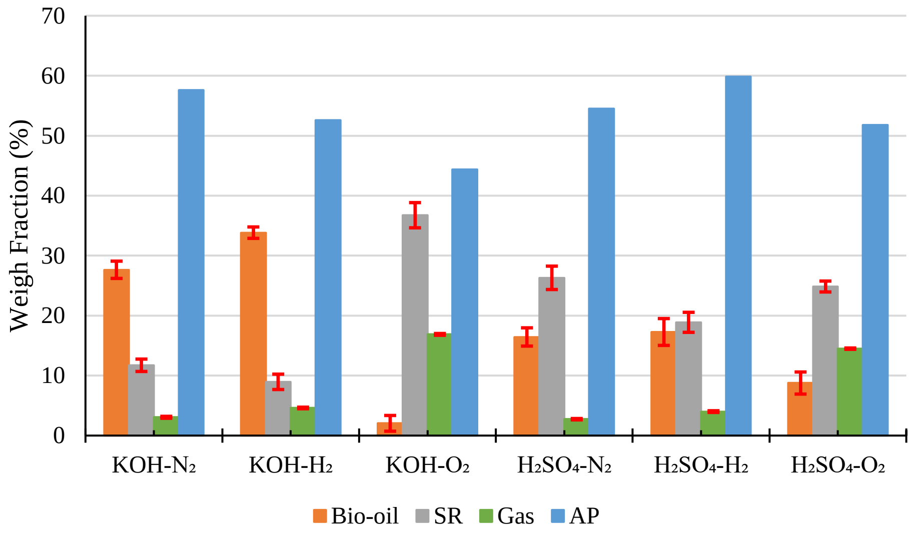

Figure 3.1: Products distribution from HTL of pinewood sawdust at 300 °C for 60 min under N_2, H_2, and O_2, respectively, with KOH or H_2SO_4 catalyst.

Table 3.2: Yield of gas products obtained from HTL of pinewood sawdust at 300 °C for 60 min under N_2, H_2, and O_2, respectively, with KOH or H_2SO_4 catalyst.

Yield of each gas species (mmol/g)	**Catalyst: KOH**			**Catalyst: H_2SO_4**		
	N_2	H_2	O_2	N_2	H_2	O_2
H_2	0.0612	-	0.0083	0.0662	-	0.0419
CH_4	0.0051	0.0024	0.0058	0.0019	0.0045	0.0103
CO	0.0818	0.1257	0.0301	0.0951	0.3487	0.1074
CO_2	0.6196	0.5562	3.7920	0.5628	0.3834	0.9146
C_2H_4	0.0004	0.0002	0.0006	0.0002	0.0011	0.0006

3.3.2 Properties of Bio-oil Products

Table 3.3 presents the results of the elemental compositions, HHV, viscosity, average molecular weights, and TAN of the obtained bio-oils from HTL of pinewood sawdust at 300 °C for 60 min under N_2, H_2, and O_2, respectively, with KOH or H_2SO_4 catalyst. In terms of elemental compositions of the bio-oil products, the effects of types of catalyst were minimal, but the atmosphere showed significant influence on elemental compositions and all other oil properties. Generally, the bio-oil obtained under N_2 and H_2 atmosphere have a better quality than those obtained under O_2 atmosphere: a higher H/C ratio, lower O/C ratio, higher HHV, lower TAN, much lower viscosity and much smaller M_n and M_w. HTL operations under N_2 and H_2 atmosphere also led to much higher energy recovery (65-73% with KOH catalyst and 35-42% with H_2SO_4 catalyst) than those under O_2 atmosphere (approx. 3% with KOH catalyst and 16% with H_2SO_4 catalyst). The HTL experiment using KOH catalyst under H_2 achieved the best energy recovery (ER ~ 73%) owing to the highest bio-oil production yield (~34 wt.%) obtained under these conditions. Surprisingly the H/C ratio of the bio-oils obtained under H_2 atmosphere (suggesting more condensed structure of the oils, whose causes require future research) is smaller than that of the oils obtained under N_2. However, different results were presented by Peng et al. [39] and Zhang et al. [46]. They reported that introducing reducing gas (e.g., H_2 and CO) in HTL process resulted in a product with slightly more C or H and less O content. The causes of this opposite result require future research. The oils obtained under H_2 atmosphere have better properties: a lower TAN, much lower viscosity and smaller Mn and Mw. Apparently, the bio-oils from the HTL experiments under H_2 atmosphere are much less viscous and have smaller molecular mass than the other oils obtained under N_2 or O_2 atmosphere, which could be attributed to reductive depolymerization reactions of the holocellulose, and lignin and hydro-cracking reactions occurs. These reactions would result in breakage of the C-O-C and C–C bonds of the complex macromolecular structure of biomass substrate/intermediates into simpler small-molecule substances [47], and hence a reduced viscosity of the bio-oil products. Compared with the average molecular weight of the Illinois shale oil (M_w = 670 g/mol, M_n = 270 g/mol) [48], the bio-oils from the HTL still have larger average molecular weights (M_w = 654-1347 g/mol, M_n = 417-753 g/mol), because deep-depolymerization of lignocellulose is very difficult by thermochemical approaches due to the unavoidable occurrence of self-condensation and repolymerization reactions during the conversion process [49].

In addition, the M_w and M_n of the bio-oils from the experiments with KOH catalyst are slightly higher than those with H_2SO_4 catalyst. This result might be owing to the acid-catalyzed cleavage of alkyl-aryl ether linkages, e.g., β-O-4 linkage, in lignin, as well as the acid-catalyzed breakage of the 1,4′-β-glycosidic bonds (β(1→4) linkage) in holocellulose [50]. Moreover, compared with oils obtained with KOH catalyst, the oils obtained with

H_2SO_4 catalyst are more acidic, and the oils obtained under O_2 atmosphere are much more acidic (with a greater TAN) than those obtained under N_2 and H_2, suggesting the presence of more organic acids in the bio-oils produced under the O_2 atmosphere, which can be confirmed by the GC-MS analysis results as discussed below.

Table 3.3: Properties of bio-oil products from HTL of pinewood sawdust at 300 °C for 60 min under N_2, H_2, and O_2, respectively, with KOH or H_2SO_4 catalyst.

	Catalyst: KOH			Catalyst: H_2SO_4		
	N_2	H_2	O_2	N_2	H_2	O_2
Ultimate analysis[a] (wt.%)						
C	72.95	72.44	51.83	72.22	71.52	69.75
H	5.86	4.63	2.95	5.55	3.78	3.18
N	0.16	0.05	0.21	0.08	0.06	0.08
S	n.d.[c]	n.d.[c]	n.d.[c]	n.d.[c]	n.d.[c]	n.d.[c]
O[b]	21.03	22.84	45.01	22.15	24.64	27.00
O/C	0.22	0.24	0.65	0.23	0.26	0.29
H/C	0.96	0.77	0.68	0.92	0.63	0.55
HHV[d](MJ/kg)	29.27	27.01	13.69	28.38	25.17	23.29
ER[e] (%)	64.76	73.14	2.81	41.91	34.81	16.34
Viscosity @ 80 °C, (cp)	84.1	51.2	113.6	86.4	64.4	109.7
TAN (mg KOH/g oil)	45.7	40.2	131.3	118.4	86.6	148.3
M_n (g/mol)	504	470	753	457	417	704
M_w (g/mol)	815	767	1347	721	654	1226
PDI	1.62	1.63	1.75	1.58	1.57	1.74

[a] On dry basis; [b] Calculated by difference %O = 100% - C% - H% - N% - S% - Ash%; [c] Not detected; [d] Calculated by Dulong equation; [e] Obtained by Eqn. (3.5)

The volatile compounds of the bio-oils were analyzed by GC-MS, as shown in **Figure 3.2**. The identified compounds are mainly carboxylic acids, alcohols, aldehydes, aromatics, esters, ethers, hydrocarbons, ketones, nitrogenous compounds, and phenols. It should be noted that only volatile fractions of bio-oils could be detected by GC-MS, accounting for only about 20 to 30 wt.% of the total bio-oil. The main volatile compounds in the oils obtained under N_2 and H_2 atmosphere with KOH catalysts are phenols and aromatic compounds, and the oils obtained under H_2 atmosphere contain more phenols than those obtained under N_2 atmosphere, likely owing to the reductive depolymerization of lignin [45, 51]. Similar results were obtained in the depolymerization of lignin conducted by Duangkaew et al. [52]. They found that condition under H_2 provided bio-oil with better quality than that under N_2 with more valuable phenolic compounds and other petrol-like products produced. In comparison to oils obtained under N_2 and H_2 atmosphere with KOH catalyst, the bio-oils obtained with H_2SO_4 catalyst contain much more carboxylic acids and ketones, suggesting acid-catalyzed degradation of cellulose and hemicellulose structures [53].

More interestingly, the oils from the HTL experiments under O_2 atmosphere contain much more acids than those obtained under H_2 or N_2. Estimated by the area %, the oils obtained under O_2 atmosphere with KOH or H_2SO_4 catalyst contain approx. 41% and 56% of acids, and hence much higher TAN and viscosity as evidenced in the results presented previously in **Table 3.3**. Under the oxygen atmosphere, phenols could also deprotonate to form phenoxy radicals by electron transfer on oxygen and be stabilized by the resonance, resulting in formation of carbonyl and carboxylic acid, and H_2SO_4 acid could also catalyze aromatic ring opening, leading to formation of pentatonic acids [54]. Similar phenomenon was confirmed in the study by Singh et al. [38]. They reported that oxidized products such as aldehydes, acids, and ketones, etc. were detected when O_2 were utilized, due to the oxidation of certain phenolic derivatives.

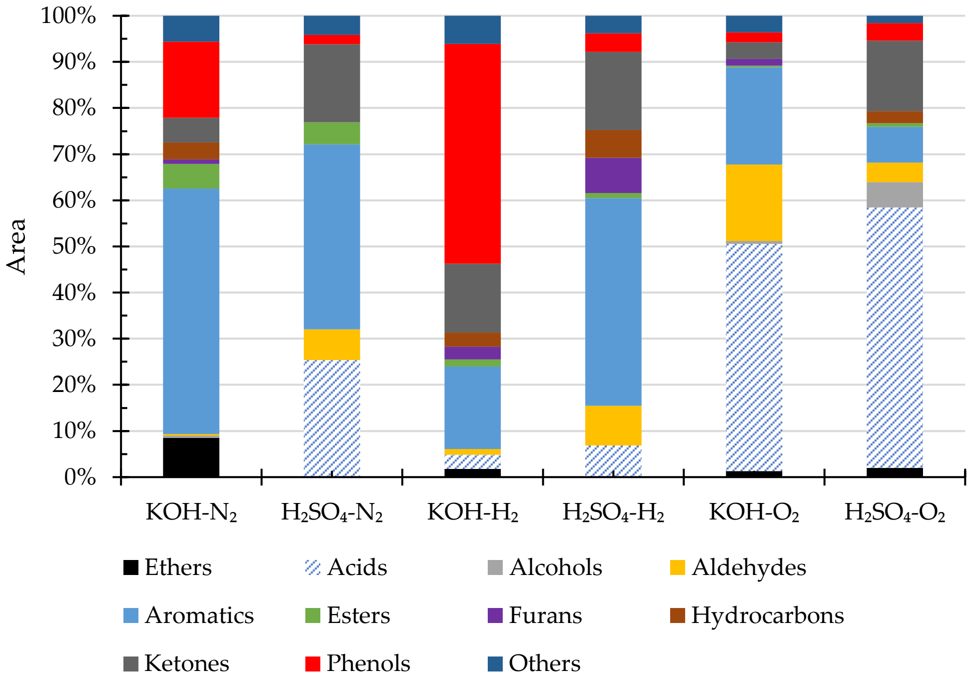

Figure 3.2: Volatile compositions (area% by GC-MS) of the bio-oil products from HTL of pinewood sawdust at 300 °C for 60 min under N_2, H_2, and O_2, respectively, with KOH or H_2SO_4 catalyst.

The functional groups of the bio-oils were identified by FT-IR and the spectra are illustrated in **Figure 3.3**. The broad IR absorption at 3350 cm^{-1} is typical of O-H stretching, suggesting the presence of alcohols, phenols, carboxylic acids, or water residues in the oils. The absorbance at 1700 cm^{-1}, representing the C=O stretching vibration of carbonyl groups, indicates the presence of ketones, aldehydes, esters or carboxylic acids in the oils. The relatively medium-intense peaks at 1611 and 1495 cm^{-1} represent aromatic nuclei, indicating the presence of aromatic rings and their derivatives. The IR absorption bands between 3000 and 2840 cm^{-1} are attributed to C-H stretching vibrations, indicating the presence of alkyl C-H in the oils. The two absorption peaks at 1370 and 1456 cm^{-1} are attributed to the bending vibrations of methyl ($-CH_3$) and methylene ($-CH_2$) groups, respectively. The presence of C-H bonds indicates the alkane groups in the bio-oils. The bands between 1280 and 1000 cm^{-1} could be related to C-O vibrations, suggesting that the oils may contain acids, phenols, furans, or alcohols. The presence of the peak at 860 cm^{-1}, attributed to C-H bending, suggests the possible presence of single, polycyclic, and substituted aromatics. In the oils obtained under O_2 atmosphere, more oxygen containing compounds were produced in the bio-oils, evidenced by the intensive peaks representing O-H, C=O and C-O bonds, compared to those of the oils obtained under N_2 or H_2 atmosphere. In addition, the intensities of aromatic absorptions at 1611 and 1495 cm^{-1} are weaker in the bio-oils obtained when using H_2SO_4 catalyst, especially under O_2 atmosphere, suggesting that the presence of oxidative agents (i.e., H_2SO_4 and O_2) could possibly restrict the aromaticity of reaction intermediates derived from lignin in pinewood.

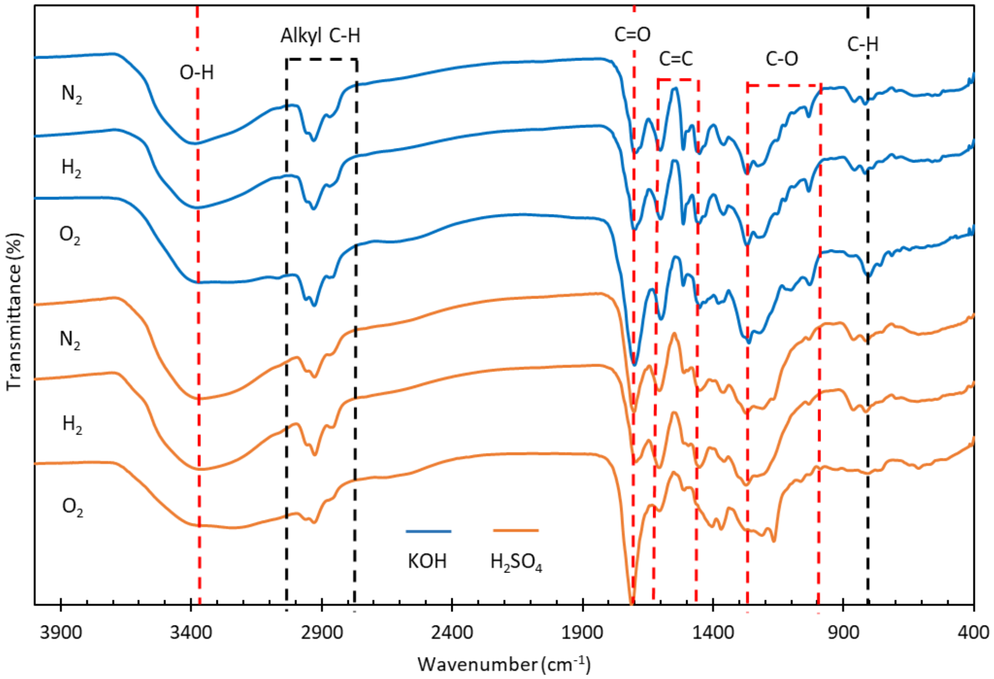

Figure 3.3: FT-IR spectra of bio-oil products from HTL of pinewood sawdust at 300 °C for 60 min under N_2, H_2, and O_2, respectively, with KOH or H_2SO_4 catalyst.

Figure 3.4 and **3.5** illustrate the thermogravimetric (TG) and derivative thermogravimetric (DTG) curves of the bio-oils obtained under N_2, H_2, and O_2, respectively, with KOH or H_2SO_4. Catalyst. The boiling point distributions of the oils, estimated from the TG curves, are presented in **Table 3.4**. The bio-oils obtained under N_2 and H_2 atmosphere had similar decomposition curves (TG). The initial decomposition of these bio-oils occurred at around 100-140 °C. Whereas, the decomposition of bio-oils from HTL of pinewood under O_2 started at around 160-180 °C. The distillate or volatile fractions of the oils (with a boiling point below 600 °C) obtained under N_2 and H_2 atmosphere vary from 59.21 wt.% to 67.26 wt.%, which fell in the range between North American tar sand bitumen (44 wt.% - 65 wt.% distillate) and the Venezuelan crude oil (66 wt.% distillate) [31,38]. However, the bio-oils produced under O_2 atmosphere are more thermally unstable with over 80 wt.% of volatile matters. Generally, the boiling point distributions of the oils obtained under N_2, and H_2 with KOH catalyst are similar, but the oil obtained under H_2 with has a higher light fraction <193 °C (23.89 wt.%). The oils obtained under O_2 have more mild boiling fractions (343 °C -538 °C) (55.85 wt.% with KOH catalyst, 35.43 wt.% with H_2SO_4 catalyst) and the least heavy residues fraction (>538 °C) (21.07 wt.% with KOH catalyst and 15.10 wt.% with H_2SO_4 catalyst).

The DTG curves (**Figure 3.5**) of the bio-oils show that the distillation peak temperatures appear at two main ranges: from room temperature to 300 °C and from 300 °C to 450 °C, respectively. The weight loss from room temperature to 300 °C could be due to the evaporation of the low molecular weight fractions in the oil samples. The major weight loss of all bio-oil samples occurred between 300 °C and 450 °C. Interestingly, intensive weight loss peaks were observed between 100 °C and 200 °C in the oils obtained under the H_2 atmosphere, likely owing to the presence of more low molecular weight compounds (e.g., phenols) that evaporate between 100 °C to 200 °C, which was confirmed by the GC-MS and GPC results discussed previously. The oils obtained under O_2 atmosphere are more thermally stable with large boiling points than those obtained under N_2 or H_2, with intensive weight loss peaks between 300 °C to 450 °C. In contrast, the DTG curves of the oils obtained under N_2 have flat and broad peaks across the entire temperature range.

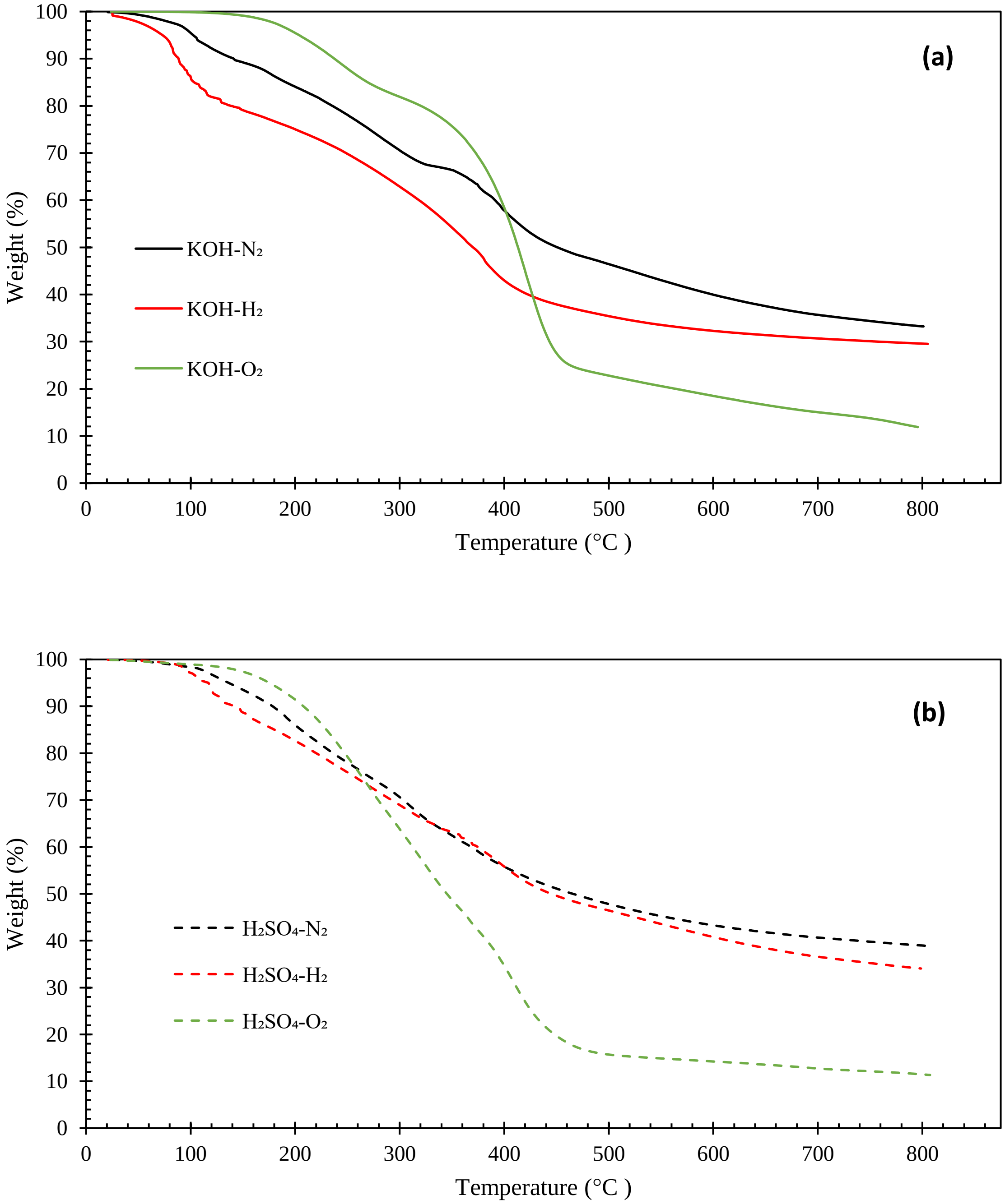

Figure 3.4: TG curves of bio-oil products from HTL of pinewood sawdust at 300 °C for 60 min under N_2, H_2, and O_2, respectively, with KOH (a) or H_2SO_4 (b) catalyst.

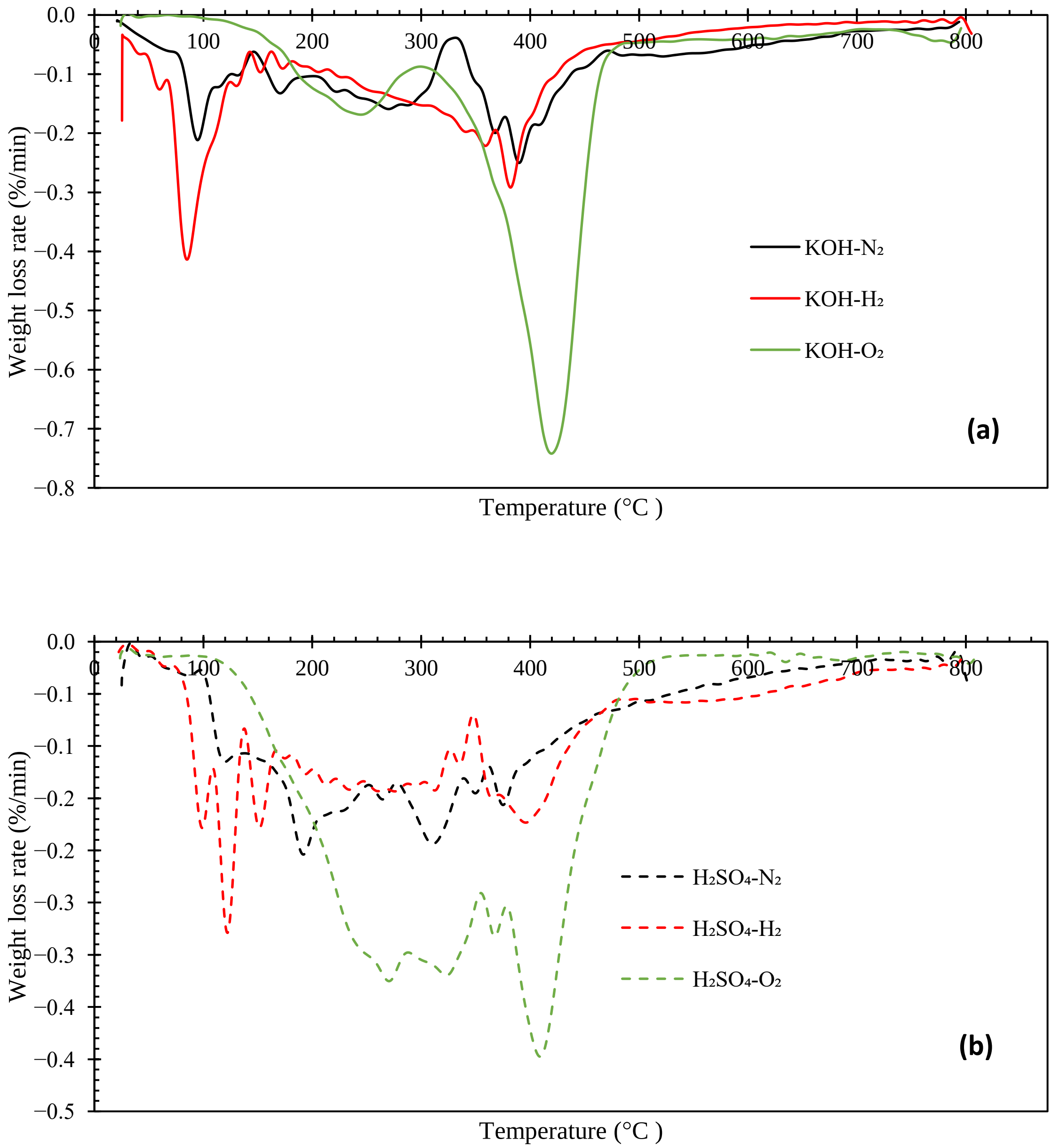

Figure 3.5: DTG curves of bio-oil products from HTL of pinewood sawdust at 300 °C for 60 min under N_2, H_2, and O_2, with KOH (a) or H_2SO_4 (b) catalyst.

Table 3.4: Boiling point distributions of the bio-oil products from HTL of pinewood sawdust at 300 °C for 60 min under N_2, H_2, and O_2, respectively, with KOH or H_2SO_4 catalyst.

Distillate range (°C)	Catalyst: KOH			Catalyst: H2SO4		
	N_2	H_2	O_2	N_2	H_2	O_2

<193 (Heavy Naphtha)	15.18	23.89	3.77	12.73	16.49	7.46
193-271 (Kerosene)	9.68	8.56	11.47	12.30	10.56	19.92
271-343 (Gas Oil)	8.27	11.64	7.84	11.56	9.28	22.09
343-538 (Vac Gas Oil)	22.97	21.52	55.85	17.56	19.42	35.43
>538 (Residues)	43.90	34.39	21.07	45.85	44.25	15.10
VM[a] (wt.%)	59.98	67.26	81.53	56.66	59.21	85.71
Ash (wt.%)	n.d[b]	n.d[b]	n.d[b]	n.d[b]	n.d[b]	n.d[b]
FC[c] (wt.%)	40.02	32.74	18.47	43.34	30.79	14.29

[a] Volatile matter, calculated by summing fractions below 600℃;

[b] Not detected;

[c] Fixed carbon, calculated by FC% = 100 - Ash - VM.

3.3.3 Cost-benefit Analysis

To perform a cost-benefit analysis of the HTL process, the costs and benefits associated with the process need to be considered, including capital investment (e.g., equipment and infrastructure, site development, engineering, etc.), operating costs (e.g., feedstock, labor, post-treatment, energy, maintenance, etc.), value of the produced oils, and environ-mental benefits. As mentioned above, the bio-oil produced under O_2 atmosphere has a higher oxygen content and average molecular weight compared to those obtained under N_2 and H_2 atmosphere and thus requires a much higher upgrading cost, including additional equipment, energy, and labor cost, to convert the bio-oil into gasoline-like products. In addition, the significant lower bio-oil yield from pinewood HTL process under O_2 atmosphere will increase the feedstock and labor cost as well due to the more raw materials consumed and longer operating time required to achieve the aimed producing capacity. Besides, the higher TAN value of bio-oil obtained under O_2 will cause corrosion problem on core HTL equipment, which will increase the maintenance costs. Although biomass HTL under H_2 atmosphere showed the best bio-oil yields and chemical properties, the safety issues accompanying H_2 will possibly cause additional operating cost (e.g., insurance, training, etc.). Thus, N_2 has been employed most often for biomass HTL. A comprehensive and detailed techno-economic assessment will be carried out in the future research.

3.4 Conclusions

The study investigated the effect of reaction atmosphere on hydrothermal liquefaction (HTL) of pinewood sawdust using KOH or H_2SO_4 catalyst at 300 °C with an initial pressure of 20 bar for 60 min under N_2, H_2, and O_2 atmospheres. The results showed that HTL under H_2 atmosphere with KOH catalyst led to the highest bio-oil yield (approx. 34 wt.%) and the lowest solid residue (SR) yield (approx. 9 wt.%). Bio-oils obtained under N_2 or H_2 exhibited higher energy recovery and better quality (higher H/C ratio, lower O/C ratio, higher HHV, lower TAN, and much lower viscosity and molecular weight) than those obtained under O_2. The oils produced in N_2 or H_2 atmosphere mainly contained phenols and aromatic compounds and showed similar boiling point distributions, while more acids were detected in the oils produced in O_2, which presented the highest mild boiling fractions and the least heavy residue fraction. Although some progress has been made in the reaction atmosphere effect on HTL process, there is still much room to explore. The influence of operating parameters (e.g., temperature, residence time) on HTL products produced under different atmospheres and the impact of more complex atmospheres comprising mixtures of gases (e.g., air, H_2 and N_2, or O_2 and N_2) requires further research, as well as the comparison of atmosphere effects in batch- and continuous HTL processes.

3.5 References

[1] M. Kumar, Y. Sun, R. Rathour, A. Pandey, I.S. Thakur, D.C. Tsang, Algae as potential feedstock for the production of biofuels and value-added products: Opportunities and challenges, Science of the Total Environment 716 (2020) 137116.

[2] E. Ahmad, N. Jäger, A. Apfelbacher, R. Daschner, A. Hornung, K. Pant, Integrated thermo-catalytic reforming of residual sugarcane bagasse in a laboratory scale reactor, Fuel Processing Technology 171 (2018) 277-286.

[3] A.I. Osman, M. Hefny, M. Abdel Maksoud, A.M. Elgarahy, D.W. Rooney, Recent advances in carbon capture storage and utilisation technologies: a review, Environmental Chemistry Letters 19(2) (2021) 797-849.

[4] S. Zhang, X. Yang, H. Zhang, C. Chu, K. Zheng, M. Ju, L. Liu, Liquefaction of biomass and upgrading of bio-oil: a review, Molecules 24(12) (2019) 2250.

[5] M. Antar, D. Lyu, M. Nazari, A. Shah, X. Zhou, D.L. Smith, Biomass for a sustainable bioeconomy: An overview of world biomass production and utilization, Renewable and Sustainable Energy Reviews 139 (2021) 110691.

[6] L. Nazari, C.C. Xu, M.B. Ray, Advanced Technologies (Biological and Thermochemical) for Waste-to-Energy Conversion, Green Chemistry and Sustainable Technology Advanced and Emerging Technologies for Resource Recovery Singapore, 2021, pp. 55-95.

[7] E. Demirkaya, O. Dal, A. Yüksel, Liquefaction of waste hazelnut shell by using sub- and supercritical solvents as a reaction medium, The Journal of Supercritical Fluids 150 (2019) 11-20.

[8] L. Cao, K. Iris, X. Xiong, D.C. Tsang, S. Zhang, J.H. Clark, C. Hu, Y.H. Ng, J. Shang, Y.S. Ok, Biorenewable hydrogen production through biomass gasification: A review and future prospects, Environmental research 186 (2020) 109547.

[9] H. Chen, W. Qiu, Key technologies for bioethanol production from lignocellulose, Biotechnology advances 28(5) (2010) 556-562.

[10] T.P.T. Pham, R. Kaushik, G.K. Parshetti, R. Mahmood, R. Balasubramanian, Food waste-to-energy conversion technologies: Current status and future directions, Waste management 38 (2015) 399-408.

[11] R. Singh, B.B. Krishna, G. Mishra, J. Kumar, T. Bhaskar, Strategies for selection of thermo-chemical processes for the valorisation of biomass, Renewable energy 98 (2016) 226-237.

[12] T.H. Seehar, S.S. Toor, K. Sharma, A.H. Nielsen, T.H. Pedersen, L.A. Rosendahl, Influence of process conditions on hydrothermal liquefaction of eucalyptus biomass for biocrude production and investigation of the inorganics distribution, Sustainable Energy & Fuels 5(5) (2021) 1477-1487.

[13] A. Weir, A.J. del Barco Carrión, C. Queffélec, B. Bujoli, E. Chailleux, C. Uguna, C. Snape, G. Airey, Renewable binders from waste biomass for road construction: A review

on thermochemical conversion technologies and current developments, Constrcution and Building Materials 330 (2022) 127076.

[14] R. Singh, B. Balagurumurthy, A. Prakash, T. Bhaskar, Catalytic hydrothermal liquefaction of water hyacinth, Bioresource technology 178 (2015) 157-165.

[15] Y. Xu, M. Li, Hydrothermal liquefaction of lignocellulose for value-added products: Mechanism, parameter and production application, Bioresource technology 342 (2021) 126035.

[16] R.K. Mishra, P. Kumar, K. Mohanty, Hydrothermal liquefaction of biomass for bio-crude production: A review on feedstocks, chemical compositions, operating parameters, reaction kinetics, techno-economic study, and life cycle assessment, Fuel 316 (2022) 123377.

[17] A. Gollakota, N. Kishore, S. Gu, A review on hydrothermal liquefaction of biomass, Renewable and Sustainable Energy Reviews 81 (2018) 1378-1392.

[18] S. Pang, Advances in thermochemical conversion of woody biomass to energy, fuels and chemicals, Biotechnology advances 37(4) (2019) 589-597.

[19] S. Nagappan, R.R. Bhosale, D.D. Nguyen, N.T.L. Chi, V.K. Ponnusamy, C.S. Woong, G. Kumar, Catalytic hydrothermal liquefaction of biomass into bio-oils and other value-added products–A review, Fuel 285 (2021) 119053.

[20] A. Dimitriadis, S. Bezergianni, Hydrothermal liquefaction of various biomass and waste feedstocks for biocrude production: A state of the art review, Renewable and Sustainable Energy Reviews 68 (2017) 113-125.

[21] L. Cao, C. Zhang, S. Hao, G. Luo, S. Zhang, J. Chen, Effect of glycerol as co-solvent on yields of bio-oil from rice straw through hydrothermal liquefaction, Bioresource technology 220 (2016) 471-478.

[22] L. Cao, C. Zhang, H. Chen, D.C. Tsang, G. Luo, S. Zhang, J. Chen, Hydrothermal liquefaction of agricultural and forestry wastes: state-of-the-art review and future prospects, Bioresource technology 245 (2017) 1184-1193.

[23] M.K. Jindal, M.K. Jha, Effect of process parameters on hydrothermal liquefaction of waste furniture sawdust for bio-oil production, RSC advances 6(48) (2016) 41772-41780.

[24] S. Cheng, I. D'cruz, M. Wang, M. Leitch, C. Xu, Highly efficient liquefaction of woody biomass in hot-compressed alcohol− water co-solvents, Energy & Fuels 24(9) (2010) 4659-4667.

[25] L. Ye, J. Zhang, J. Zhao, S. Tu, Liquefaction of bamboo shoot shell for the production of polyols, Bioresource technology 153 (2014) 147-153.

[26] I.A. Basar, H. Liu, H. Carrere, E. Trably, C. Eskicioglu, A review on key design and operational parameters to optimize and develop hydrothermal liquefaction of biomass for biorefinery applications, Green Chemistry 23(4) (2021) 1404-1446.

[27] Z. Zhu, L. Rosendahl, S.S. Toor, G. Chen, Optimizing the conditions for hydrothermal liquefaction of barley straw for bio-crude oil production using response surface methodology, Science of the Total Environment 630 (2018) 560-569.

[28] R. Obeid, N. Smith, D.M. Lewis, T. Hall, P. van Eyk, A kinetic model for the hydrothermal liquefaction of microalgae, sewage sludge and pine wood with product characterisation of renewable crude, Chemical Engineering Journal 428 (2022) 131228.

[29] F. Cheng, M.D. Porter, L.M. Colosi, Is hydrothermal treatment coupled with carbon capture and storage an energy-producing negative emissions technology?, Energy conversion and management 203 (2020) 112252.

[30] Y. Zhang, W.-T. Chen, Hydrothermal liquefaction of protein-containing feedstocks, Direct Thermochemical Liquefaction for Energy Applications, Elsevier2018, pp. 127-168.

[31] S. Yin, R. Dolan, M. Harris, Z. Tan, Subcritical hydrothermal liquefaction of cattle manure to bio-oil: Effects of conversion parameters on bio-oil yield and characterization of bio-oil, Bioresource technology 101(10) (2010) 3657-3664.

[32] A. Rahimi, A. Azarpira, H. Kim, J. Ralph, S.S. Stahl, Chemoselective metal-free aerobic alcohol oxidation in lignin, Journal of the American Chemical Society 135(17) (2013) 6415-6418.

[33] A. Rahimi, A. Ulbrich, J.J. Coon, S.S. Stahl, Formic-acid-induced depolymerization of oxidized lignin to aromatics, Nature 515(7526) (2014) 249-252.

[34] L. Qian, B. Zhao, H. Wang, G. Bao, Y. Hu, C.C. Xu, H. Long, Valorization of the spent catalyst from flue gas denitrogenation by improving bio-oil production from hydrothermal liquefaction of pinewood sawdust, Fuel 312 (2022) 122804.

[35] R. Jaswal, A. Shende, W. Nan, V. Amar, R. Shende, Hydrothermal liquefaction and photocatalytic reforming of pinewood (pinus ponderosa)-derived acid hydrolysis residue for hydrogen and bio-oil production, Energy & Fuels 33(7) (2019) 6454-6462.

[36] R. Kaur, P. Gera, M.K. Jha, T. Bhaskar, Reaction parameters effect on hydrothermal liquefaction of castor (Ricinus Communis) residue for energy and valuable hydrocarbons recovery, Renewable energy 141 (2019) 1026-1041.

[37] R. Kaur, B. Biswas, J. Kumar, M.K. Jha, T. Bhaskar, Catalytic hydrothermal liquefaction of castor residue to bio-oil: Effect of alkali catalysts and optimization study, Industrial crops and products 149 (2020) 112359.

[38] R. Singh, K. Chaudhary, B. Biswas, B. Balagurumurthy, T. Bhaskar, Hydrothermal liquefaction of rice straw: effect of reaction environment, The Journal of Supercritical Fluids 104 (2015) 70-75.

[39] W. Peng, C. Wu, S. Wu, Y. Wu, J. Gao, The effects of reaction atmosphere on composition, oxygen distribution, and heating value of products from the hydrothermal liquefaction of corn stalk, Energy Sources, Part A: Recovery, Utilization, and Environmental Effects 36(4) (2014) 347-356.

[40] Y. Hu, Z. Gu, W. Li, C.C. Xu, Alkali-catalyzed liquefaction of pinewood sawdust in ethanol/water co-solvents, Biomass and Bioenergy 134 (2020) 105485.

[41] R.V. Santos, M.A. Mendes, C. Alexandre, M.R. Carrott, A. Rodrigues, A.F. Ferreira, Assessment of Biomass and Biochar of Maritime Pine as a Porous Medium for Water Retention in Soils, Energies 15(16) (2022) 5882.

[42] S.R. Ravichandran, C.D. Venkatachalam, M. Sengottian, S. Sekar, S. Kandasamy, K.P.R. Subramanian, K. Purushothaman, A.L. Chandrasekaran, M. Narayanan, A review on hydrothermal liquefaction of algal biomass on process parameters, purification and applications, Fuel 313 (2022) 122679.

[43] S. Yin, Z. Tan, Hydrothermal liquefaction of cellulose to bio-oil under acidic, neutral and alkaline conditions, Applied Energy 92 (2012) 234-239.

[44] W. Yang, X. Li, D. Zhang, L. Feng, Catalytic upgrading of bio-oil in hydrothermal liquefaction of algae major model components over liquid acids, Energy conversion and management 154 (2017) 336-343.

[45] S. Huang, N. Mahmood, M. Tymchyshyn, Z. Yuan, C.C. Xu, Reductive de-polymerization of kraft lignin for chemicals and fuels using formic acid as an in-situ hydrogen source, Bioresource technology 171 (2014) 95-102.

[46] J. Zhang, W.-T. Chen, P. Zhang, Z. Luo, Y. Zhang, Hydrothermal liquefaction of Chlorella pyrenoidosa in sub-and supercritical ethanol with heterogeneous catalysts, Bioresource technology 133 (2013) 389-397.

[47] M. Saber, B. Nakhshiniev, K. Yoshikawa, A review of production and upgrading of algal bio-oil, Renewable and Sustainable Energy Reviews 58 (2016) 918-930.

[48] D.R. Vardon, B.K. Sharma, G.V. Blazina, K. Rajagopalan, T.J. Strathmann, Thermochemical conversion of raw and defatted algal biomass via hydrothermal liquefaction and slow pyrolysis, Bioresource technology 109 (2012) 178-187.

[49] D.R. Vardon, B. Sharma, J. Scott, G. Yu, Z. Wang, L. Schideman, Y. Zhang, T.J. Strathmann, Chemical properties of biocrude oil from the hydrothermal liquefaction of Spirulina algae, swine manure, and digested anaerobic sludge, Bioresource technology 102(17) (2011) 8295-8303.

[50] N. Mahmood, Z. Yuan, J. Schmidt, C.C. Xu, Hydrolytic depolymerization of hydrolysis lignin: Effects of catalysts and solvents, Bioresource technology 190 (2015) 416-419.

[51] B. Hao, D. Xu, G. Jiang, T.A. Sabri, Z. Jing, Y. Guo, Chemical reactions in the hydrothermal liquefaction of biomass and in the catalytic hydrogenation upgrading of biocrude, Green Chemistry 23(4) (2021) 1562-1583.

[52] N. Duangkaew, W. Pattaraprakorn, N. Grisdanurak, S. Neramittagapong, Utilization of black-liquor by hydrothermal liquefaction, Materials Today: Proceedings 75 (2023) 99-105.

[53] W.-T. Chen, Y. Zhang, J. Zhang, L. Schideman, G. Yu, P. Zhang, M. Minarick, Co-liquefaction of swine manure and mixed-culture algal biomass from a wastewater treatment system to produce bio-crude oil, Applied Energy 128 (2014) 209-216.

[54] M. Camus, O. Condassamy, F. Ham-Pichavant, C. Michaud, S. Mastroianni, G. Mignani, E. Grau, H. Cramail, S. Grelier, Oxidative Depolymerization of Alkaline Lignin from Pinus Pinaster by Oxygen and Air for Value-Added Bio-Sourced Synthons, Polymers 13(21) (2021) 3725.

Chapter 4

4 Development of a Kinetic Model based on Chemical Compositions of Lignocellulosic Biomass for Predicting Product Yields from Hydrothermal Liquefaction under N_2 Atmosphere

Abstract

This study aimed to develop a kinetic model to predict product yields from hydrothermal liquefaction (HTL) of lignocellulosic biomass based on its chemical compositions (contents of cellulose, hemicellulose, and lignin). HTL experiments were carried out with biomass model compounds (cellulose, xylan, and lignin) and lignocellulosic biomass (bamboo, cornstalk, and pinewood) at various temperatures (225-300 °C) and reaction times (10-60 min) with K_2CO_3 catalyst. Out of the three major components of lignocellulosic biomass, lignin was found to be the main contributor to bio-oil formation. A universal reaction network was proposed, and a kinetic model was developed based on the experimental results obtained from HTL of biomass model compounds. The kinetic parameters were determined by the lease-squares method using a MATLAB optimization function. Assuming no interactions among the components (cellulose, hemicellulose, and lignin) of lignocellulosic biomass during HTL, a kinetic model was developed based on the chemical compositions of lignocellulosic biomass and the kinetic parameters obtained from the model compound. The developed model was validated with our experimental results from HTL of bamboo, cornstalk, and pinewood and the publicly available HTL data in literature obtained with lignocellulosic biomass feedstocks.

Keywords: Kinetic model, Hydrothermal liquefaction, Lignocellulosic biomass, Model compounds, Reaction network

4.1 Introduction

In recent years, the rapid increase in the demand for clean energy and green chemicals as well as concerns over the supply and environmental impacts associated with fossil resources have stimulated intensive research on exploring alternatives to fossil resources for both energy and chemical production. Among all the potential alternatives, bioresources, such as lignocellulosic biomass, food waste and algal biomass, are promising candidates to produce bioenergy and bio-based chemicals owing to their renewability and sustainability characteristics [1-3].

Utilization of lignocellulosic biomass such as forestry and agricultural residues has received a particular interest in recent past, as these feedstocks are generated in abundant amounts in forestry and agricultural sectors. However, direct application of lignocellulosic biomass is challenging not only because it is usually bulky and hence difficult to transport, handle, and store, but it has a much lower energy density based on either volume or mass compared to fossil fuels [4]. It is thus desirable and necessary to convert raw biomass materials into gaseous, liquid, or solid biofuels before further applications. Typical conversion technologies include biochemical and thermochemical processes. Biochemical conversion methods, mainly referring to fermentation of wet carbohydrate materials into bioethanol and anaerobic digestion to generate biogas at ambient operation conditions [5], are sensitive to operating conditions (pH, temperature, etc.) and require long processing time ranging from days to weeks [6]. In contrast, thermochemical conversion processes, such as combustion, gasification, pyrolysis and HTL, are much faster owing to their high-temperature operating conditions. Compared to other thermochemical conversion methods, HTL is more cost-effective to process lignocellulosic biomass with moisture content of over 30% [7]. Particularly, HTL is advantageous for the conversion of wet and waste biomass feedstocks such as “black liquor” from pulp mills, wastewater sludge, food wastes and newly harvested algal biomass, etc. [4].

HTL processes are typically performed in the presence of water or water-alcohol mixed solvents or other organic solvents at mild temperature of 200–400 °C and elevated pressure of 5–25 MPa with/without a catalyst to directly decompose the macromolecules of biomass into bio-oil products - fragments of light molecules [8]. The research of biomass HTL mostly focuses on the effects of operating parameters (resistance time, reaction temperature, and feedstock to solvent ratio), biomass feedstocks (algae, lignocellulosic biomass, food waste, manure, etc.), and catalysts on production efficiency and chemical properties of the products [9-24] . Generally, the increase in the residence time and temperature, up to a certain extent, have demonstrated promoting effects on the production of bio-oil with a higher heating value (HHV), beyond which a further increase in time or temperature would inhibit oil production due to the occurrence of bio-oil cracking and repolymerization [8, 25]. Similarly, increasing solvent-to-biomass ratio to some extent resulted in higher bio-oil yields [26, 27], but a too high solvent amount would decrease oil yield, due to competition between hydrolysis and repolymerization reactions [22, 28-30]. The feedstock type and composition could also significantly affect the overall product yields and physicochemical properties of bio-oil [29, 31]. As a general trend the HTL conversion efficiency of different biomass constituents decreases in the order of lipids > proteins > hemicellulose > cellulose > lignin. Thus, the more lignin that the biomass contains, the higher operating temperature was required [20, 32]. Catalyst is another factor that affects HTL bio-oil yield. The most commonly used catalysts are homogeneous alkaline catalysts [33]. Previous studies showed that the addition of homogeneous alkaline catalysts could significantly enhance the liquefaction of lignocellulosic biomass into bio-oil products [34, 35]. During the HTL treatment of pinewood sawdust, effect of alkaline catalysts on the feedstock conversion was reported in the order of $K_2CO_3 > KOH > Na_2CO_3 > NaOH$; the corresponding conversion efficiency decreased from 96.0% to 86.0%, and the bio-oil yield from 33.7% to 22.4% [36-39]. In contrast, the addition of mineral acid catalysts, such as sulfuric acid, led to a reduction in oil yield [35]. The use of organic acid catalysts like acetic acid and formic acid increased the bio-oil yield, but these acids were found to be consumed during the reaction suggesting that they would act as both a catalyst and a reactant [40]. Heterogeneous catalysts such as metals (Pt, Pd, Mo, Ni, Ru, and others) supported on active carbon, SiO_2, Al_2O_3, and zeolite, that are widely applied in biomass gasification, were also extensively studied for biomass HTL [41, 42]. Among all homogeneous and heterogeneous catalysts, alkaline catalysts are still the most promising for HTL of lignocellulosic biomass as they could effectively enhance bio-oil yield by 50–135%, balance the pH of the reaction media, and avoid the repolymerization of biocrude-forming fragments and thus reduce the formation of solid residue/char [1].

Despite extensive study on the HTL conversion of biomass, significant knowledge gaps exist particularly in not fully elucidated reaction pathway and lack of predictability for the product yields. Recently, a few studies on the kinetics of HTL of various biomass feedstocks in lab-scale batch reactors were reported. Zhang et al. proposed a model for HTL of softwood kraft lignin based on the mechanism of two-phase reactions (the fast and the slow reaction phases) in the temperature range of 300-380 °C [43]. Hardi et al. used a face centered central composite design to correlate the yields and properties of sawdust HTL products with HTL temperature, time, and feedstock concentration [44]. However, these models are only applicable to the specific feedstock used in the corresponding studies. Thus, several attempts have been made to develop product yield-prediction models for biomass based on their composition [32, 45, 46], but these models are only able to predict HTL product yields under specific processing conditions. Valdez et al. [47], Hietala et al. [48], and Vo et al. [49] further developed kinetic models of HTL reaction networks for HTL of algal biomass based on the feedstock composition to estimate the product yields at varying reaction temperature/time. However, those models were developed and applied only to algal biomass, not applicable for HTL of lignocellulosic biomass. In this work, for the first time a kinetic model based on the chemical compositions (cellulose, hemicellulose, and lignin) of lignocellulosic biomass was developed to predict product yields (gas, liquid, and solid residue) and elucidate the reaction pathways and mechanisms in HTL of lignocellulosic biomass. Such kinetic model will be also useful for scaling up the HTL technology for industrial applications.

4.2 Materials and Methods

4.2.1 Materials

Model compounds for lignocellulosic biomass (cellulose, xylan representing hemicellulose, and alkali lignin) were all purchased from Sigma-Aldrich. lignocellulosic biomass feedstocks (bamboo sawdust, cornstalk, and pinewood sawdust) were obtained from a bamboo sawmill in South China, Ontario Federation of Agriculture (OFA) and a local wood sawmill in London Ontario, respectively. Potassium carbonate (K_2CO_3), used as the catalyst in this study, was purchased from Sigma-Aldrich. The ACS reagent-grade acetone used for bio-oil product recovery, was purchased from Caledon Laboratory Chemicals (ON, Canada). All chemicals were used as received.

4.2.2 Hydrothermal Liquefaction

HTL of the model compounds and various lignocellulosic biomass feedstocks were conducted in a 500 mL stainless steel (SS316L) batch reactor (Parr 4570 HP/HT Reactor) system, as schematically illustrated in **Figure 4.1**, to collect essential data for the development of a kinetic model for HTL of lignocellulosic biomass. The water/feedstock mass ratio was kept at 15:1 under different temperatures (225, 250, 275, or 300 °C) for various time duration (10, 20, 30, or 60 min) at the specific temperature in the presence of K_2CO_3 catalyst (catalyst loading: 5 wt.% of dry biomass). In a typical run, 10 g biomass feedstock, 150 g water, and 0.5 g K_2CO_3 were loaded into the reactor. The reactor was then sealed and the air inside was removed by vacuuming and purging with nitrogen for at least three times. Then the reactor was pressurized to 2 MPa using nitrogen and heated under stirring at 172 rpm to the desired temperature (225, 250, 275, or 300 °C) and maintained at that temperature for certain time (10, 20, 30, or 60 min).

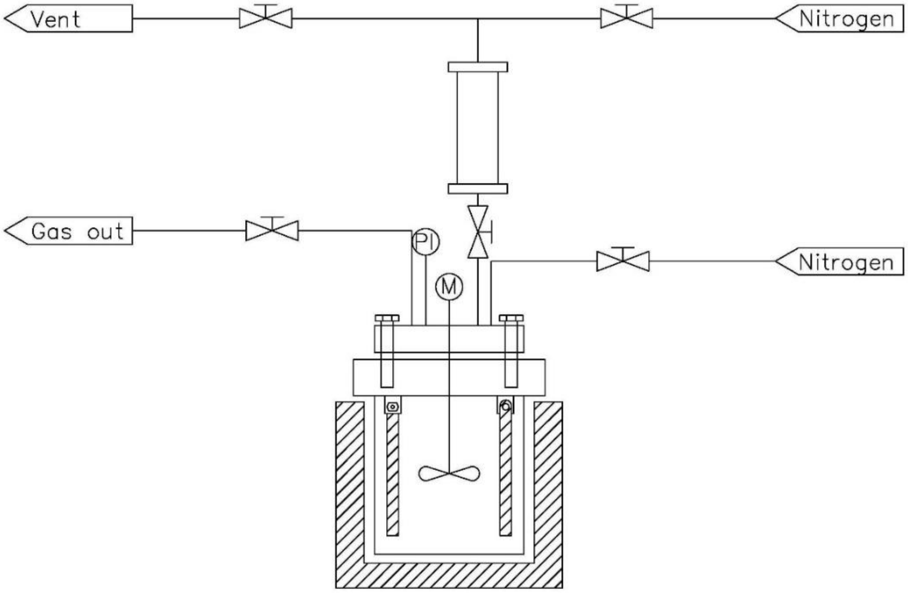

Figure 4.1: Schematic diagram of the 500 mL batch reactor for HTL.

4.2.3 Products Collection and Separation

The products were collected and separated based on the similar separation procedure of pinewood sawdust in **Section 3.2.2.2.** The products from the HTL experiments include gaseous products, bio-oil, aqueous-phase (AP) products, and solid residues (SR). The yields of products are calculated by the wt.% of the product in relation to dry mass of the feedstock, as follows:

$$\text{Yield of bio oil (wt.\%)} = \frac{\text{mass of bio oil}}{\text{dry mass of feedstock}} \times 100 \qquad (4.1)$$

$$\text{Yield of gas (wt.\%)} = \frac{\text{mass of gas}}{\text{dry mass of feedstock}} \times 100 \qquad (4.2)$$

$$\text{Yield of SR (wt.\%)} = \frac{\text{mass of solid residue}}{\text{dry mass of feedstock}} \times 100 \qquad (4.3)$$

$$\text{Yield of AP (wt.\%)} = 100 - \text{bio oil} - \text{SR} - \text{gas} \qquad (4.4)$$

4.2.4 Feedstock and Products Analysis

The moisture content was removed by drying the feedstocks in oven at 105 °C for 24 h. The element compositions (C, H, N, and S) of feedstocks were analyzed using an elemental analyzer (Vario EL Cube). The O content was calculated by difference on dry basis (%O = 100% - %Ash - %C - %H - %N - %S) where the ash contents were determined by heating the feedstocks at 700 °C in air for 4 h in a muffle furnace. The higher heating values (HHVs) of all feedstocks, bio-oil, and solid residue were calculated by Dulong equation [HHV (MJ/kg) = 0.338C + 1.428(H-O/8) + 0.095S]. The proximate analysis of the feedstocks was conducted using a thermogravimetric analyzer (Pris 1 TGA), where the sample was heated in 30 mL/min N_2 flow from 25 °C to 800 °C at 10 °C /min, followed by soaking at 800 °C for 15 min in 30 mL/min air flow for ashing. NREL/TP-510-42718 method was used to determine the compositional contents of lignin, cellulose, and hemicellulose in oven-dried lignocellulosic feedstocks.

Table 4.1 shows the proximate, compositional, and ultimate analyses of the lignocellulosic biomass model compounds and feedstocks.

Table 4.1: Proximate, compositional, and ultimate analyses of the lignocellulosic biomass model compounds and feedstocks.

Feedstock	Cellulose	Xylan	Lignin	Bamboo	Cornstalk	Pinewood
Proximate analysis (wt.%)[a]						
Volatile matters	93.08	69.67	38.01	83.39	74.65	81.54
Fixed carbon	6.92	30.33	61.99	16.17	22.91	17.84
Compositional analysis (wt.%)[a]						
Cellulose[b]	-	-	-	38.81	35.31	40.70
Xylan[c]	-	-	-	18.64	31.26	25.82
Lignin[d]	-	-	-	30.25	19.89	26.80
Ash[e]	-	-	2.31	0.44	2.44	0.63
Extractives	-	-	-	11.86	11.10	6.05
Ultimate analysis (wt.%)[a]						
C	41.81	39.93	46.70	47.24	44.85	46.96
H	6.03	6.84	4.97	6.18	5.71	6.03
N	0.04	0.03	0.11	0.21	0.50	0.01
S	<0.01	<0.01	3.75	<0.01	<0.01	<0.01
O[f]	52.12	53.20	42.16	45.93	46.50	46.37
HHV (MJ/kg)[g]	13.44	13.77	15.71	16.59	15.02	16.21

4.2.5 Reaction Network and Kinetic Model

Lignocellulosic biomass mainly contains cellulose, hemicellulose, and lignin. Under HTL conditions, initially cellulose and hemicellulose would be hydrolyzed to C_5 or C_6 sugars, which are then isomerized into aldose and alcohol sugars. They will undergo additional reactions such as degradation and dehydration to form unstable C_2–C_4-based intermediate products or stable C_2–C_4 alcohols and other substances due to the presence of carbonyl groups, some of which would contribute to the aqueous-phase products, while others can condense into solid residue or bio-oil. On the other hand, the lignin component is initially hydrolytically depolymerized/degraded into phenolic monomers/oligomers and methoxy benzene through the cleavage of C-O ether bonds, which would further condense into bio-oils or solid residue or convert/decompose into aqueous phase and gas products, following the reaction network as shown in **Figure 4.2** [50]. This reaction network, as shown in **Figure 4.2**, combines the light and heavy bio-oil fractions into a lump bio-oil and takes solid residue (SR) fraction into consideration. The reaction rates are expressed as follows:

$$\frac{dX_{feed}}{dt} = -(k_1 + k_2 + k_3)X_{feed} \tag{4.5}$$

$$\frac{dX_{AP}}{dt} = k_1X_{feed} + k_5X_{oil} - (k_4 + k_7)X_{AP} \quad (4.6)$$

$$\frac{dX_{oil}}{dt} = k_2X_{feed} + k_4X_{AP} - (k_5 + k_6 + k_8)X_{oil} \quad (4.7)$$

$$\frac{dX_{SR}}{dt} = k_3X_{feed} + k_6X_{oil} \quad (4.8)$$

$$\frac{dX_{gas}}{dt} = k_7X_{AP} + k_8X_{oil} \quad (4.9)$$

where X_{feed}, X_{AP}, X_{oil}, X_{SR}, and X_{gas} (wt.%) refer to mass fractions of the feedstock, aqueous phase product, bio-oil product, solid residue, and gaseous product, respectively. k_1-k_8 (min^{-1}) are the reaction rate constants of each reaction pathway.

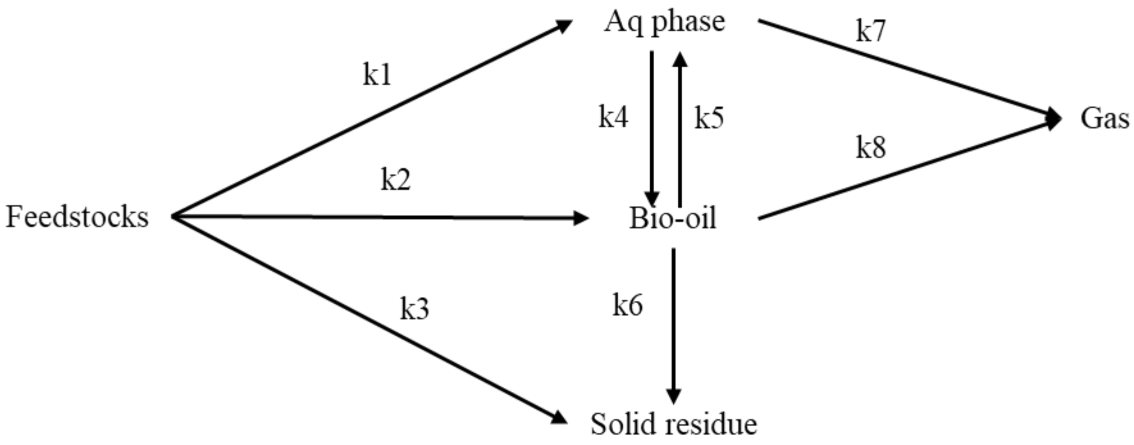

Figure 4.2: The reaction network proposed for HTL of lignocellulosic feedstocks.

The rate constants (k_i, min^{-1}) were estimated using the nonlinear least square method (i.e., minimizing the sum of the square of the difference between the simulation results Y_{cal} and the experimental data Y_{exp}), as expressed in the following objective function:

$$f = \min \sum_{i=1}^{N} (Y_{cal} - Y_{exp})^2 \quad (4.10)$$

In this work, MATLAB optimization function was used to minimize *f* at each reaction temperature. Initially, the boundary conditions of the rate constants were fixed within 0.00-0.40 min^{-1}, and the fixed-step size for the solver was 0.5 s. This step size was found to be short enough to achieve converged solutions. The determined values for the rate constant *k* at different temperatures were used to calculate the activation energy for each reaction pathway based on the Arrhenius equation:

$$\mathrm{k} = \mathrm{A}\exp\frac{-\mathrm{E}}{\mathrm{RT}} \tag{4.11}$$

where *T* is the reaction temperature, *A* is the Arrhenius constant, *E* (is the activation energy, and *R* is the molar gas constant (8.314 J/K/mol). Taking the natural logarithm, Eqn. (4.11) can be further expressed as:

$$\ln\mathrm{k} = \ln\mathrm{A} - \frac{\mathrm{E}}{\mathrm{R}}\left(\frac{1}{\mathrm{T}}\right) \tag{4.12}$$

Through linear fitting of lnk vs. $\frac{1}{T}$, the activation energies *E* and the pre-exponential factors *A* were thus determined.

The predicted yield of each product from HTL of lignocellulosic biomass, $\widehat{\mathrm{Y}_\imath}$, was calculated additively from the product yields of the compositional components in the whole biomass using the algebraic equation below:

$$\widehat{\mathrm{Y}_\imath} = \sum\nolimits_{\mathrm{i}} \widehat{y_\imath}\, \mathrm{x_i} \tag{4.13}$$

Where $\widehat{y_\imath}$ is the yield of each product calculated from the kinetic model of individual model compounds (i.e., cellulose, xylan, lignin), $\mathrm{x_i}$ is the mass fraction of compositional components (cellulose, hemicellulose, and lignin) in the dried lignocellulosic biomass.

To assess the quality/reliability of the model predictions, the root mean square deviation (RMSD) and mean absolute percentage error (MAPE) were calculated for each product yield and will be discussed in the Results and Discussion Section:

$$\mathrm{RMSD} = \sqrt{\frac{\sum_{\mathrm{i}=1}^{\mathrm{N}}\left(\mathrm{Y_i} - \widehat{\mathrm{Y}_\imath}\right)^2}{\mathrm{N}}} \tag{4.14}$$

$$\mathrm{MAPE} = \frac{1}{N}\sum\nolimits_{i=1}^{N}\left|\frac{Y_i - \widehat{Y_\imath}}{Y_i}\right| \tag{4.15}$$

Where $\widehat{Y_i}$ is the predicted yield of each product from HTL of lignocellulosic biomass, Y_i is the experimental result from HTL of real biomass, N is the number of data points.

For simplicity, the assumptions made for this kinetic model were listed as follow:

1. The reaction kinetics follow a first-order reaction model.
2. All reactions are assumed to be homogeneous, neglecting any spatial variations or concentration gradients within the system.
3. The effect of temperature on the reaction rate is considered using an Arrhenius equation, assuming no other factors significantly influence the rate of reaction.
4. The model assumes ideal reactor conditions, disregarding any potential non-idealities such as heat or mass transfer limitations.
5. There is no synergistic or antagonistic interaction between the compositional components during the whole biomass HTL process.

4.3 Results and Discussion

4.3.1 Bio-oil Production from HTL of Lignocellulosic Model Compounds and Feedstocks

The bio-oil yields from HTL of cellulose at different temperatures and reaction times are presented in **Table 4.2.** Within the tested temperature (225-300 °C) and time range (10-60 min), only a small amount of gas (<1.5 wt.%) was produced; the maximum bio-oil yield from HTL of cellulose (25.40 ± 0.48 wt.%) was obtained at 300 °C, 30 min. The bio-oil yield of HTL conversion of cellulose increased with temperature. The SR yield decreased with temperature in the range of 225-275 °C, but started to increase when further elevating temperature to 300 °C, likely due to the condensation of bio-oil/AP at higher temperatures [51]. These results are in good agreement with the results from a previous study by Xu et al. [52]. At relatively high temperature (T>250 °C), the oil yields were around 9.11-21.71 wt.% after 10 min of reaction, and raised to 20.33-25.40 wt.% as the reaction time increased to 30 min. When extending the reaction time to 60 min, the oil yields, however, decreased to 17.86-20.78 wt.%, again due to the condensation of bio-oil/AP at a long residence time. The HTL conversion of cellulose can be considered to comprise three steps:

macromolecules depolymerization into oligomers/monomers (oils), oligomers/monomers decomposition to form reactive fragments, and reactive fragments repolymerization into SR or char [53]. The above results indicate that it takes about 30 min to convert cellulose and reach the optimum bio-oil yield, after which repolymerization reactions dominate the process and lowers the oil production. Meanwhile, an increase in SR yields was observed at longer reaction time (i.e., 60 min) due to the generation of char.

Table 4.3 presents the product yields from HTL of xylan (a model compound for hemicellulose) at a temperature ranging from 225 °C to 300 °C) for reaction time from 10 min to 60 min. Compared to cellulose HTL (**Table 4.2**), no significant changes in product yields from xylan HTL were observed within the tested ranges of temperature and time, likely because xylan can be readily hydrolyzed at temperatures as low as 120 °C [54]. The bio-oil yields from xylan HTL varied from 15.06-22.90 wt.%, with the maximum obtained at 275 °C, 10 min.

The product yields from HTL of lignin at different temperatures and reaction times are presented in **Table 4.4**. It was found that the bio-oil yield increased with temperature. The oil yields at 225 °C were slightly lower than those from cellulose and xylan HTL under the same conditions, likely because the hydrolytic depolymerization of lignin is limited at such a low temperature [55, 56]. Increasing temperature to 250 °C led to a sharp growth in bio-oil yield, while no obvious increase in bio-oil yield occurred at temperatures higher than 275 °C. A similar trend was reported in previous research work [56, 57]. These results indicate that lignin depolymerization takes place rapidly at HTL temperatures over 250 °C. At above 275 °C, the repolymerization or self-condensation reactions of bio-oil fragments could become favorable [58, 59], resulting in less generation of bio-oil, accompanied by more SR formation. The effect of reaction time on oil yield exhibited the same trend as that observed in cellulose HTL, and the maximum bio-oil yield (77.58±0.69 wt.%) of lignin HTL was obtained at 300 °C, 30 min.

Table 4.2: Product yields obtained by HTL of cellulose at different temperatures and times.

Temp. (°C)	Time (min)	Bio-oil yield (wt.%)	SR yield (wt.%)	Gas yield (wt.%)	AP yield (wt.%)

225	10	7.52±0.81	59.90±0.30	0.52±0.03	32.08
	20	13.53±0.91	47.70±0.28	0.48±0.10	38.32
	30	13.04±0.96	42.60±0.42	0.53±0.04	43.87
	60	15.27±0.79	30.80±0.32	0.56±0.06	53.44
250	10	9.11±0.95	32.50±0.19	0.44±0.11	57.95
	20	13.82±0.63	18.20±0.45	0.52±0.13	67.48
	30	20.33±0.55	7.71±0.68	0.74±0.12	71.25
	60	17.86±0.76	5.40±0.77	0.89±0.14	75.91
275	10	20.03±0.49	3.30±0.95	0.91±0.09	75.79
	20	21.10±0.66	2.90±0.82	0.94±0.13	75.06
	30	24.60±0.44	2.88±0.97	1.03±0.11	71.49
	60	20.52±0.45	7.90±0.79	1.10±0.08	70.50
300	10	21.71±0.53	4.84±0.91	1.43±0.12	72.03
	20	23.35±0.42	4.26±0.85	1.52±0.13	70.92
	30	25.40±0.48	3.28±0.69	1.49±0.15	69.83
	60	20.78±0.40	4.45±0.77	1.55±0.12	73.30

Table 4.3: Product yields obtained by HTL of lignin at different temperatures and times.

Temp. (°C)	Time (min)	Bio-oil yield (wt.%)	SR yield (wt.%)	Gas yield (wt.%)	AP yield (wt.%)
225	10	15.40±0.81	3.84±0.92	0.53±0.03	80.23
	20	16.71±0.91	2.28±0.89	0.64±0.05	80.38
	30	18.55±0.91	3.36±0.84	0.79±0.10	77.35
	60	15.06±0.63	3.45±0.95	0.73±0.03	80.82
250	10	16.33±0.55	4.61±0.68	0.59±0.12	78.50
	20	17.12±0.96	4.19±0.80	0.71±0.13	78.00
	30	21.10±0.71	5.77±0.93	0.88±0.09	72.25
	60	17.28±0.68	2.55±0.87	0.87±0.11	79.38
275	10	22.90±0.63	6.60±0.69	0.92±0.16	69.58
	20	19.64±0.79	7.86±0.75	0.93±0.01	71.61
	30	18.15±0.70	2.65±1.12	0.91±0.04	78.34
	60	15.22±0.74	4.02±0.77	0.95±0.06	79.83
300	10	20.11±0.58	7.02±0.54	1.15±0.11	71.73
	20	15.40±0.81	3.84±0.92	0.53±0.03	80.23
	30	16.71±0.91	2.28±0.89	0.64±0.05	80.38
	60	18.55±0.91	3.36±0.84	0.79±0.10	77.35

Table 4.4: Product yields obtained by HTL of lignin at different temperatures and times.

Temp. (°C)	Time (min)	Bio-oil yield (wt.%)	SR yield (wt.%)	Gas yield (wt.%)	AP yield (wt.%)
225	10	2.55±1.32	1.13±0.45	0.54±0.08	95.83
	20	4.71±0.76	2.27±0.56	0.71±0.05	92.32
	30	6.23±0.92	3.90±0.47	0.88±0.13	89.02
	60	11.67±0.83	4.08±0.78	0.85±0.01	83.47
250	10	44.54±0.87	4.15±0.91	1.06±0.16	50.29
	20	57.10±0.75	4.29±0.44	1.04±0.16	37.57
	30	72.21±0.54	4.33±0.43	1.20±0.08	22.27
	60	69.89±0.60	2.61±0.59	1.30±0.15	26.29
275	10	60.02±0.65	6.37±0.55	1.55±0.07	32.08
	20	70.66±0.96	8.99±0.92	1.57±0.11	18.84
	30	75.04±0.57	10.88±0.29	1.69±0.00	12.43
	60	73.51±1.01	7.58±0.76	1.77±0.08	17.15
300	10	64.90±0.78	6.33±0.75	1.87±0.09	26.90
	20	72.16±0.53	7.54±0.38	1.90±0.05	18.46
	30	77.58±0.69	8.87±0.57	1.96±0.14	11.67
	60	74.04±0.74	6.68±0.53	1.95±0.10	17.37

4.3.2 Kinetic Model and Parameter Estimation

Figures 4.3-4.5 show the model calculated values (solid lines) and the experimental values (discrete points) from HTL of model compounds at 225 °C, 250 °C, 275 °C, and 300 °C. Overall, the calculated values based on the developed model well match the experimental values of the product yields. As shown in **Figure 4.3**, the conversion of cellulose proceeded slowly at 225 °C, and the loaded feedstock was not completely converted even after 60 min of HTL processing. Elevating temperature facilitated the cellulose HTL. When the temperature was 275 °C or higher, the cellulose could be liquefied completely within 10 min. Likewise, all product yields gradually increased at low reaction temperatures (225 and 250 °C), while at the temperature above 275 °C, the yields rapidly reached the maxima with plateaus coming after. Overall, the dominant product from HTL of cellulose was AP, followed by bio-oil, and the gas and solid products only took a small portion (<10 wt.%), and formation of these products increased by extending the residence time.

As shown in **Figure 4.4**, xylan can be quickly converted (in 10 min) under all temperatures investigated (225-300 °C) likely because xylan with amorphous structure can be readily hydrolyzed at temperatures as low as 120 °C [54], way below the reaction temperatures tested. At lower temperatures (225 and 250 °C), the product yields increased quickly in the first 10 min and leveled off afterwards. When the reaction temperature increased to 275-300 °C, the bio-oil yield gradually decreased with time after the initial 10 min, accompanied by an increase in the yield of AP, suggesting the formation of AP from reactive fragments at high HTL temperatures. Negligible amount of gases was produced from HTL of xylan and the reaction time showed insignificant effects on the SR formation.

As illustrated in **Figure 4.5**, at all temperatures there was a rapid decrease in lignin during the first 5 min, accompanied by a fast increase in the formation of AP products, likely due to the readily dissolution of alkali lignin in the alkaline reaction medium. The components in AP could subsequently be converted into bio-oil products, and such conversion became more pronounced and faster at elevated temperatures. At 275-300 °C, achieving equilibrium after 30 min of reaction, while the equilibrium time was longer at lower temperatures. In HTL of lignin, the gas yield increased linearly with reaction time at all temperatures, while the generation of SR is nearly independent of reaction time.

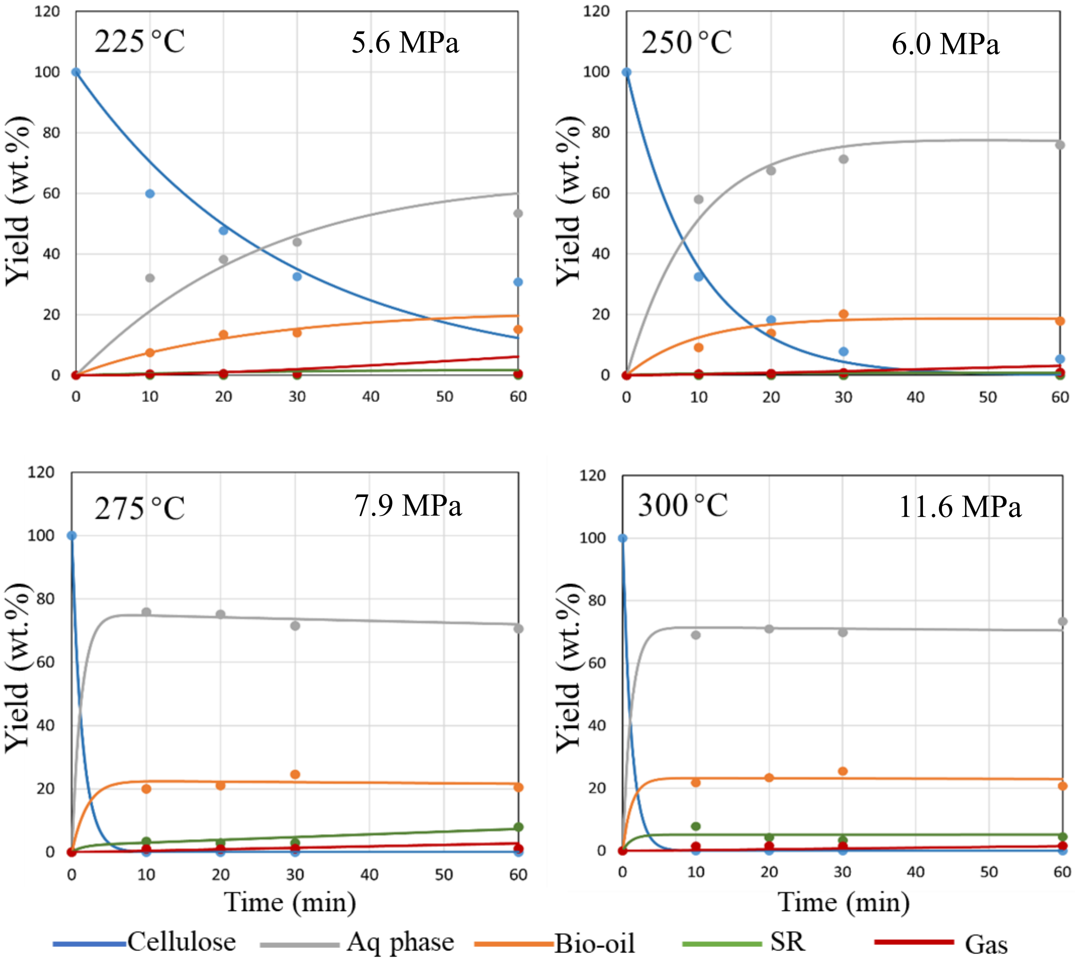

Figure 4.3: Experimental (discrete points) and calculated (continuous curves) values of product yields from HTL of cellulose as a function of time at different temperatures.

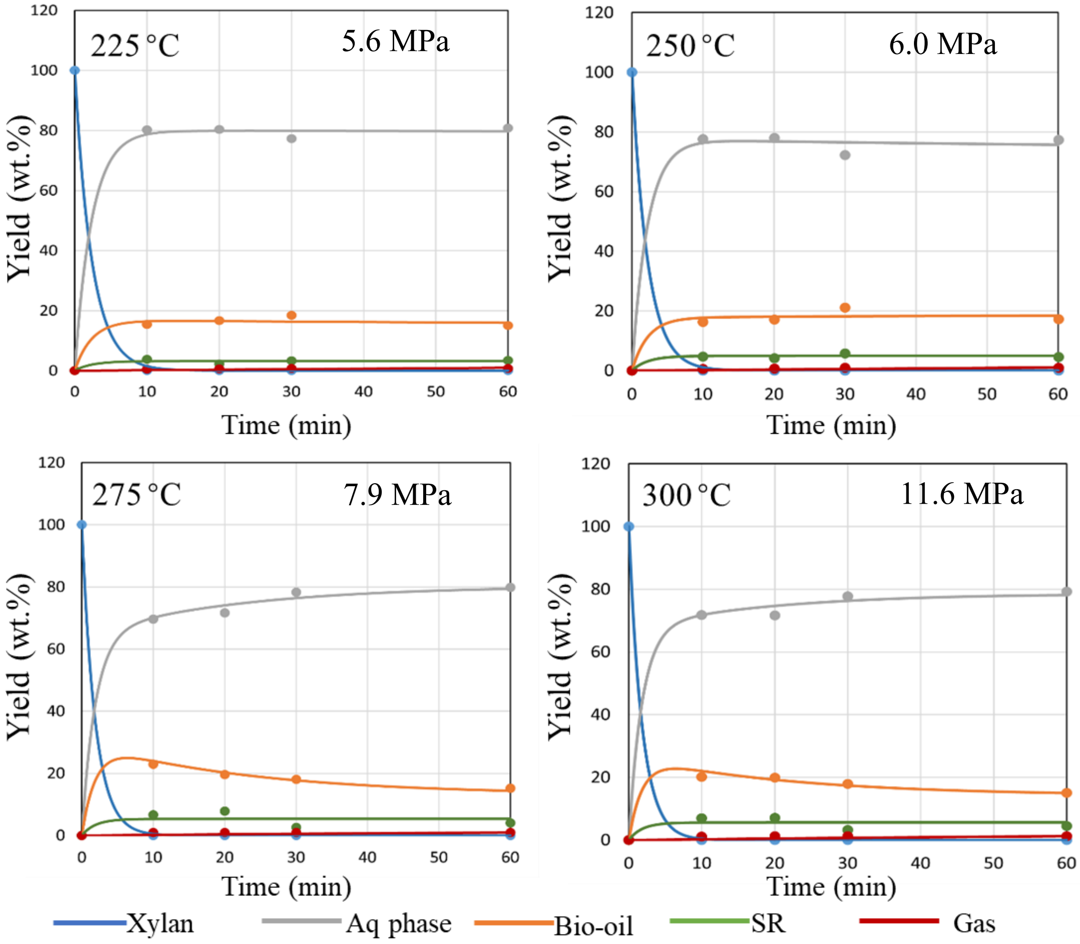

Figure 4.4: Experimental (discrete points) and calculated (continuous curves) values of product yields from HTL of xylan as a function of time at different temperatures.

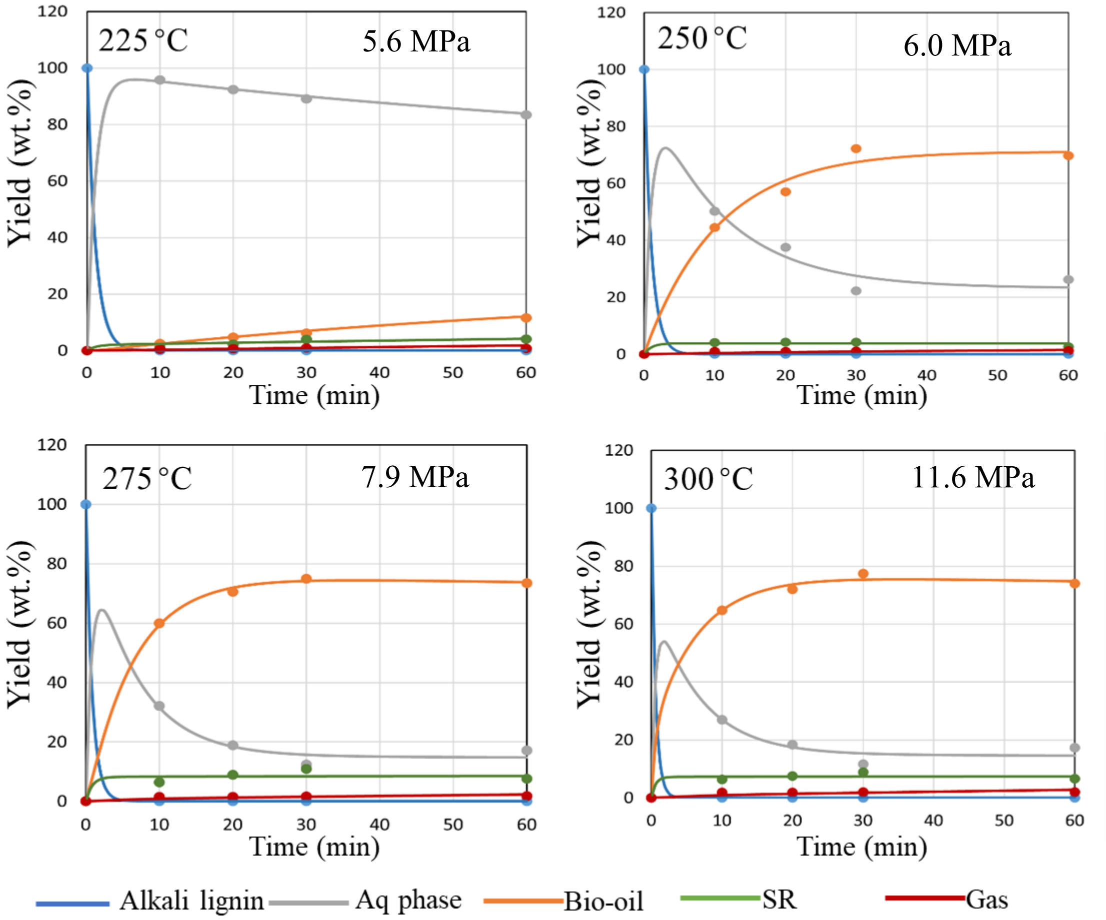

Figure 4.5: Experimental (discrete points) and calculated (continuous curves) values of product yields from HTL of alkali lignin as a function of time at different temperatures.

Table 4.5 lists the optimized values of rate constant of each reaction pathway (**Figure 4.2**) during HTL of the model compounds (cellulose, xylan and alkali lignin) at different reaction temperatures. The apparent rate constants of conversion of cellulose to AP, bio-oil, and SR, i.e., k_1, k_2 and k_3, are enhanced at elevated temperatures, as expected. The values of k_1 and k_2 are 7-116 times than that of k_3, indicating less possibility of direct formation of SR from cellulose. The rate constants of the interconversion of AP products and bio-oil also increase with temperature, and the rate constants for bio-oil generation are lower than those for bio-oil consumption. The formation of SR and gases during cellulose

HTL is less favorable compared to that of AP and bio-oil under the testing temperature range, as evidenced by the small reaction rate constants (k_3, k_6, k_7 and k_8).

In xylan HTL, k_1 and k_2 are obviously much higher than the other rate constants, indicating that the readily formation of AP products and bio-oil from xylan are the dominant reaction pathways. Temperature rarely affects the rate constants of xylan to AP, suggesting the complete dissolution or hydrolysis of xylan under the temperatures tested. The rate constants of xylan to bio-oil increase at higher temperatures as expected.

In HTL of alkali lignin, k_1 has a constant value at all temperatures, because alkali lignin is highly soluble in alkaline water, particularly in the presence of K_2CO_3 catalyst (catalyst loading: 5 wt.% of dry biomass). The bio-oil formation from alkali lignin is more pronounced at increased temperatures, as shown by the bio-oil yield results from our experiments (**Figure 4.5**) and the increasing values of k_1 with reaction temperature (**Table 4.5**). It was also reported that a higher temperature facilitated the cleavage of ether bonds in lignin and the subsequent degradation to form bio-oil products [60]. It can also be observed that the rate constants of AP→Bio-oil (k_4) are all higher than those of the reverse reaction (k_5) at temperatures above 250 °C, which should be another cause to the high bio-oil yield in lignin HTL. The activation energies of each pathway were also determined as shown in **Table 4.5**. The activation energies for the decomposition of model compounds into bio-oil in HTL are lower compared with those of pyrolysis of lignocellulosic biomass as reported in the literature [61-63]. In the kinetic model presented in this work, the pathway from cellulose to SR has the greatest activation energy at 128.9 kJ/mol. Among all the reaction pathways that lead to bio-oil, the pathways from cellulose and lignin to bio-oil require higher activity energy (74.29 and 64.83 kJ/mol), compared with that from xylan (25.74 kJ/mol). The activation energies required in all pathways to gas formation for all model compounds are relatively high, which accounts for a very low gas yield in their HTL processes.

Table 4.5: Optimized values of rate constants and activation energies for the reaction pathways proposed in Figure 4.2.

Feedstock	**Paths**	**Reactions**	**Rate constant (min^{-1})**				**E (kJ/mol)**
			225 °C	250 °C	275 °C	300 °C	
Cellulose	1	Cellulose→AP	0.034	0.10	0.26	0.27	68.92

	2	Cellulose→Bio-oil	0.020	0.022	0.15	0.16	74.29
	3	Cellulose→SR	0.00073	0.00086	0.022	0.023	128.90
	4	AP→Bio-oil	0.048	0.048	0.12	0.13	38.32
	5	Bio-oil→AP	0.12	0.14	0.37	0.40	43.93
	6	Bio-oil→SR	0.00010	0.00010	0.00018	0.0013	75.72
	7	AP→Gas	0.00010	0.00010	0.00018	0.00061	55.93
	8	Bio-oil→Gas	0.0011	0.0011	0.0070	0.0080	73.83
Xylan	1	Xylan→AP	0.34	0.35	0.35	0.37	2.88
	2	Xylan→Bio-oil	0.071	0.080	0.15	0.14	25.74
	3	Xylan→SR	0.014	0.022	0.028	0.031	26.00
	4	AP→Bio-oil	0.0038	0.0044	0.0061	0.0070	20.52
	5	Bio-oil→AP	0.019	0.024	0.037	0.038	23.93
	6	Bio-oil→SR	0.000050	0.00010	0.00050	0.00070	90.62
	7	AP→Gas	0.00010	0.00010	0.00018	0.00032	38.15
	8	Bio-oil→Gas	0.00010	0.00010	0.00049	0.00082	74.44
Alkali lignin	1	Alkali lignin→AP	0.40	0.40	0.40	0.40	-
	2	Alkali lignin→Bio-oil	0.000030	0.064	0.11	0.24	64.83
	3	Alkali lignin→SR	0.0072	0.019	0.046	0.050	64.42
	4	AP→Bio-oil	0.0031	0.072	0.13	0.13	28.06
	5	Bio-oil→AP	0.0095	0.014	0.026	0.026	28.61
	6	Bio-oil→SR	0.000020	0.00010	0.00012	0.00014	58.39
	7	AP→Gas	0.00036	0.00081	0.0019	0.0024	62.45
	8	Bio-oil→Gas	0.00010	0.00080	0.0010	0.0016	82.44

As discussed previously, in this work, the model (Eqn. 4.13) established to predict the yield of each product from HTL of lignocellulosic biomass was based on the assumption that there is no synergistic or antagonistic interaction between the compositional components during the whole biomass HTL process. To validate this assumption, the following experiments were performed. Mixtures of the three model compounds (cellulose, xylan and lignin) were prepared according to the compositional analysis (**Table 4.1**) of three whole biomass feedstocks: bamboo, cornstalk and pinewood. HTL experiments were performed on these mixtures, compared with the whole biomass feedstocks for 30 min at various temperatures. **Table 4.6** presents the HTL bio-oil yields from the model compounds mixtures (simulating the whole biomass compositions), from the whole biomass of bamboo, cornstalk, and pinewood, and from the model calculations. The results clearly indicate that at all temperatures and for each biomass feedstock, the obtained HTL bio-oil yields from the model compounds mixtures (simulating the whole biomass compositions) are similar to those from the whole biomass feedstock, as well as are close to the model (Eqn. 4.13) calculations (the mass-fraction weighted average of the product yield from individual model components). As such, the assumption for the model (Eqn. 4.13) is that there is no synergistic or antagonistic interaction between the compositional components during the whole biomass HTL process, can be validated. In addition, the experimental results in

Table 4.6 further demonstrate that the HTL bio-oil yield was strongly positively correlated to the lignin content in the feedstocks, as concluded in many previous studies in literature [64-66]. Admittedly, some differences can be observed between the HTL bio-crude yields from whole biomass and those from the model compounds mixtures could be caused by the presence of extractives in the whole biomass feedstocks [67, 68]. The extractives in the whole biomass feedstock would decompose to fatty acids [69-71], as a part of the HTL bio-oil products.

Table 4.6: HTL bio-oil yields from the model compounds mixtures (simulating the whole biomass compositions), from the whole biomass of bamboo, cornstalk, and pinewood, and from the model calculations.

Feedstock		**Bio-oil Yield (wt.%)**		
		250 °C	275 °C	300 °C
Bamboo	Model compounds mixture	27.14±2.10	29.30±2.12	32.04±1.99
	Calculated yield[a]	33.65	35.61	36.64
	Whole biomass	32.97±0.25	34.56±0.05	36.15±0.25
Cornstalk	Model compounds mixture	20.27±0.92	21.87±0.71	22.33±0.58
	Calculated yield	27.45	28.51	29.19
	Whole biomass	17.50±1.20	22.50±0.50	24.75±0.75
Pinewood	Model compounds mixture	21.12±0.72	24.98±0.44	27.05±0.54
	Calculated yield	33.06	34.79	35.73
	Whole biomass	18.00±1.10	28.50±1.50	29.67±2.00

[a] The calculated yield is the mass-fraction weighted average, based on results from the kinetic model of the individual model components.

Figure 4.6 compares the HTL product yields obtained by model calculations and by the experiments at 250, 275, 300 °C for 30 min with different lignocellulosic biomass (bamboo, cornstalk, and pinewood). The root mean square deviation (RMSD) and mean absolute percentage error (MAPE) of each type of products were calculated to assess the quality/reliability of the predictions. The interpretation of MAPE values is presented in **Table 4.7**. As shown in **Figure 4.6**, the model provides a reasonable and good accurate prediction for AP yields (MAPE: 14.3%; RMSD: ±10.12 wt.%) and bio-oil yields (MAPE: 20.7%; RMSD: ±5.64 wt.%), respectively, for all three lignocellulosic feedstocks across all experimental conditions. However, the RMSD and MAPE values for SR yields are ±11.35 wt.% and 49.7%, respectively, suggesting the model's predictions of this product is not as accurate as that of bio-oil and AP products.

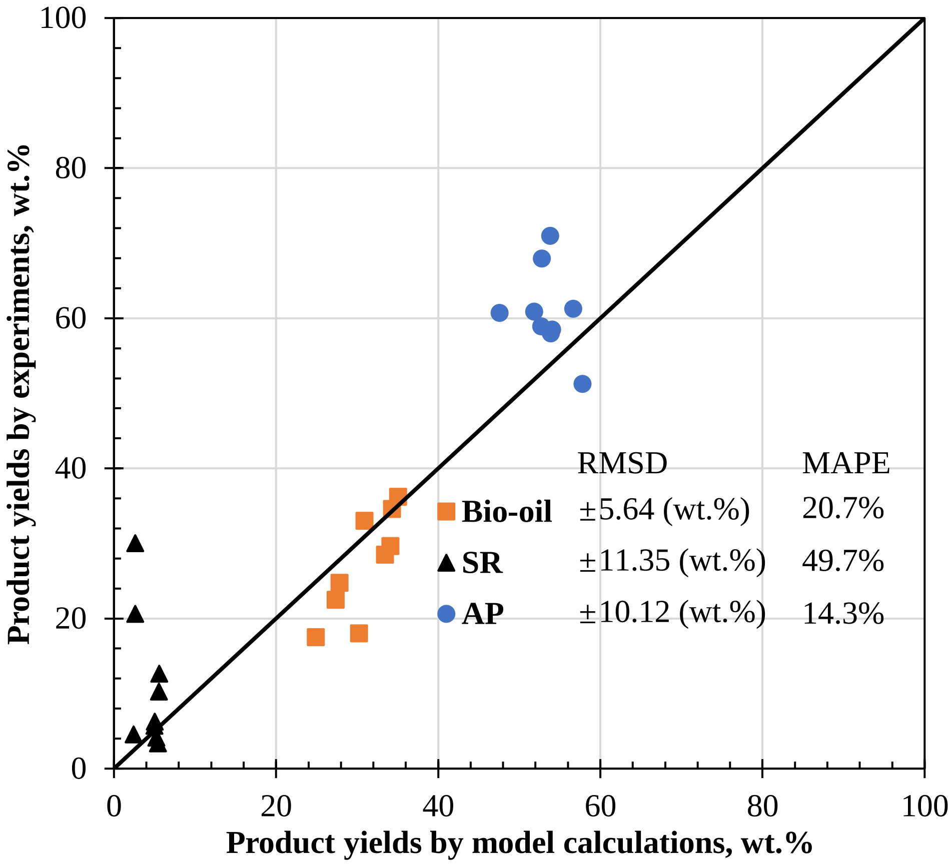

Figure 4.6: Comparison of the HTL product yields obtained by model calculations and by experiments with bamboo, cornstalk, and pinewood at 250, 275, 300 ºC for 30 min.

To further validate the generality of the developed kinetic model, the model predictions of HTL product yields are also compared to the experimental results from literature on HTL of different lignocellulosic feedstocks under various operating conditions (temperatures: 230–350 °C, residence time up to 60 min, with/without alkali catalyst) [35, 64, 68, 72-79], as illustrated in **Figure 4.7**. As clearly shown, the model provides good accurate prediction of bio-oil (RMSD: ±6.60 wt.%) yields with a MAPE of 18.9%, followed by reasonable forecasting of SR (RMSD: ±4.94 wt.%; MAPE: 24.5%) and AP (RMSD: ±7.52 wt.%; MAPE: 40.4%) yields. Admittedly there are still some deviations between model calculations and experimental results. This could be caused by the simplifications made in the model development, and the complexities in the biomass feedstock compositions and particle sizes, reactor configurations and conditions (heating rate, catalyst loading, etc.) and the complexities in the HTL reactions [32, 80]. For instance, the ash contents of the feedstocks could influence the products yields [81, 82]. K and Ca in the ash content proved to catalyze the conversion of biomass [18]. In addition, the synergistic or antagonistic effects from interactions among the components during HTL could increase or decrease the bio-oil yield [32, 83]. Furthermore, the efficiency of lignocellulosic biomass liquefaction could be constrained due to the high crystallinity and degree of polymerization of cellulose [84]. More future work will be done to further improve the accuracy and robustness of the kinetic model developed in this work.

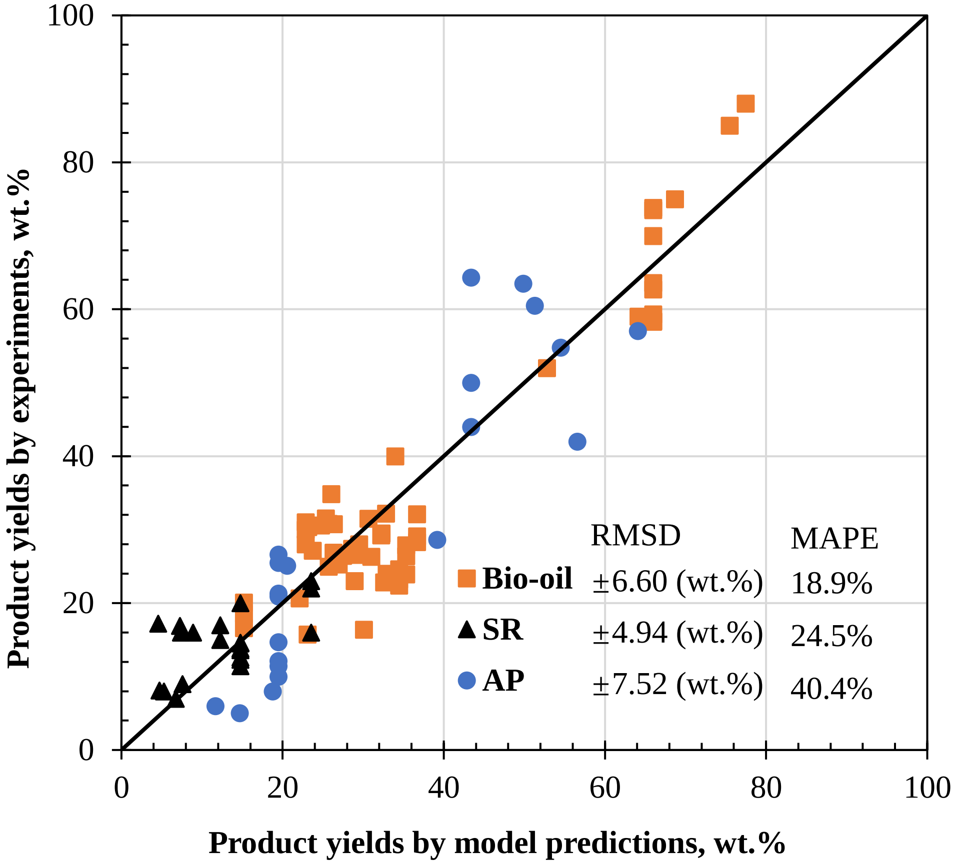

Figure 4.7: Comparison of HTL product yields obtained by model predictions and by experiments reported in literature [35, 64, 68, 72-79] on HTL of different types of lignocellulosic biomass under various operating conditions.

Table 4.7: Interpretation of typical MAPE values [85].

MAPE (%)	Interpretation
<10	Highly accurate forecasting
10-20	Good accurate forecasting
20-50	Reasonable forecasting

>50	Inaccurate forecasting

4.4 Conclusions

This study aimed to develop a kinetic model based on chemical compositions of lignocellulosic biomass for predicting HTL product yields. HTL experiments of the model compounds for lignocellulosic biomass (cellulose, xylan, and lignin) and lignocellulosic biomass (bamboo, cornstalk, and pinewood) were conducted in the temperature range of 225 °C-300 °C for a residence time from 10 min to 60 min with K_2CO_3 catalyst. Lignin was found to be the main contributor to bio-oil formation from HTL of lignocellulosic biomass. A kinetic model was developed based on the experimental results obtained from HTL of biomass model compounds to predict HTL product yields based on chemical compositions of lignocellulosic biomass (contents of cellulose, hemicellulose, and lignin). The model was validated using our experimental results from HTL of bamboo, cornstalk, and pinewood and the publicly available data in literature from HTL of various lignocellulosic biomass feedstocks. However, there are still some limitations on this kinetic model: (1) The model does not account for potential side reactions or competing reaction pathways that may occur simultaneously. (2) The model assumes steady-state conditions and does not account for transient behavior or dynamic changes in the reaction system. (3) The model does not take operating parameters like moisture content, inorganic content, and interaction of biomass component into consideration. More future work is required to further improve the accuracy and robustness of the kinetic model developed in this work.

4.5 References

[1] I.A. Basar, H. Liu, H. Carrere, E. Trably, C. Eskicioglu, A review on key design and operational parameters to optimize and develop hydrothermal liquefaction of biomass for biorefinery applications, Green Chemistry 23(4) (2021) 1404-1446.

[2] A. Gollakota, N. Kishore, S. Gu, A review on hydrothermal liquefaction of biomass, Renewable and Sustainable Energy Reviews 81 (2018) 1378-1392.

[3] P. McKendry, Energy production from biomass (part 1): overview of biomass, Bioresource technology 83(1) (2002) 37-46.

[4] C. Xu, J. Lancaster, Conversion of secondary pulp/paper sludge powder to liquid oil products for energy recovery by direct liquefaction in hot-compressed water, Water research 42(6-7) (2008) 1571-1582.

[5] D. Wen, H. Jiang, K. Zhang, Supercritical fluids technology for clean biofuel production, Progress in Natural science 19(3) (2009) 273-284.

[6] T.P.T. Pham, R. Kaushik, G.K. Parshetti, R. Mahmood, R. Balasubramanian, Food waste-to-energy conversion technologies: Current status and future directions, Waste management 38 (2015) 399-408.

[7] B. Grycová, I. Koutník, A. Pryszcz, Pyrolysis process for the treatment of food waste, Biomass Conversion and Biorefinery 218 (2016) 1203-1207.

[8] A. Dimitriadis, S. Bezergianni, Hydrothermal liquefaction of various biomass and waste feedstocks for biocrude production: A state of the art review, Renewable and Sustainable Energy Reviews 68 (2017) 113-125.

[9] H. Bayat, F. Cheng, M. Dehghanizadeh, N. Soliz, C.E. Brewer, U. Jena, Hydrothermal liquefaction of food waste: Bio-crude oil Characterization, Mass and Energy Balance, 2019 ASABE Annual International Meeting, American Society of Agricultural and Biological Engineers, 2019, p. 1.

[10] W.T. Chen, Y. Zhang, J. Zhang, G. Yu, L.C. Schideman, P. Zhang, M. Minarick, Hydrothermal liquefaction of mixed-culture algal biomass from wastewater treatment system into bio-crude oil, Bioresource technology 152 (2014) 130-139.

[11] F. Cheng, Z. Cui, L. Chen, J. Jarvis, N. Paz, T. Schaub, N. Nirmalakhandan, C.E. Brewer, Hydrothermal liquefaction of high-and low-lipid algae: Bio-crude oil chemistry, Applied Energy 206 (2017) 278-292.

[12] F. Cheng, K. Mallick, S.M.H. Gedara, J.M. Jarvis, T. Schaub, U. Jena, N. Nirmalakhandan, C.E. Brewer, Hydrothermal liquefaction of Galdieria sulphuraria grown on municipal wastewater, Bioresource technology 292 (2019) 121884.

[13] A. Mathanker, D. Pudasainee, A. Kumar, R. Gupta, Hydrothermal liquefaction of lignocellulosic biomass feedstock to produce biofuels: Parametric study and products characterization, Fuel 271 (2020) 117534.

[14] J. Lu, J. Zhang, Z. Zhu, Y. Zhang, Y. Zhao, R. Li, J. Watson, B. Li, Z. Liu, Simultaneous production of biocrude oil and recovery of nutrients and metals from human feces via hydrothermal liquefaction, Energy conversion and management 134 (2017) 340-346.

[15] L. Yang, L. Nazari, Z. Yuan, K. Corscadden, C.C. Xu, Hydrothermal liquefaction of spent coffee grounds in water medium for bio-oil production, Biomass and Bioenergy 86 (2016) 191-198.

[16] R. Singh, K. Chaudhary, B. Biswas, B. Balagurumurthy, T. Bhaskar, Hydrothermal liquefaction of rice straw: effect of reaction environment, The Journal of Supercritical Fluids 104 (2015) 70-75.

[17] D. Sahoo, A. Awasthi, V. Dhyani, B. Biswas, J. Kumar, Y.S. Reddy, V. Adarsh, A. Puthiyamadam, K.K. Mallapureddy, R.K. Sukumaran, Value-addition of water hyacinth and para grass through pyrolysis and hydrothermal liquefaction, Carbon Resources Conversion 2(3) (2019) 233-241.

[18] S. Feng, Z. Yuan, M. Leitch, C.C. Xu, Hydrothermal liquefaction of barks into bio-crude–Effects of species and ash content/composition, Fuel 116 (2014) 214-220.

[19] E. Panisko, T. Wietsma, T. Lemmon, K. Albrecht, D. Howe, Characterization of the aqueous fractions from hydrotreatment and hydrothermal liquefaction of lignocellulosic feedstocks, Biomass and Bioenergy 74 (2015) 162-171.

[20] D.R. Vardon, B. Sharma, J. Scott, G. Yu, Z. Wang, L. Schideman, Y. Zhang, T.J. Strathmann, Chemical properties of biocrude oil from the hydrothermal liquefaction of

Spirulina algae, swine manure, and digested anaerobic sludge, Bioresource technology 102(17) (2011) 8295-8303.

[21] Y. Tian, F. Wang, J.O. Djandja, S.L. Zhang, Y.P. Xu, P.G. Duan, Hydrothermal liquefaction of crop straws: Effect of feedstock composition, Fuel 265 (2020) 116946.

[22] S. Yin, R. Dolan, M. Harris, Z. Tan, Subcritical hydrothermal liquefaction of cattle manure to bio-oil: Effects of conversion parameters on bio-oil yield and characterization of bio-oil, Bioresource technology 101(10) (2010) 3657-3664.

[23] H. Li, J. Lu, Y. Zhang, Z. Liu, Hydrothermal liquefaction of typical livestock manures in China: biocrude oil production and migration of heavy metals, Journal of Analytical and Applied Pyrolysis 135 (2018) 133-140.

[24] P. Biller, D. Lawson, R.B. Madsen, J. Becker, B.B. Iversen, M. Glasius, Assessment of agricultural crops and natural vegetation in Scotland for energy production by anaerobic digestion and hydrothermal liquefaction, Biomass Conversion and Biorefinery 7(4) (2017) 467-477.

[25] S. Nagappan, R.R. Bhosale, D.D. Nguyen, N.T.L. Chi, V.K. Ponnusamy, C.S. Woong, G. Kumar, Catalytic hydrothermal liquefaction of biomass into bio-oils and other value-added products–A review, Fuel 285 (2021) 119053.

[26] H. Huang, X. Yuan, G. Zeng, J. Wang, H. Li, C. Zhou, X. Pei, Q. You, L. Chen, Thermochemical liquefaction characteristics of microalgae in sub-and supercritical ethanol, Fuel Processing Technology 92(1) (2011) 147-153.

[27] R. Singh, B. Balagurumurthy, A. Prakash, T. Bhaskar, Catalytic hydrothermal liquefaction of water hyacinth, Bioresource technology 178 (2015) 157-165.

[28] B. Jin, P. Duan, Y. Xu, F. Wang, Y. Fan, Co-liquefaction of micro-and macroalgae in subcritical water, Bioresource technology 149 (2013) 103-110.

[29] Y. Xue, H. Chen, W. Zhao, C. Yang, P. Ma, S. Han, A review on the operating conditions of producing bio-oil from hydrothermal liquefaction of biomass, International Journal of Energy Research 40(7) (2016) 865-877.

[30] H.M. Liu, M.F. Li, R.C. Sun, Hydrothermal liquefaction of cornstalk: 7-lump distribution and characterization of products, Bioresource technology 128 (2013) 58-64.

[31] B. Hao, D. Xu, G. Jiang, T.A. Sabri, Z. Jing, Y. Guo, Chemical reactions in the hydrothermal liquefaction of biomass and in the catalytic hydrogenation upgrading of biocrude, Green Chemistry 23(4) (2021) 1562-1583.

[32] J. Lu, Z. Liu, Y. Zhang, P.E. Savage, Synergistic and antagonistic interactions during hydrothermal liquefaction of soybean oil, soy protein, cellulose, xylose, and lignin, ACS Sustainable Chemistry & Engineering 6(11) (2018) 14501-14509.

[33] H. Mazaheri, K.T. Lee, S. Bhatia, A.R. Mohamed, Subcritical water liquefaction of oil palm fruit press fiber for the production of bio-oil: effect of catalysts, Bioresource technology 101(2) (2010) 745-751.

[34] Z. Bi, J. Zhang, E. Peterson, Z. Zhu, C. Xia, Y. Liang, T. Wiltowski, Biocrude from pretreated sorghum bagasse through catalytic hydrothermal liquefaction, Fuel 188 (2017) 112-120.

[35] Z. Zhu, S.S. Toor, L. Rosendahl, D. Yu, G. Chen, Influence of alkali catalyst on product yield and properties via hydrothermal liquefaction of barley straw, Energy 80 (2015) 284-292.

[36] Z. Fang, T. Minowa, R. Smith, T. Ogi, J. Koziński, Liquefaction and gasification of cellulose with Na2CO3 and Ni in subcritical water at 350 C, Industrial & Engineering Chemistry Research 43(10) (2004) 2454-2463.

[37] S. Karagöz, T. Bhaskar, A. Muto, Y. Sakata, T. Oshiki, T. Kishimoto, Low-temperature catalytic hydrothermal treatment of wood biomass: analysis of liquid products, Chemical Engineering Journal 108(1-2) (2005) 127-137.

[38] J. Akhtar, S.K. Kuang, N.S. Amin, Liquefaction of empty palm fruit bunch (EPFB) in alkaline hot compressed water, Renewable energy 35(6) (2010) 1220-1227.

[39] H. Huang, X. Yuan, H. Zhu, H. Li, Y. Liu, X. Wang, G. Zeng, Comparative studies of thermochemical liquefaction characteristics of microalgae, lignocellulosic biomass and sewage sludge, Energy 56 (2013) 52-60.

[40] R. Shakya, J. Whelen, S. Adhikari, R. Mahadevan, S. Neupane, Effect of temperature and Na2CO3 catalyst on hydrothermal liquefaction of algae, Algal research 12 (2015) 80-90.

[41] P. Biller, R. Riley, A. Ross, Catalytic hydrothermal processing of microalgae: decomposition and upgrading of lipids, Bioresource technology 102(7) (2011) 4841-4848.

[42] P. Duan, P.E. Savage, Hydrothermal liquefaction of a microalga with heterogeneous catalysts, Industrial & Engineering Chemistry Research 50(1) (2011) 52-61.

[43] B. Zhang, H.J. Huang, S. Ramaswamy, Reaction kinetics of the hydrothermal treatment of lignin, Biotechnology for fuels and chemicals, Springer2007, pp. 487-499.

[44] F. Hardi, M. Mäkelä, K. Yoshikawa, Non-catalytic hydrothermal liquefaction of pine sawdust using experimental design: material balances and products analysis, Applied Energy 204 (2017) 1026-1034.

[45] Y.H. Chan, A.T. Quitain, S. Yusup, Y. Uemura, M. Sasaki, T. Kida, Liquefaction of palm kernel shell to bio-oil using sub-and supercritical water: an overall kinetic study, Journal of the Energy Institute 92(3) (2019) 535-541.

[46] M. Déniel, G. Haarlemmer, A. Roubaud, E. Weiss-Hortala, J. Fages, Modelling and predictive study of hydrothermal liquefaction: application to food processing residues, Waste and Biomass Valorization 8(6) (2017) 2087-2107.

[47] P.J. Valdez, V.J. Tocco, P.E. Savage, A general kinetic model for the hydrothermal liquefaction of microalgae, Bioresource technology 163 (2014) 123-127.

[48] D.C. Hietala, J.L. Faeth, P.E. Savage, A quantitative kinetic model for the fast and isothermal hydrothermal liquefaction of Nannochloropsis sp, Bioresource technology 214 (2016) 102-111.

[49] T.K. Vo, S.S. Kim, H.V. Ly, E.Y. Lee, C.G. Lee, J. Kim, A general reaction network and kinetic model of the hydrothermal liquefaction of microalgae Tetraselmis sp, Bioresource technology 241 (2017) 610-619.

[50] P.J. Valdez, P.E. Savage, A reaction network for the hydrothermal liquefaction of Nannochloropsis sp, Algal research 2(4) (2013) 416-425.

[51] J. Akhtar, N.A.S. Amin, A review on process conditions for optimum bio-oil yield in hydrothermal liquefaction of biomass, Renewable and Sustainable Energy Reviews 15(3) (2011) 1615-1624.

[52] Z.X. Xu, J.H. Cheng, Z.X. He, Q. Wang, Y.W. Shao, X. Hu, Hydrothermal liquefaction of cellulose in ammonia/water, Bioresource technology 278 (2019) 311-317.

[53] K. Malins, Production of bio-oil via hydrothermal liquefaction of birch sawdust, Energy conversion and management 144 (2017) 243-251.

[54] A. Beckendorff, A. Lamp, M. Kaltschmitt, Optimization of hydrolysis conditions for xylans and straw hydrolysates by HPLC analysis, Biomass Conversion and Biorefinery (2021) 1-14.

[55] L. Yang, P. Havard, K. Corscadden, C.C. Xu, X. Wang, Co-liquefaction of spent coffee grounds and lignocellulosic feedstocks, Bioresource technology 237 (2017) 108-121.

[56] B. Biswas, A. Kumar, R. Kaur, B.B. Krishna, T. Bhaskar, Catalytic hydrothermal liquefaction of alkali lignin over activated bio-char supported bimetallic catalyst, Bioresource technology 337 (2021) 125439.

[57] P. Jia, J. Wang, W. Zhang, Catalytic hydrothermal liquefaction of lignin over carbon nanotube supported metal catalysts for production of monomeric phenols, Journal of the Energy Institute 94 (2021) 1-10.

[58] D.G. Boocock, F. Porretta, Physical aspects of the liquefaction of poplar chips by rapid aqueous thermolysis, Journal of wood chemistry and technology 6(1) (1986) 127-144.

[59] R. Shu, J. Long, Y. Xu, L. Ma, Q. Zhang, T. Wang, C. Wang, Z. Yuan, Q. Wu, Investigation on the structural effect of lignin during the hydrogenolysis process, Bioresource technology 200 (2016) 14-22.

[60] J.L. Wen, S.L. Sun, T.Q. Yuan, F. Xu, R.C. Sun, Understanding the chemical and structural transformations of lignin macromolecule during torrefaction, Applied Energy 121 (2014) 1-9.

[61] J. Cai, W. Wu, R. Liu, G.W. Huber, A distributed activation energy model for the pyrolysis of lignocellulosic biomass, Green Chemistry 15(5) (2013) 1331-1340.

[62] J. Cai, W. Wu, R. Liu, An overview of distributed activation energy model and its application in the pyrolysis of lignocellulosic biomass, Renewable and Sustainable Energy Reviews 36 (2014) 236-246.

[63] L. Gašparovič, J. Labovský, J. Markoš, L. Jelemenský, Calculation of kinetic parameters of the thermal decomposition of wood by distributed activation energy model (DAEM), Chemical and Biochemical Engineering Quarterly 26(1) (2012) 45-53.

[64] Y.H. Chan, S. Yusup, A.T. Quitain, Y. Uemura, M. Sasaki, Bio-oil production from oil palm biomass via subcritical and supercritical hydrothermal liquefaction, The Journal of Supercritical Fluids 95 (2014) 407-412.

[65] B. de Caprariis, P. De Filippis, A. Petrullo, M. Scarsella, Hydrothermal liquefaction of biomass: Influence of temperature and biomass composition on the bio-oil production, Fuel 208 (2017) 618-625.

[66] T. Belkheiri, C. Mattsson, S.-I. Andersson, L. Olausson, L.-E. Åmand, H. Theliander, L. Vamling, Effect of pH on Kraft lignin depolymerisation in subcritical water, Energy & Fuels 30(6) (2016) 4916-4924.

[67] A. Pattiya, Direct Thermochemical Liquefaction for Energy Applications, Fast Pyrolysis (2018) 3-28.

[68] P. Sun, M. Heng, S. Sun, J. Chen, Direct liquefaction of paulownia in hot compressed water: Influence of catalysts, Energy 35(12) (2010) 5421-5429.

[69] M.K. Jindal, M.K. Jha, Effect of process parameters on hydrothermal liquefaction of waste furniture sawdust for bio-oil production, RSC advances 6(48) (2016) 41772-41780.

[70] M.K. Akalın, K. Tekin, S. Karagöz, Hydrothermal liquefaction of cornelian cherry stones for bio-oil production, Bioresource technology 110 (2012) 682-687.

[71] X. Guo, S. Wang, K. Wang, Q. Liu, Z. Luo, Influence of extractives on mechanism of biomass pyrolysis, Journal of fuel Chemistry and Technology 38(1) (2010) 42-46.

[72] T. Belkheiri, S.I. Andersson, C. Mattsson, L. Olausson, H. Theliander, L. Vamling, Hydrothermal liquefaction of kraft lignin in sub-critical water: the influence of the sodium and potassium fraction, Biomass Conversion and Biorefinery 8(3) (2018) 585-595.

[73] H.N. Lyckeskog, Hydrothermal Liquefaction of Lignin into Bio-Oil, Chalmers Tekniska Hogskola (Sweden)2016.

[74] T. Belkheiri, S.I. Andersson, C. Mattsson, L. Olausson, H. Theliander, L. Vamling, Hydrothermal liquefaction of Kraft lignin in subcritical water: influence of phenol as capping agent, Energy & Fuels 32(5) (2018) 5923-5932.

[75] Y. Gao, S. Liu, J. Du, Z. Wang, H. Wang, T. Zhao, Conversion and extracting bio-oils from rod-shaped cornstalk by sub-critical water, Journal of Analytical and Applied Pyrolysis 115 (2015) 316-325.

[76] R. Singh, T. Bhaskar, S. Dora, B. Balagurumurthy, Catalytic hydrothermal upgradation of wheat husk, Bioresource technology 149 (2013) 446-451.

[77] C. Zhong, X. Wei, A comparative experimental study on the liquefaction of wood, Energy 29(11) (2004) 1731-1741.

[78] S. Cheng, I. D'cruz, M. Wang, M. Leitch, C. Xu, Highly efficient liquefaction of woody biomass in hot-compressed alcohol− water co-solvents, Energy & Fuels 24(9) (2010) 4659-4667.

[79] H. Mazaheri, K.T. Lee, A.R. Mohamed, Influence of temperature on liquid products yield of oil palm shell via subcritical water liquefaction in the presence of alkali catalyst, Fuel Processing Technology 110 (2013) 197-205.

[80] S. Mahadevan Subramanya, P.E. Savage, Identifying and modeling interactions between biomass components during hydrothermal liquefaction in sub-, near-, and supercritical water, ACS Sustainable Chemistry & Engineering 9(41) (2021) 13874-13882.

[81] W.T. Chen, W. Qian, Y. Zhang, Z. Mazur, C.-T. Kuo, K. Scheppe, L.C. Schideman, B.K. Sharma, Effect of ash on hydrothermal liquefaction of high-ash content algal biomass, Algal research 25 (2017) 297-306.

[82] D. Xu, Y. Wang, G. Lin, S. Guo, S. Wang, Z. Wu, Co-hydrothermal liquefaction of microalgae and sewage sludge in subcritical water: Ash effects on bio-oil production, Renewable Energy 138 (2019) 1143-1151.

[83] Q. Fan, P. Fu, C. Song, Y. Fan, Valorization of waste biomass through hydrothermal liquefaction: A review with focus on linking hydrothermal factors to products characteristics, Industrial crops and products 191 (2023) 116017.

[84] E. Jasiukaitytė-Grojzdek, M. Kunaver, I. Poljanšek, Influence of cellulose polymerization degree and crystallinity on kinetics of cellulose degradation, BioResources 7(3) (2012).

[85] B.C. Blasco, J.J.M. Moreno, A.P. Pol, A.S. Abad, Using the R-MAPE index as a resistant measure of forecast accuracy, Psicothema 25(4) (2013) 500-506.

Chapter 5

5 Production of Bio-oils or Depolymerized Lignin from Technical Lignin through Hydrothermal Liquefaction: Comparison of Batch and Continuous-flow Operations

Abstract

Batch reactor systems have been predominantly used for laboratory and pilot-scale hydrothermal liquefaction (HTL) of biomass. However, the development of continuous-flow reactor systems is crucial for the cost-effective industrial deployment of HTL technology. In this study, a continuous-flow HTL system capable of processing up to 6 kg/h of feed was developed and used to convert alkali lignin and kraft lignin into bio-oils or depolymerized lignin (DL) using K_2CO_3 catalyst at 300 °C for 15 min. The bio-oils or DL produced were extensively characterized using FT-IR, GPC, TGA, and elemental analysis. The study aimed to compare the performance of the HTL process in the continuous-flow HTL reactor and a batch reactor under the same reaction conditions, in terms of bio-oil or DL yields, chemistry, and energy recovery potential. The results showed that the continuous-flow HTL reactor obtained a lower yield of bio-oil or DL (28.5 wt.% and 43.9 wt.%, respectively) and lower energy recovery rate (50.8% and 50.6% for alkali and kraft lignin, respectively) than those of the batch reactor (36.9 wt.% and 50.6% for alkali lignin, 50.6 wt.% and 64.2% for kraft lignin). These results will be useful for future development and deployment of HTL technology for lignin liquefaction/depolymerization on a large scale.

Keywords: Batch reactor, Bio-oils, Continuous-flow reactor, Depolymerization, Depolymerized lignin, Hydrothermal liquefaction, Technical lignin

5.1 Introduction

The growing consciousness regarding environmental issues like global warming has prompted the exploration of alternative sources that are renewable and sustainable for both energy and chemicals production [1, 2]. Biomass is a significant component of this quest and encompasses a diverse array of materials ranging from forestry and agricultural by-products to energy crops and organic waste like sewage sludge, food waste, and sorted organic waste [3]. Given its widespread availability, biomass is more evenly distributed globally than traditional fossil fuels.

Hydrothermal liquefaction (HTL) is one of the most promising technologies to convert different types of wet biomass into bio-oils or liquid chemical feedstock through reactions such as depolymerization, bond breaking, rearrangement and decarboxylation at elevated temperatures (200–400 °C) and the pressure up to 30 MPa [4-6]. HTL has been receiving increased attention compared to pyrolysis due to its ability to generate bio-oils of superior quality, which contain a lower oxygen content (5-20 wt.%) and produce less gas and solid by-products. More advantageously, HTL can handle high-moisture (>70%) feedstocks without requiring pre-drying.

The majority of research on biomass HTL has been carried out in batch reactors, focusing on the optimisation of the process conditions such as temperature, pressure, and reaction time [3, 7], effects of feedstock type [5] and evaluation of catalysts [8, 9]. Recently, continuous-flow HTL processes have attracted particular attention due to its obvious advantages, such as flexibility, lower supply chain inventory and a higher overall equipment effectiveness as well as a smaller footprint [3, 10, 11]. A few examples of the continuous-flow HTL processes are introduced below.

A continuous-flow HTL reactor was developed by Iowa State University and assessed based on the bio-oil yields obtained during steady-state operation. However, it was observed that bio-oil production was not entirely stable [12]. A new two-stage HTL process was developed at Aalborg University in order to enhance the pumpability of lignocellulosic feedstocks containing high solid loading (25% dw) in HTL. The initial stage of alkaline treatment produced a suitable wood paste for the second stage, which was processed at 400°C and 30 MPa. This continuous bench-scale HTL system had the ability to transform lignocellulosic wood chips into bio-oil at a feed capacity of 20 kg/h [13]. Cheng et al. [14] modified a pilot-scale continuous flow reactor (CFR) for HTL of algae slurry under subcritical conditions to assess the potential for scaling up from batch to continuous processing. The modifications included a unique dual filter system capable of eliminating solids under the system pressure and temperature, as well as in-situ cleaning. Aierzhati et al. [15] presented a novel mobile pilot-scale HTL reactor system (0.57 L/min) for food waste conversion. The mobile HTL system can be delivered to everywhere by truck, and their work demonstrated the economic viability of this mobile HTL system when there is a widespread availability of biomass resources (more than 106 miles).

However, the accumulated information of continuous-flow HTL processes is quite limited and there are no clear comparisons between batch and continuous-flow HTL operations\. The findings from batch processing cannot be directly and effectively applied to the continuous-flow processes, which are more desirable for future industrial scale applications of the HTL technology [4, 16]. In addition, Lignin, as the only natural source of aromatic compounds, is a valuable renewable resource for producing biofuel or phenolic chemicals by hydrothermal liquefaction process [17]. Therefore, the objective of this study was to compare the efficacy of a continuous-flow reactor and a batch reactor in the HTL of various types of technical lignin (alkali lignin and kraft lignin). The comparison was made in terms of product yields, bio-oil or DL chemistry, and energy recovery potential. The HTL of two types of technical lignin was conducted in a plug-flow HTL reactor (with a slurry feeding capacity of up to 6 kg/h) and a 100 ml autoclave batch reactor, both operating at a temperature of 300 °C for 15 min and with the addition of K_2CO_3 catalyst. The characteristics of the resulting bio-oils or DL were analyzed by techniques such as Fourier transform infrared spectroscopy (FT-IR), gel permeation chromatography (GPC), thermogravimetric analysis (TGA), and elemental analysis.

5.2 Materials and Methods

5.2.1 Materials

The alkali lignin used in this work was provided by Shengquan Co. Ltd, Shandong, China, while the kraft lignin was provided by Lancotek Co. Ltd, Ontario, Canada. Both types of lignin were pre-drying at 105 °C in an oven for 24 h. The chemical compositions of both types of lignin are presented in **Table 5.1**. Potassium carbonate was purchased from Sigma-Aldrich (Oakville, Canada). Sulfuric acid was bought from VWR International

(Mississauga, Canada). Reagent-grade acetone and ethanol were obtained from Fisher Scientific (Ottawa, Canada).

Table 5.1: Chemical compositions of the two types of lignin.

	Alkali lignin	**Kraft lignin**
VM[a]	38.6	52.8
FC[a]	46.0	37.5
Ash[a]	15.4	9.7
Purity (%)[b]	41.7	83.6
Ultimate analysis (wt.%)[a]		
C	40.1	62.5
H	6.1	4.8
N	0.4	0.2
S	0.3	2.1
O[c]	37.7	30.4
HHV (MJ/kg)[d]	15.6	24.5

[a] On dry basis; [b]Measure by UV-Vis; [c] By difference; [d] Calculated by DuLong equation: HHV (MJ/kg) = 0.338%C + 1.428(%H-%O/8) + 0.095%S.

5.2.2 Experimental Setup

The batch-mode HTL experiments were conducted in a 100 ml autoclave reactor (Parr 4590 HP/HT reactor) under the operating conditions listed in **Table 5.2**. In a typical run, lignin, distilled water, ethanol (as a co-solvent) and K_2CO_3 (catalyst) were loaded into the reactor. After that, the reactor was sealed and purged with nitrogen to completely remove any residual air. Following that, the reactor was pressurized with nitrogen to 2 MPa and then heated under stirring at 172 rpm to the desired temperature and maintained at that temperature for 15 min as the residence time.

The continuous-flow HTL experiments were conducted on a plug flow HTL reactor (with a maximum slurry feeding capacity of 6 kg/h) designed and custom-built by our lab. **Figure 5.1** is the schematic diagram of the continuous-flow reactor. The main parts of the system include a 5/8-inch SS316L tubular reactor, two piston feeders, feed tank, HPLC pump, pre-heater, and main furnace, cooler, gas-liquid separation vessel and back pressure regulator (BPR). The feedstock slurry was first well-mixed and stored in a stirred container, and then fed into the piston feeders. At the beginning of the experiment, nitrogen purge was introduced into the system to remove any residual air. The reactor was then heated to the desired temperature while pumping distilled water through the reactor system. The pressure of the reactor system was adjusted through the back pressure regulator (BPR) to reach the desired pressure and maintained at 1500 psi in this work. As soon as the reactor reached the desired temperature (300 °C inside the reactor) and pressure, the outlet valve of one of the piston feeders was opened and the HPLC pump was switched to pump water from the water tank to the piston feeder to feed the feedstock slurry to the reactor, afterwards flowing through a pre-heater where the feed was pre-heated to approx. 140 °C. The reactor effluent was cooled in a cooler and then in a liquid-solids separation vessel. The gas and some liquids were released from the top of the separation vessels and solid/liquid products were mainly collected from the bottom of the vessel. When one of the piston feeders was empty, the outlet valve of the other one was opened to maintain a continuous flow through the system. In a typical run, the feed was prepared by mixing the lignin powder, K_2CO_3, and water/ethanol co-solvent. The mixture was fed into the reactor system and reacted at 300 °C inside the tube reactor. The estimated average residence time inside the reactor was controlled at 15 min by setting the slurry feeding speed at 20 mL/min (or 1.2 kg/h). The detailed process parameters for continuous-flow HTL experiments are presented in **Table 5.2**.

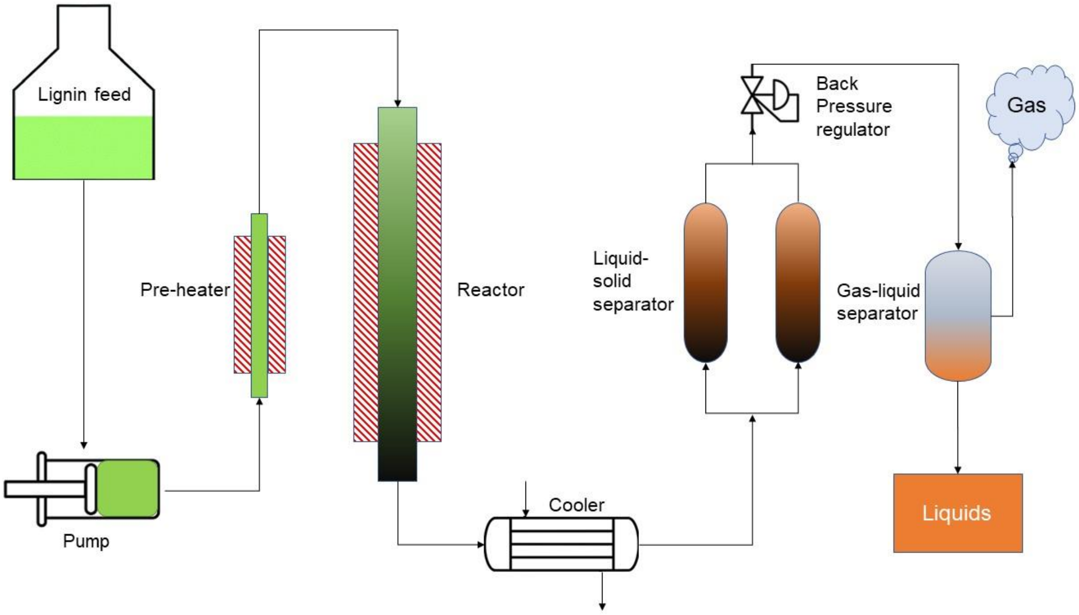

Figure 5.1: The continuous-flow reactor system used for HTL of lignin.

Table 5.2: Detailed operating conditions for HTL of alkali lignin and kraft lignin in the batch/continuous-flow reactors.

	Alkali lignin	**Kraft lignin**
Solvent	Water/EtOH (1:1, v/v)	
Solid/solvent ratio (w/w)	1:5	1:10
Catalyst	K_2CO_3 (10 wt.% of dry feedstock)	
Temperature	300 °C	
Residence time	15 min	

5.2.3 Conversion Products Separation

In the batch-mode HTL tests, the major reaction products were depolymerized lignin, which dissolves very well at alkaline pH due to the ionization of its weakly acidic phenolic and carboxyl groups. Decreasing the pH will progressively protonate these groups and lower the existing electrostatic interactions within the aqueous solution [18]. The solid/liquid products inside the reactor were washed with distilled water. The resulting suspension was acidified to pH = 2 with sulfuric acid, causing the bio-oil or DL to precipitate out of solution. The mixture was then vacuum-filtered to obtain a solid cake and a filtrate through the same pre-weighed VWR No. 413 filter paper. The dry filter cake composed of bio-oil and SR was then rinsed with acetone, followed by filtration to separate the acetone-soluble phase. The acetone insoluble SR was retained on the filter paper. The acetone-soluble phase was evaporated under reduced pressure at 50 °C wherein acetone was removed and bio-oil or DL was collected.

In the continuous-flow HTL tests, the solid/liquid products were mainly collected from the separation vessels (rinsed with acetone after the each run) and the resulting suspension was vacuum-filtered through a pre-weighed VWR No. 413 filter paper. The separated solids were then oven dried at 105 °C overnight to a constant weight to determine the yield SR. The total amount of the filtrate solution collected was weighed. A fixed amount of filtrate sample was then taken and separated using the same procedure as that for the batch-mode HTL tests to determine the bio-oil or DL yeild. In all tests, the yields of aqueous products (AP) and gaseous products (Gas) were lumped and determined by difference.

The yields of the HTL products were calculated based on dry biomass as follows:

$$\mathrm{Bio-oil\ or\ DL\ yield\ (wt.\%)} = \frac{\mathrm{Mass\ of\ bio{-}oil}}{\mathrm{Mass\ of\ feedstock}} \times 100\% \tag{5.1}$$

$$\text{SR yield (wt. \%)} = \frac{\text{Mass of SR}}{\text{Mass of feedstock}} \times 100\% \tag{5.2}$$

$$\text{(AP + Gas) yield (wt. \%)} = 1 - \text{Bio} - \text{oil or DL (wt. \%)} - \text{SR (wt. \%)} \tag{5.3}$$

$$\text{Energy recovery (\%)} = \frac{\text{HHV}_{\text{bio-oil}}}{\text{HHV}_{\text{feedstock}}} \times \text{Bio} - \text{oil (wt. \%)} \times 100\% \tag{5.4}$$

5.2.4 Lignin and Products Analysis

Fourier transform infrared (FT-IR) analyses were conducted on a PerkinElmer FT-IR spectrometer (Massachusetts, USA) to characterize the functional groups of the bio-oil or DL products. The average molecular weight (M_w, M_n), polydispersity index (PDI, PDI=M_w/M_n) of the bio-oil or DL products were determined using Gel Permeation Chromatography (GPC, Waters Breeze) equipped with 1525 binary pump, UV detector set at 270 nm, Waters Styragel HR1 column at 40 °C. The polystyrene (linear polymer) standards were used in GPC-UV calibration. The proximate analysis (volatile matters and fixed carbon contents) of lignin and the boiling point distribution of bio-oil products were determined on a thermogravimetric analyzer (Pris 1 TGA, Waltham, USA), where the sample was heated in 30 ml/min N_2 flow from 25 °C to 800 °C at 10 °C /min, followed by soaking at this temperature for 15 min in 30 mL/min air flow for ashing. The element compositions (C, H, N, and S) of the feedstocks and bio-oil or DL products were determined on an elemental analyzer (Vario EL Cube). The O content was calculated by difference on a dry basis (%O = 100% – %Ash – %C – %H – %N – %S) where the ash contents of the lignin and bio-oil or DL products were determined by ashing at 700 °C for 4 h in air in a muffle furnace. The purity of lignin was analyzed by UV–visible spectrophotometry (UV-Vis, Evolution 220). The higher heating values (HHV) of all feedstocks and bio-oils were estimated by Dulong equation.

$$\text{HHV (MJ/kg)} = 0.338\%\text{C} + 1.428(\%\text{H}-\%\text{O}/8) + 0.095\%\text{S} \tag{5.5}$$

5.3 Results and Discussion

5.3.1 Products Distribution

Figure 5.2 shows the products distribution in HTL of alkali lignin and kraft lignin in the batch/continuous-flow reactors at 300 °C for 15 min, respectively. The yields of bio-oil or DL products from alkali lignin and kraft lignin in the continuous-flow reactor (28.5 wt.% and 43.9 wt.%, respectively) were lower than those from the batch reactor (36.9 wt.% and 50.6 wt.%, respectively). Whereas the SR yields were slightly lower under the continuous-flow operation. These results are consistent with the research conducted by Erdocia et al. [19]. They observed that the bio-oil yield from organosolv lignin increased with the reaction time until reaching a maximum at a prolong residence time of 80 min, accompanied with an opposite trend of residue yield. In continuous-flow operations, the feed was controlled at the reaction temperature as it entered the reactor. In contrast, in batch operations, the feedstock was gradually heated from room temperature to the reaction temperature, and the time taken for heating (which was approximately 30-60 min in this work) was not considered as part of the reaction time. Consequently, the actual residence time in the continuous-flow operations was shorter compared to that in the batch operations. Generally, a longer reaction time would hence the degradation of lignin and increase bio-oil yield in lignin HTL [20, 21]. Besides, long reaction induction period of the intermediates enabled secondary reactions including re-polymerization, cross-linking and rearrangement, thereby forming marginally higher products yields [22]. Thus, the relatively lower residence time of the lignin feed in continuous-flow reactor could possibly cause the incomplete cracking of the easily cleaved bonds in lignin molecule such as ether bonds and carbonyl groups, resulting in the formation of bio-oil or DL with a higher molecular weight, as evidenced by the GPC analysis for the bio-oil or DL products (**Table 5.3**).

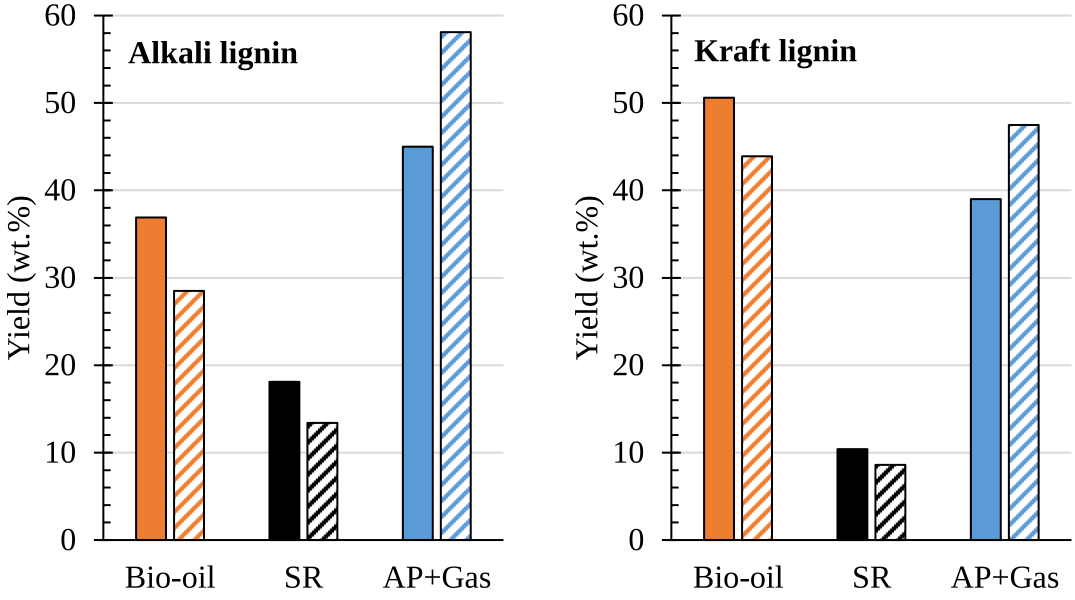

Figure 5.2: Products distribution in HTL of alkali lignin (left) and kraft lignin (right) in the batch and continuous-flow reactors at 300 °C for 15 min (Solid: Batch; Diagonal strips: Continuous-flow).

5.3.2 Chemical Analysis of Bio-oils

Table 5.3 presents the elemental compositions, HHVs, energy recovery rates and molecular weights and distribution of the bio-oil or DL derived from alkali and kraft lignin in the batch/continuous-flow HTL operations. Compared to the bio-oil or DL products obtained from HTL of alkali lignin in the batch reactor, the products from the continuous-flow operation have much higher oxygen content (32.4 wt.% vs 17.9 wt.%), leading to a lower HHV value and the energy recovery rate (31.0 MJ/kg and 64.2% from the batch reactor vs. 28.2 MJ/kg and 50.6 % from the continuous-flow reactor). These again could result from the enhanced deoxygenation reactions owing to a relatively longer reaction time in the batch operations [23]. Similar results were observed in the HTL process of kraft lignin. In addition, as shown in **Table 5.3** and **Figure 5.3**, the molecular weights of the bio-oil or DL products from the continuous-flow reactor are higher than those obtained from the batch reactor with both alkali lignin and kraft lignin, which was likely due to the shorter residence time in the continuous operations leading to incomplete depolymerization of lignin. Longer residence time favored the formation of simple compounds [24], since an extended reaction time could ensure the complete degradation of all ether bonds in lignin and subsequent gradual degradation of the stable C-C bonds [22]. As reported by Tolesa et al., increasing the reaction time from 30 min to 60 min, the values of average M_w further decrease down in the case of alkali lignin depolymerization [25]. Consistent results were observed in the study from Erdocia et al. as well [19].

Table 5.3: Comparison of chemical properties of the bio-oil or DL products derived from alkali lignin and kraft lignin in the batch/continuous-flow HTL operations at 300 °C for 15 min.

	Alkali lignin		**Kraft lignin**	
	Batch	Continuous-flow	Batch	Continuous-flow
Yields (wt.%)	36.9	28.5	50.6	43.9
Ash [a]	1.8	2.5	3.2	4.8
Ultimate analysis (wt.%)[a]				
C	72.0	63.8	73.3	59.7
H	6.9	6.3	6.3	8.1
N	0.3	0.5	0.1	0.1
S	1.1	0.8	1.2	5.0
O[b]	17.9	32.4	15.9	22.3
HHV (MJ/kg)[c]	31.0	24.8	31.0	28.2
Energy recovery (%)[d]	82.2	50.8	64.2	50.6
Molecular weight				
M_w (g/mol)	468	812	995	1229
M_n (g/mol)	322	514	602	718
PDI	1.45	1.57	1.65	1.71

[a] On dry basis; [b] By difference, assuming negligible ash content; [c] Calculated by DuLong equation; [d] Energy recovery (%) $= \frac{\mathrm{HHV_{oil}} \times \mathrm{Weight_{oil}}}{\mathrm{HHV_{feedstock}} \times \mathrm{Weight_{feedstock}}} \times 100$.

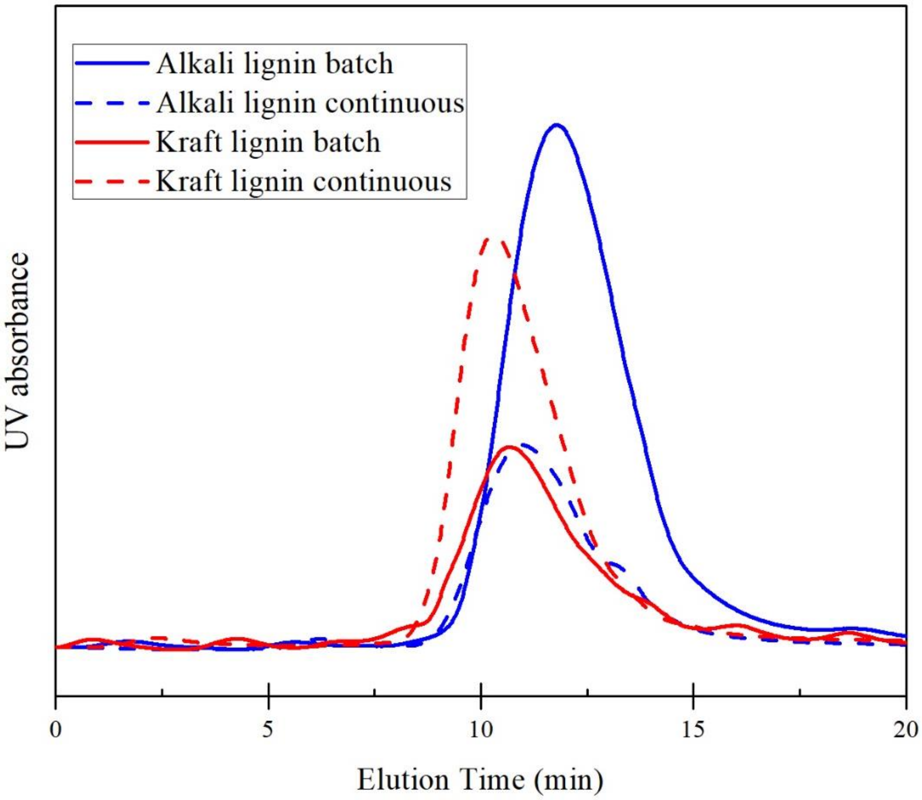

Figure 5.3: The GPC curves of bio-oil or DL products obtained from HTL of alkali lignin and kraft lignin in the batch/continuous-flow operations at 300 °C for 15 min.

Figure 5.4 shows the FT-IR spectra of the bio-oil, or DL products obtained from HTL of lignin in the batch /continuous-flow reactors. As clearly shown in the figure, the FT-IR spectra of all bio-oil/DL products are almost the same. The broad IR absorption at 3500 cm^{-1} is typical of O-H stretching, suggesting the presence of alcohols, phenols, carboxylic acids, or water residues in the products. The absorbance at 1700 cm^{-1}, representing the C=O stretching vibration of carbonyl groups, indicates the presence of ketones, aldehydes, esters or carboxylic acids. These bands are more pronounced in the product from alkali lignin in the continuous-flow operation, suggesting the presence of more conjugated C=O groups in the product. The relatively medium-intense peaks at 1611 and 1495 cm^{-1} represent aromatic nuclei, indicating the presence of aromatic rings and their derivatives in the DL products as expected. The IR absorption bands between 3000 and 2840 cm^{-1} are attributed to C-H stretching vibrations, indicating the presence of alkyl C-H in the products. The two absorption peaks at 1370 and 1456 cm^{-1} are attributed to the bending vibrations of methyl

(-CH_3) and methylene (-CH_2) groups, respectively. The presence of C-H stretching vibration and the C-H blending indicates the alkane groups in the bio-oil/DL products. The peaks between 1280 and 1000 cm^{-1} are likely related to vibrations of C-O ether linkages in the DL products. The peak at 860 cm^{-1} in the products from the continuous-flow operations, attributed to C-H bending, suggests the presence of single, polycyclic, and substituted aromatics.

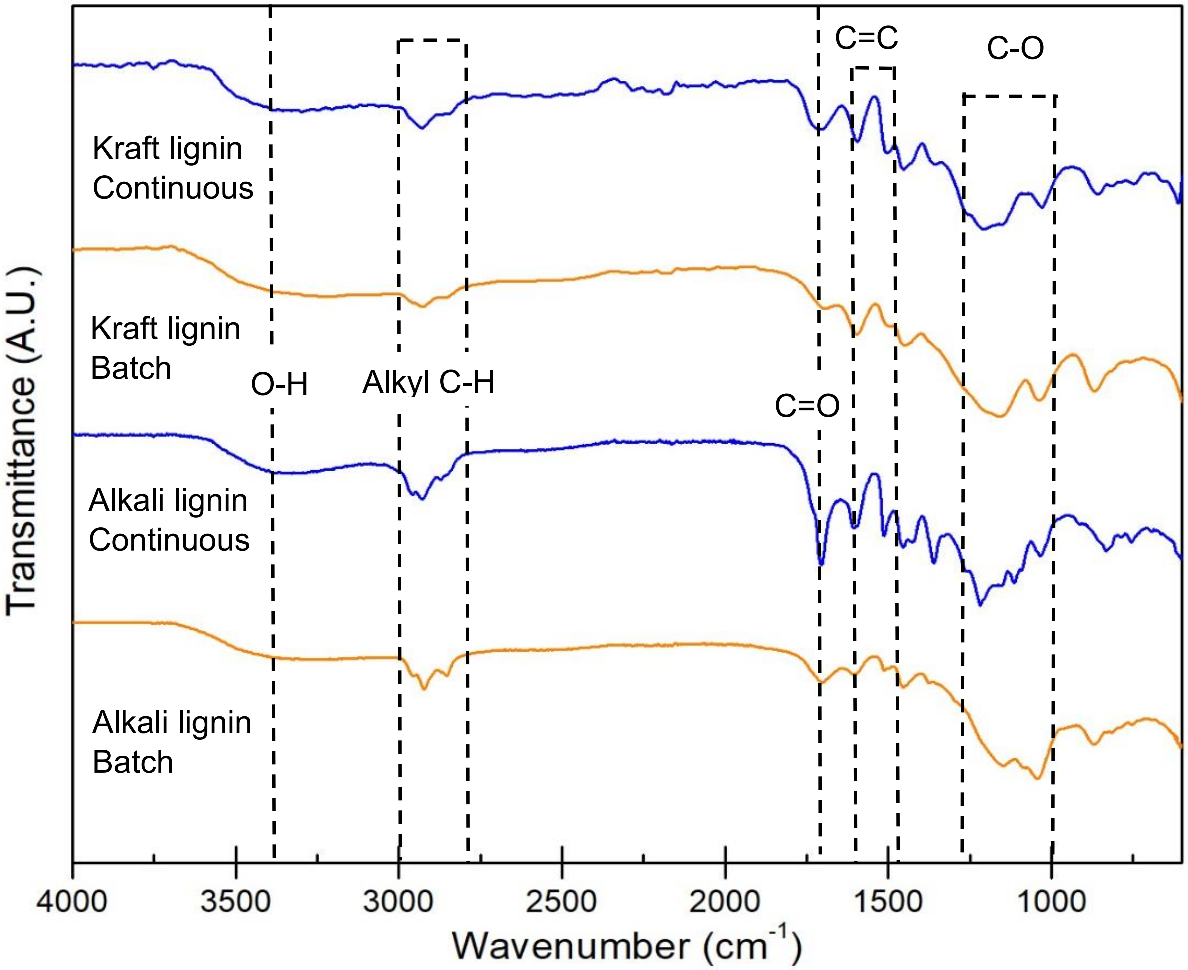

Figure 5.4: FT-IR spectra of bio-oil/DL products obtained from HTL of alkali lignin and kraft lignin in the continuous-flow and batch reactors at 300 °C for 15 min.

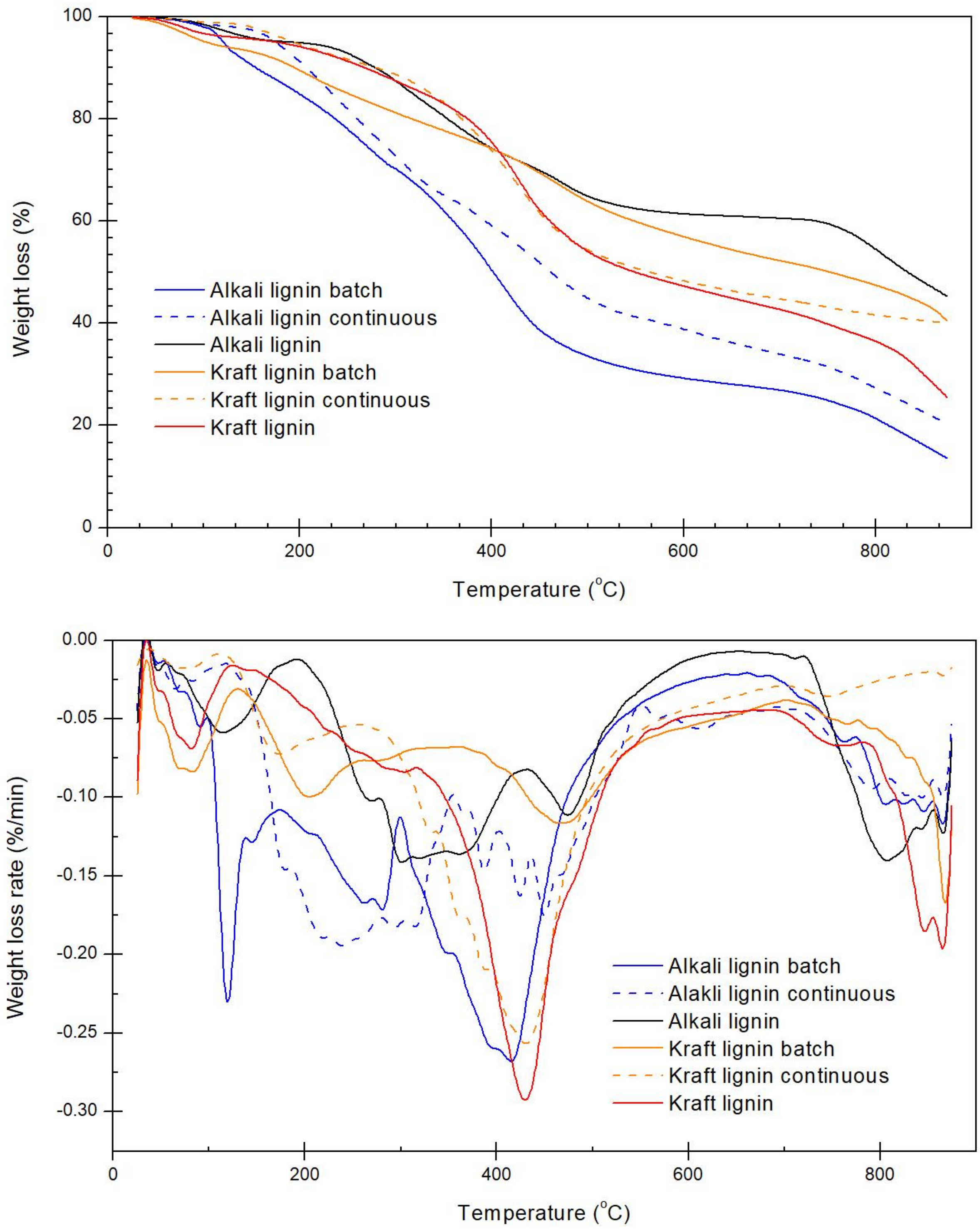

Figure 5.5: TG (a) and DTG (b) curves of the alkali lignin and kraft lignin feedstocks and the bio-oil/DL products from HTL in the continuous-flow and batch reactors at 300 °C for 15 min.

Figures 5.5a and **5.5b** illustrate the thermogravimetric (TG) and derivative thermogravimetric (DTG) curves, respectively, of the alkali lignin and kraft lignin feedstocks and their derived bio-oil/DL products obtained from HTL in the batch and continuous reactors. The boiling point distributions of the bio-oils, estimated from the TG curves, are presented in **Table 5.4**. Generally, the boiling point distributions of the oils obtained from the batch reactor have a larger light fraction (<193 °C) than those from the continuous-flow reactor (alkali lignin: 14.3 wt.% vs. 7.5 wt.%; kraft lignin: 9.5 wt.% vs. 4.9 wt.%). For both types of lignin, the oils from both reactors have similar boiling point distributions in the distillate ranges of 193-271 °C (Kerosene) and 271-343 °C (Gas Oil). The alkali lignin-derived oil from the batch reactor has a higher fraction (32%) of the distillate range 343-538 °C (Vac Gas Oil) than that (24.1%) from the continuous-flow reactor, corresponding to a lower Residues (>538 °C) fraction for the oil from the batch reactor. In contrast, a reverse trend was obtained for HTL of kraft lignin, with the produced oils from the batch reactor having a lower fraction (17.5%) of the distillate range 343-538 °C (Vac Gas Oil) than that (32.7%) from the continuous-flow reactor, as well as a larger Residues (>538 °C) fraction for the oil from the batch reactor. Such inconsistency was likely due to the differences in the chemical compositions and purities of the two types of lignin.

As shown in the DTG curves (**Figure 5.5b**), the initial decomposition of both oils obtained in the batch reactor occurred at around 100-130 °C, whereas that the decomposition of oils from the continuous-flow HTL reactor started from around 200 °C, suggesting that the oils from the batch reactor have lower boiling points. With both types of lignin, the oil obtained from both types of reactors thermally degraded mainly between 200-300 °C and 400-500 °C.

Table 5.4: Boiling point distributions of the bio-oil products from HTL of alkali lignin and kraft lignin at 300 °C for 15 min.

Distillate range (°C)	Alkali lignin		Kraft lignin	
	Batch	Continuous-flow	Batch	Continuous-flow
<193 (Heavy Naphtha)	14.3	7.5	9.5	4.9
193-271 (Kerosene)	11.2	14.5	6.8	4.5
271-343 (Gas Oil)	11.1	12.1	5.2	6.3
343-538 (Vac Gas Oil)	32.0	24.1	17.5	32.7

>538 (Residues)	31.3	41.8		60.7	51.5

5.4 Conclusions

This study compared the performance of lignin HTL/depolymerization in a continuous-flow reactor and a batch reactor operating at 300 °C for 15 minutes. The yields of bio-oil/DL from alkali and kraft lignin were found to be lower (28.5 wt.% and 43.9%, respectively) in the continuous-flow reactor compared to those produced in the batch reactor (36.9 wt.% and 50.6%, respectively), as well as having a lower energy recovery rate. Additionally, the bio-oil/DL products produced from the continuous-flow reactor have lower HHVs, lower fractions of light oil with boiling points (<193 °C), but higher molecular weights due to the shorter reaction time in the continuous-flow operations. These findings would be useful for development of continuous-flow HTL systems for production of biofuel or phenolic chemicals from lignin on a large-scale.

5.5 References

[1] H.C. Ong, W.-H. Chen, A. Farooq, Y.Y. Gan, K.T. Lee, V. Ashokkumar, Catalytic thermochemical conversion of biomass for biofuel production: A comprehensive review, Renewable and Sustainable Energy Reviews 113 (2019) 109266.

[2] S. Pang, Advances in thermochemical conversion of woody biomass to energy, fuels and chemicals, Biotechnology advances 37(4) (2019) 589-597.

[3] I.A. Basar, H. Liu, H. Carrere, E. Trably, C. Eskicioglu, A review on key design and operational parameters to optimize and develop hydrothermal liquefaction of biomass for biorefinery applications, Green Chemistry 23(4) (2021) 1404-1446.

[4] D. Castello, T.H. Pedersen, L.A. Rosendahl, Continuous hydrothermal liquefaction of biomass: A critical review, Energies 11(11) (2018) 3165.

[5] A. Dimitriadis, S. Bezergianni, Hydrothermal liquefaction of various biomass and waste feedstocks for biocrude production: A state of the art review, Renewable and Sustainable Energy Reviews 68 (2017) 113-125.

[6] J. Ni, L. Qian, Y. Wang, B. Zhang, H. Gu, Y. Hu, Q. Wang, A review on fast hydrothermal liquefaction of biomass, Fuel 327 (2022) 125135.

[7] R.K. Mishra, P. Kumar, K. Mohanty, Hydrothermal liquefaction of biomass for bio-crude production: A review on feedstocks, chemical compositions, operating parameters, reaction kinetics, techno-economic study, and life cycle assessment, Fuel 316 (2022) 123377.

[8] Y. Wu, H. Wang, H. Li, X. Han, M. Zhang, Y. Sun, X. Fan, R. Tu, Y. Zeng, C.C. Xu, Applications of catalysts in thermochemical conversion of biomass (pyrolysis, hydrothermal liquefaction and gasification): A critical review, Renewable energy (2022).

[9] S. Nagappan, R.R. Bhosale, D.D. Nguyen, N.T.L. Chi, V.K. Ponnusamy, C.S. Woong, G. Kumar, Catalytic hydrothermal liquefaction of biomass into bio-oils and other value-added products–A review, Fuel 285 (2021) 119053.

[10] A. Lababpour, Continuous hydrothermal liquefaction for biofuel and biocrude production from microalgal feedstock, ChemBioEng Reviews 5(2) (2018) 90-103.

[11] S. Sahu, N. Sahoo, S. Naik, D. Mahapatra, Advancements in hydrothermal liquefaction reactors: Overview and prospects, Bioreactors (2020) 195-213.

[12] A.R. Suesse, G.A. Norton, J. van Leeuwen, Pilot-scale continuous-flow hydrothermal liquefaction of filamentous fungi, Energy & Fuels 30(9) (2016) 7379-7386.

[13] I.M. Sintamarean, I.F. Grigoras, C.U. Jensen, S.S. Toor, T.H. Pedersen, L.A. Rosendahl, Two-stage alkaline hydrothermal liquefaction of wood to biocrude in a continuous bench-scale system, Biomass Conversion and Biorefinery 7 (2017) 425-435.

[14] F. Cheng, T. Le Doux, B. Treftz, S. Woolf, J. Yu, J. Miller, U. Jena, C.E. Brewer, Modification of a pilot-scale continuous flow reactor for hydrothermal liquefaction of wet biomass, MethodsX 6 (2019) 2793-2806.

[15] A. Aierzhati, J. Watson, B. Si, M. Stablein, T. Wang, Y. Zhang, Development of a mobile, pilot scale hydrothermal liquefaction reactor: Food waste conversion product

analysis and techno-economic assessment, Energy Conversion and Management: X 10 (2021) 100076.

[16] Y. Fan, C. Prestigiacomo, M. Gong, T. Tietz, U. Hornung, N. Dahmen, Comparative investigation on the value-added products obtained from continuous and batch hydrothermal liquefaction of sewage sludge, Frontiers in Environmental Science 10 (2022) 996353.

[17] K.R. Arturi, M. Strandgaard, R.P. Nielsen, E.G. Søgaard, M. Maschietti, Hydrothermal liquefaction of lignin in near-critical water in a new batch reactor: Influence of phenol and temperature, The Journal of Supercritical Fluids 123 (2017) 28-39.

[18] S. Gillet, M. Aguedo, L. Petitjean, A. Morais, A. da Costa Lopes, R. Łukasik, P. Anastas, Lignin transformations for high value applications: towards targeted modifications using green chemistry, Green Chemistry 19(18) (2017) 4200-4233.

[19] X. Erdocia, R. Prado, M.Á. Corcuera, J. Labidi, Influence of reaction conditions on lignin hydrothermal treatment, Frontiers in Energy Research 2 (2014) 13.

[20] Y. Cao, C. Zhang, D.C. Tsang, J. Fan, J.H. Clark, S. Zhang, Hydrothermal liquefaction of lignin to aromatic chemicals: impact of lignin structure, Industrial & Engineering Chemistry Research 59(39) (2020) 16957-16969.

[21] J. Schuler, U. Hornung, N. Dahmen, J.J.G.B. Sauer, Lignin from bark as a resource for aromatics production by hydrothermal liquefaction, Gcb Bioenergy 11(1) (2019) 218-229.

[22] Y. Alhassan, U. Hornung, I.M. Bugaje, Lignin hydrothermal liquefaction into bifunctional chemicals: a concise review, IntechOpen2020.

[23] R.B. Carpio, Y. Zhang, C.-T. Kuo, W.-T. Chen, L.C. Schideman, R. de Leon, Effects of reaction temperature and reaction time on the hydrothermal liquefaction of demineralized wastewater algal biomass, Bioresource Technology Reports 14 (2021) 100679.

[24] Y. Ye, J. Fan, J. Chang, Effect of reaction conditions on hydrothermal degradation of cornstalk lignin, Journal of Analytical and Applied Pyrolysis 94 (2012) 190-195.

[25] L.D. Tolesa, B.S. Gupta, M.-J. Lee, Degradation of lignin with aqueous ammonium-based ionic liquid solutions under milder conditions, New Journal of Chemistry 43(8) (2019) 3357-3365.

Chapter 6

6 Production of Bio-oils from Various Bio-feedstocks through Hydrothermal Liquefaction: Comparison of Batch and Continuous-flow Operations

Abstract

Laboratory- and pilot- scale hydrothermal liquefaction (HTL) of biomass has predominantly been carried out in batch reactor systems. However, the development of continuous-flow reactor systems is critical for industrial deployment of HTL technology in a cost-competitive manner. In this study, a continuous-flow HTL system (with a feed capacity up to 6 kg/h) was developed and employed to convert various types of bio-feedstocks (wood sawdust, cornstalk, and black liquor) into bio-oils in the presence of K_2CO_3 catalyst at 300 °C for 12 min. The produced bio-oils were characterized in detail by using GC-MS, FT-IR, GPC, and elemental analysis. This work compared the performance of the continuous-flow HTL process with that of a batch HTL process under the same conditions in terms of the yields and chemistry of the bio-oil products as well as the energy recovery potential. The results indicated that HTL of different bio-feedstocks, particularly cornstalk and pinewood, in the continuous-flow reactor led to a higher yield of bio-oil (32.4 and 34.5 wt.%, respectively) with lower molecular weights and less solid residue (2.9 and 4.6 wt.%, respectively) as well as a higher energy recovery rate (53.3 and 52.0%, respectively) compared with those in the batch reactor (Cornstalk: 23.8 wt.%, 6.2 wt.% and 46.5%; Pinewood: 28.5 wt.%, 10.3 wt.% and 50.8%, respectively). These promising results shall advance the future development and deployment of the HTL technology in Canadian and global bioenergy sectors.

Keywords: Batch reactor, Bio-oils, Black liquor, Continuous reactor, Hydrothermal liquefaction, Wood sawdust

6.1 Introduction

Serious environmental concern and increasing demands for clean and renewable energy and chemicals have significantly propelled the development and deployment of advanced bioenergy production and application technologies. Biomass is a plant-based renewable resource, including mainly forestry and agricultural residues, energy crops, sewage sludge, microalgae, food and other organic wastes [1]. Compared with fossil resources, biomass is renewable in nature [2-5], making it as a very important alternative for fossil resources for global energy and chemical production.

Pyrolysis and hydrothermal liquefaction (HTL) are two main thermochemical pathways developed for the transformation of raw biomass materials into liquid products that can be further processed to produce biofuels or bio-based chemicals. Over the past decades, HTL has developed to be one of the most promising thermochemical conversion methods to valorize different types of biomass feedstocks, ranging from lignocellulosic biomass to microalgae and organic wastes, in particular for wet bio-feedstocks. Recently HTL has gained more attention than pyrolysis because it produces higher quality bio-oils with a lower oxygen content (5-20 wt.%) and much less by-production of gas and solid products [6], and it can process high-moisture (>70%) feedstocks without the requirement for pre-drying [7, 8]. HTL of biomass or organic wastes operates at mild temperatures (200–400 °C) and the pressure range of 5–25 MPa due to the presence of water or an organic solvent or a mixed solvent [9].

Intensive efforts have been made in biomass HTL in batch reactors, generating abundant information on the effects of different operating parameters and a variety of feedstocks on the yields and properties of bio-oils [7, 10-14]. However, precise control of residence time and pressure in a batch reactor are quite challenging due to the variability in reactor heating/cooling rates, and the autogenic pressure (temperature, solvent and reactor volume dependent) during the HTL processes [15]. Thus, the findings from batch processing cannot be directly and effectively applied to the continuous-flow processes, which are more desirable for future industrial scale applications of the HTL technology [1, 16]. Recently, continuous-flow HTL processes has attracted particular attention due to its obvious advantages, such as flexibility, lower supply chain inventory and a higher overall equipment effectiveness [3, 17, 18]. For example, researchers from the Pacific Northwest National Laboratory (PNNL) have accumulated considerable experience in continuous-flow biomass HTL. They developed a continuous-flow HTL reactor system comprising a continuous-flow stirred-tank reactor and a horizontal tubular reactor, and conducted continuous-flow HTL investigations on a variety of wet-waste feedstocks (fermentation waste, sludge, manure, food waste, and mixed waste) [19-21]. The University of Bath's continuous HTL reactor proved to be a cost-effective solution, which made it a viable option for large-scale implementation. The reactor's unique design, consisting of a double tube with an inner tube placed within a reactor, enabled the cold algae feed to be introduced through the top of the inner tube, where it was gradually heated. The resulting products were then directed up through the annulus of the reactor and exited from the top [22]. Anastasakis et al. [23] developed a pilot-scale continuous- flow biomass HTL system employing a hydraulic oscillation device to boost the turbulence inside the tube reactor (with a slurry feeding capacity up to 100 L/h). The oscillators improved the overall mixing and heat transfer inside the reactor system by increasing the turbulence throughout the reactor. In addition to this, they demonstrated the efficiency of a customized heat exchanger, being able to recover up to 80% of heat in the reactor effluent. Aierzhati et al. [24] presented a novel mobile pilot-scale HTL reactor system (0.57 L/min) for food waste conversion. The mobile HTL system can be delivered to everywhere by truck, and their work demonstrated the economic viability of this mobile HTL system when there is a widespread availability of biomass resources (more than 106 miles). However, the accumulated information of continuous-flow HTL processes is quite limited and there are no clear comparisons between batch- and continuous-HTL modes. Also, it is unclear about the role of biomass types (especially biowastes) on the performance of continuous HTL processes.

In summary, most of the HTL research has been conducted in batch reactors, and continuous-flow reactor systems are more desirable for industrial applications of biomass HTL. Therefore, this study aimed to compare the performance of a continuous-flow reactor and a batch reactor in HTL of various types of bio-feedstocks (pinewood sawdust, cornstalk, and black liquor) in terms of product yields and chemistry of the bio-oils as well as the energy recovery potential. In this work, HTL of the three types of biomasses were processed in a plug-flow HTL reactor (with a slurry feeding capacity of up to 6 kg/h) and a 100 ml autoclave batch reactor at 300 °C for 12 min in the presence of K_2CO_3 catalyst.

The physicochemical characteristics of the bio-oils were analyzed using Fourier transform infrared spectroscopy (FT-IR), gas chromatography mass spectrometry (GC-MS), gel permeation chromatography (GPC), and elemental analysis techniques.

6.2 Materials and Methods

6.2.1 Materials

Cornstalk used in this work was provided by Ontario Federation of Agriculture collected from South Ontario, Canada. Pinewood sawdust was collected from a local sawmill in London, Canada. The black liquor used in this study was provided by FPInnovations Bioeconomy Technology Centre, Thunder Bay, Canada. The cornstalk and pinewood sawdust were pre-drying at 105 °C in an oven for 24 h and grounded to particles finer than 40 mesh. The chemical compositions of the three bio-feedstocks are presented in **Table 6.1**. Potassium carbonate and sodium carboxymethyl cellulose (CMC) were purchased from Sigma-Aldrich (Oakville, Canada). Sulfuric acid was bought from VWR International (Mississauga, Canada). Reagent-grade acetone and ethanol were obtained from Fisher Scientific (Ottawa, Canada).

Table 6.1: Chemical compositions of the bio-feedstocks.

	Cornstalk	**Pinewood**	**Black liquor**
Proximate analysis (wt.%)			
Moisture content	6.1	12.4	-
Cellulose[a]	35.3	40.7	-
Hemicellulose[a]	32.6	25.8	-
Lignin[a]	18.6	26.8	42.0
Extractives[a]	11.1	6.1	-
Ash[a]	2.4	0.6	32.1
Ultimate analysis (wt.%)[a]			
C	46.0	47.0	37.3
H	5.9	6.0	3.9
N	0.6	0.01	0.03
S	<0.01	<0.01	1.6
O[b]	46.5	46.4	25.0
HHV (MJ/kg)[c]	15.0	16.2	13.9

[a] On dry basis; [b] By difference; [c] Calculated by DuLong equation: HHV (MJ/kg) = 0.338%C + 1.428(%H-%O/8) + 0.095%S.

6.2.2 Experimental Setup

The batch-mode HTL experiments were conducted in a 100 ml autoclave reactor (Parr 4590 HP/HT reactor) under the operating conditions listed in **Table 6.2**. In a typical run, biomass feedstock, distilled water, ethanol (as a co-solvent) and K_2CO_3 (catalyst) were loaded into the reactor. After that, the reactor was sealed and purged with nitrogen to completely remove any residual air. Following that, the reactor was pressurized with nitrogen to 2 MPa and then heated under stirring at 172 rpm to the desired temperature and maintained at that temperature for 12 min as the residence time.

The continuous-flow HTL experiments were conducted on a plug flow HTL reactor (with a maximum slurry feeding capacity of 6 kg/h) designed and custom-built at our lab. **Figure 6.1** is the schematic diagram of the continuous-flow reactor for biomass HTL. The detailed information of this setup was described in **Section 5.2.2**. In a typical run, the feedstock was prepared by mixing the ground biomass particles, K_2CO_3, and water or water/ethanol co-solvent. To facilitate pumping the cornstalk or pinewood slurry with high solids concentration, CMC as a dispersant was added to the feedstock slurry at an amount of 3 wt.% of the total reaction mixture to obtain a homogeneous suspension. The slurry was fed into the reactor system and reacted at 300 °C inside the tube reactor. The estimated average residence time inside the reactor was controlled at 12 min by setting the slurry feeding speed at 25 mL/min (or 1.5 kg/h). The detailed process parameters for continuous-flow HTL experiments are presented in **Table 6.2**. The purpose of adding EtOH in HTL of cornstalk and pinewood was to prevent potential clogging of the reactor by the bio-oils as ethanol could dissolve the bio-oils produced. The bio-oils produced from cornstalk and pinewood were highly viscous and thus could not be dissolved in water after passing through the cooler in the continuous-flow system, consequently resulting in clogging problem in the continuous-flow operations. Whereas the bio-oil converted from black liquor was water-soluble due to its high alkali content.

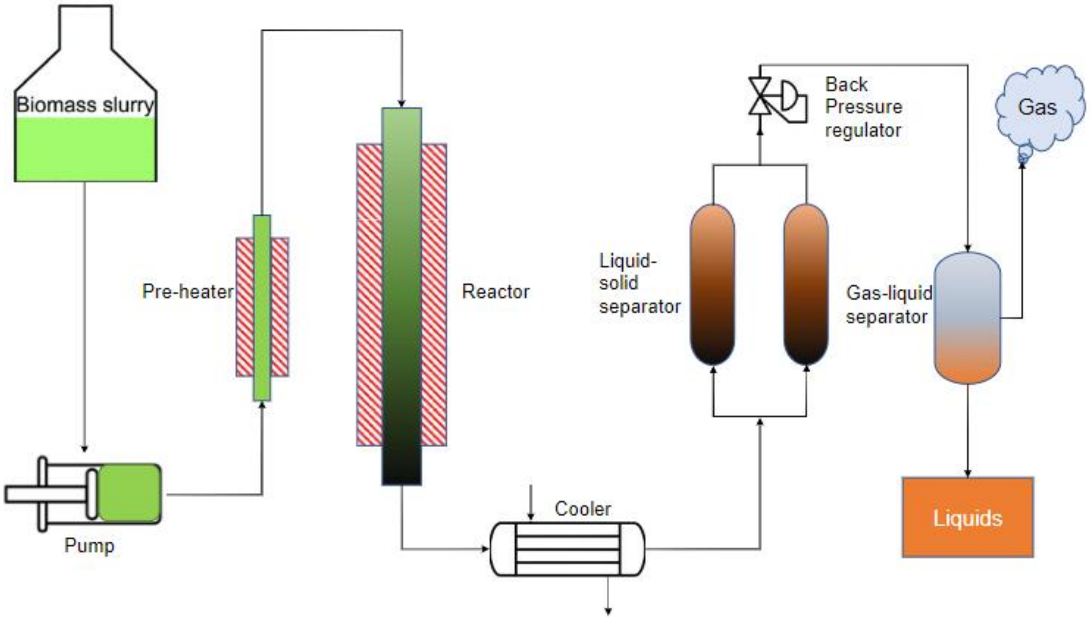

Figure 6.1: The continuous-flow reactor system used for HTL of bio-feedstocks.

Table 6.2: Detailed operating conditions for the batch/continuous-flow HTL of cornstalk, pinewood, and black liquor.

Feedstock	**Cornstalk, Pinewood**	**Black liquor**
Solvent	Water/EtOH (9:1, v/v)	Water
Solid/solvent ratio (w/w)	1:19	1:9
Viscosity modifier	CMC (3 wt.% for the continuous-flow reactor only)	n.a.
Catalyst	K_2CO_3 (5 wt.% of dry feedstock)	
Temperature	300 °C	
Residence time	12 min	

6.2.3 Conversion Products Separation

The products from HTL processes include gaseous products (Gas), bio-oil, aqueous phase (AP), and solid residue (SR). In the batch-mode HTL tests for cornstalk and pinewood, the products were collected and separated based on the similar separation procedure of pinewood sawdust in **Section 3.2.2.2.** For the batch-mode HTL tests of black liquor, the products were collected and separated based on the similar separation procedure of batch-mode lignin HTL process in **Section 5.2.3**.

In the continuous-flow HTL tests, the solid/liquid products were mainly collected from the separation vessels (rinsed with acetone after the each run with cornstalk or pinewood) and the resulting suspension was vacuum-filtered through a pre-weighed VWR No. 413 filter paper. The separated solids were then oven dried at 105 °C overnight to a constant weight to determine the yield of SR. The total amount of the filtrate solution collected was weighed. A fixed amount of filtrate sample was then taken and separated using the same procedure as that for the batch-mode HTL tests.

The yields of the HTL products were calculated based on dry biomass as follows:

$$\text{Bio} - \text{oil yield (wt.\%)} = \frac{\text{Mass of bio−oil}}{\text{Mass of feedstock}} \times 100 \tag{6.1}$$

$$\text{SR yield (wt.\%)} = \frac{\text{Mass of SR}}{\text{Mass of feedstock}} \times 100 \tag{6.2}$$

$$(\text{AP} + \text{ Gas}) \text{ yield (wt.\%)} = 100 - \text{Bio} - \text{oil (wt.\%)} - \text{SR (wt.\%)} \tag{6.3}$$

$$\text{Energy recovery (\%)} = \frac{\text{HHV}_{\text{bio−oil}}}{\text{HHV}_{\text{feedstock}}} \times \text{Bio} - \text{oil (wt.\%)} \times 100 \tag{6.4}$$

6.2.4 Feedstocks and Products Analysis

Fourier transform infrared (FT-IR) analyses on a PerkinElmer FT-IR spectrometer (Massachusetts, USA) were conducted to characterize the functional groups of the bio-oils. The average molecular weight (M_w, M_n) and polydispersity index (PDI, PDI=M_w/M_n) of the bio-oils were determined using Gel Permeation Chromatography (GPC, Waters Breeze) equipped with 1525 binary pump, UV detector set at 270 nm, Waters Styragel HR1 column at 40 °C. The polystyrene (linear polymer) standards were used in GPC-UV calibration. The volatile compositions were analyzed with Gas Chromatograph-Mass Spectrometer (GC–MS, Agilent Technologies, 5977A MSD) equipped with an HP-5MS column (30 m × 250 μm × 0.25 μm). The GC temperature program was set as: held at 40 °C for 5 min, then increased by 10 °C/min to 150 °C and held for 2 min, then increased by 10 °C/min to 290 °C and held for 5 min. The injection mode and ionization mode were split mode and electron ionization (EI), respectively. After a solvent delay of 3.0 min, full scan mass spectra were acquired from 40 to 400 m/z. It should be noted that some low molecular-weight oil compounds might be lost in the solvent evaporation stage, and most of the heavy compounds cannot be eluted into the column [25]. The identification of the peaks was conducted based on the NIST Library with 2011 Update and then integrated and normalized to 100 to get a semi-quantitative result. According to their functional groups, the main chemical compounds in bio-oils were categorized into furans, acids, aldehydes, phenols, esters, alcohols, ketones, aromatic compounds, and others (e.g., sulfides, chlorides). The element compositions (C, H, N, and S) of the feedstocks and bio-oils were determined on an elemental analyzer (Vario EL Cube). The O content was calculated by difference on a dry basis (%O = 100% – %Ash – %C – %H – %N – %S) where the ash contents of the feedstocks and bio-oils were determined by ashing at 700 °C for 4 h in air in a muffle furnace. NREL/TP-510-42718 method was used to determine the compositional contents of lignin, cellulose, and hemicellulose in oven-dried lignocellulosic feedstocks. FPI-in-house method was used to determine the lignin content in black liquor. The moisture content in the lignocellulosic biomass was determined by drying in an oven at 105 °C for 12 h. The higher heating values (HHV) of all feedstocks and bio-oils were estimated by Dulong equation.

$$\mathrm{HHV\,(MJ/kg)} = 0.338\%\mathrm{C} + 1.428(\%\mathrm{H}-\%\mathrm{O}/8) + 0.095\%\mathrm{S} \tag{6.5}$$

6.3 Results and Discussion

6.3.1 Cornstalk and Pinewood HTL

6.3.1.1 Products Distribution

Figure 6.2 shows the product yields in HTL of cornstalk and pinewood in the batch/continuous-flow reactor at 300 °C for 12 min. It should be noted that all batch tests were repeated 2-3 times and the relative errors are presented as error bars, while the continuous-flow tests were not repeated due to their long-time operations. The yields of bio-oil from cornstalk and pine sawdust in the continuous-flow reactor (32.4 wt.% and 34.5 wt.%, respectively) were both noticeably higher than those from the batch reactor (23.8 wt.% and 28.5 wt.%, respectively). Moreover, the SR yields were much lower under the continuous-flow operations. The different reactor type thus accounted for the differences in the products distributions in HTL of both lignocellulosic feedstocks. Some possible reasons are discussed here. First of all, the differences in heat/mass transfer in the batch and continuous-flow reactor systems would certainly influence the biomass HTL reactions.

In addition, in the continuous-flow operations, the feed reached the reactor controlled at the reaction temperature, whereas in the batch operations, the feedstock was progressively heated from room temperature to the reaction temperature, and the heating time (approx. 30-60 min) was not counted in the reaction time. As such, the actual residence time in the continuous-flow operations would be shorter than that occurred in the batch operations. In a HTL process, a shorter residence time was found to be generally preferrable for bio-oil production, especially in the operations with a low biomass-to-water ratio [6, 7, 26]. A longer residence time would induce repolymerization and condensation of intermediate products into insoluble large molecules or SR [3], hence lowering the yield of bio-oil [27-29]. Different results were described in others' research. Barreiro et al. [30] provides a comparison between the performance of CSTR and batch reactors on HTL of microalgal species. The bio-oil yield decreased for both strains when using a CSTR. (from 51.5 ± 2.1 wt.% in batch to 42.6 ± 5.5 wt.% in CSTR for S. almeriensis; from 52.6 ± 2.3 wt.% in batch to 50.8 ± 1.1 wt.% in CSTR for N. gaditana). Similarly, Laleh reported that the yield of bio-oil from HTL of waste activated sludge in the continuous-flow reactor (25.3 wt.%) is slightly lower than that from the batch reactor (~30 wt.%) [31]. It should be noted that the higher bio-oil yield in the continuous-flow operation could also be attributed to the conversion of some CMC added as the feedstock dispersant in the continuous-flow operations [32, 33]. In addition, the higher bio-oil yield obtained from pinewood HTL process could possibly be due to the higher cellulose and lignin content in pinewood sawdust [34, 35].

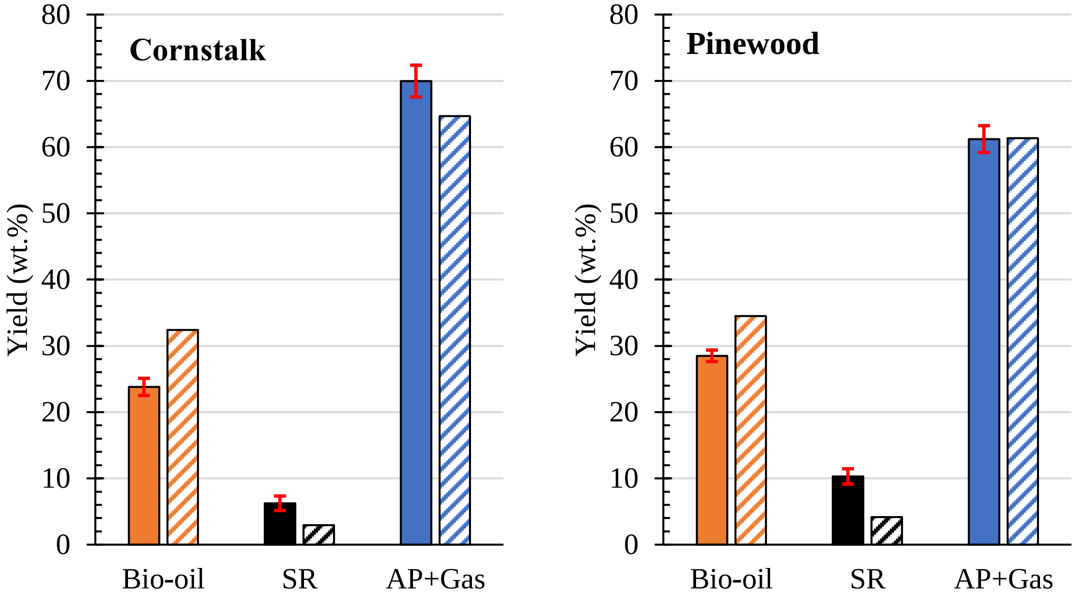

Figure 6.2: Products yields from HTL of cornstalk (left) and pinewood (right) in the batch and continuous-flow reactors at 300 °C for 12 min (Solid: Batch; Diagonal strips: Continuous-flow).

6.3.1.2 Chemical Analysis of the Bio-oils

Table 6.3 summarizes the chemical property results for the bio-oils obtained in the batch-mode/continuous-flow HTL of cornstalk and pinewood at 300 °C, for 12 min: their elemental compositions, HHV, energy recovery and molecular weights. Compared with those obtained from the continuous-flow operations with both feedstocks, the bio-oils obtained from the batch operations have slightly higher carbon contents, lower oxygen contents, and higher HHVs (29.3 MJ/kg and 28.9 MJ/kg, respectively, from the batch reactor vs 24.7 MJ/kg and 24.4 MJ/kg, respectively, from the continuous-flow operations reactor). These could result from the enhanced deoxygenation reactions owing to a relatively longer reaction time in the batch operations [36]. Similar trend was reported by Fan et al. [16]. Higher content of oxygen was found in the bio-oil from continuous flow HTL of sewage sludge. They indicated that a faster heating rate in continuous operation improves the formation of oxygenates. Although a greater HHV of bio-oil is always desirable, a balance on bio-oil yield and HHV must be considered to have better energy recovery rate for bio-oil production from biomass HTL [37]. As shown in **Table 6.3**, the energy recovery into the bio-oil produced from cornstalk and pinewood was slightly higher in the continuous-flow reactor (53.3% and 52.0%, respectively) compared to that in the batch reactor (46.5% and 50.8%, respectively). The bio-oils obtained from both reactors have similar M_w (572-742 g/mol) and M_n (410-476 g/mol), as presented in **Table 6.3**.

Table 6.3: Comparison of chemical properties of the bio-oils derived from cornstalk/pinewood in the batch/continuous-flow HTL processes at 300 °C for 12 min.

	Cornstalk		**Pinewood**	
	Batch	Continuous-flow	Batch	Continuous-flow
Yields (wt.%)	23.8	32.4	28.5	34.5
Ultimate analysis (wt.%)[a]				
C	70.5	67.6	69.8	66.1
H	6.7	4.7	6.6	5.0
N	0.05	0.3	0.86	0.2
S	<0.01	0.1	<0.01	0.05
O[b]	22.8	27.3	22.8	28.6
HHV (MJ/kg)[c]	29.3	24.7	28.9	24.4
Energy recovery (%)[d]	46.5	53.3	50.8	52.0
Molecular weight				
M_w (g/mol)	708	742	632	572
M_n (g/mol)	453	476	410	422
PDI	1.56	1.56	1.54	1.36

[a] On dry basis; [b] By difference, assuming negligible ash content; [c] Calculated by DuLong equation; [d]Energy recovery (%) $= \frac{\mathrm{HHV_{oil}} \times \mathrm{Weight_{oil}}}{\mathrm{HHV_{feedstock}} \times \mathrm{Weight_{feedstock}}} \times 100$.

The GC-MS analysis results of main volatile chemical compounds in the bio-oils from HTL of cornstalk and pinewood sawdust in the batch/continuous-flow operations are compared in **Figure 6.3**. The major components detected by GC-MS are aromatic and phenolic compounds, and some ketones, which could be derived from cellulose in the cornstalk/pinewood feedstocks. Compared with the oils from the batch operations, the bio-oils obtained from the continuous-flow operations contain higher amount of furan compounds, with relatively smaller molecular weight. This could be due to the longer retention times in the batch HTL process , causing condensation/repolymerization of the furans into large-molecule compounds or even hydrochar [3].

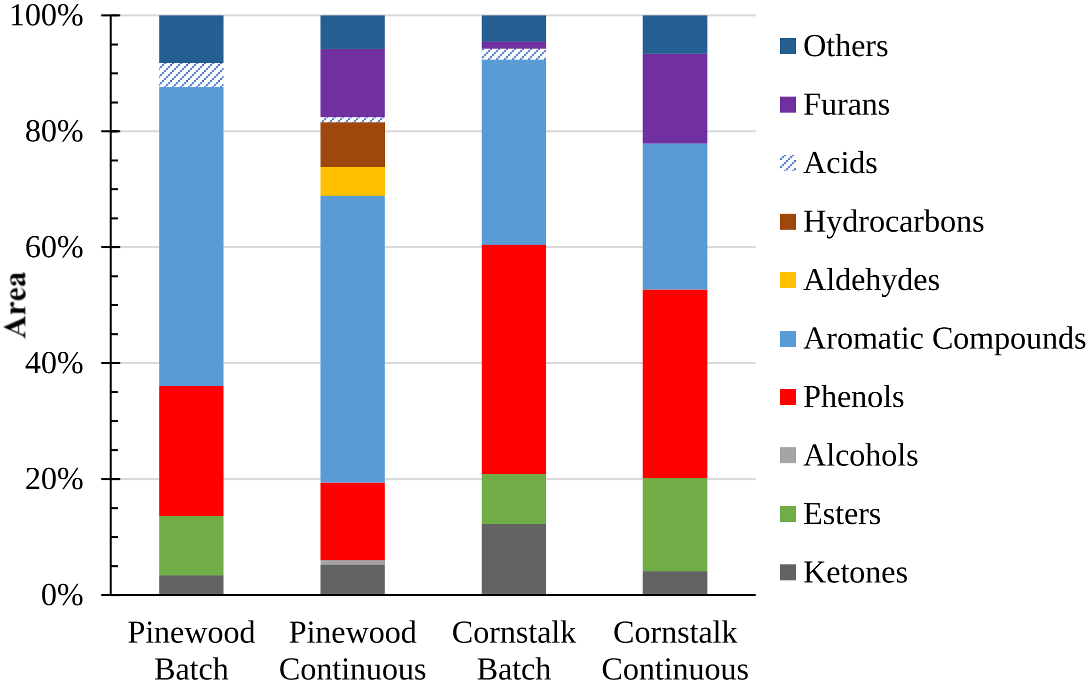

Figure 6.3: GC-MS analysis results for the bio-oils obtained from HTL of cornstalk and pinewood in the batch/continuous-flow operations at 300 °C for 12 min.

Figure 6.4 shows the FT-IR spectra of the bio-oils converted from HTL of cornstalk and pinewood sawdust in the batch /continuous-flow reactors. The broad IR absorption at 3350 cm^{-1} is typical of O-H stretching, suggesting the presence of alcohols, phenols, carboxylic acids, or water residues in the oils. The absorbance at 1700 cm^{-1}, representing the C=O stretching vibration of carbonyl groups, indicates the presence of ketones, aldehydes, esters or carboxylic acids in the oils. These peaks were observed to be more intensive in the bio-oils obtained in the batch-mode experiments, indicating possible formation of esters between acid intermediates and alcohol. In addition, these peaks are relatively stronger in the bio-oils obtained from HTL of pinewood possibly due to the higher cellulose content in pinewood leading to the production of more ketones or acids [38]. The relatively medium-intense peaks at 1611 and 1495 cm^{-1} represent aromatic nuclei, indicating the presence of aromatic rings and their derivatives. The IR absorption bands between 3000 and 2840 cm^{-1} are attributed to C-H stretching vibrations, indicating the presence of alkyl C-H in the oils. The two absorption peaks at 1370 and 1456 cm^{-1} are attributed to the bending vibrations of methyl ($-CH_3$) and methylene ($-CH_2$) groups, respectively. The presence of C-H stretching vibration and the C-H blending indicates the alkane groups in the bio-oils. The peaks between 1280 and 1000 cm^{-1} could be related to C-O vibrations. These peaks are relatively stronger in the bio-oils obtained in the continuous-flow operations, suggesting that the oils may contain higher concentrations of acids, phenols, furans, or alcohols. The peak at 860 cm^{-1} in the oils from the continuous-flow HTL of cornstalk, attributed to C-H bending, suggests the possible presence of single, polycyclic, and substituted aromatics. In general, the shorter residence time in continuous HTL process could lead to the higher content of small-molecule compounds, such as furans, as indicated in the GC-MS results (Figure 3) and the relatively stronger peaks at 1100 cm^{-1} representing C-O vibration.

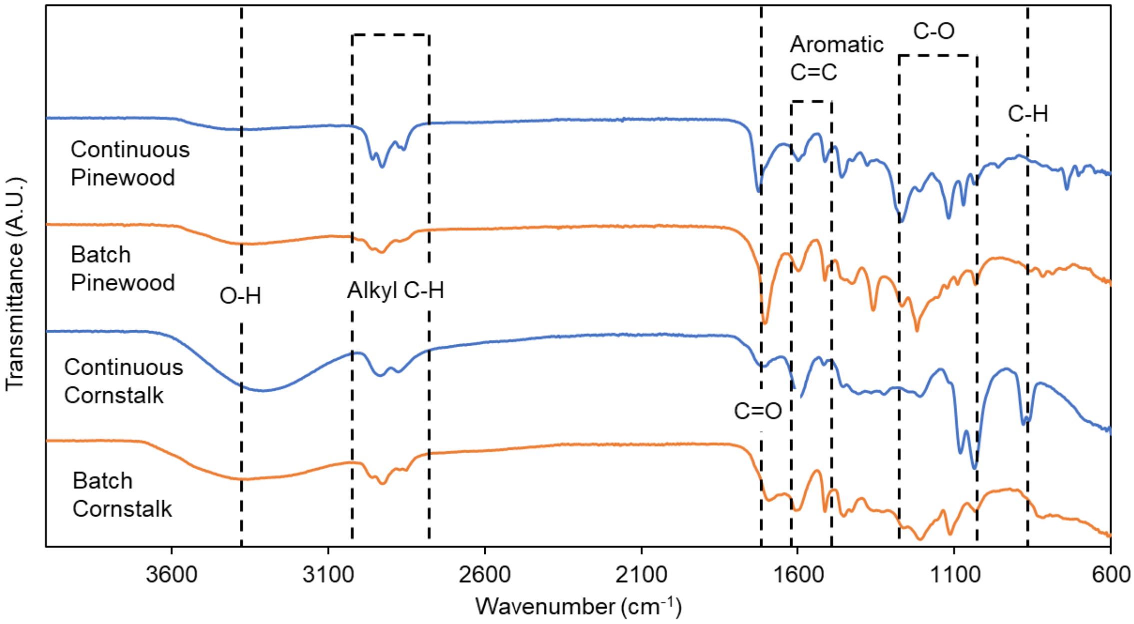

Figure 6.4: FT-IR spectra of bio-oils obtained from HTL of cornstalk and pinewood in continuous and batch-mode reactors at 300 °C for 12 min.

6.3.2 Biowaste-Black Liquor HTL

6.3.2.1 Products Distribution

The products distribution for HTL of black liquor on the batch/continuous-flow reactors at 300 °C, for 12 min are compared in **Figure 6.5**. The bio-oil, SR, and (AP+Gas) yields from black liquor processed in the continuous-flow reactor were 53.0, 4.2, and 42.8 wt.%, respectively, which are closed to those in the batch reactor (52.8, 4.5, and 42.7 wt.%, respectively). These results indicate that the differences in the types of operations (batch vs. continuous-flow) had negligible effects on the products distribution for the black liquor HTL, likely owing to the faster conversion of lignin in the black liquor, which is different from what was observed in HTL of lignocellulosic feedstocks (pinewood and cornstalk) (**Figure 6.2**). A higher bio-oil yield was obtained in black liquor HTL process than those of cornstalk and pinewood, since the major organic compounds in black liquor is lignin which produces higher amount of bio-oil than cellulose and hemicellulose [39].

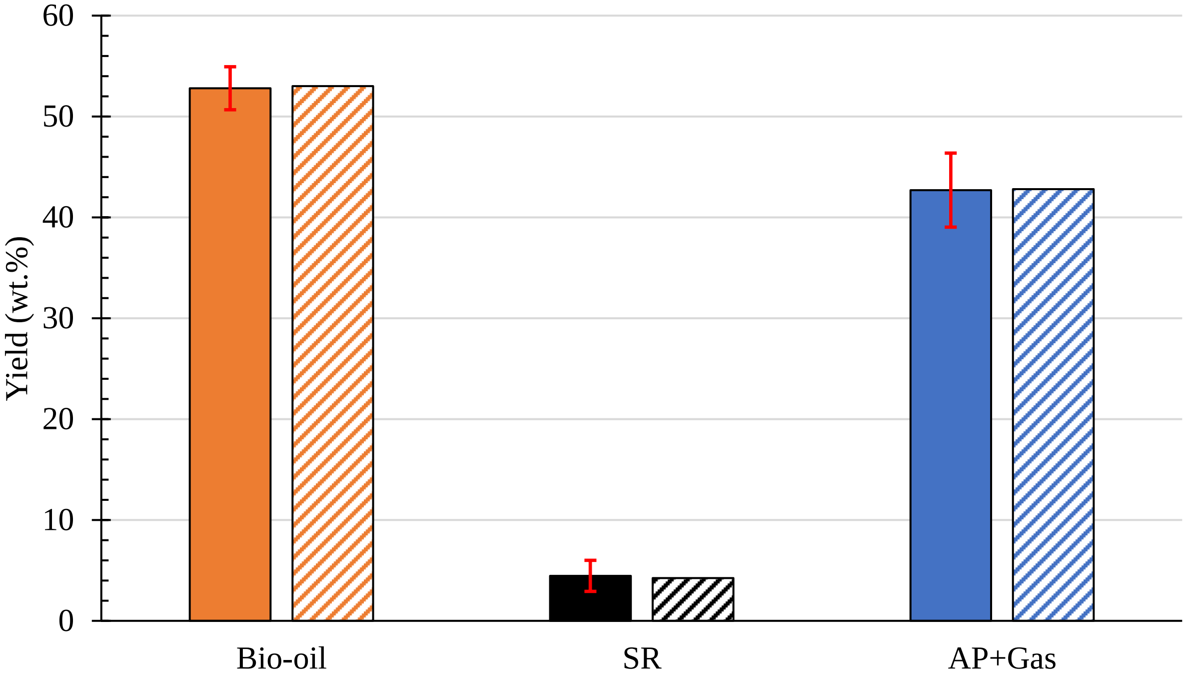

Figure 6.5: Products yields from HTL of black liquor in the batch/continuous-flow reactors at 300 °C for 12 min (Solid: Batch; Diagonal strips: Continuous-flow).

6.3.2.2 Chemical Analysis of Bio-oils

Table 6.4 presents the elemental compositions, HHVs, energy recovery rates and molecular weights of the bio-oils derived from black liquor in the batch/continuous-flow HTL operations. Both batch and continuous-flow HTL of black liquor produced bio-oils with lower HHVs (20-23 MJ/kg), compared with 24-29 MJ/kg for the oils obtained from pinewood and cornstalk. Compared with the batch HTL system, the continuous-flow reactor system produced bio-oils with a slightly higher oxygen content and hence lower HHV, and a reduced energy recovery rate (78% in the continuous-flow process vs. 86% in the batch process), as similarly reported in previous studies [16, 30, 31]. These results could be due to the shorter in-reactor reaction time and less deoxygenation of reaction intermediates during the continuous-flow HTL process [40, 41]. Similar results were Furthermore, the molecular weights (M_w=1089 g/mol, M_n=672 g/mol) are also lower for the oil obtained from the continuous-flow system in comparison with those of the batch system (M_w=1348 g/mol, M_n=805 g/mol). As discussed previously, the shorter in-reactor residence time in the continuous-flow operation could reduce the extent of repolymerization of the reaction intermediates, and hence produce bio-oils with reduced molecular weights [36, 40]. Similar results were obtained by Barreiro et al. [30]. They found that batch experiments led to a bio-oil containing molecules with higher molecular weight. The reduced heating and cooling durations in the continuous reactor, combined with the ongoing extraction of products from the reaction mixture, could diminish the occurrence of repolymerization reactions. As a result, this can lead to the production of a bio-oil with a lower concentration of heavy molecules [30].

Table 6.4: Comparison of chemical properties of the bio-oils derived from black liquor in the batch/continuous-flow HTL operations at 300 °C for 12 min.

	Batch	**Continuous-flow**
Yields (wt.%)	52.8	53.0
Ultimate analysis (wt.%)[a]		
Ash (wt.%)	11.7	6.9
C	58.8	55.7
H	4.2	4.1
N	0.08	0.2
S	4.7	6.1
O[b]	20.5	27.0
HHV (MJ/kg)[c]	22.7	20.4
Energy recovery (%)[d]	86.0	77.6
Molecular weight		
M_w (g/mol)	1348	1089
M_n (g/mol)	805	672
PDI	1.67	1.62

[a] On dry basis; [b] By difference; [c] Calculated by DuLong equation;

[d]Energy recovery (%) $= \frac{\mathrm{HHV_{oil} \times Weight_{oil}}}{\mathrm{HHV_{feedstock} \times Weight_{feedstock}}} \times 100.$

As also observed from **Table 6.4**, the ash of bio-oil from the batch operation is almost two times of that from the continuous-flow HTL operation. The relatively longer retention time in batch reactors could possibly enhance the release of ash from the bio-feedstocks into subcritical water, which may facilitate the combination between ash component and bio-oil intermediates, leading to the higher ash content in bio-oil produced from the batch operation.

The compositions of volatile fractions of the bio-oil samples obtained from batch and continuous-flow HTL of black liquor were analyzed by GC-MS and the results are compared in **Figure 6.6**. The major volatile compounds of both bio-oil samples are phenolic and aromatic compounds, as expected, because of the dominant presence of lignin in the black liquor feedstock. The bio-oil obtained from the batch HTL process contains more long-chain esters compared with that from the continuous-flow process, possibly due to the repolymerization of small-molecule reaction intermediates during the relatively longer in-reactor residence time in the batch system as discussed previously. This result can be further evidenced by the FTIR spectra of the bio-oils as illustrated in **Figure 6.7**. The relatively stronger peaks at 1700 cm^{-1}, 1280 cm^{-1}, and 1000 cm^{-1} indicate that the bio-oil sample from batch system contains a higher content of esters. In addition, the peaks between 1611 and 1495 cm^{-1} were observed to be more intensive in the bio-oil obtained in the continuous HTL system, which suggests the presence of more aromatic compounds or phenols. Furthermore, the stronger peak of O-H at 3500 cm^{-1} indicates that the bio-oil from batch-mode process contained more phenols.

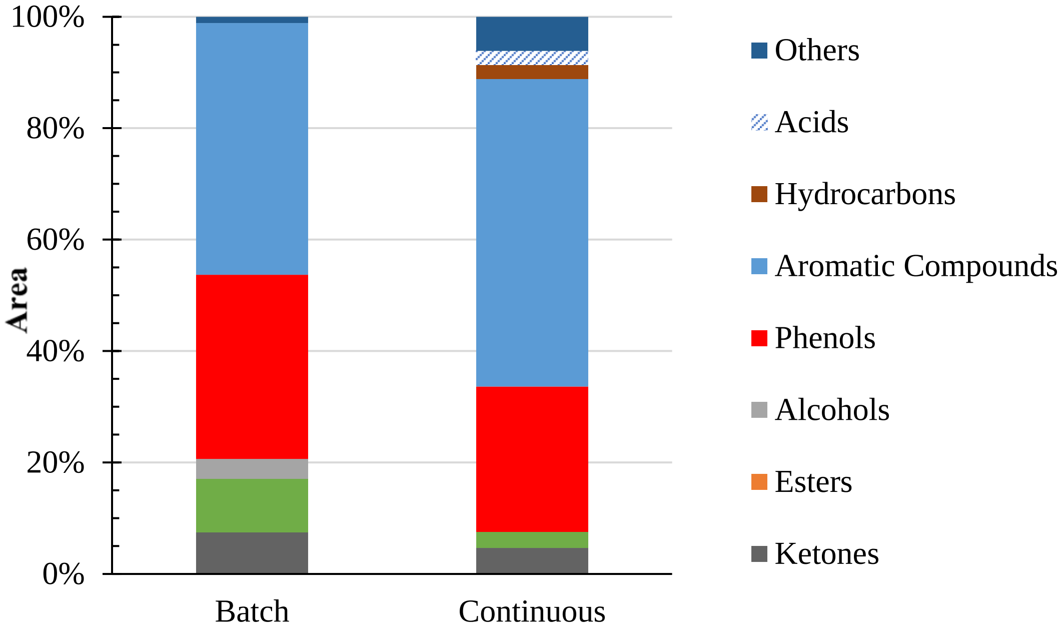

Figure 6.6: GC-MS analysis results of the bio-oils obtained from HTL of black liquor in the batch/continuous-flow reactors at 300 °C for 12 min.

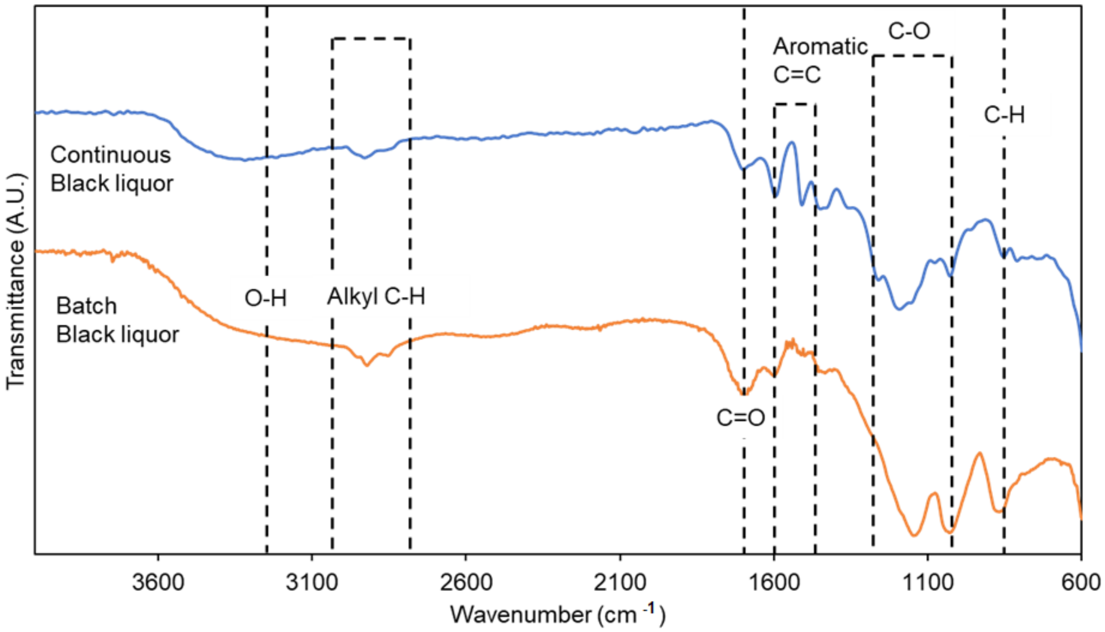

Figure 6.7: FT-IR spectra of the bio-oils obtained from HTL of black liquor in the batch/continuous-flow reactors at 300 °C for 12 min.

6.4 Conclusions

In this study, the performance of a continuous-flow HTL process against that of a batch HTL process was compared for processing three types of bio-feedstocks at 300 °C for 12 min. The HTL of cornstalk and pinewood in the continuous-flow reactor produced more bio-oils (32.4 and 34.5 wt. %, respectively) and less solid residues (2.9 and 4.6 wt.%, respectively) as well as higher energy recovery rates (53.3 and 52.0 %, respectively) compared with those in the batch reactor (Cornstalk: 23.8 wt.%, 6.2 wt.% and 46.5%, respectively; Pinewood: 28.5 wt.%, 10.3 wt.% and 50.8%), although the HHVs of the bio-oils from the continuous-flow reactor are slightly lower. The bio-oils obtained from these lignocellulosic biomass feedstocks in both reactors have similar molecular weights (M_w:572-742 g/mol and M_n: 410-476 g/mol), while the oils obtained from the continuous-flow operations contain higher amounts of furan compounds. The HTL product yields from black liquor do not exhibit significant difference between the continuous-flow and batch operations, while the bio-oil obtained from the continuous operation has a slightly lower HHV (20.4 vs. 22.7 MJ/kg) and smaller molecular weights (M_w:1089 vs. 1348 g/mol and M_n: 672 vs. 805 g/mol). These results would be helpful for designing the HTL systems for continuous production of bio-oil and drop-in fuels at a larger scale, using lignocellulosic biomass or biowaste.

While HTL has undergone significant improvements, there are still some major challenges to be addressed for commercializing the HTL process. The availability and storage of biomass can present logistical challenges. The lower density of biomass compared to fuel density has a detrimental effect on processing and transportation costs and logistics [42]. Feeding biomass to continuous reactors can also pose challenges when dealing with slurries that contain a high content of solid particles, especially under high pressures. The presence of solid particles in the feed can lead to blockages in both the reactor's inlet and outlet. An additional challenge in large-scale applications is the presence of solids in the product stream. The gravitational separation currently used could be time consuming with a time up to 90 min for the solid products to settle [43]. Other challenges allied with HTL continuous operations including potential corrosion caused by ash content in biomass, the replacement of catalyst, the excess need of water for specific types of biomasses (e.g. microalgae and lignocellulosic biomass) and etc.

6.5 References

[1] D. Castello, T.H. Pedersen, L.A. Rosendahl, Continuous hydrothermal liquefaction of biomass: A critical review, Energies 11(11) (2018) 3165.

[2] L. Cao, K. Iris, X. Xiong, D.C. Tsang, S. Zhang, J.H. Clark, C. Hu, Y.H. Ng, J. Shang, Y.S. Ok, Biorenewable hydrogen production through biomass gasification: A review and future prospects, Environmental research 186 (2020) 109547.

[3] I.A. Basar, H. Liu, H. Carrere, E. Trably, C. Eskicioglu, A review on key design and operational parameters to optimize and develop hydrothermal liquefaction of biomass for biorefinery applications, Green Chemistry 23(4) (2021) 1404-1446.

[4] A. Gollakota, N. Kishore, S. Gu, A review on hydrothermal liquefaction of biomass, Renewable and Sustainable Energy Reviews 81 (2018) 1378-1392.

[5] T.H. Seehar, S.S. Toor, K. Sharma, A.H. Nielsen, T.H. Pedersen, L.A. Rosendahl, Influence of process conditions on hydrothermal liquefaction of eucalyptus biomass for biocrude production and investigation of the inorganics distribution, Sustainable Energy & Fuels 5(5) (2021) 1477-1487.

[6] Y. Xu, M. Li, Hydrothermal liquefaction of lignocellulose for value-added products: Mechanism, parameter and production application, Bioresource technology 342 (2021) 126035.

[7] R.K. Mishra, P. Kumar, K. Mohanty, Hydrothermal liquefaction of biomass for bio-crude production: A review on feedstocks, chemical compositions, operating parameters, reaction kinetics, techno-economic study, and life cycle assessment, Fuel 316 (2022) 123377.

[8] A. Weir, A.J. del Barco Carrión, C. Queffélec, B. Bujoli, E. Chailleux, C. Uguna, C. Snape, G. Airey, Renewable binders from waste biomass for road construction: A review on thermochemical conversion technologies and current developments, Constrcution and Building Materials 330 (2022) 127076.

[9] A. Dimitriadis, S. Bezergianni, Hydrothermal liquefaction of various biomass and waste feedstocks for biocrude production: A state of the art review, Renewable and Sustainable Energy Reviews 68 (2017) 113-125.

[10] S. Nagappan, R.R. Bhosale, D.D. Nguyen, N.T.L. Chi, V.K. Ponnusamy, C.S. Woong, G. Kumar, Catalytic hydrothermal liquefaction of biomass into bio-oils and other value-added products–A review, Fuel 285 (2021) 119053.

[11] L. Cao, C. Zhang, H. Chen, D.C. Tsang, G. Luo, S. Zhang, J. Chen, Hydrothermal liquefaction of agricultural and forestry wastes: state-of-the-art review and future prospects, Bioresource technology 245 (2017) 1184-1193.

[12] M.K. Jindal, M.K. Jha, Effect of process parameters on hydrothermal liquefaction of waste furniture sawdust for bio-oil production, RSC advances 6(48) (2016) 41772-41780.

[13] R. Kaur, P. Gera, M.K. Jha, T. Bhaskar, Reaction parameters effect on hydrothermal liquefaction of castor (Ricinus Communis) residue for energy and valuable hydrocarbons recovery, Renewable energy 141 (2019) 1026-1041.

[14] Y. Wu, H. Wang, H. Li, X. Han, M. Zhang, Y. Sun, X. Fan, R. Tu, Y. Zeng, C.C. Xu, Applications of catalysts in thermochemical conversion of biomass (pyrolysis, hydrothermal liquefaction and gasification): A critical review, Renewable energy (2022).

[15] B. Patel, K. Hellgardt, Hydrothermal upgrading of algae paste in a continuous flow reactor, Bioresource technology 191 (2015) 460-468.

[16] Y. Fan, C. Prestigiacomo, M. Gong, T. Tietz, U. Hornung, N. Dahmen, Comparative investigation on the value-added products obtained from continuous and batch hydrothermal liquefaction of sewage sludge, Frontiers in Environmental Science 10 (2022) 996353.

[17] A. Lababpour, Continuous hydrothermal liquefaction for biofuel and biocrude production from microalgal feedstock, ChemBioEng Reviews 5(2) (2018) 90-103.

[18] S. Sahu, N. Sahoo, S. Naik, D. Mahapatra, Advancements in hydrothermal liquefaction reactors: Overview and prospects, Bioreactors (2020) 195-213.

[19] D. Cronin, A.J. Schmidt, J. Billing, T.R. Hart, S.P. Fox, X. Fonoll, J. Norton, M.R. Thorson, Comparative Study on the Continuous Flow Hydrothermal Liquefaction of Various Wet-Waste Feedstock Types, ACS Sustainable Chemistry & Engineering 10(3) (2021) 1256-1266.

[20] D.C. Elliott, T.R. Hart, G.G. Neuenschwander, L.J. Rotness, G. Roesijadi, A.H. Zacher, J.K. Magnuson, Hydrothermal processing of macroalgal feedstocks in continuous-flow reactors, ACS Sustainable Chemistry & Engineering 2(2) (2014) 207-215.

[21] P.A. Marrone, D.C. Elliott, J.M. Billing, R.T. Hallen, T.R. Hart, P. Kadota, J.C. Moeller, M.A. Randel, A.J. Schmidt, Bench-Scale Evaluation of Hydrothermal Processing Technology for Conversion of Wastewater Solids to Fuels: Marrone et al, Water Environment Research 90(4) (2018) 329-342.

[22] J.L. Wagner, C.D. Le, V.P. Ting, C. Chuck, Design and operation of an inexpensive, laboratory-scale, continuous hydrothermal liquefaction reactor for the conversion of microalgae produced during wastewater treatment, Fuel Processing Technology 165 (2017) 102-111.

[23] K. Anastasakis, P. Biller, R.B. Madsen, M. Glasius, I. Johannsen, Continuous hydrothermal liquefaction of biomass in a novel pilot plant with heat recovery and hydraulic oscillation, Energies 11(10) (2018) 2695.

[24] A. Aierzhati, J. Watson, B. Si, M. Stablein, T. Wang, Y. Zhang, Development of a mobile, pilot scale hydrothermal liquefaction reactor: Food waste conversion product analysis and techno-economic assessment, Energy Conversion and Management: X 10 (2021) 100076.

[25] P. Sun, M. Heng, S. Sun, J. Chen, Direct liquefaction of paulownia in hot compressed water: Influence of catalysts, Energy 35(12) (2010) 5421-5429.

[26] B. Zhang, M. von Keitz, K. Valentas, Thermochemical liquefaction of high-diversity grassland perennials, Journal of Analytical and Applied Pyrolysis 84(1) (2009) 18-24.

[27] F. Wang, Z. Chang, P. Duan, W. Yan, Y. Xu, L. Zhang, J. Miao, Y. Fan, Hydrothermal liquefaction of Litsea cubeba seed to produce bio-oils, Bioresource technology 149 (2013) 509-515.

[28] Y. Xue, H. Chen, W. Zhao, C. Yang, P. Ma, S. Han, A review on the operating conditions of producing bio-oil from hydrothermal liquefaction of biomass, International Journal of Energy Research 40(7) (2016) 865-877.

[29] L. Tai, R. Hamidi, L. Paglia, P. De Filippis, M. Scarsella, B. de Caprariis, Lignin-enriched waste hydrothermal liquefaction with ZVMs and metal-supported Al2O3 catalyst, Biomass and Bioenergy 165 (2022) 106594.

[30] D.L. Barreiro, B.R. Gómez, U. Hornung, A. Kruse, W. Prins, Hydrothermal liquefaction of microalgae in a continuous stirred-tank reactor, Energy & Fuels 29(10) (2015) 6422-6432.

[31] L. Nazari, Hydrothermal liquefaction of high-water content biomass and waste materials for the production of biogas and bio-crude oil, The University of Western Ontario (Canada), 2016.

[32] K.R. Arturi, S. Kucheryavskiy, R.P. Nielsen, M. Maschietti, F. Vogel, S. Bjelić, E.G. Søgaard, Molecular footprint of co-solvents in hydrothermal liquefaction (HTL) of Fallopia Japonica, The Journal of Supercritical Fluids 143 (2019) 211-222.

[33] M. Kröger, F. Hartmann, M. Klemm, Hydrothermal Treatment of Carboxy-methyl Cellulose Salt: Formation and Decomposition of Furans, Pentenes and Benzenes, Chemical Engineering & Technology 36(2) (2013) 287-294.

[34] Y. Tian, F. Wang, J.O. Djandja, S.L. Zhang, Y.P. Xu, P.G. Duan, Hydrothermal liquefaction of crop straws: Effect of feedstock composition, Fuel 265 (2020) 116946.

[35] M. Tymchyshyn, C.C. Xu, Liquefaction of bio-mass in hot-compressed water for the production of phenolic compounds, Bioresource technology 101(7) (2010) 2483-2490.

[36] R.B. Carpio, Y. Zhang, C.-T. Kuo, W.-T. Chen, L.C. Schideman, R. de Leon, Effects of reaction temperature and reaction time on the hydrothermal liquefaction of demineralized wastewater algal biomass, Bioresource Technology Reports 14 (2021) 100679.

[37] W.S. Villaver, R.B. Carpio, K.J. Yap, R. De Leon, Effects of temperature and reaction time on yield and properties of biocrude oil produced by hydrothermal liquefaction of Spirulina platensis, Int. J. Smart Grid Clean Energy 7 (2018).

[38] J. Lu, Z. Liu, Y. Zhang, P.E. Savage, Synergistic and antagonistic interactions during hydrothermal liquefaction of soybean oil, soy protein, cellulose, xylose, and lignin, ACS Sustainable Chemistry & Engineering 6(11) (2018) 14501-14509.

[39] A. do Couto Fraga, M.B.B. de Almeida, E.F. Sousa-Aguiar, Hydrothermal liquefaction of cellulose and lignin: a new approach on the investigation of chemical reaction networks, Cellulose 28(4) (2021) 2003-2020.

[40] J. Ni, L. Qian, Y. Wang, B. Zhang, H. Gu, Y. Hu, Q. Wang, A review on fast hydrothermal liquefaction of biomass, Fuel 327 (2022) 125135.

[41] B. Patel, P. Arcelus-Arrillaga, A. Izadpanah, K. Hellgardt, Catalytic Hydrotreatment of algal biocrude from fast Hydrothermal Liquefaction, Renewable energy 101 (2017) 1094-1101.

[42] M. Fahim, T. Alsahhaf, A. Elkilani, Refinery feedstocks and products, Fundamenatl of petroleum refining (2010) 11-31.

[43] T.H. Pedersen, I. Grigoras, J. Hoffmann, S.S. Toor, I.M. Daraban, C.U. Jensen, S. Iversen, R. Madsen, M. Glasius, K.R. Arturi, Continuous hydrothermal co-liquefaction of aspen wood and glycerol with water phase recirculation, Applied Energy 162 (2016) 1034-1041.

Chapter 7

7 Roles of Biomass Feedstocks and Corresponding Organic Products on Corrosion of SS316L under Hydrothermal Liquefaction (HTL) Conversion

Abstract

The industrial application of hydrothermal liquefaction technology is retarded due to limited materials and corrosion knowledge on corrosion of reactor alloys. To fill knowledge gaps and partially support the development of material technology guideline on HTL plant construction, this study investigated the effects of biomass feedstocks and organic products on the corrosion of a candidate construction alloys (SS316L) in catalytic hydrothermal liquefaction environments. It is found that some organic compounds produced from the conversion of bamboo may act as corrosion inhibitors to facilitate the formation of a carbon-rich layer on the surface oxide scale of the steel. The presence of excessive amounts of S^{2-} and ash in black liquor feedstocks can completely change the corrosion mode of SS316L in the HTL environments and significantly accelerate the corrosion process.

Keywords: Bamboo, Bio-oil, Black liquor, Corrosion, Hydrothermal liquefaction, SS316L

7.1 Introduction

Over the past decades, serious environmental concerns caused by the production and application of conventional fossil resources and continuously increasing demand for energy supply have prompted extensive R&D activities on the development of reliable, clean and sustainable energy alternatives to partially and even completely replace the fossil fuels [1, 2]. Among the identified alternatives, raw biomass materials, such as food residues, energy crops, forest and agricultural products and residues, and waste from industry, farms and households, have been widely recognized as one of the most promising resources since the conversion of them into marketable biofuels and biochemicals can help achieve environmental-friendly and renewable targets [3-5]. It is estimated that the annual global primary energy production from biomass resources can be roughly equivalent to the 4,500 EJ (1 EJ = 10^{18} J) of solar energy captured per year [6]. More attractively, abundant industrial and municipal biowastes can also be directly and rapidly converted into green bioenergy products via either biochemical or thermochemical processes. Compared with the biochemical methods, the thermochemical pathways are more efficient in terms of process duration, the ability to decompose the biomass fractions, and carbon conversion efficiency [7].

Hydrothermal liquefaction (HTL) is a thermochemical conversion process in which hot-compressed water, water-alcohol mixed solvents, or other organic solvents are used as a medium to convert wet biomass and biowaste feedstocks into crude biooil at temperatures ranging from 200-400 °C and pressure up to 35 MPa [8-10]. This process has attracted particular attention for the conversion of wet energy crops and biowaste streams, such as black liquor, wastewater sludge, food waste, and freshly harvested algal biomass, etc. [11-13]. These feedstocks generally consist of a complicated mixture of carbohydrates, proteins, and minerals and pose unique chemical and physical characteristics [14, 15]. Different from them, the agricultural and forest feedstocks, such as straw, corn stalks, soft and hard woods, and bamboo [16], are mainly composed of three major compounds, namely cellulose, hemicellulose and lignin [15, 17]. Among the HTL feedstocks, municipal or industrial waste stream is likely to be the most complicated feedstock which usually consists of highly aggressive components, such as hydroxide, sulfide, and thiosulphate. It is worth noticing that the components and elements within the biowastes could be remarkably different, depending on their original sources and processing conditions.

Despite the different compositions of HTL feedstocks, the general HTL conversion mechanism involves the breakdown of intermolecular hydrogen bonds into monomers, followed by the hydrolysis of biopolymers. However, the chemical content (such as O, H, and C), structural components (such as hemicellulose and lignin), lipid, and carbohydrate composition of different biomass feedstocks can vary significantly, resulting in significant difference of reaction processes and kinetics and consequently leading to different final yield and quality of bio-oils. In recent years, several studies [18-20] have been conducted to predict the yield and quality of bio-oil from different biomass feedstocks based on kinetic modeling and/or lab-scale testing. However, a general kinetic model is still not available to quantitively predict HTL product yields based on feedstock chemistry and processing parameters. Additionally, compared with the biooil produced via pyrolysis process (14–20 MJ/kg), HTL-generated oil has reduced oxygen and moisture contents, higher HHV (25–35 MJ/kg), and less corrosivity [21, 22].

To achieve optimum carbon conversion efficiency and obtain high-quality bio-oil, a heterogeneous (e.g., ZSM-5, Pt/C, Pd/C, and Ru/C) or homogeneous (such as K_2CO_3, KOH, Na_2CO_3, NaOH and H_2SO_4) catalyst is also introduced into the HTL processes [23-26]. Among all the catalysts, alkaline catalysts are seen as the most promising and cost-effective options for HTL conversion as they can effectively prevent the repolymerization of biocrude-forming fragments and enhance bio-oil yield by 50–135 % [27]. The overall rank of catalyst activity on the HTL conversion has been proposed as K_2CO_3 > KOH > Na_2CO_3 > NaOH [28]. It is worth noticing that the major challenge of using homogeneous catalysts lies in the difficulty of isolating the product from liquid media and the associated acceleration in the corrosion rates of reactor alloys as their addition can make the process environmental chemistry more aggressive. For instance, a recent study reported that the addition of 0.5 M K_2CO_3 could increase the environmental pH up to ~ 12 at room temperature, at which the major alloying elements (Cr, Fe, Ni) in reactors alloys would suffer active corrosion instead of protective oxidation [29].

Despite its simplicity and high suitability for wet feedstocks, the widespread commercialization of HTL technology has not been established due to several economic concern and knowledge gaps, including high capital investment and technical obstacles such as clogging and corrosion of core components. In the case of water HTL conversion, the operating environments are expected to be highly corrosive to the refining reactor alloys due to the presence of hot-pressurized water medium, caustic catalysts, and the by-production of organic acids and inorganic corrodents (such as Cl^- and S^{2-}) [30-32]. Previous operation experience and knowledge accumulated on high-temperature aqueous systems, such as boiling and pressurized water nuclear reactors, have shown that the corrosion of constructional alloys must be a significant factor for safe long-term operation [33-38]. Moreover, recent studies in simulated HTL environments indicated that the presence of an alkaline catalyst could cause a remarkable increase in corrosion rate as the formed surface scale was composed of porous hydroxides with high solubility in high temperature aqueous environments instead of stable and compact oxides [39, 40]. Furthermore, the feedstock type and composition will affect the overall bio-oil yield, compositions, and the contents of corrodants released. For instance, industrial bio-wastes can contain more than 10,000 ppm of Cl^- and S^{2-} ions, which are well known agents to facilitate localized pitting and stress corrosion cracking of Fe-based steels and Ni-based alloys [32, 41-44]. The organic acids generated from the HTL processes shall change the environmental pH and possibly change the corrosion mode and extent of reactor alloys [39, 45].

Fe-based stainless steels, such as SS316L, have been widely used as construction materials in high temperature aqueous environments [46, 47]. Recent studies in simulated HTL environments indicated that SS316L could be a very promising candidate for the construction of HTL reactors [31, 48]. According to our knowledge, however, few corrosion studies have been conducted in real biomass HTL conversion environments. Compared with the simulated HTL environments, the chemistry of real biomass conversion environments is much more complicated as inorganic corrodants (e.g., Cl^- and S^{2-}) and organic products (such as phenolic and carboxyl compounds) are produced during the conversion and the environmental pH remarkably varies with the conversion processes. According to pilot-scale testing results, the HTL processes with K_2CO_3 catalyst are likely operated at the pH range of 6–12 [49-51]. To accelerate the development and deployment of HTL technology in Canada and the global bioenergy industry in a cost-competitive manner, it is important to determine whether the steel is the suitable materials of construction for the HTL reactor and explore the influence of biomass types and major conversion product on corrosion. Therefore, this study investigates the corrosion modes and extents of SS316L steel under the catalytic batch-mode HTL conversions of two representative feedstocks, bamboo (similar to sawdust) and black liquor, and analyzes the conversion products to advance fundamental mechanistic understanding of the HTL conversion processes and related corrosion mechanisms.

7.2 Materials and Methods

7.2.1 Raw Materials and Chemicals

Bamboo and black liquor, obtained from a bamboo sawmill in South China and FPInnovations Bioeconomy Technology Centre, Thunder Bay, Canada, were used as the feedstocks in this study. The bamboo sawdust was pre-dried at 105 °C in an oven for 24 h and grounded to fine particles less than 40 mesh size. The chemical compositions of those two bio-feedstocks are listed in **Table 7.1**. As expected, the black liquor has much higher S content, but lower oxygen compared to bamboo. As mentioned above, the addition of homogeneous alkaline catalysts can significantly enhance the liquefaction of biomass into bio-oil products [27]. During the HTL treatment of pinewood sawdust, the effect of these catalysts on feedstock conversion was in the rank of K_2CO_3> KOH> Na_2CO_3> NaOH; the corresponding conversion efficiency decreased from 96.0% to 86.0%, and the bio-oil production yield from 33.7% to 22.4% [28, 52-54]. Thus, the catalyst employed in the batch-mode tests was K_2CO_3 (99%, purchased from Sigma-Aldrich, Oakville, Canada) at a concentration of 5 wt.% of dry feedstock, which optimized the conversion of bamboo; and 0.5 M in the static test of simulated conditions, which optimized the conversion of general forest, agricultural and microalgae feedstocks. Other chemicals used, including KOH (99%), phenolphthalein, reagent-grade acetone (99.5%) and sulfuric acid (98%) were obtained from Sigma-Aldrich (Oakville, Canada), VWR International (Mississauga, Canada) and Fisher Scientific (Ottawa, Canada).

Table 7.1: Chemical compositions of bio-feedstocks used in this study.

	Bamboo	**Black liquor**
Ash (wt.%)^a	0.44	32.1
Ultimate analysis (wt.%)^a		
C	47.24	37.32
H	6.18	3.93
N	0.21	0.03
S	<0.01	1.64
O^b	45.93	24.98
HHV (MJ/kg)^c	16.59	13.92

^{a} On dry basis; ^{b} By difference; ^{c} Calculated by DuLong equation

7.2.2 Corrosion Test Specimen Preparation

Testing coupons (20 mm long x 10 mm wide x 2 mm thick) were machined from a commercial SS316L plate and its composition is presented in **Table 7.2** based on the certificate provided by the supplier. A small hole with a radius of 2 mm was drilled into each coupon near the top to facilitate mounting on a homemade sample holder. Prior to each corrosion test, the coupons were well polished with SiC papers up to 600 grits in deionized water to completely remove possible contamination and defects introduced during machining, rinsed using ethanol in an ultrasonic bath for 10 minutes, cleaned with ultrapure water, and finally dried using pressurized air. After that, a sample ID was stamped on each coupon near its top-left edge based on the in-house standard method. Before a batch-mode HTL test, each coupon was weighed using a micro-balance with a precision of 1 μg, and its dimensions were measured using a digital caliper with a precision of 10 μm. For each test, two coupons of stainless steel were used to ensure the accuracy and precision of obtained results.

Table 7.2: Chemical Compositions of SS316L in this study.

Element	**Cr**	**Ni**	**Mo**	**Mn**	**C**	**Si**	**P**	**Fe**
Composition (wt.%)	16.60	10.0	1.60	1.20	0.02	0.30	0.02	Bal.

7.2.3 Test Facility and Procedure

Table 7.3 shows the autoclave test matrix which was performed to identify the effect of feedstocks and organic products on corrosion under simulated and real biomass-contained catalytic HTL conversion conditions. Note that the concentration of Cl^- and S^{2-} in test #1 was chosen based on their maximum contents in industrial biowastes and the feeding water/solid mass ratio of 15:1. Note that 10 wt.% of acetic acid was added in the test to simulate the production of organic acids during the batch-mode tests, and the final pH value after the simulated test is around 5.4, close to that after bamboo-contained HTL test (test #2), which is 4.8-5.3. As shown in **Figure 7.1**, the test #1 was conducted in an Alloy C-276 autoclave based on ASTM G31 standard [55], with a pre-oxidized Alloy 625 liner to mitigate the influence of autoclave wall alloy. Note that Alloy 625 liner was pre-oxidized in an air furnace at 400 °C for 24 hours and used for accommodating testing solution and samples. Before the testing, the freshly prepared samples were loaded on the Alloy 625 holder using 20Cr-80Ni alloy wires, which were also pre-oxidized to avoid the galvanic effect between testing samples and the holder. The autoclave was then sealed and purged with nitrogen gas for at least 60 min to produce a deaerated environment, following the leaking test under high pressure N_2 condition. After that, the autoclave was powered on to reach the target temperature. Once the temperature reached 310 °C, the time was recorded as the start point and the test was allowed to proceed for 10 days. When the exposure duration was reached, the heater was powered off, and the autoclave was allowed to cool down to room temperature, before removing the exposed SS316L samples for subsequent cleaning and characterizations.

Test #2 and 3 (batch-mode real HTL conversion experiments) were performed in a 500 ml autoclave reactor (Parr 4575A HP/HT reactor). Although the concentration of K_2CO_3 in the two tests is much lower than that in the simulated HTL test, the initial pH value of the two tests is still higher than that of test #1 due to the addition of acidic acid. **Figure 7.2** schematically shows the experimental setup for the tests. **Figure 7.3** are the photo images of batch reactor and sample holder used in this study. The testing samples were hung on a pre-oxidized SS316L holder, which was placed at the bottom of the reactor during the tests. Before a real HTL test, the oxygen in the reactor was completely removed by N_2 purging. After that, 2 MPa of nitrogen was charged into the reactor at room temperature. All alloy coupons were subjected to cyclic batch-mode exposures for a total of 20 cycles at 300 °C with the designed water/dried feedstock mass ratio of 15:1. The residence time of each cycle was 30 min, which is also the duration required to completely convert the feedstocks into bio-oils. Thus, the total exposure time for the corrosion tests was 10 hours. Afterwards, the corroded coupons were removed from the reactor and rinsed with distilled water for 5 min, followed by acetone cleaning in an ultrasonic cleaner for 5 min. The collected corroded samples were then used for subsequent corrosion rate measurements and corrosion product characterizations. Meanwhile, the conversion products were also collected for chemical analyses as described in the following section. In addition, the autoclave reactor was cleaned using acetone and water before and after each cycle.

Table 7.3: Test matrix conducted to identify the influence of biomass feedstocks and organic products under simulated and real biomass-contained HTL conversion conditions.

Test #	Testing Conditions
#1	in a **static** Alloy C-276 autoclave with an Alloy 625 liner containing deaerated 0.5 M K_2CO_3 + 3500 ppm Cl^- + 2500 ppm S^{2-} + 10 wt.% acetic acid at 310 °C for 10 days
#2	in a **batch-mode** autoclave containing deaerated 0.024 M K_2CO_3 (5 wt.% of dry biomass) and 6.25 wt.% bamboo (on dry basis) at 300 °C for 10 hours
#2	in a **batch-mode** autoclave containing deaerated 0.024 M K_2CO_3 (5 wt.% of dry biomass) and 6.25 wt.% black liquor (on dry basis) at 300 °C for 10 hours

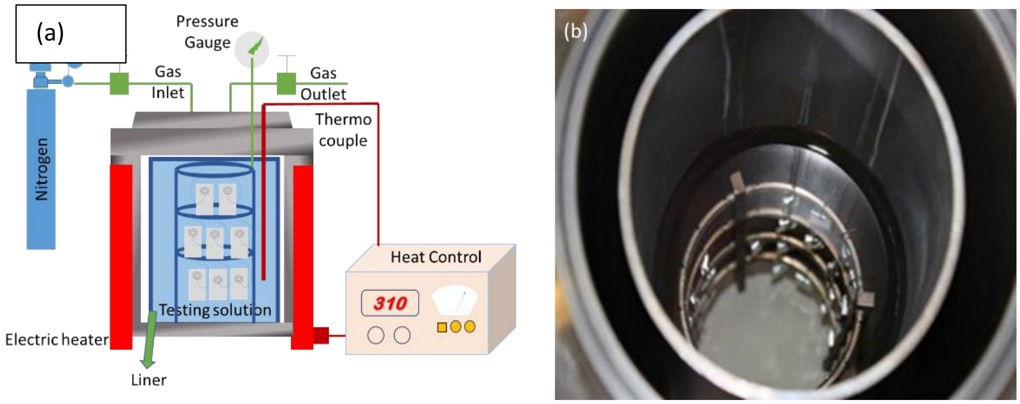

Figure 7.1: (a) Schematic of the static autoclave setup used for test #1 in this study; (b) Top-view photograph of the Alloy 625 liner, testing samples and sample holder.

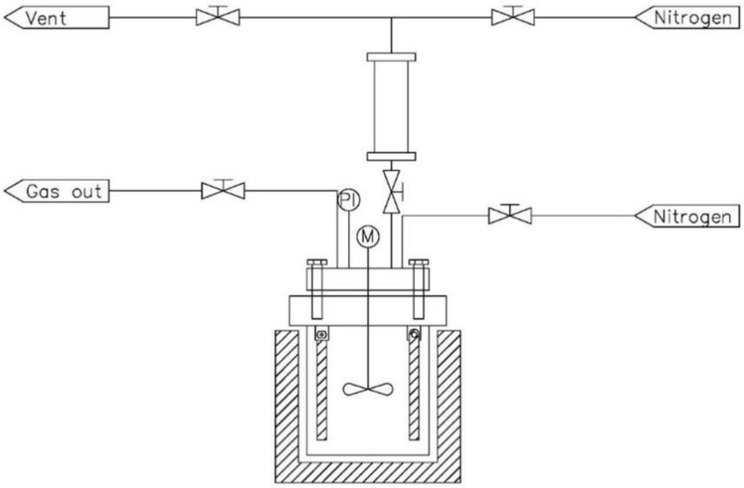

Figure 7.2: Schematic of the experimental set-up used for batch-mode read HTL tests (tests #2 and 3).

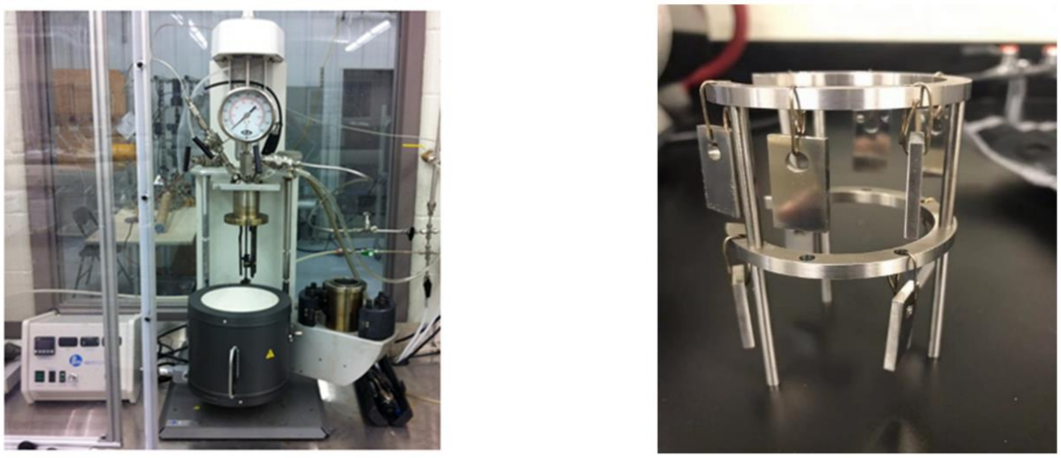

Figure 7.3: Photographs of a 500 ml batch reactor and test coupon holder.

7.2.4 Conversion Products Separation and Analysis

The products from HTL processes include gaseous products (Gas), bio-oil, aqueous phase (AP), and solid residue (SR). In the bamboo HTL tests, the products were collected and separated based on the similar separation procedure of pinewood sawdust in **Section 3.2.2.2.** For the black liquor HTL tests, the products were collected and separated based on the similar separation procedure of batch-mode lignin HTL process in **Section 5.2.3**.

Fourier transform infrared (FT-IR) analyses on a PerkinElmer FT-IR spectrometer (Massachusetts, USA) were conducted to characterize the functional groups of the bio-oils. The volatile compositions were analyzed with Gas Chromatograph-Mass Spectrometry (GC–MS, Agilent Technologies, 5977A MSD) equipped with an HP-5MS column (30 m × 250 μm × 0.25 μm). The GC temperature program was set as: held at 40 °C for 5 min, then increased by 10 °C/min to 150 °C and held for 2 min, then increased by 10 °C/min to 290 °C and held for 5 min. The element compositions (C, H, N, and S) of the feedstocks and bio-oils were determined using an elemental analyzer (Vario EL Cube). The O content was calculated based on the difference on a dry basis (%O = 100% – %Ash – %C – %H – %N – %S) where the ash contents of the feedstocks and bio-oils were determined by ashing at 700 °C for 4 h in air in a muffle furnace. The higher heating values (HHV) of all feedstocks and bio-oils were estimated by [56, 57].

$$\mathrm{HHV\ (MJ/kg)} = 0.388\%\mathrm{C} + 1.428(\%\mathrm{H} - \%\mathrm{O}/8) + 0.095\%\mathrm{S} \tag{7.1}$$

The total acid number (TAN) of the bio-oil products was evaluated by using 0.01 N KOH and phenolphthalein as the titration solution and indicator, respectively. TAN was then calculated in milligrams of KOH/gram of sample as follows:

$$\mathrm{TAN} = [(\mathrm{A} - \mathrm{B})\mathrm{N} \times 56.1]/\mathrm{W} \qquad (7.2)$$

where:

A=KOH solution required for titration of the sample, ml,

B=KOH solution required for titration of the blank, ml,

N=normality of the KOH solution,

W=weight of sample used, g.

7.2.5 Corrosion Rate Measurement

Two weight change measurement methods, including direct weight change and indirect weight loss measurements, are usually employed to determine the corrosion rates of candidate alloys in high temperature environments. As considerable chemical dissolution and localized breakdown of the formed corrosion layers as well as organic compound deposition possibly occur during the exposures to the HTL environments, indirect weight loss measurement is therefore seen as a more accurate method for assessing corrosion rates in this study.

Based on ASTM G1 standard [58], the indirect weight loss measurement involves two major steps: (a) descaling the formed surface corrosion products on an alloy coupon; and (b) calculating the mass change of the coupon before a corrosion test and after the descaling. Descaling can be achieved by immersing the coupons in specific chemical solutions, which do not corrode metal substrates, but effectively remove the formed corrosion layers through chemical dissolution reactions. In this study, the descaling was achieved by immersing the corroded coupons in solution A (composed of citric acid, dibasic ammonium citrate, and Disodium EDTA) at 90 °C for one hour, and then submerging in solution B (composed of potassium permanganate and caustic soda) at 90 °C for another hour. After weighing, the coupon is then immersed in solution A for one hour again and weighed. The above immersion treatment process was applied repeatedly until the weight of the coupon reached a constant value. The descaling procedure has been demonstrated to be an effective way to remove the oxide scale formed on Fe-based alloys when exposed to subcritical and supercritical water environments [59, 60]. After the descaling, the coupons were cleaned using ethanol and deionized water, dried with pressurized air, and weighed using a microbalance. The corrosion rate of an alloy in millimeters per year was thus calculated by:

$$\mathrm{Corrosion\ Rate} = 8.763 \times 10^4 \cdot \frac{\Delta \mathrm{m}}{\mathrm{dSt}} \tag{7.3}$$

where Δm is the mass loss of the coupon in gram, d is the alloy density in g/cm^3, S is the measured surface area of the coupon (cm^2), and t is the testing duration in hours [61].

7.2.6 Corrosion Products Characterization

After a corrosion test, primary optical examination on the corroded samples were performed to roughly identify corrosion modes and extents of the tested materials. Following that, one of the corroded coupons was selected from the replicate set for microscopic electron characterizations. The corrosion products on the SS316L samples were examined in detail using a FEI Nova NanoSEM 650 scanning electron microscope (SEM) system and a Hitachi SU3900 large chamber variable pressure scanning electron microscope system to identify corrosion modes (active corrosion, general oxidation, and/or pitting) of oxide layers, respectively. A Rigaku SmartLab X-ray diffractometer (XRD) with a Cu X-ray and Co Kα X-ray was used to determine the phase compositions of the corrosion products formed. FT-IR (Bruker Tensor II system equipped with Hyperion 2000 microscope) were applied to identify the organic compounds deposited on the sample surfaces.

7.3 Results and Discussion

7.3.1 Chemical Properties of HTL Products

The chemical compositions of produced bio-oils were analyzed using GC-MS, and the results are summarized in **Figure 7.4**. The major compounds of bio-oils produced from the two feedstocks are phenolic and aromatic compounds. The bio-oil derived from black liquor contains more phenols and aromatics, but fewer ketones compared to that converted from bamboo. This can be attributed to the fact that the major organic compound in black liquor is lignin (42 wt.% of the dried solid contents), while bamboo contains 57 wt.% of carbohydrate (cellulose and hemicellulose) and 30 wt.% of lignin. The difference in feedstock types and compositions can significantly affect the overall bio-oil compositions due to various reaction behaviors of major components in raw biomass during HTL conversion. Carbohydrates, including cellulose and hemicellulose, are firstly hydrolyzed into monosaccharides and then undergo Retro-Aldol condensation to produce organic acids, ketones, and alcohols [62]. Different from them, lignin is converted to aromatic compounds via hydrolysis, C-C bond cleavage, and C-O bond cleavage [62].

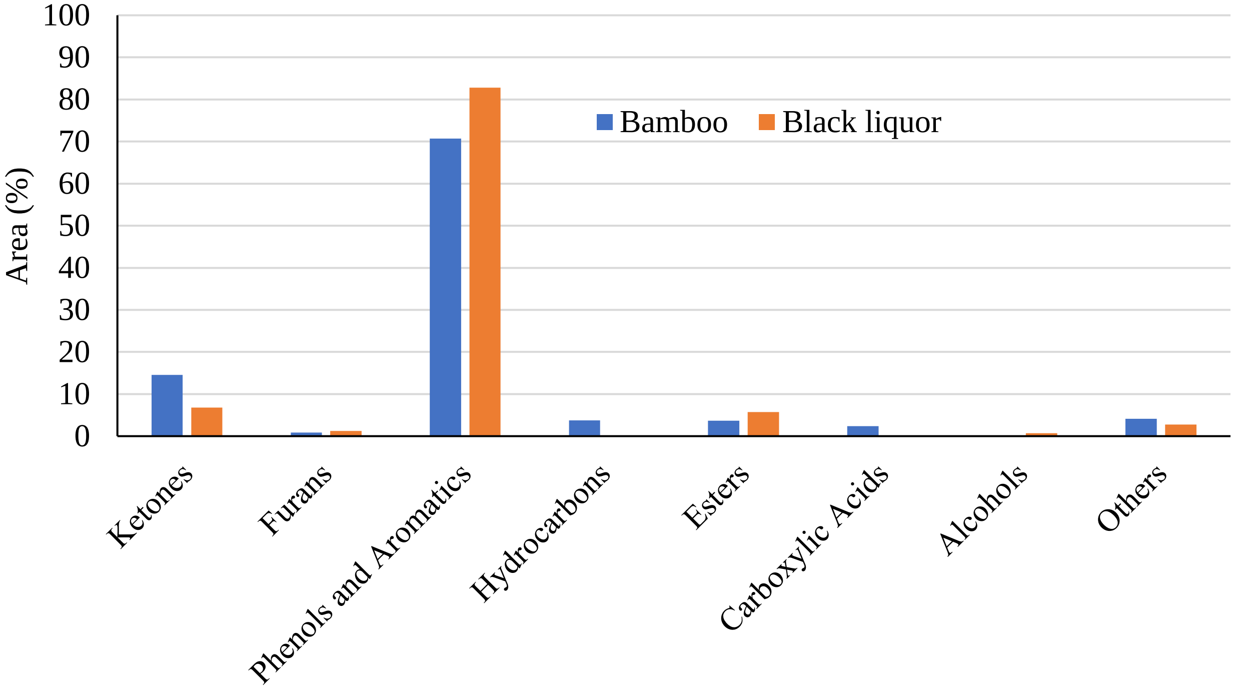

Figure 7.4: GC-MS analysis of the bio-oil obtained from the HTL of bamboo and black liquor at 300 °C for 30 min, respectively.

FT-IR analyses of the bio-oil samples in the range of 4000-400 cm^{-1} were performed to identify the functional groups, and the collected spectra are presented in **Figure 7.5**. The bands between 3000 and 2840 cm^{-1} represent C-H stretching vibrations, indicating the presence of alkyl C-H. The two absorptions at 1370 and 1456 cm^{-1} are attributed to the bending vibrations of methyl ($-CH_3$) and methylene ($-CH_2$) groups, respectively. The peak at 1456 cm^{-1} may be related to aromatic compounds presented in the oil. The broad absorption at 3350 cm^{-1} is typical of O-H stretching, suggesting the presence of alcohols, phenols, carboxylic acids, and water residues in the bio-oil. The absorbance at 1700 cm^{-1} represents the C=O stretching vibration of carbonyl groups and indicates the presence of ketones, aldehydes, and carboxylic acids in oils. The peaks at 1611 and 1456 cm^{-1} represent aromatic rings and their derivatives. The bands between 1280 and 1000 cm^{-1} could be related to C-O vibrations, suggesting the possible presence of acids, phenols, furans, or alcohols in the bio-oil. The peak at 860 cm^{-1} attributed to C-H bending suggests the possible presence of single, polycyclic, and substituted aromatics.

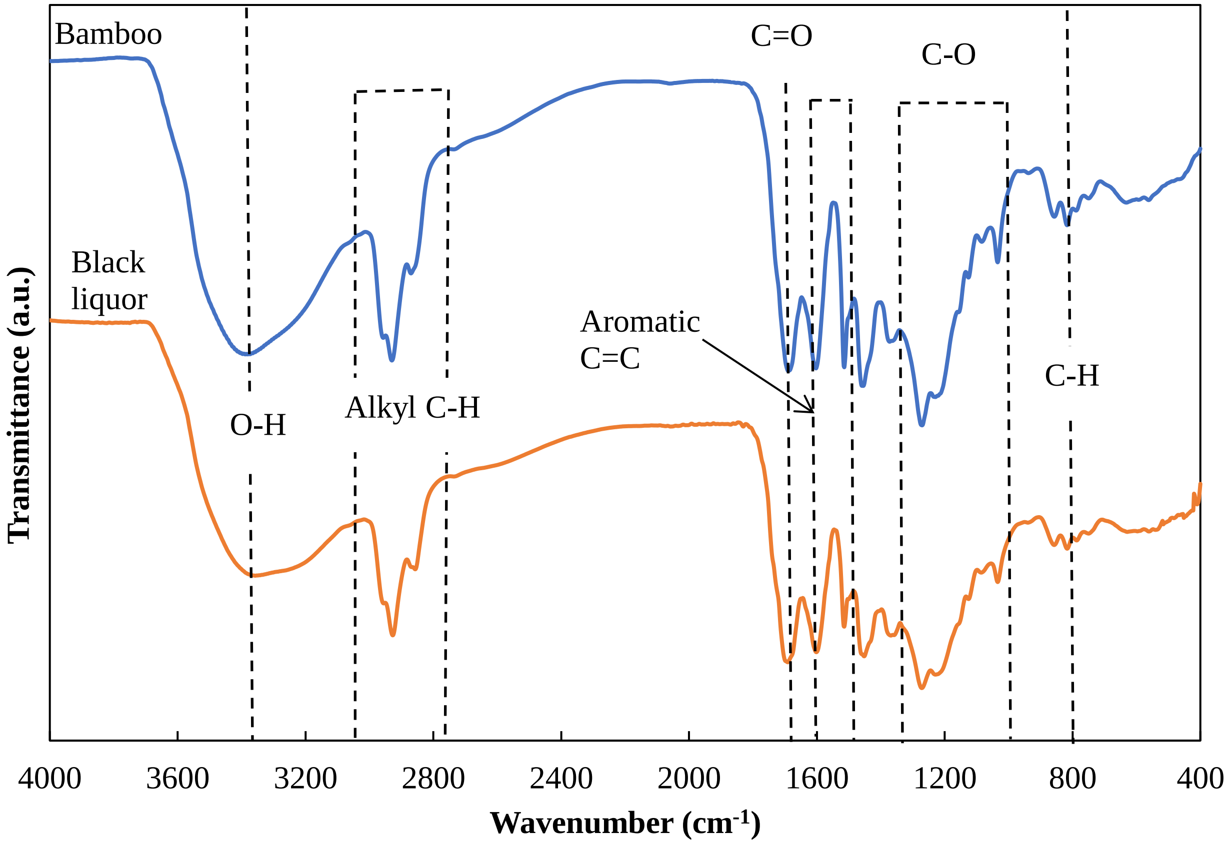

Figure 7.5 : FT-IR spectrum of the bio-oil from the liquefaction of bamboo and black liquor at 300 °C for 30 min, respectively.

Table 7.4 summarizes the ultimate analysis results of bio-oils as well as the TAN value of the produced bio-oils. From the corrosion perspective, the bio-oil produced from black liquor is much more aggressive as it contains higher sulfur content (4.71 wt.%) and has a higher TAN value of 106.22 ± 2.76 mg KOH/g compared to those generated from bamboo. Note that a higher TAN value indicates the presence of a high concentration of organic acids.

Table 7.4: Ultimate analysis results and associated TANs of produced bio-oils.

Feedstock	**Bamboo**	**Black liquor**
Ash (wt.%)	n.d.	11.71
Ultimate analysis (wt.%)[a]		
C	70.40	58.83
H	6.38	4.20
N	0.33	0.08
S	<0.01	4.71
O[b]	22.89	20.47
HHV (MJ/kg)[c]	28.82	22.68
TAN (mg KOH/g)	40.07 ± 3.52	106.22 ± 2.76

[a] On dry basis; [b] By difference; [c] Calculated by DuLong equation.

7.3.2 Characterization of Formed Corrosion Products and Deposited Organic Products

The representative photographic images of SS316L samples before and after the exposures to different HTL environments are shown in **Figure 7.6**. Before the tests, the surface of a freshly prepared coupon was shining metal luster. However, after the exposures to the simulated and real HTL conversion environments, the steels exhibited dark surface color, implying the formation of thick corrosion layers and/or the deposition of organic compounds. In addition, the samples exposed to bamboo and black liquor-contained solution have relatively large black deposits on the surface, probably due to the formation and agglomeration of organic compounds above the surface oxide layers. It is also noticed that spallation occurred on the sample exposed to the black liquor-contained HTL environment.

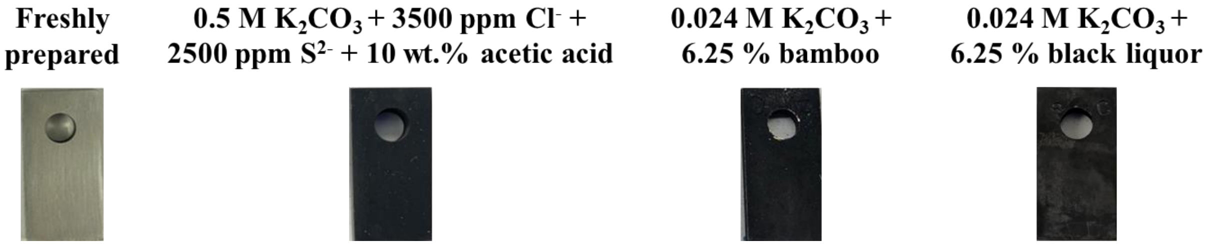

Freshly prepared

0.5 M K_2CO_3 + 3500 ppm Cl^- + 2500 ppm S^{2-} + 10 wt.% acetic acid

0.024 M K_2CO_3 + 6.25 % bamboo

0.024 M K_2CO_3 + 6.25 % black liquor

Figure 7.6: Photographic images of SS316L before and after the exposures to simulated HTL environment at 310 °C for 10 days and biomass-contained HTL environments at 300 °C for 10 hours, respectively.

In order to further explore the impact of organic feedstocks and organic deposits, top-view SEM images were obtained and are shown in **Figure 7.7**. In the simulated HTL environment, the steel experienced general oxidation and suffered considerable chemical dissolution of formed oxides. Localized nodular oxidation and corrosive product deposition were observed. Note that the deposition was likely to occur during the autoclave cooling-down as described in a recent study [63]. As suggested in previous studies [64, 65], stable Fe and Cr oxide are thermodynamically unfavorable to be formed in the simulated catalytic HTL environments, and would have relatively high chemical dissolution rates in the environment . Moreover, the addition of inorganic and organic corrodants (S^{2-}, Cl^- and acetic acid) into the simulated catalytic environment could further enhanced their dissolution due to the following reactions:

$$CH_3COOH + OH^- = CH_3COO^- + H_2O \quad (7.4)$$

$$S^{2-} + H_2O = HS^- + OH^- \quad (7.5)$$

This corrosion mechanism shall also be applied on the steel exposed to the real HTL conversion environments.

For the corrosion in real biomass conversion environment, a unique feature observed is the localized accumulation of organic compounds on the steels, as shown in **Figure 7.7 (b)** and **(c)**. After the 10 hours exposure to the bamboo HTL environment, a porous and thick carbon-rich deposition layer was presented on the steel, below which an oxide scale was possibly formed. Cracks were found to develop along the whole surface layer. Different from that, obvious spalling of the outer surface layer occurred on the steel exposed to the black liquor HTL conversion environment. Below the carbon-rich layer, a corrosion layer was grown on the steels, accompanied by randomly distributed nodular oxides. Interestingly, micro-pores and cracks are not observed on the corrosion layer. More importantly, S^{2-} and ash are known to facilitate the steels susceptible to pitting [66-68]. However, the results indicated that pitting would be unlikely to occur even under the black liquor HTL conversion.

The formation of organic compounds above the oxide layer implies that their functional group might interact with oxide cation/anion and/or their vacancies. For instance, CH_3COO^- ions produced from the reaction (4) could also interact with metal cations (M^{n+}) in the oxide to form dissolvable metal acetate based on previous studies [29]:

$$\mathrm{nCH_3COO^-} + \mathrm{M^{n+}_{oxide}} \rightarrow \mathrm{M(CH_3COO)_n} \tag{7.6}$$

The interaction could be quite complicated during the HTL conversion of bamboo or black liquor due to the existence of numerous functional groups, as suggested by **Figure 7.8** below.

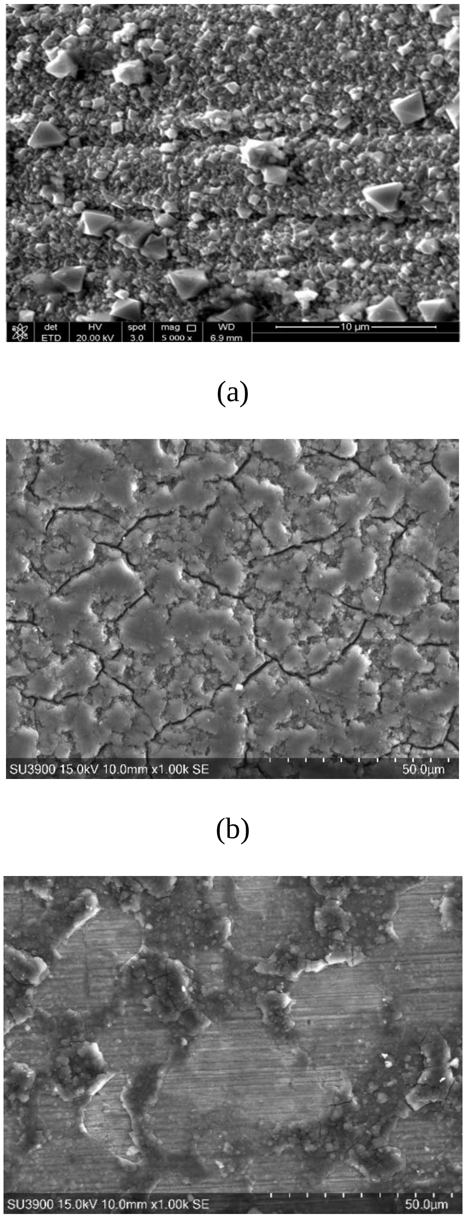

(a)

(b)

(c)

Figure 7.7: Top-view SEM images collected on SS316L samples after the exposures to (a) simulated HTL environment at 310 °C for 10 days, (b) bamboo-contained HTL environments at 300 °C for 10 hours, and (c) black liquor-contained HTL environments at 300 °C for 10 hours.

Figure 7.8 shows the FTIR spectrum collected on a SS316L sample after being corroded in the bamboo-contained HTL at 300 °C for 10 hours. The absorbance at 1700 cm^{-1}, representing the C=O stretching vibration of carbonyl groups, indicated the presence of ketones, aldehydes, esters, or carboxylic acids within the deposited carbon-rich layer. The relatively medium-intense peaks at 1611 and 1495 cm^{-1} represented aromatic nuclei, suggesting the presence of aromatic rings and their derivatives. The IR absorption bands between 3000 and 2840 cm^{-1} would be attributed to C-H stretching vibrations from alkyl C-H in the oils. The two absorption peaks at 1370 and 1456 cm^{-1} were attributed to the bending vibrations of methyl ($-CH_3$) and methylene ($-CH_2$) groups, respectively. The presence of C-H stretching vibration and the C-H blending was possibly due to the alkane groups. The peaks between 1280 and 1000 cm^{-1} were related to C-O vibrations, suggesting the possible presence of acids, phenols, furans, or alcohols. The peak at 860 cm^{-1} is attributed to C-H bending suggested the possible presence of single, polycyclic, and substituted aromatics. The functional groups observed on the SS316L corroded in black liquor-contained environment were similar to that exposed to bamboo-containing environment. In general, the carbon-rich layer deposited on the steel are mainly composed of phenolic and carboxyl compounds. The roles of these compounds on corrosion will be discussed in detail in **Section 7.3.4** below.

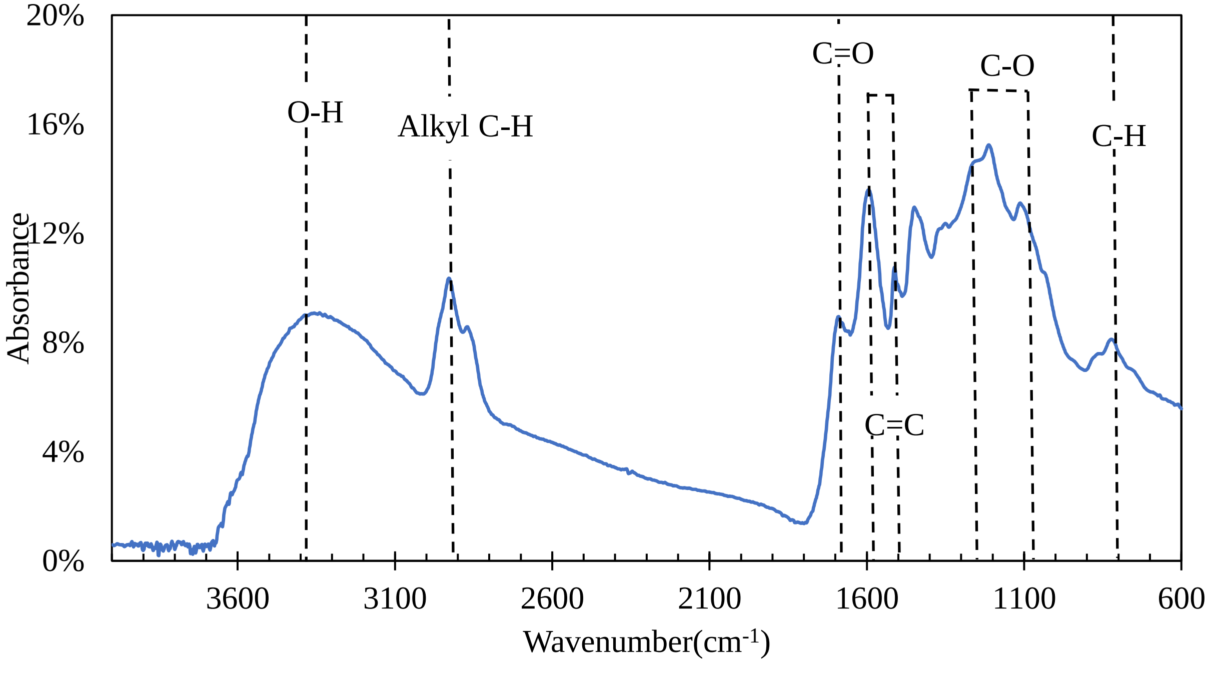

Figure 7.8: FT-IR spectrum collated on a SS316L sample after exposed to the bamboo-contained HTL at 300 °C for 10 hours.

To explore the chemical composition of corrosion layer formed, XRD spectra were collected on the steel samples exposed to different HTL environments, and the results are shown in **Figure 7.9**. The major oxide compounds formed under simulated HTL environment are Fe and Cr spinel oxides as well as magnetite. Note that the spectrum has been smoothed to better illustrate the location of minor peaks. Different from that, the oxide layer formed under bamboo-contained environment might be quite thin and only the bulk metal phase was detected. Note that the broad peak at 25° possibly referred to the uncrystallized carbon-rich layer. In high-temperature aqueous solutions, a Cr-rich oxide layer is expected to form on SS316L due to its Cr content > 16%. Thermodynamic calculation suggested that the alloying elements (Cr and Fe) would be ready for the oxide formation in all the three testing environments because of the negative formation energy of their oxides [33]. The undetected Cr/Fe oxide signals on the sample exposed to bamboo-contained environment could be attributed to the following factors: (1) the formed surface scale might be too thin; and/or (2) the chemical dissolution of Cr oxides be remarkably enhanced in the conversion environment. Compared with bamboo, the corrosion layer in the black liquor HTL environment would be relatively thicker as the signals of FeS, Fe_3O_4, and (Fe, Ni) Cr_2O_4 were collected. The FeS and Fe_3O_4 might be formed from the deposition of corrosive ions or above the Cr-enriched oxides, since Cr oxides should be more chemically stable in the testing environment compared to Fe compounds. Cross-section TEM characterization is needed to further confirm the observations.

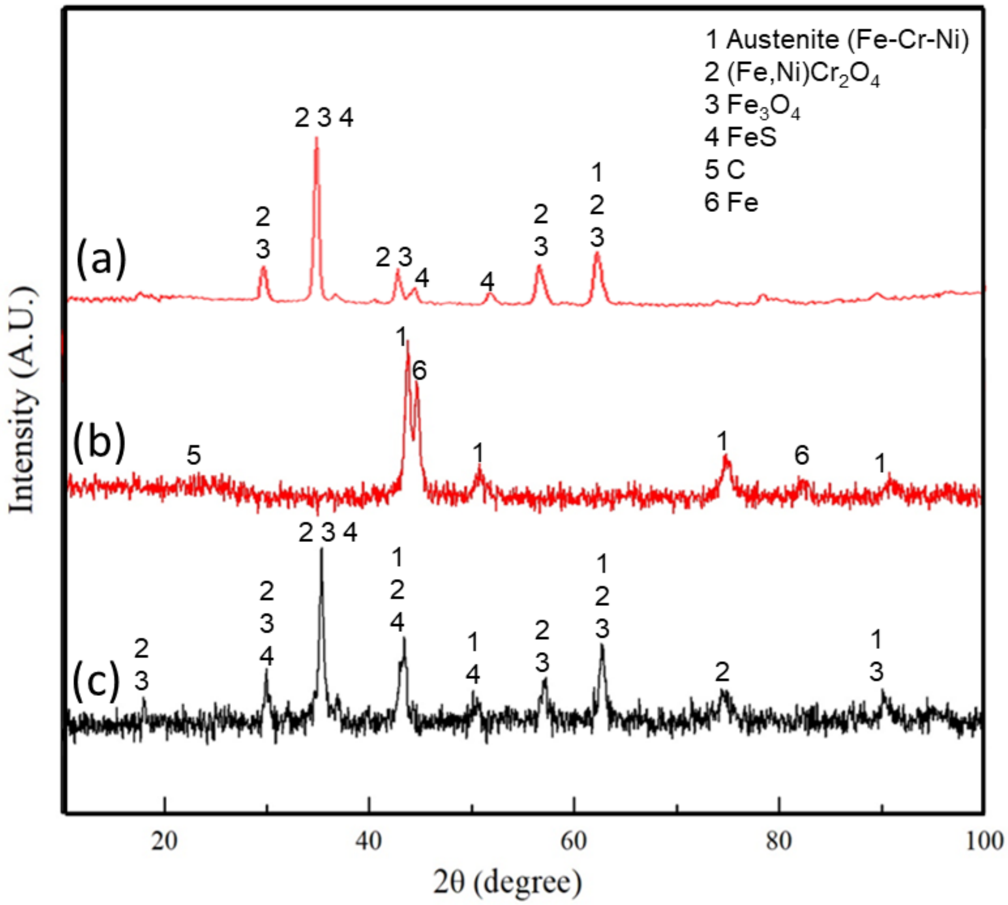

Figure 7.9: XRD spectra collected on SS316L samples after the exposures to (a) simulated HTL environment at 310 °C for 10 days, (b) bamboo-contained HTL environments and (c) black liquor-contained HTL at 300 °C for 10 hours, respectively.

7.3.3 Corrosion Rates of SS316L in Different HTL Environments

The average corrosion rates of SS316L in different HTL environments were estimated based on the weight loss measurement and Eqn. (7.3) as described in **Section 7.2.5**, and the obtained results are shown in **Figure 7.10**. Following observations and discussions are made:

(1) SS316L suffered the highest corrosion rate (336 µm/year) in the black liquor-contained HTL environment, while experienced the lowest corrosion rate (62 µm/year) in the bamboo-contained HTL environment at 300 °C, consistent with the observations in **Figure 7.7**. Given the pH value of conversion media and thermodynamic predications conducted in a previous study [29], the major alloying

elements (Fe, Cr, and Ni) in the steel would experience active corrosion in the black liquor HTL environment, but undergo passivation and relatively high chemical dissolution of surface oxide in the other two HTL environments. Although the final pH value (~ 4.8-5.3) of bamboo-contained HTL environment after the conversion is close to that (~ 5.4), of simulated HTL environment the corrosion rate of SS316L in the simulated condition is noticeably higher than that in the bamboo-contained environment, implying that (1) the presence of Cl and S anions could enhance the chemical dissolution of surface oxides; and/or (2) certain organic products produced during the conversion of bamboo might act as corrosion inhibitor to somewhat protect the surface scales formed.

(2) Compared with the rate obtained in the simulated HTL environment, the highest corrosion rate of the steel in the black liquor HTL environment suggests that the excessive amounts of S^{2-} and ash in the black liquor could make the environment more aggressive to the steel even though some organic products and functional groups (e.g., carboxylic group and phenolic hydroxyl) produced from this feedstock might serve as corrosion inhibitors to mitigate the corrosion damage. This also implies that the S^{2-} and ash could act as more dominant factors on the corrosion compared to the organic intermediate and products. Additionally, the results also suggest that there might be critical contents of S^{2-} and ash, above which the surface oxide scale formed on the steel would become unprotective to the metal substrate, leading to the corrosion mode controlled by the active corrosion. Further work is needed to determine the critical levels of two corrodants for long-term safe operation of HTL reactor.

(3) As there is no materials technology guideline available to define the maximum allowable corrosion rate of the HTL reactor alloys, one can assume that the maximum limit should be less than 100 um/year based on existing operating experience and knowledge at paper and mill plants [69, 70]. Therefore, SS316L is likely to be a suitable candidate of construction for common forest or agricultural biomass conversion, but unapplicable for handling highly corrosive biowastes such as black liquor.

In general, the above findings indicate that except for hot pressurized water, basic catalyst and corrodants release during the conversion, the organic intermediates, and products during the catalytic HTL conversion could also affect the corrosion kinetic of SS316L steel. More importantly, the corrodants (S^{2-} and ash) presented in the biowastes possibly act as more dominant factors on corrosion process compared with other operating parameters.

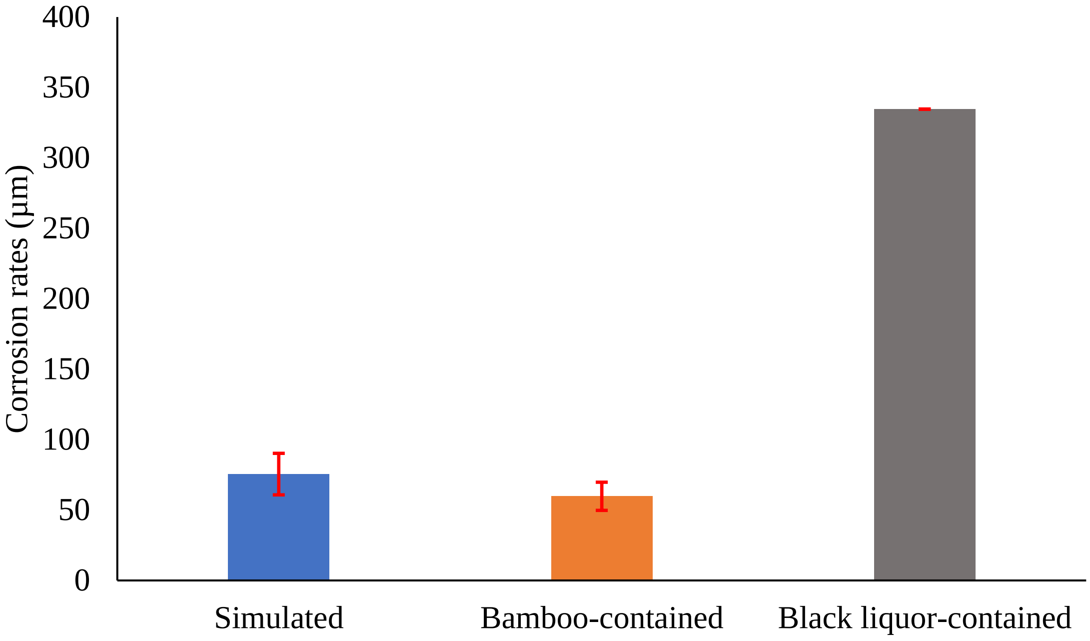

Figure 7.10: Variation of corrosion rates of SS316L in (a) simulated HTL environment at 310 °C for 10 days, (b) biomass-contained HTL environments at 300 °C for 10 hours, and (c) black liquor-contained HTL environments at 300 °C for 10 hours.

7.3.4 Possible Role of Organic Compounds on Corrosion

As described above, the organic compounds deposited on of the corroded SS316L could act as inhibitors to reduce corrosion damage. The chemistry of HTL environment is quite complicated and it is different to clarify the role of each organic compound on corrosion. Theoretically, the efficiency of organic corrosion inhibitors is controlled by multiple factors, including the size of the organic molecules, the types and numbers of bonding atoms or functional groups, and the nature of the surface charge and its distribution (electron releasing or withdrawing) [71-73].

According to previous studies [74, 75], there are two major pathways in which organic inhibitors would absorb and deposit on the metal/oxide surface. The first is physisorption, in which positively charged inhibitor and metallic surface interacted through electrostatic force. Another way is named chemisorption, where non-bonding or π-electrons were shared between inhibitors and metallic d-orbital. As shown in **Figure 7.8**, several bonding and corresponding functional groups, including -OH (in alcohol, carboxylic acid, and phenol), C-H (in alkane, alkene, and methyl), C=C, C=O and C-O., are detected in the deposited organic layer on SS316L surface after the exposed to bamboo-contained HTL conversion. These functional groups may act as the inhibitor by imposing electrostatic force with the formed oxides and then retaining on the surface oxide through physical approaches. Moreover, the produced polar functional groups, which have sulfur, oxygen, or nitrogen atoms (see **Figures 7.4** and **7.5)**, can also improve the performance of these organic inhibitors.

Based on previous studies [76-78], the organic compounds produced during the HTL catalytic conversion could exhibit different ways to reduce corrosion damage and protect the steel. Firstly, primary alcohol functional groups could suppress the accessibility of Cl^- to the steel surface and consequently reduce localized pitting susceptibility. Secondly, carboxylate might inhibit the chemical dissolution of oxides in alkaline solutions with pH of ~11.5. Thirdly, the -OCH3 groups can facilitate both physical and chemical adsorption on the steel surface for the formation of a carbon-rich corrosion barrier.

Fourthly, the polar functional groups with hetero atoms, such as O, S and N, could be benefit to the adsorption on the steel surface to reduce cathodic and anodic reactions occurred at the steel/solution interface. These atoms have also been found to perform well on stainless steels in acidic environment by interacting with metals to increase their surface hydrophobicity [79-82].

It is worth noticing that most of the previous corrosion studies on inhibitors are conducted at room or moderate temperatures, the effects of these functional groups in alkaline solutions at elevated temperature (> 300 °C) have not yet been well studied. In this study, even though the relatively low corrosion rate of SS316L during bamboo-contained HTL conversion suggests that protective oxide layer would likely to form on the surface, previous thermodynamic calculations [29] implying that in the initial catalytic environment (pH > 10.5) or after fully converted (pH= 4.8 ~ 5.3), the steels would not only experience general oxidation, but also suffered high chemical dissolution of formed oxides. In this case, the hetero atoms within the formed organic compounds may donate lone electrons to the cations in the oxides to form a persistent organic layer, which consequently retard the reaction rate of both cathodic and anodic reactions occurred on steel/solution interface. According to former studies [83] , they are likely to form strong covalent bond and chemisorption would thus to be the dominant approach in this HTL environment. Further microscopic characterization on the oxide/organic layer interface is required to reveal the puzzle.

7.4 Conclusions

This chapter investigated the influence of biomass feedstocks (bamboo and black liquor) and organic products on corrosion of SS316L during catalytic HTL conversion. Following preliminary conclusions are made:

(1) The major compounds presenting in both bio-oils from bamboo and black liquor are phenolic and aromatic compounds. The bio-oil derived from black liquor contains more phenols and aromatics, but fewer ketones compared to that converted from HTL of bamboo. In addition, the application of black liquor leads to the produced bio-oils with higher concentrations of S and organic acids compared to bamboo feedstock.

(2) SS316L steel exhibits the lowest in bamboo-contained HTL environment, but suffers the highest attack during the HTL conversion of black liquor. Compared with the corrosion in simulated catalytic HTL environment, it is likely that the application of bamboo somewhat reduces corrosion damage, likely due to the formation of Carbon-rich inhibition layer on the surface scale.

(3) There are possible critical contents of S^{2-} and ash in biowaste, above which the use of the wastes for the conversion could lead to unacceptable damage on HTL conversion reactors. Further work is required to determine these limits.

7.5 References

[1] N. Sharma, K.K. Jaiswal, V. Kumar, M.S. Vlaskin, M. Nanda, I. Rautela, M.S. Tomar, W. Ahmad, Effect of catalyst and temperature on the quality and productivity of HTL bio-oil from microalgae: A review, Renewable energy 174 (2021) 810-822.

[2] J. Ni, L. Qian, Y. Wang, B. Zhang, H. Gu, Y. Hu, Q. Wang, A review on fast hydrothermal liquefaction of biomass, Fuel 327 (2022) 125135.

[3] L. Nazari, C.C. Xu, M.B. Ray, Advanced Technologies (Biological and Thermochemical) for Waste-to-Energy Conversion, Green Chemistry and Sustainable Technology Advanced and Emerging Technologies for Resource Recovery Singapore, 2021, pp. 55-95.

[4] E. Demirkaya, O. Dal, A. Yüksel, Liquefaction of waste hazelnut shell by using sub- and supercritical solvents as a reaction medium, The Journal of Supercritical Fluids 150 (2019) 11-20.

[5] L. Cao, K. Iris, X. Xiong, D.C. Tsang, S. Zhang, J.H. Clark, C. Hu, Y.H. Ng, J. Shang, Y.S. Ok, Biorenewable hydrogen production through biomass gasification: A review and future prospects, Environmental research 186 (2020) 109547.

[6] A. Sertolli, Z. Gabnai, P. Lengyel, A. Bai, Biomass Potential and Utilization in Worldwide Research Trends—A Bibliometric Analysis, Sustainability 14(9) (2022) 5515.

[7] T.H. Seehar, S.S. Toor, K. Sharma, A.H. Nielsen, T.H. Pedersen, L.A. Rosendahl, Influence of process conditions on hydrothermal liquefaction of eucalyptus biomass for biocrude production and investigation of the inorganics distribution, Sustainable Energy & Fuels 5(5) (2021) 1477-1487.

[8] C.C. Xu, Y. Shao, Z. Yuan, S. Cheng, S. Feng, L. Nazari, M. Tymchyshyn, Hydrothermal liquefaction of biomass in hot-compressed water, alcohols, and alcohol-water co-solvents for biocrude production, Application of hydrothermal reactions to biomass conversion, Springer2014, pp. 171-187.

[9] Y. Zhang, W.-T. Chen, Hydrothermal liquefaction of protein-containing feedstocks, Direct Thermochemical Liquefaction for Energy Applications, Elsevier2018, pp. 127-168.

[10] R.K. Mishra, P. Kumar, K. Mohanty, Hydrothermal liquefaction of biomass for bio-crude production: A review on feedstocks, chemical compositions, operating parameters, reaction kinetics, techno-economic study, and life cycle assessment, Fuel 316 (2022) 123377.

[11] C. Xu, J. Lancaster, Conversion of secondary pulp/paper sludge powder to liquid oil products for energy recovery by direct liquefaction in hot-compressed water, Water research 42(6-7) (2008) 1571-1582.

[12] F. Conti, S.S. Toor, T.H. Pedersen, T.H. Seehar, A.H. Nielsen, L.A. Rosendahl, Valorization of animal and human wastes through hydrothermal liquefaction for biocrude production and simultaneous recovery of nutrients, Energy conversion and management 216 (2020) 112925.

[13] C. Tian, B. Li, Z. Liu, Y. Zhang, H. Lu, Hydrothermal liquefaction for algal biorefinery: A critical review, Renewable and Sustainable Energy Reviews 38 (2014) 933-950.

[14] G.G. Zaimes, V. Khanna, Microalgal biomass production pathways: evaluation of life cycle environmental impacts, Biotechnology for Biofuels 6(1) (2013) 88.

[15] C.L. Williams, T.L. Westover, R.M. Emerson, J.S. Tumuluru, C. Li, Sources of Biomass Feedstock Variability and the Potential Impact on Biofuels Production, BioEnergy Research 9(1) (2016) 1-14.

[16] M. Saleem, Possibility of utilizing agriculture biomass as a renewable and sustainable future energy source, Heliyon 8(2) (2022) e08905.

[17] R. Singh, A. Prakash, B. Balagurumurthy, R. Singh, S. Saran, T. Bhaskar, Hydrothermal liquefaction of agricultural and forest biomass residue: comparative study, Journal of Material Cycles and Waste Management 17(3) (2015) 442-452.

[18] A.R. Maag, A.D. Paulsen, T.J. Amundsen, P.E. Yelvington, G.A. Tompsett, M.T. Timko, Catalytic hydrothermal liquefaction of food waste using CeZrOx, Energies 11(3) (2018) 564.

[19] H.-j. Huang, X.-z. Yuan, H.-n. Zhu, H. Li, Y. Liu, X.-l. Wang, G.-m. Zeng, Comparative studies of thermochemical liquefaction characteristics of microalgae, lignocellulosic biomass and sewage sludge, Energy 56 (2013) 52-60.

[20] J. Lu, J. Watson, J. Zeng, H. Li, Z. Zhu, M. Wang, Y. Zhang, Z. Liu, Biocrude production and heavy metal migration during hydrothermal liquefaction of swine manure, Process Safety and Environmental Protection 115 (2018) 108-115.

[21] S. Bensaid, R. Conti, D. Fino, Direct liquefaction of ligno-cellulosic residues for liquid fuel production, Fuel 94 (2012) 324-332.

[22] L. Yang, L. Nazari, Z. Yuan, K. Corscadden, C.C. Xu, Hydrothermal liquefaction of spent coffee grounds in water medium for bio-oil production, Biomass and Bioenergy 86 (2016) 191-198.

[23] H. Hwang, J.H. Lee, I.-G. Choi, J.W. Choi, Comprehensive characterization of hydrothermal liquefaction products obtained from woody biomass under various alkali catalyst concentrations, Environmental technology 40(13) (2019) 1657-1667.

[24] L. Yan, Y. Wang, J. Li, Y. Zhang, L. Ma, F. Fu, B. Chen, H. Liu, Hydrothermal liquefaction of Ulva prolifera macroalgae and the influence of base catalysts on products, Bioresource technology 292 (2019) 121286.

[25] Y. Zhuang, J. Guo, L. Chen, D. Li, J. Liu, N. Ye, Microwave-assisted direct liquefaction of Ulva prolifera for bio-oil production by acid catalysis, Bioresource technology 116 (2012) 133-139.

[26] C. Ma, J. Geng, D. Zhang, X. Ning, Hydrothermal liquefaction of macroalgae: Influence of zeolites based catalyst on products, Journal of the Energy Institute 93(2) (2020) 581-590.

[27] I.A. Basar, H. Liu, H. Carrere, E. Trably, C. Eskicioglu, A review on key design and operational parameters to optimize and develop hydrothermal liquefaction of biomass for biorefinery applications, Green Chemistry 23(4) (2021) 1404-1446.

[28] S. Karagöz, T. Bhaskar, A. Muto, Y. Sakata, T. Oshiki, T. Kishimoto, Low-temperature catalytic hydrothermal treatment of wood biomass: analysis of liquid products, Chemical Engineering Journal 108(1-2) (2005) 127-137.

[29] M. Liu, Y. Zeng, J.-L. Luo, Impacts of catalyst, inorganic and organic corrodants on corrosion under batch-mode catalytic biomass hydrothermal liquefaction conversion, Corrosion Science 204 (2022) 110409.

[30] M.P. Brady, J.R. Keiser, D.N. Leonard, L. Whitmer, J.K. Thomson, Corrosion considerations for thermochemical biomass liquefaction process systems in biofuel production, JOM 66(12) (2014) 2583-2592.

[31] M. Liu, Y. Zeng, J.-L. Luo, Impacts of Catalyst, Inorganic and Organic Corrodants on Corrosion under Batch-mode Catalytic Biomass Hydrothermal Liquefaction Conversion, Corrosion Science (2022) 110409.

[32] T. Tran Thi Thuy, K. Kannoorpatti, A. Padovan, S. Thennadil, Effect of alkaline artificial seawater environment on the corrosion behaviour of duplex stainless steel 2205, Applied Sciences 10(15) (2020) 5043.

[33] M. Liu, Y. Zeng, J.-L. Luo, Influence of Major Operating Parameters (Temperature, Pressure, and Flow Rate) on the Corrosion of Candidate Alloys for the Construction of Hydrothermal Liquefaction Biorefining Reactors, Energy & Fuels 36(6) (2022) 3134-3153.

[34] H. Kim, D. Mitton, R. Latanision, Corrosion behavior of Ni-base alloys in aqueous HCl solution of pH 2 at high temperature and pressure, Corrosion Science 52(3) (2010) 801-809.

[35] W. Sun, H. Wei, X. Li, Z.-a. Xiong, C.J.C.E. Sun, Science, Technology, Effects of different inorganic anions on equipment material corrosion behaviour in subcritical water oxidation, Corrosion Enigineering, Science and Technology 53(6) (2018) 403-412.

[36] X. Guo, Y. Fan, W. Gao, R. Tang, K. Chen, Z. Shen, L. Zhang, Corrosion resistance of candidate cladding materials for supercritical water reactor, Annals of Nuclear Energy 127 (2019) 351-363.

[37] D. Rodriguez, A. Merwin, Z. Karmiol, D. Chidambaram, Surface chemistry and corrosion behavior of Inconel 625 and 718 in subcritical, supercritical, and ultrasupercritical water, Applied Surface Science 404 (2017) 443-451.

[38] K. Chen, J. Wang, Z. Shen, D. Du, X. Guo, B. Gong, J. Liu, L. Zhang, Comparison of the stress corrosion cracking growth behavior of cold worked Alloy 690 in subcritical and supercritical water, Journal of Nuclear Materials 520 (2019) 235-244.

[39] C.A. de Wolf, H.A. Nasr-El-Din, A. Bouwman, E.R. Bang, E. Naylor, Corrosion rates of Cr-and Ni-based alloys with organic acids and chelating agents used in stimulation of deep wells, SPE Production & Operations 32(02) (2017) 208-217.

[40] J. Shao, C. Du, X. Zhang, L. Cui, Effects of lead on the initial corrosion behavior of 316LN stainless steel in high-temperature alkaline solution, Acta Metallurgica Sinica 32(1) (2019) 89-97.

[41] W. Tsai, T. Wu, Pitting corrosion of Alloy 690 in thiosulfate-containing chloride solutions, Journal of Nuclear Materials 277(2-3) (2000) 169-174.

[42] M. Abdallah, B. Jahdaly, M. Salem, A. Fawzy, A.A. Fattah, Pitting corrosion of nickel alloys and stainless steel in chloride solutions and its inhibition using some inorganic compounds, J. Mater. Environ. Sci 8(7) (2017) 2599-2607.

[43] J. Yang, S. Wang, D. Xu, Y. Guo, C. Yang, Y. Li, Effect of ammonium chloride on corrosion behavior of Ni-based alloys and stainless steel in supercritical water

gasification process, International Journal of Hydrogen Energy 42(31) (2017) 19788-19797.

[44] J. Zhang, B. Li, Y. Li, J. Lu, K. Wang, H. Zhang, Effect of sulfide on corrosion behavior of stainless steel 316SS and Hastelloy C276 in sub/supercritical water, International Journal of Hydrogen Energy 46(42) (2021) 22222-22233.

[45] M. Quraishi, D.S. Chauhan, F.A. Ansari, Development of environmentally benign corrosion inhibitors for organic acid environments for oil-gas industry, Journal of Molecular Liquids 329 (2021) 115514.

[46] R.K. Desu, H. Nitin Krishnamurthy, A. Balu, A.K. Gupta, S.K. Singh, Mechanical properties of Austenitic Stainless Steel 304L and 316L at elevated temperatures, Journal of Materials Research and Technology 5(1) (2016) 13-20.

[47] L. Gardner, A. Insausti, K.T. Ng, M. Ashraf, Elevated temperature material properties of stainless steel alloys, Journal of Constructional Steel Research 66(5) (2010) 634-647.

[48] M. Liu, Y. Zeng, J.-L. Luo, Roles of Major Alloying Elements in Steels and Alloys on Corrosion under Biomass Hydrothermal Liquefaction (HTL) Conversion, Corrosion Science (2023) 111148.

[49] P. Körner, D. Jung, A. Kruse, Influence of the pH Value on the Hydrothermal Degradation of Fructose, Chemistry Open 8(8) (2019) 1121-1132.

[50] X. Zhang, J. Scott, B.K. Sharma, N. Rajagopalan, Advanced treatment of hydrothermal liquefaction wastewater with nanofiltration to recover carboxylic acids, Environmental Science: Water Research & Technology 4(4) (2018) 520-528.

[51] T. Belkheiri, S.I. Andersson, C. Mattsson, L. Olausson, H. Theliander, L. Vamling, Hydrothermal liquefaction of kraft lignin in sub-critical water: the influence of the sodium and potassium fraction, Biomass Conversion and Biorefinery 8(3) (2018) 585-595.

[52] Z. Fang, T. Minowa, R. Smith, T. Ogi, J. Koziński, Liquefaction and gasification of cellulose with Na2CO3 and Ni in subcritical water at 350 C, Industrial & Engineering Chemistry Research 43(10) (2004) 2454-2463.

[53] J. Akhtar, S.K. Kuang, N.S. Amin, Liquefaction of empty palm fruit bunch (EPFB) in alkaline hot compressed water, Renewable energy 35(6) (2010) 1220-1227.

[54] H. Huang, X. Yuan, H. Zhu, H. Li, Y. Liu, X. Wang, G. Zeng, Comparative studies of thermochemical liquefaction characteristics of microalgae, lignocellulosic biomass and sewage sludge, Energy 56 (2013) 52-60.

[55] Standard Practice for Laboratory Immersion Corrosion Testing of Metals.

[56] H. Guan, W. Ding, S. Liu, B. Zhao, H. Zhang, C. Zhong, B. Chen, A. Song, D. Zhu, H. Li, Catalytic hydrothermal liquefaction of Chinese herb residue for the production of high-quality bio-oil, International Journal of Hydrogen Energy 48(30) (2023) 11205-11213.

[57] R. Kaur, P. Gera, M.K. Jha, T. Bhaskar, Reaction parameters effect on hydrothermal liquefaction of castor (Ricinus Communis) residue for energy and valuable hydrocarbons recovery, Renewable energy 141 (2019) 1026-1041.

[58] A.C.G.-o.C.o. Metals, Standard practice for preparing, cleaning, and evaluating corrosion test specimens, ASTM international, 2017.

[59] R.A. Antunes, M.C.L. de Oliveira, Corrosion in biomass combustion: A materials selection analysis and its interaction with corrosion mechanisms and mitigation strategies, Corrosion Science 76 (2013) 6-26.

[60] D. Guzonas, W. Cook, Cycle chemistry and its effect on materials in a supercritical water-cooled reactor: A synthesis of current understanding, Corrosion Science 65 (2012) 48-66.

[61] ASTM, Corrosion tests and standards, Application and Interpretation, Baboian-Editor, Phil., PA, 1995, p. 499.

[62] S. He, M. Zhao, J. Wang, Z. Cheng, B. Yan, G. Chen, Hydrothermal liquefaction of low-lipid algae Nannochloropsis sp. and Sargassum sp.: Effect of feedstock composition and temperature, Science of the Total Environment 712 (2020) 135677.

[63] M. Liu, Y. Zeng, J.-L. Luo, Influence of Major Operating Parameters (Temperature, Pressure, and Flow Rate) on the Corrosion of Candidate Alloys for the Construction of Hydrothermal Liquefaction Biorefining Reactors, Energy & Fuels (2022).

[64] G. Tranchida, M. Clesi, F. Di Franco, F. Di Quarto, M. Santamaria, Electronic properties and corrosion resistance of passive films on austenitic and duplex stainless steels, Electrochimica Acta 273 (2018) 412-423.

[65] J. Robertson, The mechanism of high temperature aqueous corrosion of stainless steels, Corrosion Science 32(4) (1991) 443-465.

[66] P. Vainikka, D. Bankiewicz, A. Frantsi, J. Silvennoinen, J. Hannula, P. Yrjas, M. Hupa, High temperature corrosion of boiler waterwalls induced by chlorides and bromides. Part 1: Occurrence of the corrosive ash forming elements in a fluidised bed boiler co-firing solid recovered fuel, Fuel 90(5) (2011) 2055-2063.

[67] S.C. Srivastava, K.M. Godiwalla, M.K. Banerjee, Fuel ash corrosion of boiler and superheater tubes, Journal of Materials Science 32(4) (1997) 835-849.

[68] D. Bankiewicz, P. Vainikka, D. Lindberg, A. Frantsi, J. Silvennoinen, P. Yrjas, M. Hupa, High temperature corrosion of boiler waterwalls induced by chlorides and bromides – Part 2: Lab-scale corrosion tests and thermodynamic equilibrium modeling of ash and gaseous species, Fuel 94 (2012) 240-250.

[69] M. Davies, N.D. Institute, Alloy Selection for Service in Caustic Soda: A Guide to the Use of Nickel-containing Alloys, Nickel Institute2019.

[70] R. Francis, S. Clarke, Corrosion in Caustic Soda in Mineral Processing Operations, Corrosion 76(7) (2020) 707-715.

[71] S. Abd El-Maksoud, The effect of organic compounds on the electrochemical behaviour of steel in acidic media. A review, International Journal of Electrochemical Science 3(5) (2008) 528-555.

[72] M.A. Ameer, A.M. Fekry, Inhibition effect of newly synthesized heterocyclic organic molecules on corrosion of steel in alkaline medium containing chloride, International Journal of Hydrogen Energy 35(20) (2010) 11387-11396.

[73] L. Rivera-Grau, M. Casales, I. Regla, D. Ortega-Toledo, J. Ascencio-Gutierrez, J. Porcayo-Calderon, L. Martinez-Gomez, Effect of organic corrosion inhibitors on the corrosion performance of 1018 carbon steel in 3% NaCl solution, International Journal of Electrochemical Science 8(2) (2013) 2491-2503.

[74] B. Chugh, S. Thakur, B. Pani, M. Murmu, P. Banerjee, A.M. Al-Mohaimeed, E.E. Ebenso, M. Singh, J. Singh, A.K. Singh, Investigation of phenol-formaldehyde resins as corrosion impeding agent in acid solution, Journal of Molecular Liquids 330 (2021) 115649.

[75] M. Goyal, S. Kumar, I. Bahadur, C. Verma, E.E. Ebenso, Organic corrosion inhibitors for industrial cleaning of ferrous and non-ferrous metals in acidic solutions: A review, Journal of Molecular Liquids 256 (2018) 565-573.

[76] E. Rakanta, T. Zafeiropoulou, G. Batis, Corrosion protection of steel with DMEA-based organic inhibitor, Construction and Building Materials 44 (2013) 507-513.

[77] M. Cabrini, F. Fontana, S. Lorenzi, T. Pastore, S. Pellegrini, Effect of Organic Inhibitors on Chloride Corrosion of Steel Rebars in Alkaline Pore Solution, Journal of Chemistry 2015 (2015) 521507.

[78] B. Lin, Y. Zuo, Corrosion inhibition of carboxylate inhibitors with different alkylene chain lengths on carbon steel in an alkaline solution, RSC Advances 9(13) (2019) 7065-7077.

[79] S. Ali, A. El-Shareef, R. Al-Ghamdi, M. Saeed, The isoxazolidines: The effects of steric factor and hydrophobic chain length on the corrosion inhibition of mild steel in acidic medium, Corrosion Science - CORROS SCI 47 (2005) 2659-2678.

[80] C. Verma, L. Olasunkanmi, E. Ebenso, M. Quraishi, Substituents effect on corrosion inhibition performance of organic compounds in aggressive ionic solutions: A review, Journal of Molecular Liquids 251 (2017).

[81] X.L. Cheng, H.Y. Ma, S.H. Chen, R. Yu, X. Chen, Z.M. Yao, Corrosion of stainless steels in acid solutions with organic sulfur-containing compounds, Corrosion Science 41(2) (1998) 321-333.

[82] N.F. Atta, A.M. Fekry, H.M. Hassaneen, Corrosion inhibition, hydrogen evolution and antibacterial properties of newly synthesized organic inhibitors on 316L stainless steel alloy in acid medium, International Journal of Hydrogen Energy 36(11) (2011) 6462-6471.

[83] L.T. Popoola, Organic green corrosion inhibitors (OGCIs): a critical review, Corrosion Reviews 37(2) (2019) 71-102.

Chapter 8

8 Conclusions and Recommendations for Future Work

8.1 Conclusions

The major objectives of this research were to develop a kinetic model based on chemical compositions (cellulose, hemicellulose, and lignin) for predicting HTL product yields (gas, liquid, and solid residue) from various types of lignocellulosic biomass with different chemical compositions, investigate the corrosion-resistance performance of various candidate alloys in HTL of various types of lignocellulosic biomass under varying conditions, in order to establish guidelines for selecting proper materials for HTL reactor construction and to develop corrosion-preventing strategies to achieve long-term operation of HTL reactors, as well as compare the performance of HTL of lignocellulosic biomass (pinewood, cornstalk, alkali lignin, kraft lignin, and black liquor) under various atmospheres (N_2, H_2, or O_2) or in various types of reactor (continuous-flow vs. batch). The following detailed conclusions were drawn from this research:

(1) Effects of reaction atmosphere on hydrothermal liquefaction (HTL) of pinewood sawdust were investigated in a batch reactor using KOH or H_2SO_4 catalyst at 300 °C with an initial pressure of 20 bar for 60 min under N_2, H_2, and O_2 atmospheres. The results showed that HTL under H_2 atmosphere with KOH catalyst led to the highest bio-oil yield (approx. 34 wt.%) and the lowest solid residue (SR) yield (approx. 9 wt.%). Bio-oils obtained under N_2 or H_2 exhibited higher energy recovery and better quality (higher H/C ratio, lower O/C ratio, higher HHV, lower TAN, and much lower viscosity and molecular weight) than those obtained under O_2. The oils produced in N_2 or H_2 atmosphere mainly contained phenols and aromatic compounds and showed similar boiling point distributions, while more acids were detected in the oils produced in O_2, which presented the highest mild boiling fractions and the least heavy residue fraction.

(2) A kinetic model was developed for predicting HTL product yields from various types of lignocellulosic biomass based on its chemical compositions. HTL experiments of the model compounds for lignocellulosic biomass (cellulose, xylan, and lignin) and lignocellulosic biomass (bamboo, cornstalk, and pinewood) were first conducted in the temperature range of 225 °C-300 °C for a residence time from 10 min to 60 min with K_2CO_3 catalyst. Lignin was found to be the main contributor to bio-oil formation from HTL of lignocellulosic biomass. A kinetic model was then developed based on the experimental results obtained from HTL of biomass model compounds to predict HTL product yields based on chemical compositions of lignocellulosic biomass (contents of cellulose, hemicellulose, and lignin). The model was validated using our experimental results from HTL of bamboo, cornstalk, and pinewood and the publicly available data in literature from HTL of various lignocellulosic biomass feedstocks.

(3) This study compared the performance of lignin HTL/depolymerization in a continuous-flow reactor and a batch reactor operating at 300°C for 15 minutes. The yields of bio-oil/DL from alkali and kraft lignin were found to be lower (28.5 wt.% and 43.9%, respectively) in the continuous-flow reactor compared to those produced in the batch reactor (36.9 wt.% and 50.6%, respectively), as well as having a lower energy recovery rate. Additionally, the bio-oil/DL products produced from the continuous-flow reactor have lower HHVs, lower fractions of light oil with boiling points (<193 °C), but higher molecular weights due to the shorter reaction time in the continuous-flow operations. These findings would be useful for the development of continuous-flow HTL systems for production of biofuel or phenolic chemicals from lignin on a large-scale.

(4) The performance of a continuous-flow HTL process against that of a batch HTL process was compared for processing three types of bio-feedstocks at 300 °C for 12 min. The HTL of cornstalk and pinewood in the continuous-flow reactor produced more bio-oils (32.4 and 34.5 wt. %, respectively) and less solid

residues (2.9 and 4.6 wt.%, respectively) as well as a higher energy recovery rate (53.3 and 52.0 %, respectively) compared with those in the batch reactor (Cornstalk: 23.8 wt.%, 6.2 wt.% and 46.5%; Pinewood: 28.5 wt.%, 10.3 wt.% and 50.8%), although the HHVs of the bio-oils from the continuous-flow reactor are slightly lower. The bio-oils obtained from these lignocellulosic biomass feedstocks in both reactors have similar molecular weights (Mw:572-742 g/mol and Mn: 410-476 g/mol), while the oils obtained from the continuous-flow operations contain higher amounts of furan compounds. The HTL product yields from black liquor did not exhibit significant difference between the continuous-flow and batch operations, while the bio-oil obtained from the continuous operation has a slightly lower HHV (20.4 vs. 22.7 MJ/kg) and smaller molecular weights (Mw:1089 vs. 1348 g/mol and Mn: 672 vs. 805 g/mol). These outcomes can be utilized to design pilot-scale systems for continuous production of bio-oil on a larger scale, using lignocellulosic biomass or biowaste. The data provided is valuable for selecting suitable bio-feedstocks for producing drop-in fuels through HTL processes and estimating fuel products. While HTL has undergone significant improvements, there are still some major challenges to be addressed, such as blockages in either the reactor outlet or downstream systems during continuous processing, as well as potential corrosion caused by ash content in bio-feedstocks.

(5) The major compounds presenting in both bio-oils from bamboo and black liquor are phenolic and aromatic compounds. The bio-oil derived from black liquor contains more phenols and aromatics, but fewer ketones compared to that converted from HTL of bamboo. In addition, the application of black liquor leads to the produced bio-oils with higher concentrations of S and organic acids compared to bamboo feedstock. SS316L steel exhibits the lowest in bamboo-contained HTL environment, but suffers the highest attack during the HTL conversion of black liquor. Compared with the corrosion in simulated catalytic HTL environment, it is likely that the application of bamboo somewhat reduces corrosion damage, likely due to the formation of Carbon-rich inhibition layer on the surface scale. There are possible critical contents of S^{2-} and ash in

biowaste, above which the use of the wastes for the conversion could lead to unacceptable damage on HTL conversion reactors. Further work is required to determine these limits.

8.2 Recommendations for Future Work

(1) Impact of more complex atmospheres comprising mixtures of gases (e.g., air, H_2 and N_2, or O_2 and N_2) on biomass HTL process need to be explored. In addition, a comprehensive and detailed techno-economic assessment should be carried out to evaluate the economic feasibility of the HTL process under various reaction atmospheres for large-scale application of HTL technology.

(2) Although a kinetic model has been developed for the prediction of HTL product yields (gas, liquid, and solid residue) from various types of lignocellulosic biomass, there are still some deviations between model calculations and experimental results. This could be caused by the simplifications made in the model development, and the complexities in the biomass feedstock compositions, reactor configurations and conditions (heating rate, catalyst loading, etc.) and the complexities in the HTL reactions. More future work is required to further improve the accuracy and robustness of the kinetic model developed in this work.

(3) The continuous-flow HTL process needs to be optimized to maximize the bio-oil yield, including optimization of catalyst and reaction conditions, such as residence time, solid loading in the feed, and temperature. In addition, there are still some major challenges in operating a continuous-flow HTL process, such as the pumpability of a feed containing a high solid loading, blockages of the reactor outlet or downstream systems by biochar or bio-oil during the continuous-flow operations, as well as potential corrosion caused by ash in bio-feedstocks. Moreover, a detailed comparison between various types of reactors (e.g., tubular, CSTR, and PFR) needs to be addressed.

(4) Long-term corrosion tests are needed to determine whether the candidate alloys are suitable for construction of HTL reactors. Given the presence of high operating

pressure, it is necessary to investigate the stress corrosion cracking (SCC) susceptibility of the testing alloys under HTL conditions. In addition, the conversion chemistry of typical lignocellulosic biomass model compounds in HTL environments and the corrosion performance of candidate alloys in such environments need to be comprehensively investigated in order to facilitate the development of corrosion mechanisms of candidate alloys in HTL of various lignocellulosic bio-feedstocks.

8.3 Contributions and Novelties

Based on the results from this research, the main contributions and novelties of the thesis are summarized as follows:

In Chapter 3, the influence of reaction atmosphere on HTL of woody biomass was for the first time comprehensively investigated in terms of bio-oil yields and properties. Bio-oils obtained under N_2 or H_2 exhibited higher energy recovery and better quality.

In Chapter 4, a kinetic model was developed based on the chemical compositions of lignocellulosic biomass and was validated with our experimental results from HTL of bamboo, cornstalk, and pinewood and the publicly available HTL data in literature obtained with lignocellulosic biomass feedstocks.

In Chapter 5, HTL of lignin for the production of bio-oil or depolymerized lignin was realized for the first time in a continuous-flow reactor, although the continuous-flow operations led to lower yields of bio-oil/depolymerized lignin and larger molecular weights, compared with the batch operation, due to the shorter reaction time in the continuous-flow operations.

In Chapter 6, performance of HTL of lignocellulosic biomass (cornstalk, pinewood) and biowaste (black liquor) in a continuous-flow reactor and a batch reactor was compared. The continuous-flow operations resulted in higher yields of bio-oil, although with slightly poorer qualities compared with those obtained from batch operations.

In Chapter 7, the effects of biomass feedstocks and organic products on the corrosion of a candidate construction alloys (SS316L) in catalytic hydrothermal liquefaction environments were investigated for the first time.

Appendices

Appendix A: Detailed chemical compounds identified in the bio-oil obtained from HTL of pinewood sawdust at 300 °C for 60 min under N_2, H_2, and O_2, respectively, with KOH or H_2SO_4 catalyst.

RT[a] (min)	**Compounds Name**	**Relative Composition by Percent Area**					
		$KOH\text{-}N_2$	**$KOH\text{-}H_2$**	**$KOH\text{-}O_2$**	**$H_2SO_4\text{-}N_2$**	**$H_2SO_4\text{-}H_2$**	**$H_2SO_4\text{-}O_2$**
3.780	Acetic acid		3.036				
5.967	2-Pentanone, 4-hydroxy-4-methyl-	1.409		1.025	2.917	2.731	0.824
7.700	2-Cyclopenten-1-one, 2-methyl-	0.435					
8.517	1,3-Dioxolane-4-methanol, 2,2-dimethyl-, (S)-	0.468					
8.948	Benzaldehyde		0.640				
9.142	2-Cyclopenten-1-one, 3-methyl-		1.036				
9.527	Phenol		0.658				
9.908	Cyclotetrasiloxane, octamethyl-		0.789				
10.288	2,5-Furandione, dihydro-3-methyl-			0.900			
10.555	2-Cyclopenten-1-one, 2,3-dimethyl-		1.264			0.569	
10.868	DL-Norvaline, N-[(phenylmethoxy)carbonyl]-		0.838				
11.054	Acetophenone	1.284	3.519			1.320	
11.109	Pentanoic acid, 4-oxo-			0.927	25.374	6.830	51.470
11.464	Phenol, 2-methoxy-	4.110	42.040			1.627	
11.959	2-Isopropylbenzenethiol, S-methyl-				2.366		
12.204	N-Chlorocarbonyl-N-methoxy-N-isopropylamine		2.131				
12.284	Pentanoic acid, 2-methyl-4-oxo-						1.155
12.454	Phenol, 2,6-dimethyl-		0.902				
12.919	2-Cyclopenten-1-one, 2,3,4,5-tetramethyl-		0.935				
13.028	Benzoic acid			11.585			1.545
13.143	Creosol	2.549	1.818			0.656	
13.232	Catechol		2.648		1.136		

13.341	Butanedioic acid, monopropargyl ester			0.400			
13.460	1H-Benzimidazole, 2-ethyl-		0.723				
13.895	Butanedioic acid, methyl-			0.780			
14.022	4-Nonanol, 4-methyl-			0.615			
14.200	Cyclohexene, 1-methyl-4-(1-methylethylidene)-	0.926	1.700			0.966	
14.230	Naphthalene, 2,6-bis(1,1-dimethylethyl)-				1.404		0.734
14.327	Benzoic acid, 3-methyl-			2.079			
14.420	Phenol, 4-ethyl-2-methoxy-	4.622	2.253	1.428			
14.445	1H-Inden-1-one, 2,3-dihydro-				1.314	1.479	
14.805	1-Methylindan-2-one		1.250	0.869			
15.067	2-Cyclopenten-1-one, 2,3-dimethyl-			0.733	1.958	1.482	
15.113	3-Cyclohexen-1-one, 2-isopropyl-5-methyl-		0.834				0.445
15.210	Hydrocinnamic acid			1.012			0.170
15.325	1,4-Benzenediol, 2-methyl-		0.516				
15.405	1(3H)-Isobenzofuranone			0.891			
15.418	7-Methylindan-1-one	0.370	1.520		1.395	0.484	
15.553	Benzaldehyde, 3-hydroxy-			2.111			
15.629	Phenol, 2-methoxy-4-propyl-	3.286				1.121	
15.963	Benzene, 1-ethenyl-4-methyl-	1.105			0.812	2.971	
16.001	Ethanone, 1-(3-hydroxyphenyl)-		1.363				0.865
16.048	Vanillin	0.578	0.260	5.944	0.508		1.040
16.149	Benzoic acid, 3-(1-methylethyl)-			0.882			
16.293	1H-Inden-1-one, 2,3-dihydro-3,3-dimethyl-	1.203					
16.331	1,2-Diethoxybenzene		0.809	2.494	1.059		0.900
16.412	2-(Cyclohex-1-enyl)-furan					1.896	
16.623	Acetophenone, 4′-hydroxy-			1.674			
16.754	Phenol, 2-methoxy-4-(1-propenyl)-	1.309					
16.792	Benzoic acid, 3-formyl-			1.281			
16.953	3-Ethenylheptan-2,6-dione			0.932			
16.961	Phenol, 2-(1,1-dimethylethyl)-						0.531

17.067	4-Methylphthalaldehyde			0.556			
17.071	1,4-Benzenediamine, N,N,N′,N′-tetramethyl-	1.014					
17.169	1-Tetralone, 8-hydroxy-		0.267				
17.287	Benzoic acid, 4-hydroxy-						0.342
17.355	Apocynin	1.549		10.221			0.470
17.384	Ethyl 3-(2-furyl)propenoate		0.615				
17.782	4-Hydroxy-3-methylacetophenone			0.602			
17.883	2-Cyclopentenecarboxylic acid, 5-hydroxy-5-methyl-2-(1-methylethyl)-, methyl ester, trans-		0.681				
18.175	2-Propanone, 1-(4-hydroxy-3-methoxyphenyl)-	1.637			2.935	0.868	
18.196	1-(4-methylthiophenyl)-2-propanone		1.716				
18.234	Benzenamine, 4-methyl-3-nitro-			0.930			
18.462	4-Acetylbenzoic acid			4.376			
18.648	Phenol, 2-(1,1-dimethylethyl)-4-methyl-			0.509			
18.813	Benzene, 1-methyl-3,5-bis[(trimethylsilyl)oxy]-			2.952			0.223
18.890	4-Hexylphenol, trimethylsilyl ether		1.816				
19.109	4-Ethoxy-3-anisaldehyde			3.261			
19.460	Phthalan		0.563				
19.562	Phenol, 2,6-dimethyl-4-nitro-			0.261			
19.630	Benzofuran, 2,3-dihydro-		0.558				0.477
19.659	1,4-Benzenedicarboxaldehyde, 2-methyl-			0.405			
19.828	Aminosalicylic Acid			0.487			0.218
19.951	Benzene, 1-methoxy-4-(1-methyl-2-propenyl)-	1.820					0.183
19.968	Benzaldehyde, 3-methyl-			1.708			
20.146	Homovanillic acid	1.719					
20.213	Naphthalene, 2-ethoxy-					0.689	
20.315	Ether, bis(p-tert-butylphenyl)			1.287			
20.365	2-Naphthalenol, 3-methoxy-	1.046					
20.391	9-Methyl-3,4-dihydro-2H-pyrido(1,2-a)pyrimidin-2-one		0.465				

20.446	4-Hydroxy-3,5-dimethylbenzoic acid			0.375			
20.496	4,6-Dimethoxy-1-naphthaldehyde					2.105	
20.539	Terephthalic acid			0.226			
20.547	Benzofuran, 2,3-dihydro-2,2,4,6-tetramethyl-	0.965	1.511				
20.695	1,2-Dihydropyrido(3,2,1-kl)phenothiazin-3-one				1.450		
20.704	Butan-1-one, 1-(2,3-dihydro-7,8-dinitro-1,4-benzodioxin-6-yl)-		0.984				
20.962	10H-Phenothiazine, 2-(trifluoromethyl)-				1.202		
20.983	2-Propenoic acid, 3-(3-hydroxyphenyl)-, methyl ester		0.736				
21.122	5-Hydroxy-1-tetralone		0.553				
21.148	Salicylhydroxamic acid			0.692			
21.258	1,4-Benzenediamine, N,N'-diethyl-			2.026			
21.346	Benzaldehyde, 2-nitro-, diaminomethylidenhydrazone	1.575			1.229		
21.363	Methyleugenol		0.777			1.482	
21.389	2-Methyl-5-nitrobenzoic acid			1.085			
21.397	1H-Benzotriazole-5,6-dicarbonitrile						0.481
21.592	Pyridine, 4-(5-benzo[1,3]dioxol-5-yl-[1,2,4]oxadiazol-3-yl)-			1.139			
21.735	Benzenesulfonic acid, 4-methyl-			0.628			
21.820	4-Methoxycinnamaldehyde					1.680	
21.854	Dihydrofuranno(3,2-f)coumaran	2.134	1.056	1.447			0.584
22.006	4,4'-Stilbenedicarbonitrile					1.748	
22.010	(6,7-Dimethoxy-3,4-dihydro-1-isoquinolinyl)acetonitrile		0.941	1.290	1.385		0.363
22.137	1-[2,2':5',2'']Terthiophen-5-yl-ethanone				1.232		
22.209	Benzene, 1-phenyl-4-(2,2-dicyanoethenyl)				1.378		
22.213	Benzo(a)phenazine					1.615	
22.222	Dibenzo[c,h][2,6]naphthyridine						0.481
22.230	2,2′-Bi-1H-indene		1.321				

22.340	1,4-Dimethyl-4,5,7,8-tetrahydroimidazo-[4,5-E]-1,4-diazepin-5,8(6H)-dione		1.538		2.477	2.927	1.088
22.509	2-Ethoxyphenyl isocyanate	1.220		1.912			
22.535	Asarone		0.785		0.977	1.374	0.789
22.683	Tricyclo[4.3.0.0(7,9)]nonane, 2,2,5,5,8,8-hexamethyl-, (1.alpha.,6.beta.,7.alpha.,9.alpha.)-	1.683				0.934	
22.924	Benzaldehyde, 2-methoxy-4-methyl-			0.944			
23.106	6-Acetyl-5-hydroxy-2,7-dimethyl-1,4-naphthoguinone					1.211	
23.135	Benzoic acid, 3-methoxy-			0.643			0.495
23.321	As-Indacene, 1,2,3,6,7,8-hexahydro-1,1,6,6-tetramethyl-4-(1-methylethyl)-					2.247	
23.385	(+)-3-Carene, 2-.alpha.-isopropenyl-	1.063					
23.402	2,2'-Isopropylidenebis(3-methylbenzofuran)				1.837	1.728	
23.579	2,4,5,6-Tetrachloro-nicotinamide				0.587		
23.588	9,10-Dihydro-12H-5-oxabenzocyclodecene-6,11-dione	1.082					
23.596	Fluorene, 2,7-bis(1-hydroxyethyl)-					3.234	
23.681	1,3-Benzodioxole, 4-methoxy-6-(2-propenyl)-						0.287
23.824	[1,2,4]Triazolo[1,5-a]pyrimidine, 6-chloro-2-(2-furanyl)-5,7-dimethyl-	1.299					
23.884	Benzene, 2-ethyl-1,3-dimethyl-					1.862	
23.968	Dithiocarbonic acid, O-ethyl ester, methylene-S(IV)-trifluoromethyl ester	0.689					
24.006	Estra-1,3,5(10)-trien-3-ol					0.564	
24.019	n-Hexadecanoic acid			1.996			1.063
24.159	7-Oxabicyclo[4.1.0]heptane, 1-(2,3-dimethyl-1,3-butadienyl)-2,2,6-trimethyl-, (E)-	0.419					
24.180	1,2-Dimethyl-3-nitro-4-nitroso-benzene			0.532			
24.302	Benzenemethanol, 2-methyl-.alpha.-phenyl-						0.595

24.311	1-Phenanthrenecarboxaldehyde, 1,2,3,4,4a,9,10,10a-octahydro-1,4a-dimethyl-7-(1-methylethyl)-, [1S-(1.alpha.,4a.alpha.,10a.beta.)]-					2.870	
24.412	Methyl 2-hydroxy-4-methoxybenzoate, trimethylsilyl ether	1.238					
24.488	Phenol, 4,4'-methylenebis-			0.412			
24.531	7,8-Dihydro-9H-cyclopenta[a]pyren-9-one				1.256	1.563	0.684
24.552	1,4-Cyclohexanedicarboxylic acid, 2,5-dioxo-, diethyl ester		0.877				
24.704	Ketone, 7-methoxy-2-benzofuranyl methyl					1.641	
24.729	2-Acetyl-3-methylbenzo[b]thiophene		1.523				
24.742	Benzo[b]thiophene, 2,3-diethyl-						0.969
24.801	2,4(1H,3H)-Quinazolinedione, 1,3-diethyl-				0.811		
24.818	1-METHOXY-2-TERT.-BUTYL-4,6-DINITROBENZENE					1.304	
24.962	di-p-Tolylacetylene						0.863
25.118	5-Methoxy-2-naphthalen-2-yl-2H-indazole				0.659		
25.127	Silane, dimethyl(2-naphthoxy)isobutoxy-		0.598				
25.199	Homovanillic acid	4.555					
25.211	2,3,6-Trimethoxybenzoic acid						0.723
25.216	Imidazo[1,2-b]-1,2,4-triazine, 6-(3-methoxyphenyl)-2,3-dimethyl-					1.817	
25.372	Androstane-3,17-dione, (5.alpha.)-			0.398	2.705	1.271	1.073
25.385	2,5-Diethyl-3,4-diphenyl cyclopentadienone	1.263	0.974				
25.478	1,2,3,4-Tetrahydrobenz[a]anthracene	1.459				1.355	
25.512	9H-Xanthen-9-one, 1,3-dihydroxy-2-methyl-			0.807			
25.541	3,5-di-tert-Butyl-4-hydroxybenzyl alcohol					1.207	
25.736	Naphthalene, 1-(2-naphthalenyloxy)-	3.021	1.884		4.552		2.427
25.833	cis-Vaccenic acid			9.907			
25.842	4-Methoxyphenol, pentafluoropropionate				2.017		

25.871	2-Hexanone, phenyl(2-propenyl)hydrazone	0.664	0.925				
26.066	Ethyl Oleate	3.889		3.408	4.803	1.827	1.477
26.192	1,2-Epoxy-3,4-dihydroxycyclohexano[a]pyrene, (3s,4s-)						1.911
26.205	2H-1-Benzopyran-3(4H)-one, 8-methoxy-2-(1-naphthalenyl)-, oxime				1.142	0.851	
26.273	3H-Benzo[f]chromen-3-one, 2-(4-methoxyphenyl)-		0.812				
26.328	3,4-Dimethoxychalcone					1.625	
26.450	Benzoic acid, 4,5-dimethoxy-2-(2-phenylethenyl)-				1.794		
26.455	Estra-1,3,5(10)-triene-6,17-dione, 3-hydroxy-					1.055	
26.543	1,3-Cyclohexanedione, 2-[4-(4-methoxyphenylamino)-2-thiazolyl]-	1.047		1.159			
26.590	Retene					2.830	2.305
26.708	Benzene, 1,3-dimethoxy-5-[(1E)-2-phenylethenyl]-	1.780			1.156		
26.713	p-Bis(p-methoxyphenyliminomethyl)benzene				2.831	0.880	
26.806	trans-3′,4′,5′-Trimethoxy-4-(methylthio)chalcone		0.696			2.653	1.466
26.899	1-Benzhydrylazetidin-3-ol						0.574
26.966	2-(((6-Fluoro-4H-1,3-benzodioxin-8-yl)methyl)sulfanyl)-1H-benzimidazole				1.289		
26.975	Benzoic acid, 4,5-dimethoxy-2-(2-phenylethenyl)-					0.877	
26.983	2-Amino-4-azido-5-[3,4,5-trimethoxybenzyl]pyrimidine	0.965					
26.987	3Alpha,5-cyclo-6beta,19-epoxy-5alpha-androstan-17-one						0.663
27.148	Acridin-9-yl-(2,4-dimethoxy-phenyl)-amine	0.979					

27.203	13-(2-Methoxyphenyl)tricyclo[8.2.2.24,7] hexadeca-1(13),4,6,10(14),11,15-hexaene-5-carbaldehyde						2.588
27.254	Estra-1,3,5(10)-trien-17-one, 3-methoxy-					1.301	
27.296	(.+/−.)-Uleine				1.801		
27.322	N,N-Dimethylindoaniline	4.244					
27.457	2-[4-(1,2-Diphenyl-but-1-enyl)-phenoxy]-ethylamine				1.827		
27.461	Benzofuran-5-ol, 3-(2-furanoyl)-4-dimethylaminomethyl-					1.432	
27.567	Homovanillic acid			1.146			
27.571	Ethyl homovanillate	5.919					
27.732	Benzeneacetic acid, 4-hydroxy-3-methoxy-, methyl ester		0.713		2.750	2.782	
27.740	3-Penten-2-one, 4-(2,2,6-trimethyl-7-oxabicyclo[4.1.0]hept-1-yl)-, (E)-	4.038					3.109
27.829	2(1H)-Pyrazinone, 3,5,6-tris(1,1-dimethylethyl)-						0.788
27.931	Pyridine, 2-(phenylethynyl)-				0.556		
27.969	8H-5,12b-(Iminoethano)-1H-phenanthro[3,2-d][1,3]dioxin, 2,3,4,4a,5,6-hexahydro-15-methyl-, [4aR-(4a.alpha.,5.alpha.,12b.alpha.)]-					1.431	
28.146	1-(10-Methylanthracen-9-yl)ethanone			0.522			3.722
28.239	1H-1,2,3,4-Tetrazole-1,5-diamine, N(1)-[(2-ethoxy-3-methoxyphenyl)methyl]-			0.385			
28.243	3-(3-Hydroxy-4-methoxyphenyl)-l-alanine	0.769					
28.315	Benzaldehyde, 2-nitro-, diaminomethylidenhydrazone					1.978	
28.556	Methyl p-(trans-styryl)-trans-cinnamate	1.551					
28.772	1-.beta.-d-Ribofuranosylpyrazolo[3,4-d]pyrimidin-4(5H)-one	1.052					

29.229	Benzene, 1-methoxy-4-(2-cyano-2-phenylethenyl)	0.661					1.046
29.415	2-(E)-Heptenoic acid, (4S)-4-[(t-butoxycarbonyl-(R)-alanyl)amino]-6-methyl-, ethyl ester					1.102	
29.664	4H-1-Benzopyran-4-one, 5-hydroxy-7-methoxy-2-phenyl-				2.369		1.245
29.685	Dinaphtho[2,1-b:1′,2′-d]furan					2.566	
30.096	4-Methoxy-4′,5′-methylenedioxybiphenyl-2-carboxylic acid	2.098					
30.282	i-Propyl nonadecanoate	1.419					
30.336	2,5-Cyclohexadien-1-one, 4-[[4-(dimethylamino)phenyl]imino]-2,5-dimethyl-						0.674
30.425	Dibenz[a,h]anthracene, 1,2,3,4-tetrahydro-				0.801		0.612
30.455	4H-1-Benzopyran-4-one, 5,7-dimethoxy-2-phenyl-					1.208	
30.540	Benzene, 1-(1,1-dimethylethyl)-3,5-dimethyl-2,4,6-trinitro-				0.547		
30.722	4H-1-Benzopyran-4-one, 5,7-dimethoxy-2-phenyl-				2.505	4.742	2.323
31.309	Dimethyldaidzin						0.944
31.318	3H-1,3,4-Benzotriazepine, 7-chloro-2-(methylamino)-5-phenyl-					3.414	
31.457	4-(1,1-Dimethylallyl)-9-methoxy-7H-furo[3,2-g][1]benzopyran-7-one	2.442					
31.690	Benzothiophen-3(2H)-one, 2-(4-ethoxy-3-methoxybenzylideno)-	0.889					
31.952	Benzaldehyde, 2,4-dihydroxy-		0.633	0.807	4.897	2.024	
31.969	2-Cyclohexen-1-one, 2-methyl-5-(1-methylethenyl)-, O-methyloxime, (+)-	8.108					

32.942	Silane, [[(16.alpha.,17.alpha.)-16,17-epoxyestra-1,3,5(10)-trien-3-yl]oxy]trimethyl-	1.385

[a] Retention time

Appendix B: The GPC curves of bio-oils obtained from HTL of cornstalk and pinewood in the batch/continuous-flow operations at 300 ºC for 12 min.

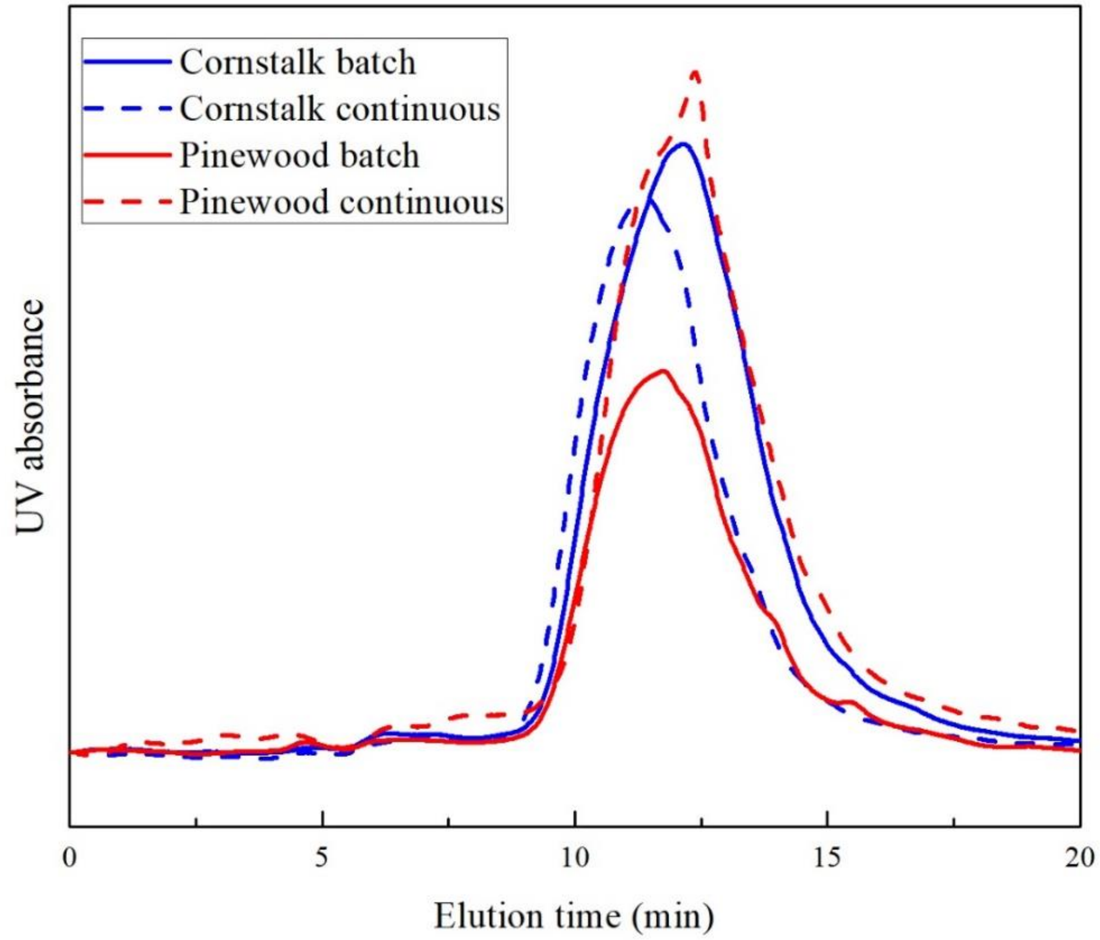

Appendix C: The GPC curves of bio-crude oils obtained from HTL of cornstalk and pinewood in the batch/continuous-flow operations at 300 ºC for 12 min.

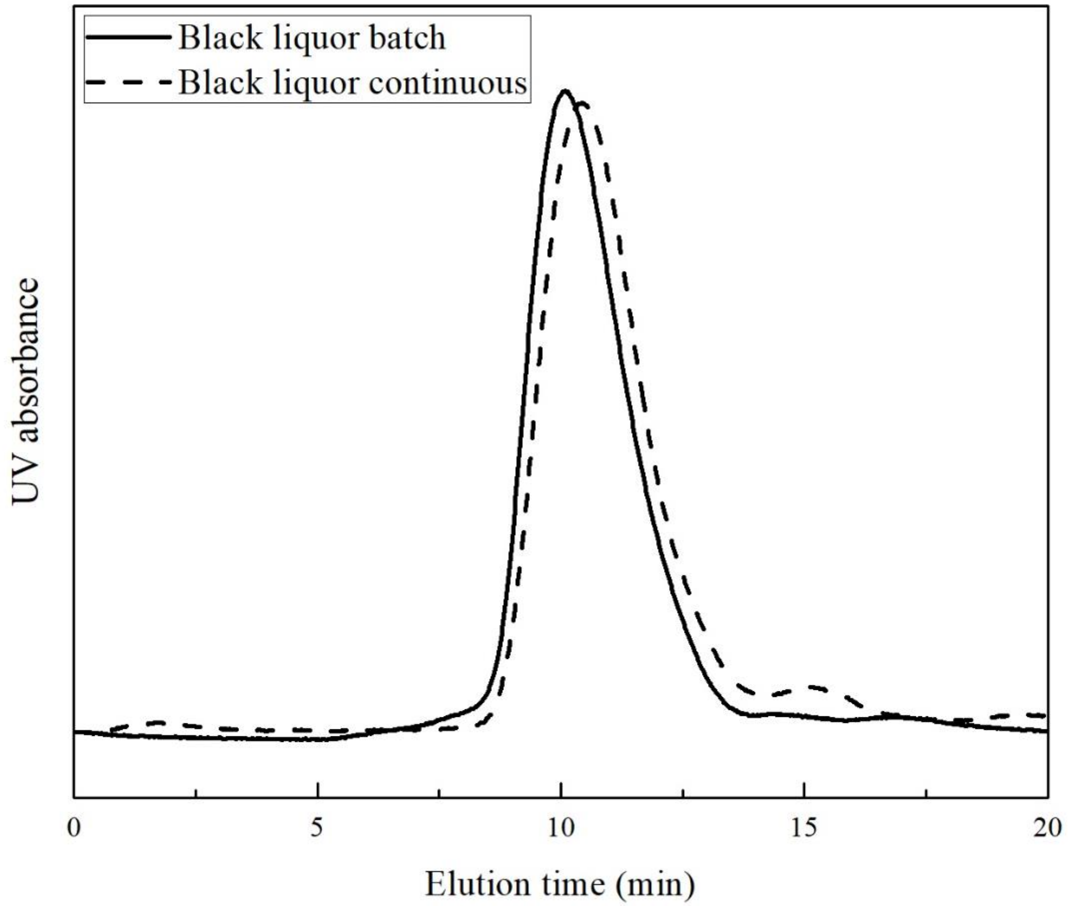

Appendix D: The GC-MS chromatograms of bio-oils obtained from HTL of cornstalk in the batch/continuous-flow operations at 300 ºC for 12 min.

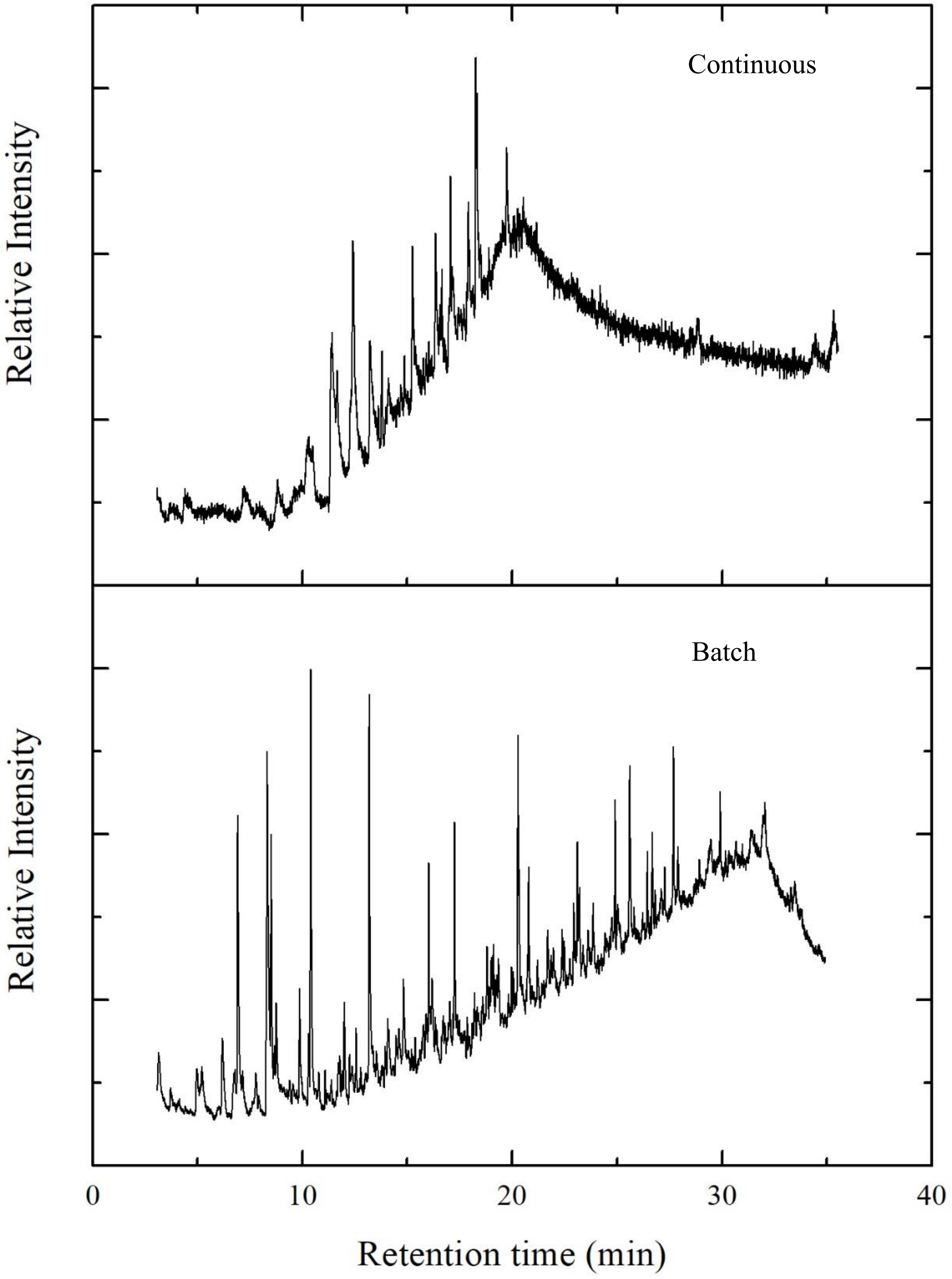

Appendix E: The GC-MS chromatograms of bio-oils obtained from HTL of pinewood in the batch/continuous-flow operations at 300 ºC for 12 min.

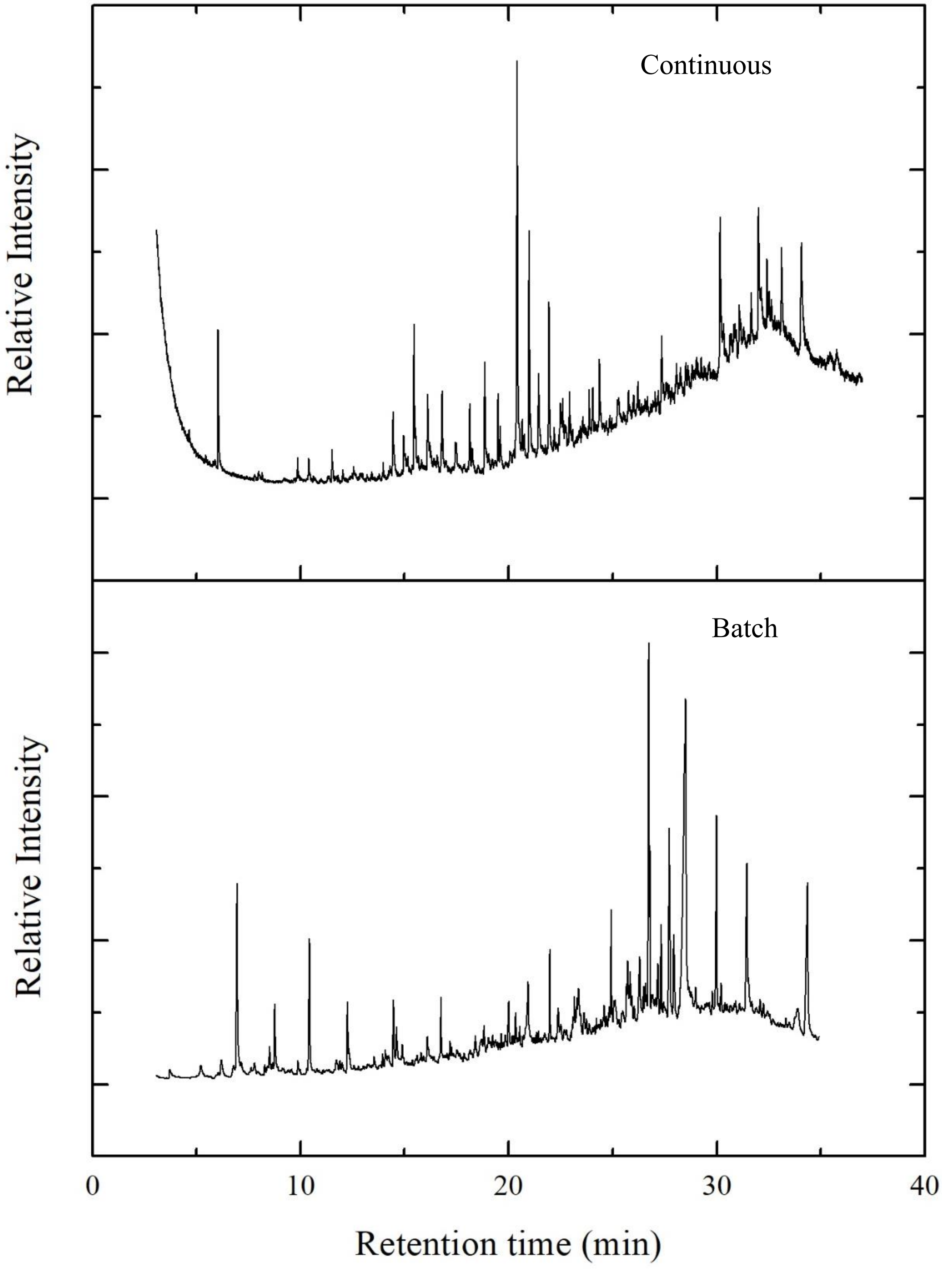

Appendix F: The GC-MS chromatograms of bio-oils obtained from HTL of black liquor in the batch/continuous-flow operations at 300 ºC for 12 min.

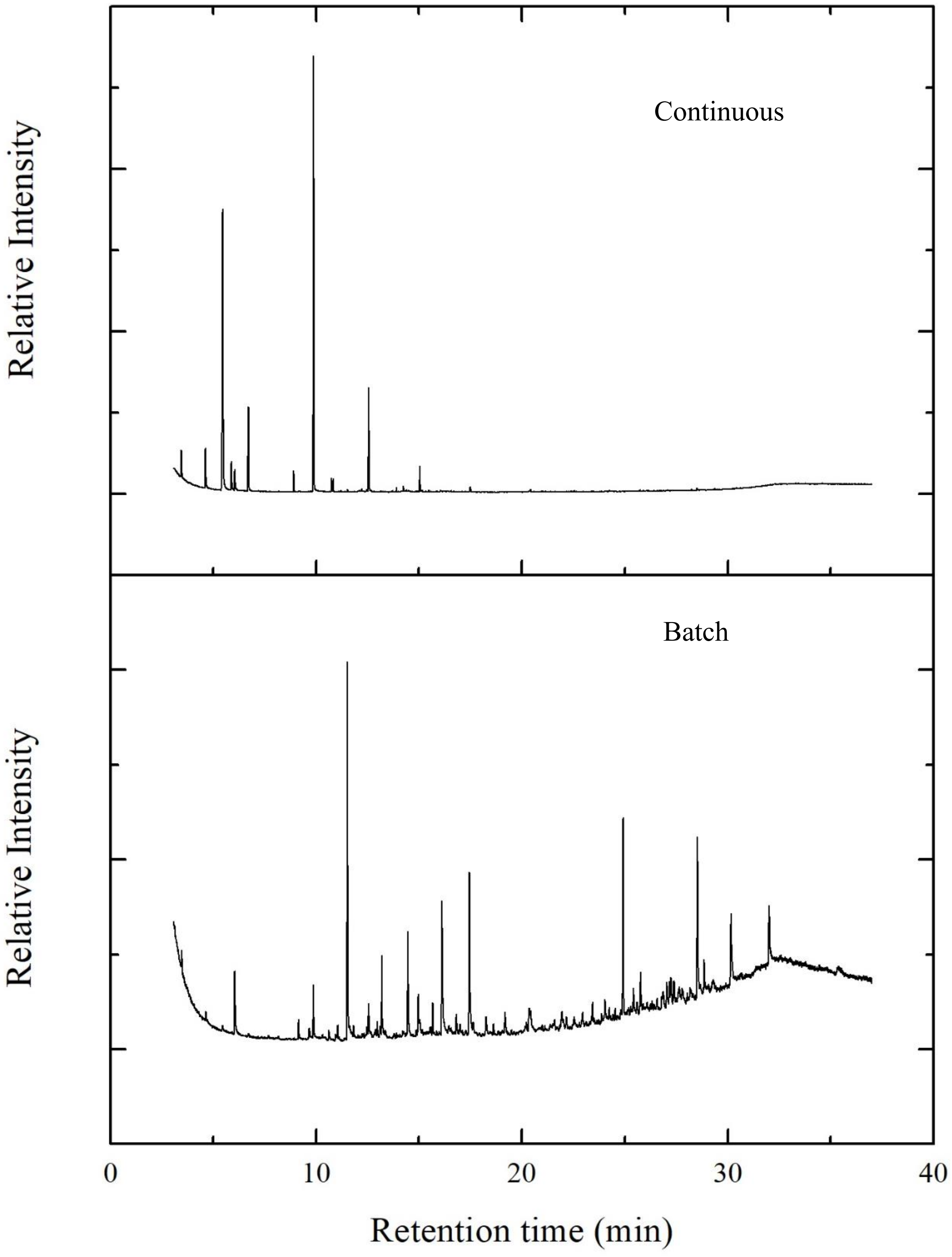

Curriculum Vitae

HAOYU WANG

Summary:

Current Chemical and Biochemical Engineering Graduate student at University of Western Ontario. Strong self-motivation, proactive attitude towards teamwork, good time management skills and a quick learner.

Education:

2019.1-present	**Western University, London, Canada** Major: Chemical and Biochemical Engineering Degree: Doctor of Philosophy
2018.1-2018.12	**Western University, London, Canada** Major: Chemical and Biochemical Engineering-Particle Technology and Fluidization Degree: Master of Engineering (Project based)
2014.9-2015.7	**Loughborough University, Loughborough, UK** Major: Chemical Engineering Degree: Other (3+1 program)
2011.9-2014.7	**Beijing University of Chemical Technology, Beijing, China** Major: Chemical Engineering Degree: Bachelor of Engineering (3+1 program)
2012.7-2012.8	**Summer school of Cambridge University, Cambridge, UK** Major: Chemical Engineering and Biotechnology (CEB) Degree: Other

Work/Research Experience

2019.1-present	**Western University** **Position: Research Assistant** Conduct literature reviews and surveys. Investigate *Kinetics of Hydrothermal Liquefaction of Biomass with Various Temperature, Reaction time and Pressure.* Investigate *Corrosion Performance of Reactor Materials in Hydrothermal Liquefaction Environment*. Conduct process scale-up and comparative studies between

	batch and continuous processes. Prepare of Journal articles, conference papers and presentation of research at academic conferences
2018.5-2018.12	**Western University** **Position: Research Assistant** Investigate *kinetics of Hydrothermal Liquefaction of Biomass with various temperature, reaction time and pressure.* Analyse the products from the research and a scale-up reaction process with GC-MS and FT-IR.
2016.9-2017.2	**China Kunlun Contracting & Engineering Company** **Position: Process Engineer** Participated in the *Coal to Ethylene Glycol* Process Packages Design. Performed process simulation, equipment calculation and flow chart drawing.
2015.9-2016.4	**Loughborough University** **Position: Lab Assistant** Worked on *Fabrication and Environmental and Biomedical Application of Micro-porous Capillary Films (MCFs).* Optimized the process condition of MCFs' Fabrication. Built up several value-added application data.
2014.3-2014.6	**Beijing University of Chemical Technology** **Position: Research Assistant** Synthesized metal-organic frameworks with different functional groups. Assisted in the data collection of the scale-up reaction process.
2013.7-2013.9	**China Kunlun Contracting & Engineering Company** **Position: Trainee** Received professional training on AutoCAD, ASPEN Hysys and 3D Piping. Assisted Bill of Materials (BOM) support and integration. Helped engineers draw Process Flow Diagram.
2011.6-2011.7	**Shanghai Only Educational Institution** **Position: Teaching Assistant**

Worked as a part-time assistant.
Solved the questions asked by the students.

2011.1-2011.2 **Tieling Paint Manufacturing Company**
Position: Observer
Learned how Trimethylamine hydrochloride is manufactured.
Got the knowledge of reaction, crystallization, evaporation, and centrifugation.

Skills:

- **Process Simulation**-- Aspen Hysys and Honeywell Unisim
- **Process design**--PFD and P&ID
- **Chemical drawing**—AutoCAD
- **Data processing**--Origin 8.0
- **Programming**--C language and Matlab
- **MS Office**-- MSWord/Excel/PowerPoint

Awards:

- 3rd prize of Public Scholarship (Undergraduate, 2012, 2013, 2014)
- Excellent Student of the year (Undergraduate, 2012, 2013, 2014)
- 3rd prize in National Chemistry Competition (Senior high school, 2010)
- 2nd prize in National Mathematics Competition (Senior high school, 2010)
- 3rd prize in 24th Youth Science Excellent Project Competition (Senior high school, 2009)

Conference Attended:

- Virtual oral presentation at National Association of Corrosion Engineers (NACE) Corrosion conference 2020, Mar 15-19, 2020.
- Virtual oral presentation at 60th Conference of Metallurgists, Aug 17-19, 2021.
- Virtual oral presentation at The Association of Materials Protection and Performance (AMPP) conference 2022, Mar 6-10, 2022.
- Oral presentation at 72nd Canadian Chemical Engineering Conference (CCEC 2022), Vancouver, British Columbia, Canada, Oct 23-26, 2022.

Publications:

- Wang H, Jiang Y, Park E, Han X, Zeng Y, Xu C. Hydrothermal Liquefaction of Pinewood Sawdust: Influence of Reaction Atmosphere. *Sustainability*. 2023; 15(8):6698.

- Wang H, Zhang M, Han X, Zeng Y, Xu C. Production of biocrude oils from various bio-feedstocks through hydrothermal liquefaction: Comparison of batch and continuous-flow operations. *Biomass and Bioenergy*. 2023; 173:106810.

- Zeng Y, Han X, Xu C, Wang H, Li H. "Biomass Conversion by Hydrothermal

Liquefaction Technology", Encyclopedia of Renewable Energy, Sustainability and the Environment, Elsevier, 2023. (Accepted)

- Wang, H., Han, X., Zeng, Y., & Xu, C. C. (2023). Development of a Global Kinetic Model based on Chemical Compositions of Lignocellulosic Biomass for Predicting Product Yields from Hydrothermal Liquefaction. Renewable Energy. (Accepted)

- Wang, Y. F., Yang, T., Wang, H. Y., Ding, L., Luo, Y. F., & Long, H. M. (2023). Application of steam injection in iron ore sintering: fuel combustion efficiency and CO emissions. Journal of Iron and Steel Research International, 30(1), 31-39.

- Wu, Y., Wang, H., Li, H., Han, X., Zhang, M., Sun, Y., ... & Xu, X. (2022). Applications of catalysts in thermochemical conversion of biomass (pyrolysis, hydrothermal liquefaction and gasification): A critical review. Renewable Energy.

- Li, H., Hu, Y., Wang, H., Han, X., El-Sayed, H., Zeng, Y., & Xu, C. C. (2022). Supercritical water gasification of lignocellulosic biomass: Development of a general kinetic model for prediction of gas yield. Chemical Engineering Journal, 433, 133618.

- Qian, L., Zhao, B., Wang, H., Bao, G., Hu, Y., Xu, C. C., & Long, H. (2022). Valorization of the spent catalyst from flue gas denitrogenation by improving bio-oil production from hydrothermal liquefaction of pinewood sawdust. Fuel, 312, 122804.

- Wang, H., Han, X., Li, K., Li, H., Liu, M., Zeng, Y., & Xu, C. C. (2022, March). Corrosion Performance of Reactor Candidate Alloys During Hydrothermal Liquefaction (HTL) of Cellulose in a Batch Reactor. In AMPP Annual Conference+ Expo. OnePetro.

- Zhao, B., Wang, H., Xu, S., Qian, L., Li, H., Gao, J., ... & Xu, C. C. (2022). Influence of extraction solvents on the recovery yields and properties of bio-oils from woody biomass liquefaction in sub-critical water, ethanol or water–ethanol mixed solvent. Fuel, 307, 121930.

- Zhao, B., Li, H., Wang, H., Hu, Y., Gao, J., Zhao, G., ... & Xu, C. C. (2021). Synergistic effects of metallic Fe and other homogeneous/heterogeneous catalysts in hydrothermal liquefaction of woody biomass. Renewable Energy, 176, 543-554.

- Zhang, M., Hu, Y., Wang, H., Li, H., Han, X., Zeng, Y., & Xu, C. C. (2021). A review of bio-oil upgrading by catalytic hydrotreatment: Advances, challenges, and prospects. Molecular Catalysis, 504, 111438.

- Feng, S., Shui, T., Wang, H., Ai, X., Kuboki, T., & Xu, C. C. (2021). Properties of phenolic adhesives formulated with activated organosolv lignin derived from cornstalk. Industrial Crops and Products, 161, 113225.

- Zhao, B., Wang, H., Hu, Y., Gao, J., Zhao, G., Ray, M. B., & Xu, C. C. (2020). Hydrothermal co-liquefaction of lignite and lignocellulosic biomass with the addition of formic acid: study on product distribution, characteristics, and synergistic

effects. Industrial & Engineering Chemistry Research, 59(50), 21663-21675.

- Wang, H., Zeng, Y., Liu, M., & Xu, C. C. (2020, June). Corrosion Performance of Candidate Constructional Steels Under Batchmode Hydrothermal Liquefaction (HTL) Conditions. In CORROSION 2020. OnePetro.

- Hu, Y., Gong, M., Xing, X., Wang, H., Zeng, Y., & Xu, C. C. (2020). Supercritical water gasification of biomass model compounds: A review. Renewable and Sustainable Energy Reviews, 118, 109529.